Investigation of Graphene Oxide and Au Based Monometallic and Alloy Nanoparticles as Nanocatalysts for Coupling and Oxidative Organic Transformations

Ph.D. Thesis

by

Ms. Tamalika Bhattacharya

Roll no. 1010406

Discipline of Chemistry, School of Basic Sciences

Indian Institute of Technology Indore

Investigation of Graphene Oxide and Au Based Monometallic and Alloy Nanoparticles as Nanocatalysts for Coupling and Oxidative Organic Transformations

A THESIS

Submitted in partial fulfillment of the

requirements for the award of the degree of

DOCTOR OF PHILOSOPHY

Ms. Tamalika Bhattacharya

Roll no. 1010406

Discipline of Chemistry, School of Basic Sciences

Indian Institute of Technology Indore

INDIAN INSTITUTE OF TECHNOLOGY INDORE

CANDIDATE'S DECLARATION

I hereby certify that the work which is being presented in the thesis entitled **Investigation of Graphene Oxide and Au Based Monometallic and Alloy Nanoparticles as Nanocatalysts for Coupling and Oxidative Organic Transformations** for the partial fulfillment of the requirements for the award of the degree of **DOCTOR OF PHILOSOPHY** and submitted in the **DISCIPLINE OF CHEMISTRY, Indian Institute of Technology Indore**, is an authentic record of my own work carried out during the time period from JULY, 2010 to JUNE, 2015 under the supervision Dr. Tridib Kumar Sarma, Assistant Professor.

The matter presented in this thesis has not been submitted by me for the award of any other degree of this or any other institute.

Signature of the student with date
(TAMALIKA BHATTACHARYA)

This is to certify that the above statement made by the candidate is correct to the best of my knowledge.

Signature of Thesis Supervisor with date
(Dr. TRIDIB KUMAR SARMA)

TAMALIKA BHATTACHARYA has successfully given her Ph.D. Oral Examination held on ...………..

Signature of Thesis Supervisor
Date:

Convener, DPGC
Date:

Signature of PSPC Member #1
Date:

Signature of PSPC Member #1
Date:

Signature of External Examiner
Date:

ACKNOWLEDGEMENTS

I need to express my deepest love and gratitude to my lovable parents Mr. Dilip Kumar Bhattacharya, Mrs. Supriti Bhattacharya and uncle Pradeep kumar Bhattacharya and my brothers Tuhin Subhra Bhattacharya, Arakhadip Bhattacharya, also my sweetest sister Paramita Bhtatacharya for their unconditional love, support, unending encouragement and patience during this tenure.

I would like to take this opportunity to express my respect, love and gratitude to all the teachers from Vivekananda Mission Ashram and Haldia Govt. Sponsored Vivekananda Vidybhawan, Haldia Government College.

-

Tamalika

Dedicated to

My Family

-Tamalika

Abstract

The development of green and sustainable chemical processes towards meeting the increasing demands of synthetic functional materials, while balancing the rapidly depleting natural resources has been a key focus area of research activities. Nanoparticles have attracted bulk of the interest towards the development of heterogeneous catalytic systems due to their large surface to volume ratio, tunable catalytic properties by controlling the structural and compositional complexities, possibilities of surface functionalization as required and stabilization of various active catalytic agents (such as free radicals, enzymes etc.) on their surface.

The objective of this thesis is to explore the inherent catalytic activity of an important carbonaceous material graphene oxide and Au based monometallic and alloy nanoparticles towards the development of greener and highly efficient synthetic methods for useful organic transformations. The rationale for these studies is to exploit the structural and compositional intricacies of the nanoparticles for catalytic organic reactions with high activity, selectivity, atom-efficiency and step-efficiency.

In this direction, we have developed the following nanocatalytic systems for various important organic transformations under mild reaction conditions:

1) Graphene oxide based metal-free carbocatalytic system for multicomponent coupling reactions under solvent free condition.

2) Self-assembled monolayer coated gold nanoparticles through thiol binding which catalyze the aerobic oxidation of aryl substituted α-hydroxy ketones to aryl 1,2-diketones as well as one-pot synthesis of quinoxalines via *in situ* oxidation of α-hydroxy ketones and subsequent condensation with aryl 1,2-diamines in water.

3) Bimetallic AuPd nanoparticle catalyzed selective oxidation of α-hydroxy esters and phosphonates as well as aerobic oxidative cross-dehydrogenative coupling for the synthesis of α-ketamide.

4) Aerobic Oxidative cross-dehydrogenative C-C coupling reaction catalyzed by shape controlled Au-Pd bimetallic Nanoparticles.

The thesis is divided into the following chapters based on nanocatalytic systems used for various organic transformations:

1. Introduction:

In the first chapter, we have summarized the historical and recent perspectives in the development of carbonaceous materials as catalysts for various organic transformations. Further, the basic concepts of monometallic and bimetallic Au based nanoparticle catalysts and the subsequent developments regarding their performance as efficient catalysts with respect to structural and compositional variations in important organic transformations have been highlighted. Further a brief summary of the research reported in this thesis and their relevance in the prospects of recent developments are discussed.

2. Ultrasound mediated synthesis of α-aminophosphonates and 3,4-dihydropyrimidin-2-ones using graphene oxide as a recyclable catalyst under solvent-free conditions

In this chapter, we have shown the exploitation of the acidic oxygenated groups on the graphene oxide (GO) sheets towards the applicability of GO as a potent catalyst for the three-component one-pot synthesis of α-aminophosphonates, 3,4-dihydropyrimidin-2-one (DHPM) and 3-substitued Indole which are important classes of biologically active compounds. Due the presence of numerous hydroxy, epoxy and carboxylic groups on their surface and the presence of large surface area, graphene oxide can act as an exciting and efficient metal-free heterogeneous catalyst following green organic protocols. The methodology resulted in high yield of the desired products in a very short reaction time.

3. Self-assembled monolayer coated gold-nanoparticle catalyzed aerobic oxidation of α-hydroxy ketones in water: an efficient one-pot synthesis of quinoxaline derivatives

In this chapter, we have displayed the catalytic activity of self-assembled monolayer-coated Au-NPs for the aerobic oxidation of aryl substituted α-hydroxy ketones to aryl 1,2-diketones and extended this reaction for a one-pot synthesis of biologically significant quinoxaline derivatives in water. Majority investigations related to the catalytic activity of Au have been oriented towards the morphology of the nanoparticles and the nature of the support, where the Au-NPs are bound by weak coordination to the supported polymeric or solid surfaces.

4. Selective oxidation of α-hydroxy esters and α-hydroxy phosphonates catalyzed by Au-Pd alloy nanoparticles

We report that alloying Au with intrinsically active Pd lead to a catalyst with fine-tuned activity for this specific reaction. It has been well established that bimetallic NPs offer greater reaction specific catalyst tunability and superior performance compared to their monometallic counterparts owing to the synergistic effect between two different metals. The selectivity in oxidation of substrates having esters and phosphonate groups were controlled by tuning the Au:Pd ratio (1:1) in a bimetallic nanoparticle catalyst under a base-free and solventless condition.

5. Aerobic Oxidative Cross-Dehydrogenative Coupling catalyzed with heterogeneous spherical Au-Pd bimetallic Nanoparticles: synthesis of α-ketamide

In this chapter, we have shown a new methodology for the synthesis of α-ketoamides from phenylglyoxal and aromatic amines using heterogeneous Au-Pd alloy nanoparticle as catalyst in presence of molecular oxygen as oxidant. This kind of coupling reactions using molecular oxygen as the sole oxidant still remains a challenge. The α-ketoamides, as the key structural skeletal framework of many

natural products and pharmaceuticals, have attracted interest because of their important biologically active properties.

6. Aerobic Oxidative Cross-Dehydrogenative C-C Coupling reaction catalyzed with shape controlled Au-Pd bimetallic Nanoparticles

In this chapter, we report the cross-dehydrogenative coupling of 1,2,3,4-tetrahydroisoquinoline with nitromethane catalyzed by shape controlled urchin like AuPd bimetallic nanoparticle without any external oxidant. It has now been established that shape controlled nanoparticles with well-defined facets can be used as heterogeneous catalysts with enhanced activity and selectivity. Towards have a better understanding in enhancement of catalytic activities to the surface crystal structure, we synthesized urchin shaped AuPd nanoparticles using a modified polyol method. The co-reduction of Au^{3+} and Pd^{2+} salt in ethylene glycol and PVP led to the formation of branched AuPd nanoparticles, when Br^- was used as an oxidative etchant.

7. Relevance and Scope of our work:

In this chapter, we have summarized the works described in this thesis. Further, we have discussed the relevance of our works for the industrial applications and future prospects.

List of Publications:

1. T. Bhattacharya, B. Majumdar, D. Dey, T. K. Sarma*, Ultrasound mediated synthesis of α-aminophosphonates and 3,4- dihydropyrimidin-2-ones using graphene oxide as a recyclable catalyst under solvent-free conditions. *RSC Adv.*, 2014, **4**, 45831- 45837.

2. D. Dey*, T. Bhattacharya, B. Majumdar, S. Mandani, B. Sharma, T. K. Sarma*, Carbon dot reduced palladium nanoparticles as active catalysts for carbon–carbon bond formation, *Dalton Trans.,* 2013, **42**, 13821-13825.

3. T. Bhattacharya, T. K. Sarma*, S. Samanta*, Self-assembled monolayer coated gold- nanoparticle catalyzed aerobic oxidation of α-hydroxy ketones in water: an efficient one- pot synthesis of quinoxaline derivatives. *Catal. Sci. Technol.*, 2012, **2**, 2216-2220.

4. T. Bhattacharya, B. Majumdar and T. K. Sarma*, Selective oxidation of α-hydroxy esters and α-hydroxy phosphonates catalyzed by Au-Pd alloy nanoparticles, manuscript under preparation.

5. B. Majumdar, T. Bhattacharya and T. K. Sarma*, Selective oxidation of benzylic C(sp^3)-H bonds using Au nanoparticle-reduced graphene oxide composite and *N*-hydroxyphthalimide under mild conditions, , manuscript submitted for publication.

6. T. Bhattacharya, B. Majumdar and T. K. Sarma*, Aerobic oxidative cross-dehydrogenative C-C coupling reaction catalyzed with shape controlled AuPd bimetallic nanoparticles, manuscript under preparation.

7. T. Bhattacharya, B. Majumdar and T. K. Sarma*, Aerobic oxidative cross-dehydrogenative coupling catalyzed with heterogeneous spherical AuPd bimetallic nanoparticles: Synthesis of α-ketoamide, manuscript under preparation.

TABLE OF CONTENTS

Chapter-3 Self-assembled monolayer coated gold-nanoparticle catalyzed aerobic oxidation of α-hydroxy ketones in water: an efficient one-pot synthesis of quinoxaline derivative

Chapter-3: Self-assembled monolayer coated gold-nanoparticle catalyzed aerobic oxidation of α-hydroxy ketones in water: an efficient one-pot synthesis of quinoxaline derivative

20 nm and the average particle size 5±2 nm scale bar 20 nm. c) after oxidation reaction average particle size 7±3 nm scale bar 10 nm

Chapter-5 : Aerobic oxidative cross- dehydrogenative coupling reactions catalyzed by heterogeneous spherical Au-Pd bimetallic nanoparticles: synthesis of *α*-ketoamide

Chapter 6: Aerobic Oxidative Cross-Dehydrogenative C-C Coupling reaction catalyzed with shape controlled Au-Pd bimetallic Nanoparticles

LIST OF SCHEMES

LIST OF TABLES

General Introduction

Ultrasound mediated synthesis of α-aminophosphonates and 3, 4-dihydropyrimidin-2-ones using graphene oxide as a recyclable catalyst under solvent-free conditions

Self-assembled monolayer coated gold-nanoparticle catalyzed aerobic oxidation of α-hydroxy ketones in water: an efficient one-pot synthesis of quinoxaline derivatives

Selective aerobic oxidation of α-hydroxy esters and α-hydroxy phosphonates using AuPd nanoparticles

Aerobic oxidative cross- dehydrogenative coupling reactions catalyzed by heterogeneous spherical Au-Pd bimetallic nanoparticles: synthesis of *α*-ketoamide

Aerobic Oxidative Cross-Dehydrogenative C-C Coupling reaction catalyzed with shape controlled Au-Pd bimetallic Nanoparticles

ACRONYMS

XRD	X-ray diffraction
NMR	Nuclear Magnetic Resonance
DMF	Dimethylformamide
DCM	Dichloromethane
TGA	Thermogravimetric Analysis
ph	phenyl
IR	Infrared
UV-Vis	UV-Visible Spectroscopy
$CDCl_3$	Chloroform-d
EtOH	Ethanol
MeOH	Methanol
THF	Tetrahydrofuran
TLC	Thin Layer Chromatography
TEA	Triethylamine
TBHP	tert-Butyl hydroperoxide
Au	gold
Pd	palladium

NOMENCLATURE

α	Alfa
β	Beta
π	Pi
σ	Sigma
Å	Angstrom
nm	Nanometer
cm	Centimeter
°	Degree
°C	Degree Centigrade
mmol	Millimol
mL	Milliliter
μL	Microliter
a. u.	Arbitrary Unit

Chapter 1

General Introduction

In recent years, there has been tremendous emphasis towards developing greener methodologies in synthetic organic chemistry. The need for clean processes in the industrial production of fine and commodity chemicals is becoming increasingly urgent and is reflected in the attention it receives from government policies, media and commercially funded research. Anastas and Warner's 12 points of Green Chemistry address specific criteria that must be developed in order to attain a clean, sustainable industry whilst continuing to meet with the chemical demands of a growing population.[1] The focal point towards these developments has been towards waste prevention, atom economy, designing safer chemicals, safer solvents and auxiliaries, energy efficiency, use of renewable feed-stocks, reduce derivatization and inherently safer chemistry.
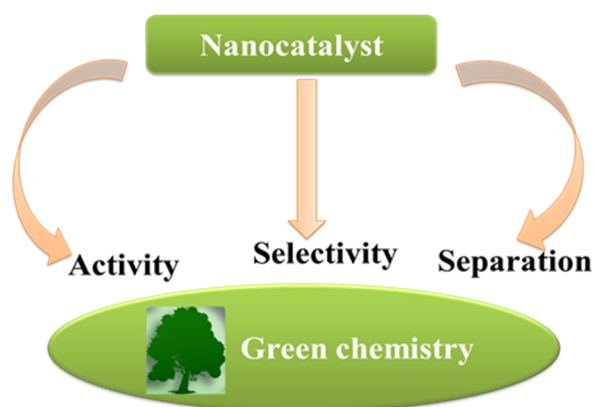
Figure 1.1 *Development of nanocatalyst from green chemistry point of view.*

Towards the development of green and economical pathways for the large scale synthesis at the industrial level, the ideal protocol is judged in terms of catalytic activity, selectivity, atom-efficiency and step-efficiency. The terms are briefly described as follows: The rate at which a reaction occurs is determined by the activation energy of the rate determining step. By providing an alternative reaction pathway with a lower energy barrier, a catalyst can be used to enhance reaction rate. If there are several products and several reaction barriers, catalysts may also direct the formation of one product over another because the reaction path is easier; the catalyst drives the reaction selectivity towards a particular product. The efficiency of a catalyst lies in the achievement of the desired chemical reaction with high yield and selectivity at

a mild reaction condition. Designing new methodology to achieve green and sustainable production of chemicals is the need of the hour in which the use of catalyst along with reduction of toxic and hazardous chemicals, stoichiometric amount of promoter, less consumption of energy, fewer side-products and less number of steps is involved.[2] A variety of catalysts have been developed, both homogenous and heterogeneous since many years but the field still demands more research as it has a vast scope from green chemistry point of view. Among various methodologies in the synthesis process in organic chemistry, fabricating a one-pot method with heterogeneous catalysis is extremely challenging goal, because it aims at decreasing the energy and time consumption by operation of multi-steps at a time which eliminates the need of separation of products from the reaction mixture again and again.
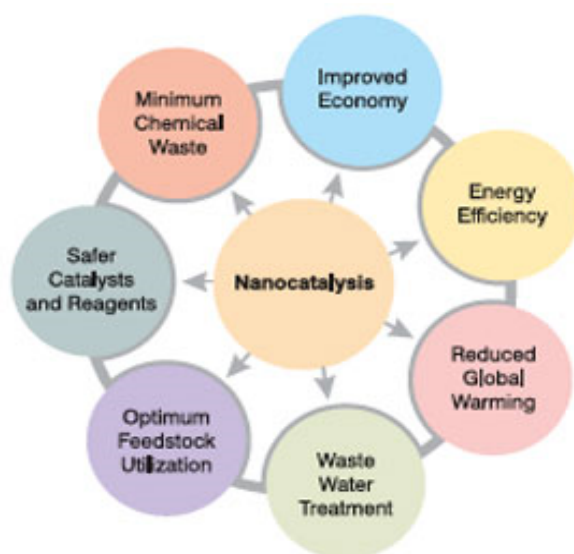
Figure 1.2 *Benefits of heterogeneous nanocatalysts in the chemical industry.*

1. 1 Heterogeneous vs homogeneous catalyst

If the catalyst is in the same phase as the reaction mixture it is defined as a homogeneous catalyst, if the two phases are different it is a heterogeneous catalyst. The active site of homogeneous catalysts is more clearly defined, thus advances in catalyst design for more complex reactions, such as in the fine chemicals and pharmaceutical industries, have generally centered on homogeneous catalysis.[3] However, there are disadvantages to using

homogeneous catalysts: they are often more corrosive, more harmful and more expensive than heterogeneous catalysts, and they are difficult and costly to separate from the product reaction mixture. Heterogeneous catalysts remove the necessity for using stoichiometric reagents and if selectivity can be appropriately controlled and significantly reduce waste, they meet some important criteria in the principles of green chemistry. A heterogeneous catalytic reaction involves adsorption and activation of reactants on specific sites of a solid surface, chemical transformation of adsorbed species and desorption of products. The catalyst surface is complex and understanding the various surface reactions at the molecular level is often very tedious for designing catalysts with suitable selectivity and activity. Many factors such as size, shape, composition and several other variables in a chemical reactor will influence the surface properties and thus the catalyst reactivity during reaction. Deactivation of the catalyst is also a major issue in the employment of these materials in industry. Consequentially, advances in heterogeneous catalyst design and improved understanding of the active site is crucial to the development of clean industrial technologies.[4]

In homogeneous catalytic systems, the reactions can be efficiently carried out with high yields and less reaction time but the main disadvantage of this process is that the catalyst cannot be recycled. Generally, expensive metal catalysts are used and if they are quite difficult to recover then the whole cost of reaction goes high. Heterogeneous catalytic systems have exhibited many advantages over homogeneous catalysts, the most extraordinary being the easy and faster separation process and facile recovery of the solid heterogeneous catalyst from the products for recycling without tedious experimental workup. Furthermore, the heterogeneous catalysts can easily operate under hazardous condition with elevated temperature when compared to the homogeneous catalysts. The mechanistic pathways of both heterogeneous and homogeneous catalyst are totally different in nature. In case of homogeneous catalyst, the oxidation state of principal metal changes in intermediate steps of the reaction process and after the reaction the metal comes back to its initial oxidation state. On the other hand, the heterogeneous catalytic reaction involves surface initiated and activated chemical transformations. The possibility of product

elimination with loss of selectivity of desired product in homogeneous catalysis is much greater than the heterogeneous catalytic pathway due to involvement of metal in the reaction of the homogeneous catalytic systems. The heterogeneous catalysis depends on the nature of catalytically active surface, specific properties of support material like surface area, morphology, porosity and active centers dispersion, metal-support interactions and mobility on the surface.[5]

In recent years, inorganic or organic nanoparticles have been explored as effective catalysts for industrial production of fine chemicals and pharmaceuticals. Using bottom-up chemistry approaches, the composition, size and shape of the nanocrystals can be controlled as desired. The recent developments on the size, composition and facet dependent catalytic performance of the nanosystems in various organic transformations are of great importance for modern heterogeneous catalysis research.[6] The desired activity and selectivity of catalytic reactions can be obtained by simply tuning the size, shape and morphology of the nanoparticles. These will be highlighted in the subsequent chapters.

Carbocatalysts

Graphene Oxide

Heterogeneous nanocatalysts

Metal nanocatalysts

1. Monometallic nanoparticles
2. Bimetallic alloy nanoparticles
3. Shape controlled nanoparticles
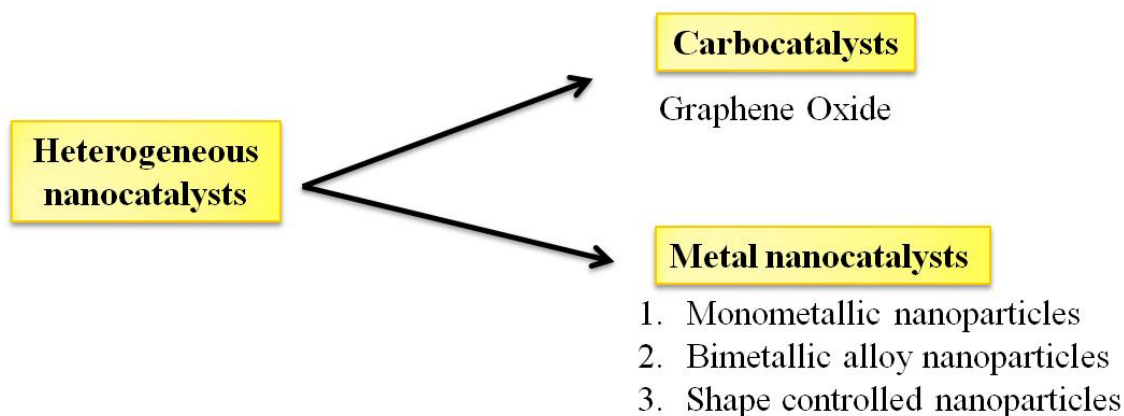
Figure 1.3 *Nanocatalysts used in this thesis work.*

1.2 Carbonaceous Nanomaterials for catalysis

Metal-free nanostructure of elemental carbons and carbonaceous materials has been demonstrated as excellent catalysts for a variety of significant organic transformations. Metal-free carbon nanostructures consist of the wide range of carbon based materials with sp^2 or sp^3 hybridized carbon which can be easily customized in nanoscale dimensions. With varying the feature of carbon materials, their inherent functional properties can be easily tuned.[7]
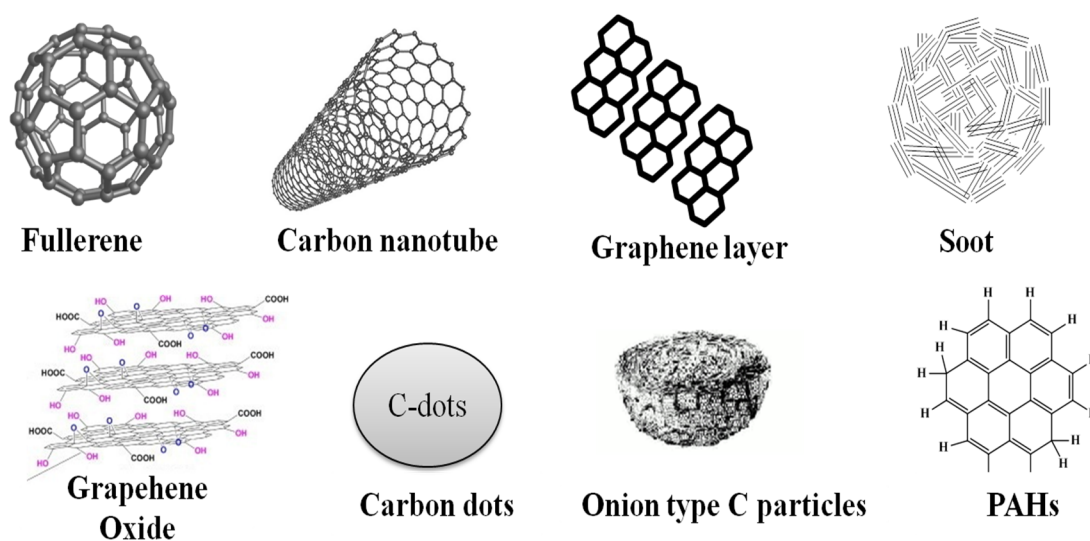
Figure 1.4 *Different types of carbon nanomaterials.*

Carbon based nanomaterials exist is a diverse range of forms such as carbon black, carbon nanotubes, carbon nanofibers, graphene, carbon nanotubes, fullerene, -coils, -nanodiamonds, -horns, and onions. For the applications in the area of catalysis, the carbonaceous nanomaterials have been used mostly as a support for anchoring active metal nanoparticles, thus imparting heterogeneity to the nanocatalytic systems.[8] The ordered porous network in mesoporous carbons have been used to impregnate metal nanoparticles for further performance as effective catalysts for numerous organic transformations. Doped fullerenes have shown activity as a cathode catalyst in hydrogen fuel cells. Carbon nanotubes show tremendous activity for oxygen reduction reactions, where they show better activity even than platinum for fuel cell applications. Metal nanoparticles immobilized on carbon nanotubes

have shown very high catalytic activity for several important organic reactions. In recent years, there has been huge excitement in the scientific community about the two-dimensional nanosheet form of carbon: graphenes.[9] Graphene is the basic building block for carbonaceous materials of different dimensionalities: fullerenes (0D), nanotubes (1D) or graphite (3D). Their importance in technological applications arise from the fact that graphenes have higher electrical and thermal conductivities, better transparency, mechanical strength and larger surface area due to their unique structure containing of sp^2 bonded carbon atoms.[10] For chemistry applications, however, the oxygenated form of grapheme namely graphene oxide has found more relevance due to their high water dispersibility, negligible toxicity and possibility of further functionalization of various inorganic or organic components on their surface. Due to the presence of oxygenated functionalities as well as the large specific surface area, graphene oxide nanosheets are emerging as promising smart supports for various graphene-based hybrid nanomaterials with significant applications in sensors, optical and electronic devices, energy conversion and storage, and catalysis.[11] While the array of possible oxygen containing functional groups that can associate with graphene oxide has been found to catalyse a variety of reactions such as oxidation and hydration reactions, aza-michael addition reaction and so on. These functional groups also allow attachment and decoration of graphene oxide surface with various metal nanoparticles for a range of electronic, charge storage, sensor and catalysis applications.[12] While GO supported Au or Pd NPs have been explored as catalysts for Suzuki-Miyaura coupling reactions, Fe based catalysts were used for Fischer-Tropsch synthesis, Pt and Pt-Pd NPs supported on GO have been studied for methanol electro-oxidation etc. Further, enhancement of recyclability is done by incorporating magnetic iron oxide to the Pd/graphene nanocomposite and used for Suzuki-Miyaura coupling.[13] Moreover, nanohybrid materials involving graphene supported porphyrin derivatives have shown excellent catalytic activities for oxidation reactions with twofold increase in catalytic activity compared to free porhyrin, which has opened up a new outlook for using grapheme oxide as a support material. The hemin-graphene nanohybrid has proved as highly effective catalyst for

toluene oxidation reaction under mild conditions. The hemin-graphene conjugates have also performed as an effective catalyst for the oxidation of pyrogallol with exceptionally high catalytic activity.[14] The inherent π- π interactions between hemin and graphene where hemin retains its catalytically active monomeric form accounts the activity of the conjugate system.

The high activity of graphene oxide based multicomponent catalytic systems over other nanohybrids might be due to the synergetic effect between the metal and graphene oxide components. Synergetic effect in multicomponent catalytic systems represents interaction between the active metal or metal oxide catalyst and the supporting material. Theses resulting enhanced catalytic performances of the hybrid material compared to combined activity of individual components. Also, carbonaceous supports impart high thermal stability for the metal nanoparticles preventing agglomeration during high temperature annealing required for several nanocatalytic systems for better performance as catalysts in chemical reactions. In case of graphene oxide, due to their high dispersibility in polar solvents, the adsorption of metal salts and further nucleation and growth of the metal nanoparticles on their surface is much easier leading to high catalyst loading on the graphene oxide surface.[15]

1.3 Development of Gold based Nanocatalysts

Metallic nanoparticles occupy a special place in catalysis and several metallic nanoparticles such as Au, Ag, Cu, Pd, Pt, Ru, Rd etc. have demonstrated excellent activity as catalysts for several important organic transformations such as hydrogenation of alkenes, alkynes and aromatics and C-C bond formations such as hydroformylation, methanol carbonylation, coupling reactions and Pauson – Khand reactions, oxidation, dehydrocoupling and hydrosilylation.[16-17] With the development of bottom-up approaches for the precise size and shape selective synthesis of nanoparticles, excitement in developing metal nanoparticle based catalytic systems for selective synthesis of chemicals has increased manifold. Nanoparticles occur in a variety of sizes ranging from 10 to 10^6 atoms per clusters. Metal nanoparticles having diameter smaller than 2 nm contain less than 100 atoms and have an especially

large surface area to volume ratio with high surface energy, which is highly desired in catalysis.[18]

Decrease of surface-to-volume ratio

92 %   76 %   63 %   52 %
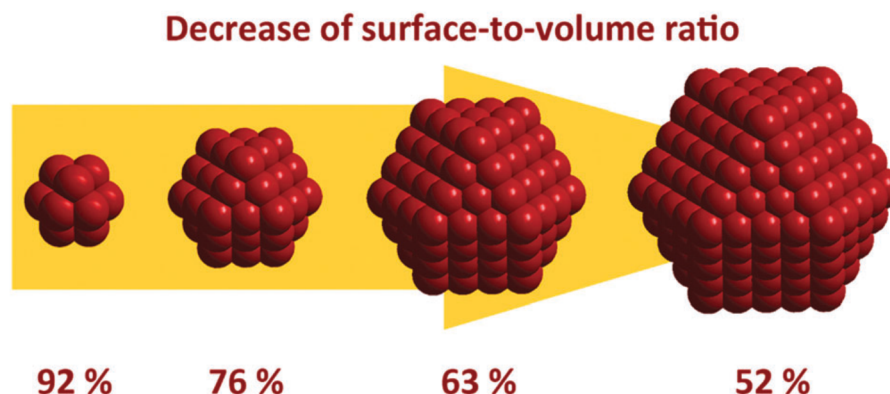
Figure 1.5 Decrease of surface-to-volume ratio for cuboctahedral nanoparticles (fraction of surface atoms given in %).

At the nanoscale level, the exposed surface atoms are more active and have physico-chemical properties completely different from their bulk counterparts. The high activity of these metallic nanoparticles is reflected in an impressive number of catalytic reactions that are achieved under milder reaction conditions. Further these nanoparticles can also be used as catalysts in homogeneous systems or alternatively they can be heterogenized by fixation onto a heterogeneous support such as silica, alumina, other oxides or carbon.[19-20] Thus, the field of nanoparticle catalysis involves both the homogeneous and heterogeneous catalysis communities and these catalysts are therefore called "semi-heterogeneous". Nanocatalysts are selective, efficient and recyclable and thus meet the modern requirements for *green catalysts*.

Au is considered to be a noble metal, as the nobility of metals are entirely connected to the chemisorption of oxygen to the metal surface with simple bond formation. On Au metal surface, the dissociative chemisorption of oxygen is thermodynamically forbidden. Correlating with the chemisorption energy of different transition metals in the periodic table as shown in Figure 1.6, Au is the only metal with endothermic chemisorption energy and has weak oxygen binding capability.[21]

Cr	Mn	Fe -6.30	Co -5.07	Ni -3.90	Cu -2.51
Mo -7.48	Tc	Ru -4.62	Rh -4.03	Pd -1.20	Ag -0.65
W -8.62	Re	Os	Ir -4.65	Pt -2.17	Au +0.54

Figure 1.6 *Chemisorption energy of different transition metals.*

However the seminal discovery by Prof. Haruta's group that Au nanoparticles immobilized on oxide supports (TiO_2, Fe_2O_3 or Co_3O_4) could effectively catalyze CO oxidation to CO_2 by O_2 even below 200K with the crucial requirement for the small size of the Au NPs (< 5 nm), has completely changed the way the chemists look at this magic metal.[21] Subsequently, there was a flurry of research with respect to activity of Au nanocatalysts with respect to size and shape, role of support and their applicability in various organic transformations. Detailed mechanistic investigations, both experimentally and theoretically, have been explored for understanding the complicated surface reactions occurring during these catalytic reactions. Au nanoparticles have shown tremendous potential as oxidation catalysts and various supported and unsupported Au nanocatalytic systems have been developed towards realizing oxidation of organic substrates.[22] The developments are summarized in Figure 1.7. Along with oxidation reactions Au nanoparticles have also shown catalytic activities in several other important organic transformations such as selective hydrogenation[23] (e.g., CO_2 reduction to CO, nitrophenol to aminophenol, and chemoselective hydrogenation of α,β-unsaturated ketones to α,β-unsaturated alcohols). Au nanoparticles have also shown high activity in C-C couplings reactions like ullmann homocoupling of halides, oxidative homocoupling of organoboronates,[24] Suzuki cross-coupling of phenylboronic acid and halides,

Sonogashira cross-coupling of iodobenzene and phenylacetylene, and A^3 - coupling reaction of phenylacetylene, amines, and aryl or alkyl aldehydes.[32]
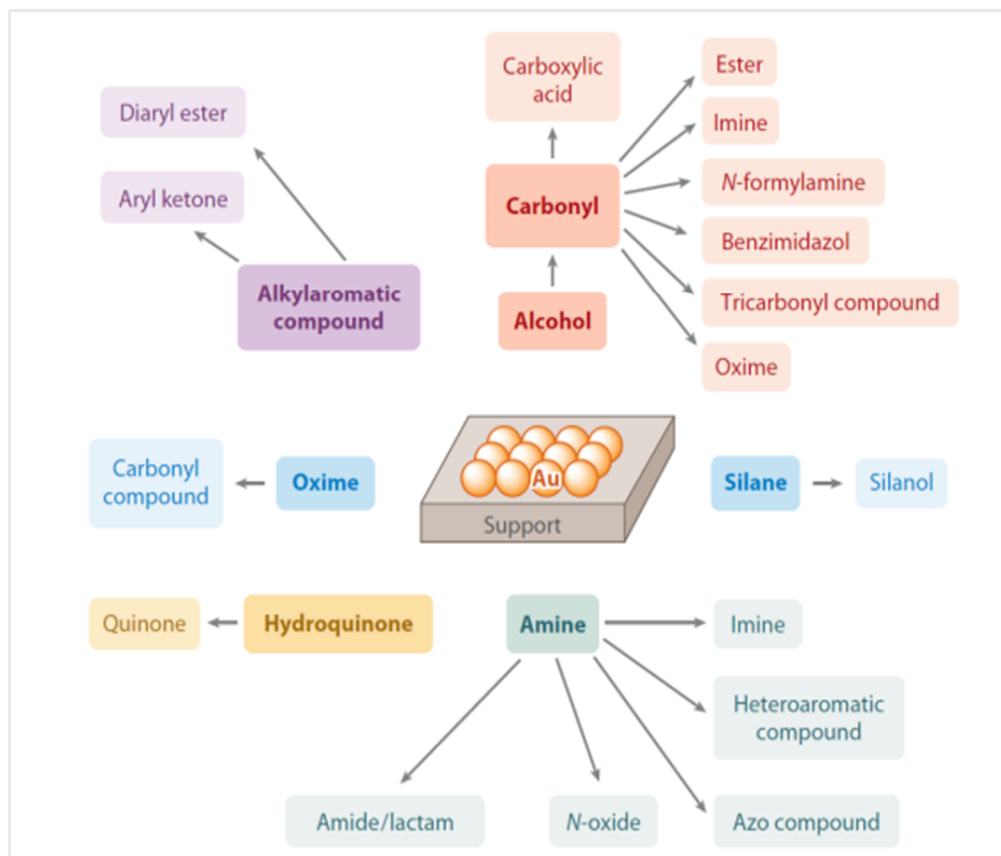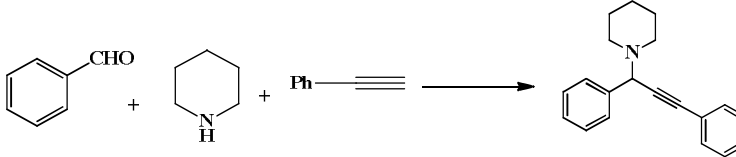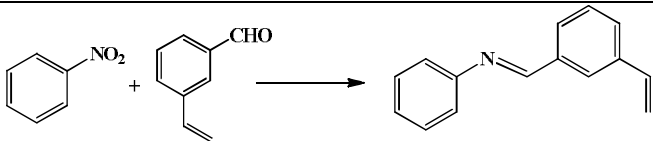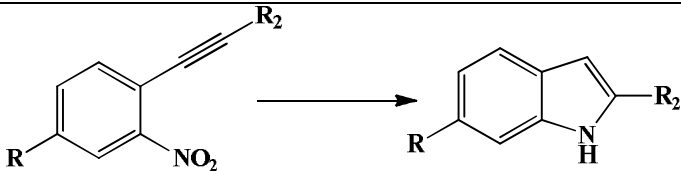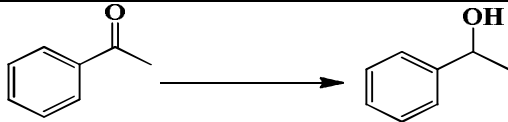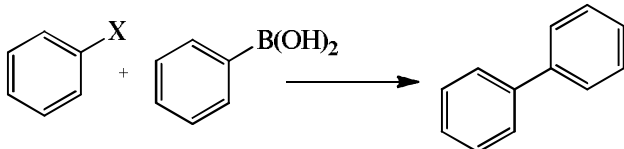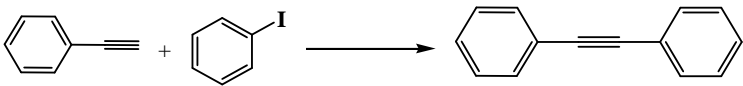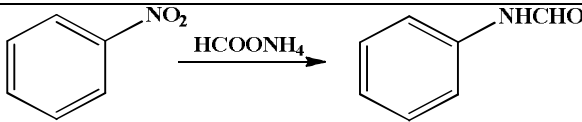
Figure 1.7 *Important aerobic oxidations in fine chemical syntheses catalysed by supported and unsupported Au nanocatalysts (adopted from Annual Review of Chemical and Bimolecular Engineering[22]).*

Some of the important organic transformations catalysed by Au nanoparticles are summarized in Table 1.1. These carbon-carbon bond formations are very important in organic synthesis especially for production of natural products such as alkaloids, biologically active compounds in pharmaceutical and agrochemical industries.

Table 1.1 *Few Important organic transformations catalyzed by Au nanoparticles*

Entry	Gold nanocatalyst	Reactions
1	Au/CeO$_2$ Ref25	
2	Au/TiO$_2$ Ref-26	
3	Au/Fe$_2$O$_3$ Ref-27	
4	AuTiO$_2$ Ref-28	
5	Au/PATP Ref-29	
6	Au/CeO$_2$ ref-30	
7	Au/TiO$_2$ Ref-31	

.

1.4 Role of Support

For the nanocatalytic systems, stability of the nanoparticles in the reaction medium is a critical issue as electrostatic, steric or ligand interactions often lead to agglomeration of the nanoparticles.[33] This leads to decreased surface area to volume ratio, resulting in decrease in activity of the nanocatalysts. This is important as nanoparticles are expected to be reused over several cycles

without major loss in activity. Therefore there has been continuous effort to use nanoparticles in homogeneous, heterogeneous, supported and biphasic medium including also studies in non-classical conditions (solvent-free, aqueous, use of ionic liquids, fluorine chemistry, microemulsions, micelles, reverse micelles, vesicles, surfactants, aerogels, polymers or dendrimers) to obtained optimized catalytic conditions.[34] In case of Au nanocatalysts, for the CO oxidation to CO_2 in presence of molecular O_2, Haruta *et. al.* showed that the activated metal oxide support was involved in the mechanism. Haruta suggested that CO probably adsorbs on the edge and step sites of AuNP surfaces and O_2 adsorbs on the support surfaces.[35] Subsequently several other groups have reported the role of various metal oxide supports on hydrogenation, C-C coupling and oxidation reactions. With a well-developed porous structure and high surface area combined with high thermal and chemical stability, a variety of oxides of metals such as Si, Al, Ti, Fe, Zn, Ni, Ca, Mg etc. have been studied as supports for Au nanoparticle catalysts for important transformations. Charcoal adequately modified to have high surface area, porosity and pore size distribution, as well as carbon nanotubes have also been used as supports for immobilizing metal nanoparticles for catalysis.[36] Recently, nanoparticles immobilized in metal-organic frameworks have also shown high activity as catalysts for chemical reactions.[37]

In this thesis, we have investigated the catalytic activity of Au based nanocatalysts stabilized in a polymer matrix namely poly(N-vinyl-2-pyrrolidone) (PVP). Polymers provide metal NP stabilization not only because of the steric bulk of their framework, but also by weak binding to the NP surface by the heteroatom, playing the role of ligands. PVP is one of the most commonly used polymers for nanoparticle stabilization and catalysis, as it fulfils both the stabilization and ligand requirements. Several metal nanoparticle-PVP composites such as Pd, Pt, Au and Rh nanoparticles have been evaluated for catalysis. PVP weakly interacts with the nanocluster through the -N-C=O sites of their functional groups where the oxygen binds to the metal nanoclusters surface.[38] The size tunability of the nanoparticles can be controlled by varying the polymer:metal salt ratio by properly controlling the reaction conditions. Further, PVP has been used as a shape-directing agent

towards the synthesis of nanoparticles with exposed facets by the well-known polyol method. Hence a proper understanding towards the correlation of size, shape and morphology of nanoparticles and catalytic activity can be achieved by using this nanocomposite system. Other conventional polymers like polyvinyl alcohol (PVA), polyaniline, polyacralamide, poly(N-isopropylacrylamide) (PNIPAM), polystyrene based polymers, poly(2-amino-thiophenol) etc.[39-40] have been utilized for stabilizing the metal nanoclusters through their weak interaction with the metal surface and catalytic activity of these nanocomposites have been performed.

1.5 Bimetallic nanoparticles

Bimetallic nanoparticles, that comprises two metallic constituents in the same nanoparticles has attracted tremendous research activities, as they show better reactivity, selectivity and stability compared to their monometallic counterparts.[41] Bimetallic nanoparticles not only combine the properties of their individual constituents, but also it is possible to change the reaction pathway dramatically in catalysis when one metal is combined with a second metal. Among bimetallic catalysts, AuPd has received a great deal of attention because of its superior activity in a number of reactions. AuPd catalysts are used in the industrial synthesis of vinyl acetate (VA).[42] AuPd catalysts also catalyze low-temperature CO oxidation, direct H_2O_2 synthesis from H_2 and O_2, hydrodechlorination of Cl-containing pollutants in underground water, hydrodesulfurization of S-containing organics, hydrogenation of hydrocarbons, acetylene trimerization, and many other reactions.[43]

Catalytic performances of bimetallic nanomaterials

1. Structure effect

2. Composition effect

3. Morphology effect

AuPd catalysts are termed as ''alloy'' when Pd and Au are intimately mixed otherwise ''bimetallics'' when Pd and Au are segregated. The chemical and physical properties of bimetallic nanoparticles can be tuned by altering the size, composition and atomic ordering of the corresponding metal components which is explained as follows.

Structure effect

Bimetallic nanocatalysts demonstrate structure dependent performance which is associated with the electronic states of the nanoparticles surface, as it leads to modification of specific geometric structure with varying the local strain and atomic coordination number of the corresponding alloy nanocatalyst.[44] The catalytic efficiency of bimetallic nanoparticles mainly depends upon two factors:

1. Ensemble effect: ascribed with bimetallic nanomaterials that composed of different metal atoms or clusters of atoms, which facilitates more than one active site for a particular catalytic reaction. In case of AuPd system, the catalytically more active component (Pd) is diluted by the less active component (Au). As the surface ratio of Au–Pd increases, sizes of contiguous Pd ensembles decrease and eventually all Pd atoms are separated by Au as isolated Pd monomers.[45]

2. Ligand effect: electronic modifications resulting from hetero-nuclear metal–metal bond formation. It involves the charge transfer between two metals or orbital rehybridization of one or both metallic components. In case of AuPd bimetallic nanoparticles, it is expected that there will be charge transfer from Pd to more electronegative Au. Upon alloying, whereas Au gains s, p electrons while loses d electrons, Pd loses s, p electrons and gains d electrons. For transition metals like Au and Pd, chemisorption and catalytic properties are governed by d-characters more than s and p characters. Gaining d electrons in Pd results in weaker interaction between the adsorbates and Pd surface atoms.[46] Thus Au effectively weakens the binding strength of Pd by perturbing the d-band. However the catalytic activity of Pd is enhanced within AuPd alloy, possibly due to diminished self-poisoning by reactants/products.

Composition effect

In alloy nanoparticles, the composition effect is closely related to structure effect. Since the addition of another metal greatly influences the electronic properties of the primary metal, it is easily comprehensible that the molar ratio of two metals plays an important

role in determining the catalytic performance of bimetallic nanoparticles. Due to the change in the geometric and coordinating parameters of the surface atoms in alloy nanoparticles (which is governed by the molar ratio of the two components) the probability of binding of the substrate molecules to the surface increases.[47] The strong metal-metal interactions tune the bonding between the catalysts surfaces and reactants, where the extra stabilization of the transition state on the alloy catalysts in comparison to the corresponding interaction on the monometallic catalyst surface is an additional benefit. Furthermore, the metal−metal bonds in bimetallic nanoparticles with intrinsic polarity govern unique reaction pathways for catalytic reactions. Thus cooperativity and synergistic effects that arises from the simultaneous or consecutive actions of different metal centers usually result in higher catalytic activity.[48]

A	**B**	**C**
Interaction of substrate in a monometallic system	Stereoelectric effect of a second metal on the M1-Substrate interaction	Combined effect of the two metals on substrate binding
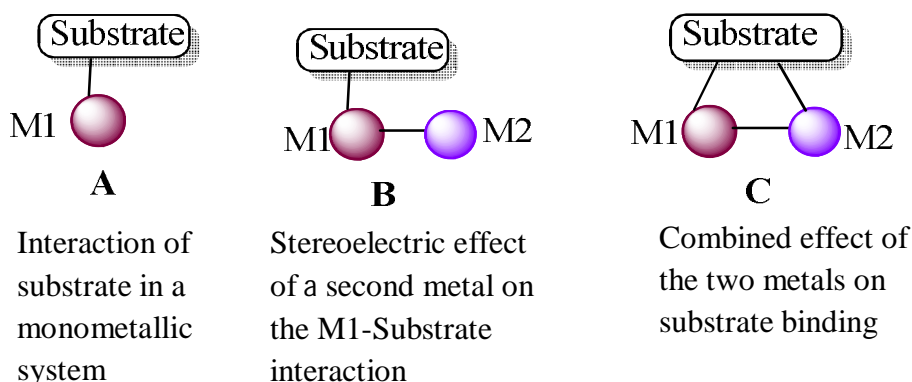
Figure 1.8 *Influence of a chemically different second metal on the binding of a substrate (synergistic effect)*

Morphology effect

The catalytic action of bimetallic nanoparticles is a surface phenomenon; therefore it is naturally expected that the activity and selectivity of these nanoparticles will be dependent on the morphology of the nanoparticles. Based on the mixing pattern, bimetallic nanoparticles can be divided into three main types: Core– shell structures, heterostructures, and intermetallic or alloyed structures. Core–shell structures are formed if one type of metal is reduced first to form an inner core and another type of metal prefers to nucleate and

grow around the core to form a shell. In heterostructured NPs, individual nucleation and growth of two kinds of metal atoms occur with the sharing of a mixed interface during the growth process. Alloy NPs are homogeneous mixtures of two metals on the atomic level and can be distinguished owing to the formation of metal-metal bonds. In several catalytic reactions, the mechanism involves leached metallic species in solution act as the catalytically active ones, and they are redeposited at the end of the reaction making the reaction quasi-homogeneous.[49, 50]
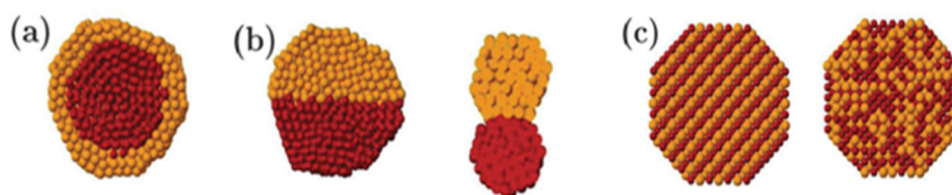
Figure 1.9 *schematic representations of some possible mixing patterns in bimetallic systems: (a) core–shell alloys, (b) sub-cluster segregated alloys, (c) ordered and random homogeneous alloy. The diagrams show cross-sectional representations of the clusters (adopted from ref 50).*

1.6 Shape effect

Catalytic reactions following the heterogeneous pathway can be categorized into structure-sensitive and structure-insensitive or facile reactions. In case of facile reactions, the turn-over frequency of the catalyst that signifies the rate per exposed surface atom does not depend on the structural characteristics of the surface (such as smooth or rough surface, exposed crystal planes etc.). In case of structure-sensitive reactions, the turn-over frequency changes appreciably, in several cases by many orders of magnitude, depending on the exposed facets. Therefore, for these kinds of reactions, catalyst design with more reactive crystal planes on the surface to optimize the structure of the active site is highly desirable for better activity. Shape-controlled synthesis of NCs presents great opportunity for the synthesis of catalytic materials with such desirable features.
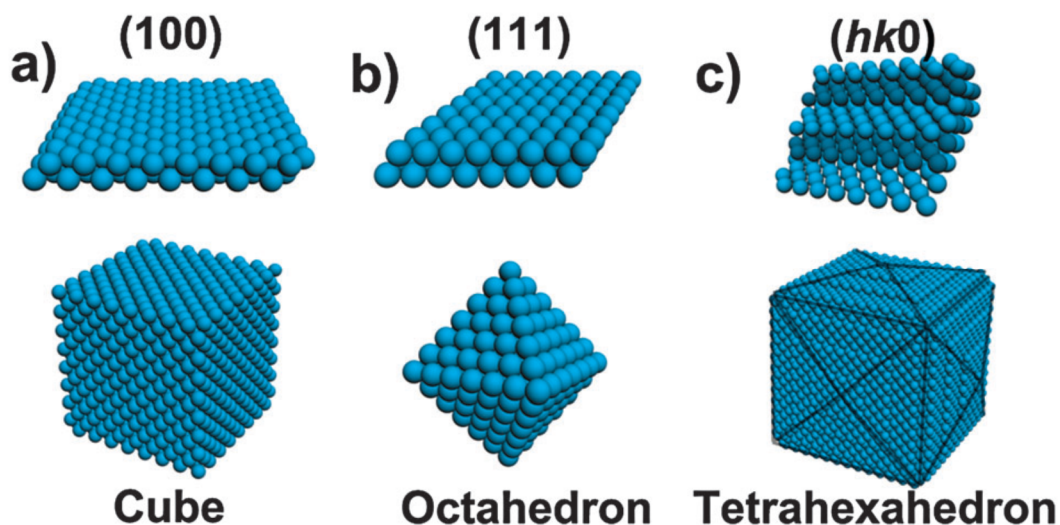
Fig. 1.10 *Schematic of some examples of atomic arrangement on the surface of face centred cubic (fcc) metal crystals with different shapes. (a) Cube exposes {100} facets. (b) Octahedron exposes {111} facets. (c) Tetrahexahedron exposes {hk0} facets containing atomic steps and terraces. (adapted from Reference 52).*

During the last decade, shape-controlled synthesis of nanocrystals have attracted increasing interest and semiconductors, metals, metal oxides as well as alloys have been exploited to discover structurally unprecedented motifs including polyhedrons, rods and belts, plates and prisms with corresponding crystal planes exposed. Several groups have performed various catalytic reactions using these shape-selective nanoparticles and have identified the activity of exposed facets in these reactions. Zhou et. al. summarized facet dependent heterogeneous catalytic reactions in an excellent review.[51a] It is worth mentioning that capping agents or morphology controlling agents that controls the shape-directing synthesis of nanocrystals might not be easily removed from the surface. These stabilizers might play an influential role on the catalytic activity and selectivity of the nanocrystals.

1.7 Organization of the thesis

The aim of our works is to explore the inherent catalytic activity of an important carbonaceous material graphene oxide and Au based monometallic and alloy nanoparticles towards the development of greener and highly efficient synthetic methods for useful organic transformations. The use of nanocatalysts along with avoiding organic solvents and harsh reaction conditions is of significant importance in modern organic chemistry. Recently carbonaceous materials such as graphene oxide and ultrasmall carbon dots have shown tremendous activity in the area of catalysis. On the other hand, there has been a tremendous focus on Au based monometallic and bimetallic nanoparticles for catalysis. There has been significant focus on attaining high activity and selectivity by controlling the composition and structural parameters such as formation of two metal composites (alloy and core-shell) and shape controlled nanoparticles where the preferential exposure of facets activate the catalytic reactions.

Chapter 2: In this chapter, we have shown the exploitation of the acidic oxygenated groups on the graphene oxide (GO) sheets towards the applicability as an efficient catalyst for the three-component coupling reaction to synthesis of α-aminophosphonates, 3,4-dihydropyrimidin-2-one (DHPM) and 3-substituted indole which are important motif of various biologically active compounds. Due the presence of numerous hydroxy, epoxy and carboxylic groups on their surface and the presence of large surface area, graphene oxide can act as an exciting and efficient metal-free heterogeneous catalyst following green organic protocols. The methodology of three component coupling resulted in high yield of the desired products in a very short reaction time. Major advantages of use of graphene oxide as a catalyst, it could be separated easily from the reaction mixture and could be reused for several cycles without major loss in catalytic activity.

Chapter 3: Here we explored the catalytic activity of self-assembled monolayer-coated Au-NPs for the aerobic oxidation of aryl substituted α-hydroxy ketones to aryl 1,2-diketones and extended this reaction for a one-pot synthesis of biologically significant quinoxaline derivatives in water. The

catalytic behavior of self-assembled monolayer-coated Au-NPs would be helpful in establishing the guiding principles for the rational design of active Au-NP-based catalytic systems. We have shown that 4-aminothiophenol self-assembled monolayer-coated gold-nanoparticles (Au-NPs) could catalyze aerobic oxidation of aryl substituted α-hydroxy ketones to aryl 1, 2-diketones in aqueous medium at 80 °C in presence of K_2CO_3. The use of our methodology allows skipping hazardous acid catalysts, organic solvents, avoiding the use of stoichiometric amounts of potentially toxic oxidants and often saving time and reagents.

Chapter 4: *α*-keto esters and *α*-keto phosphonates are structural motifs of various natural products, pharmaceuticals and biologically active compounds and have been found at the core of numerous analgesic, non-steroidal anti-inflammatory drugs and phytohormonal growth regulators. Hence, development of a nanoparticle based reusable catalyst that exhibit a wide range of substrate tolerance for the direct oxidation of *α*-hydroxy esters and *α*-hydroxy phosphonates to their keto counterparts is crucial from both synthetic and green chemistry point of view. It has been well established that bimetallic NPs offer greater reaction specific catalyst tunability and superior performance compared to their monometallic counterparts owing to the synergistic effect between two different metals. The selectivity in oxidation of substrates having esters and phosphonate groups were controlled by tuning the Au:Pd ratio (1:1) in a bimetallic nanoparticle catalyst under a base-free and solventless condition.

Chapter 5: In this chapter, we have shown a new methodology for the synthesis of α-ketoamides from phenylglyoxal and aromatic amines using heterogeneous Au-Pd alloy nanoparticle as catalyst in presence of molecular oxygen as oxidant. The monometallic Au or Pd nanoparticles stabilized by poly(*N*-vinyl-2-pyrrolidone (PVP) yielded very less coupling product, however the alloy AuPd nanoparticles afforded high yield of the coupling product in DMSO at 60 °C. The substrate scope was evaluated by varying the amines and phenylglyoxals. AuPd alloy nanoparticles showed high yield for the coupling products under our reaction conditions.

Chapter 6: In this chapter, we report the cross-dehydrogenative coupling of 1,2,3,4-tetrahydroisoquinoline with nitromethane catalyzed by shape controlled urchin like AuPd bimetallic nanoparticle without any external oxidant. It has now been established that shape controlled nanoparticles with well-defined facets can be used as heterogeneous catalysts with enhanced activity and selectivity. It was observed that monometallic Au or Pd nanoparticles were unable to catalyze the cross-dehydrogenative coupling reaction even at elevated temperature. When spherical AuPd nanoparticles were used for the reaction in DMSO using triethyl amine at 60 °C, 30 % of the coupling product was obtained. On the other hand, in presence of the urchin shaped AuPd nanoparticles, we obtained 88 % yield of the coupling product under the similar reaction conditions. A detailed mechanistic study revealed that the Br$^-$ ions bound on the nanoparticle surface played a pivotal role in enhancing the catalytic activity and reactivity.

1.8 References

1. (a) Dahl J. a., Maddux B. L. S., & Hutchison J. E. (2007), Toward greener nanosynthesis. *Chem. Rev.*, 107, 2228–2269 (DOI:10.1021/cr050943k); (b) Albrecht M. A., Evans C. W., & Raston C. L. (2006), Green chemistry and the health implications of nanoparticles, *Green Chem.*, 8, 417–432 (DOI:10.1039/B517131H).

2. Zhou Z.-Y., Tian N., Li J.-T., Broadwell I., & Sun S.-G. (2011), Nanomaterials of high surface energy with exceptional properties in catalysis and energy storage, *Chem. Soc. Rev.*, 40, 4167–4185 (DOI:10.1039/c0cs00176g).

3. (a) Gorin D. J., & Toste F. D. (2007), Relativistic effects in homogeneous gold catalysis, *Nature*, 446, 395–403 (DOI.org/10.1038/nature05592); (b) Li Z., Brouwer C., & He, C. (2008), Gold-catalyzed organic transformations, *Chem. Rev.*, 108, 3239–3265 (DOI:10.1021/cr068434l).

4. Heveling J. (2012), Heterogeneous catalytic chemistry by example of industrial applications, *J. Chem. Educ*, *89*, 1530–1536 (DOI:10.1021/ed200816g).

5. (a) Johnstone R. A. W., Wilby A. H., & Entwistle, I. D. (1985), Heterogeneous catalytic transfer hydrogenation and its relation to other methods for reduction of organic compounds, *Chem. Rev.*, 85, 129–170 (DOI:10.1021/cr00066a00); (b) Stracke J. J., & Finke R. G. (2014), Distinguishing Homogeneous from Heterogeneous Water Oxidation Catalysis when Beginning with Polyoxometalates, *ACS Catalysis*, 4, 909–933 (DOI:10.1021/cs4011716);

6. (a) Pagliaro M., Pandarus V., Ciriminna R., Béland F., & Demma Carà P. (2012), Heterogeneous versus Homogeneous Palladium Catalysts for Cross-Coupling Reactions, *ChemCatChem*, 4, 432–445 (DOI:10.1002/cctc.201100422); (b) Glasnov T. N., Findenig S., & Kappe C. O. (2009), Heterogeneous Versus Homogeneous Palladium Catalysts for Ligandless Mizoroki–Heck Reactions: A Comparison of Batch/Microwave and Continuous-Flow Processing, *Chem. Eur. J.*, 15, 1001–1010 (DOI:10.1002/chem.200802200).

7. Su D. S., Perathoner S., & Centi G. (2013), Nanocarbons for the development of advanced catalysts, *Chem. Rev.*, 113, 5782–5816 (DOI:10.1021/cr300367d).

8. (a) Scheuermann G. M., Rumi L., Steurer P., Bannwarth W., Mu R., & Albert-ludwigs-uni V. (2009), Palladium Nanoparticles on Graphite Oxide and Its Functionalized Graphene Derivatives as Highly Active Catalysts for the Suzuki - Miyaura Coupling Reaction, *J. Am. Chem. Soc.*, 131, 8262–8270; (b) Zhou X., Huang X., Qi X., Wu S., Xue C., Boey F. Y. C., Zhang, H. (2009), In Situ Synthesis of Metal Nanoparticles on Single-Layer Graphene Oxide and Reduced Graphene Oxide Surfaces, *J. Phys. Chem. C*, 113, 10842–10846; (c) Stankovich S., Dikin D. a, Dommett G. H. B., Kohlhaas K. M., Zimney E. J., Stach E. A, Ruoff R. S. (2006), Graphene-based composite materials, *Nature*, 442, 282–286 (DOI:10.1038/nature04969).

9. Gao F., Zhao G., Yang S., & Spivey J. J. (2012), Nitrogen-doped Fullerene as a Potential Catalyst for Hydrogen Fuel Cells Nitrogen-doped Fullerene as a Potential Catalyst for Hydrogen Fuel Cells, *J. Am. Chem. Soc.*, 135, 3315−3318.

10. (a) Sun Y., Wu Q., & Shi G. (2011), Graphene based new energy materials, *Energy. Environ. Sci.,* 4, 1113 (DOI:10.1039/c0ee00683a); (b) Zhao G., Wen T., Chen C., & Wang X. (2012), Synthesis of graphene-based nanomaterials and their application in energy-related and environmental-related areas, *RSC Advances*, 2, 9286 (DOI:10.1039/c2ra20990j); (c) Sun M., Liu H., Liu Y., Qu J., & Li J. (2015), Graphene-based transition metal oxide nanocomposites for the oxygen reduction reaction, *Nanoscale*, 7, 1250–1269 (DOI:10.1039/C4NR05838K).

11. (a) Fan X., Zhang G., & Zhang F. (2015), Multiple roles of graphene in heterogeneous catalysis, *Chem. Soc. Rev.*, 44, 3023–3035 (DOI:10.1039/C5CS00094G); (b) Rajesh R., Sujanthi, E., Senthil Kumar, S., & Venkatesan, R. (2015), Designing versatile heterogeneous catalysts based on Ag and Au nanoparticles decorated on chitosan functionalized graphene oxide, *Phys. Chem. Chem. Phys.*, 17, 11329–11340 (DOI:10.1039/C5CP00682A); (c) Lim E. J., Kim Y., Choi S. M., Lee S., Noh Y., & Kim W. B. (2015), Binary Pd-M catalysts (M = Ru, Sn, or Ir) over a reduced graphene oxide support for electro-oxidation of primary alcohols (methanol, ethanol, 1-propanol) under alkaline conditions, *J. Mater. Chem. A.*, 3, 5491–5500 (DOI:10.1039/C4TA06893A).

12. (a) Chang H., & Wu H. (2013), Graphene-based nanocomposites: preparation, functionalization, and energy and environmental applications, *Energy. Environ. Sci.*, 6, 3483 (DOI:10.1039/c3ee42518e); (b) Machado B. F., & Serp P. (2012), Graphene-based materials for catalysis, *Catal. Sci. Technol.,* 2, 54 (DOI:10.1039/c1cy00361e); (c) Navalon S., Dhakshinamoorthy A., Alvaro M., & Garcia H. (2014), Carbocatalysis by Graphene-Based Materials, *Chem. Rev.,* 114, 6179−6212 (DOI.org/10.1021/cr4007347).

13. Scheuermann G. M., Rumi L., Steurer P., Bannwarth W., Mu R., & Albert-ludwigs-uni V. (2009), Palladium Nanoparticles on Graphite Oxide and Its Functionalized Graphene Derivatives as Highly Active Catalysts for the Suzuki - Miyaura Coupling Reaction, *J. Am. Chem. Soc.,* 131, 8262–8270.

14. Xue T., Jiang S., Qu Y., Su, Q., Cheng R., Dubin S., Duan X. (2012), Graphene-supported hemin as a highly active biomimetic oxidation catalyst, *Angew. Chem. Inter. Ed.*, 51, 3822–3825 (DOI:10.1002/anie.201108400).

15. Shi J. (2013), On the Synergetic Catalytic Effect in Heterogeneous Nanocomposite catalysis, *Chem. Rev.*, 113, 2139−2181.

16. (a) Zhang Y., Cui X., Shi F., & Deng Y. (2012), Nano-gold catalysis in fine chemical synthesis, *Chem. Rev.*, 112, 2467–2505 (DOI:10.1021/cr200260m); (b) Hervés P., Pérez-Lorenzo M., Liz-Marzán L. M., Dzubiella J., Lu Y., & Ballauff M. (2012), Catalysis by metallic nanoparticles in aqueous solution: model reactions, *Chem. Soc. Rev.*, 41, 5577 (DOI:10.1039/c2cs35029g).

17. Fihri A., Bouhrara M., Nekoueishahraki B., Basset J.-M., & Polshettiwar V. (2011), Nanocatalysts for Suzuki cross-coupling reactions, *Chem. Soc. Rev.*, 40, 5181 (DOI:10.1039/c1cs15079k).

18. (a) Sonström P., & Bäumer M. (2011), Supported colloidal nanoparticles in heterogeneous gas phase catalysis: on the way to tailored catalysts, *Phys. Chem. Chem. Phys.*, 13, 19270 (DOI:10.1039/c1cp22048a); (b) Requejo-Isidro J., del Coso R., Solis J., Gonzalo J., & Afonso C. N. (2005), Role of surface-to-volume ratio of metal nanoparticles in optical properties of $Cu : Al_2O_3$ nanocomposite films, *Appl. Phys. Lett.*, 86, 193104 (DOI:10.1063/1.1923198)

19. (a) Astruc D., Lu F., & Aranzaes J. R. (2005), Nanoparticles as Recyclable Catalysts: The Frontier between Homogeneous and Heterogeneous Catalysis, *Angew. Chem. Int. Ed.*, 44, 7852–7872 (DOI:10.1002/anie.200500766); (b) Moreno-man M., Pleixats R., & Universitat C. (2003), Formation of Carbon - Carbon Bonds under Catalysis by Transition-Metal Nanoparticles, 36, 638–643 (DOI; 10.1021/ar020267y); (c) Yin L. (2007), Carbon − Carbon Coupling Reactions Catalyzed by Heterogeneous Palladium Catalysts, *Chem. Rev.*, 107, 133-173 (DOI: 10.1021/cr0505674); (d) Wang D., & Astruc D. (2014), Fast-growing field of magnetically recyclable nanocatalysts, *Chem. Rev.*, 114, 6949–85 (DOI:10.1021/cr500134h).

20. (a) Lykakis I. N., Psyllaki A., & Stratakis M. (2011), Oxidative cycloaddition of 1,1,3,3-Tetramethyldisiloxane to alkynes catalyzed by supported gold nanoparticles, *J. Am. Chem. Soc.*, 133, 10426–10429 (DOI:10.1021/ja2045502); (b) Likhar P. R., Roy M., Roy S., Subhas M. S., Kantam M. L., & Sreedhar B. (2008), Highly efficient and reusable polyaniline-supported palladium catalysts for open-air oxidative heck reactions under base-and ligand-free conditions, *Adv. Synth. Catal.*, 350, 1968–1974 (DOI:10.1002/adsc.200800329); (c) Mohapatra S., Kumar R. K., & Maji T. K. (2011), Green synthesis of catalytic and ferromagnetic gold nanoparticles. *Chem. Phys. Letts*, 508, 76–79 (DOI:10.1016/j.cplett.2011.04.006); (d) Wang L., Liu Y., Chen M., Cao Y., He H., & Fan K. (2008), MnO$_2$ Nanorod Supported Gold Nanoparticles with Enhanced Activity for Solvent-free Aerobic Alcohol Oxidation, *J. Phys. Chem. C.,* 112, 6981–6987; (e) Corma A., & Garcia H. (2008), Supported gold nanoparticles as catalysts for organic reactions, *Chem. Soc. Rev.*, 37, 2096–2126 (DOI:10.1039/b707314n).

21. Haruta M., Yamada N., Kobayahsi T., & Lijima S. (1989), Gold catalysts prepared by coprecipitation for low-temperature oxidation of hydrogen and of carbon monoxide, *Journal of Catalysis*, 115, 301–309 (DOI:10.1016/0021-9517(89)90034-1).

22. Mallat T., & Baiker A. (2012), Potential of Gold Nanoparticles for Oxidation in Fine Chemical Synthesis, *Annual Review of Chemical and Biomolecular Engineering*, 3, 11–28 (DOI:10.1146/annurev-chembioeng-062011-081046).

23. Mitsudome T., & Kaneda K. (2013), Gold nanoparticle catalysts for selective hydrogenations, *Green Chem.*, 15, 2636–2654 (DOI:10.1039/c3gc41360h).

24. Tsunoyama H., Sakurai H., Ichikuni N., Negishi Y., & Tsukuda T. (2004), Colloidal Gold Nanoparticles as Catalyst for Carbon−Carbon Bond Formation: Application to Aerobic Homocoupling of Phenylboronic Acid in Water, *Langmuir*, 20, 11293–11296 (DOI:10.1021/la0478189).

25. Zhang X., & Corma A. (2008), Supported gold(III) catalysts for highly efficient three-component coupling reactions, *Angew. Chem. Int. Ed.*, 47, 4358–4361 (DOI:10.1002/anie.200800098).

26. Santos L. L., Serna P., & Corma A. (2009), Chemoselective synthesis of substituted imines, secondary amines, and β-amino carbonyl compounds from nitroaromatics through cascade reactions on gold catalysts, *Chem. Eur. J.*, 15, 8196–8203 (DOI:10.1002/chem.200900884).

27. Yamane Y., Liu X., Hamasaki A., Ishida T., Haruta M., Yokoyama T., & Tokunaga M. (2009), One-Pot synthesis of indoles and aniline derivatives from nitroarenes under hydrogenation condition with supported gold nanoparticles. *Org. Lett.*, 11, 5162–5165 (DOI:10.1021/ol902061j).

28. Su F.-Z., He L., Ni J., Cao Y., He H.-Y., & Fan K.-N. (2008), Efficient and chemoselective reduction of carbonyl compounds with supported gold catalysts under transfer hydrogenation conditions, *Chem. Commun.*, (30), 3531–3533 (DOI:10.1039/b807608a).

29. Han J., Liu Y., & Guo R. (2009), Facile Synthesis of Highly Stable Gold Nanoparticles and Their Unexpected Excellent Catalytic Activity for Suzuki−Miyaura Cross-Coupling Reaction in Water *J. Am. Chem. Soc.*, 131, 2060–2061 (DOI:10.1021/ja808935n).

30. González-Arellano C., Abad A., Corma A., García H., Iglesias M., & Sánchez F. (2007), Catalysis by gold(I) and gold(III): A parallelism between homo- and heterogeneous catalysts for copper-free sonogashira cross-coupling reactions, *Angew. Chem. Inter. Ed.*, 46, 1536–1538 (DOI:10.1002/anie.200604746).

31. Lou X. B., He L., Qian Y., Liu Y. M., Cao Y., & Fan K. N. (2011), Highly Chemo- and Regioselective Transfer Reduction of Aromatic Nitro Compounds using Ammonium Formate Catalyzed by Supported Gold Nanoparticles, *Adv. Synth. Catal.*, 353, 281–286 (DOI:10.1002/adsc.201000621)

32. Sonström P., & Bäumer M. (2011), Supported colloidal nanoparticles in heterogeneous gas phase catalysis: on the way to tailored catalysts, *Phys. Chem. Chem. Phys.*, 13, 19270 (DOI:10.1039/c1cp22048a).

33. (a) Campelo J. M., Luna D., Luque R., Marinas J. M., & Romero A. A. (2009), Sustainable preparation of supported metal nanoparticles and their applications in catalysis, *ChemSusChem.*, 2, 18–45. DOI:10.1002/cssc.200800227; (b) Crooks R. M., Zhao M., Sun L. I., Chechik V., & Yeung L. K. (2001), Dendrimer-Encapsulated Metal Nanoparticles : Synthesis, Characterization and Applications to Catalysis, *Accounts of Chemical Research.*, 34, 181–190 (DOI: 10.1021/ar000110a); (c) Biondi I., Laurenczy G., & Dyson P. J. (2011), Synthesis of gold nanoparticle catalysts based on a new water-soluble ionic polymer, *Inorg. Chem.*, 50, 8038–8045 (DOI:10.1021/ic200334m); (d) Stratakis M., & Garcia H. (2012), Catalysis by Supported Gold Nanoparticles: Beyond Aerobic Oxidative Processes, *Chem. Rev.*, 112, 4469–4506 (DOI:10.1021/cr3000785); (e) Lang H., Maldonado S., Stevenson K. J., & Chandler B. D. (2004), Synthesis and characterization of dendrimer templated supported bimetallic Pt-Au nanoparticles, *J. Am. Chem. Soc.*, 126, 12949–12956 (DOI:10.1021/ja046542o).

34. (a) Fierro-Gonzalez J. C., & Gates B. C. (2008), Catalysis by gold dispersed on supports: the importance of cationic gold, *Chem. Soc. Rev.*, 37, 2127–2134 (DOI:10.1039/b707944n); (b) Keller M., Perrier A., Linhardt R., Travers L., Wittmann S., Caminade A.-M., Ouali, A. (2013), Dendrimers or Nanoparticles as Supports for the Design of Efficient and Recoverable Organocatalysts, *Advanced Synthesis & Catalysis*, 355, 1748–1754. (DOI:10.1002/adsc.201300120).

35. Haruta M. (1997), Size- and support-dependency in the catalysis of gold, *Catalysis Today*, 36, 153–166 (DOI:10.1016/S0920-5861(96)00208-8).

36. Barakat T., Rooke J. C., Tidahy H. L., Hosseini M., Cousin R., Lamonier J.-F., Siffert S. (2011), Noble-Metal-Based Catalysts Supported on Zeolites and Macro-Mesoporous Metal Oxide Supports for the Total Oxidation of Volatile Organic Compounds, *ChemSusChem*, 4, 1420–1430 (DOI:10.1002/cssc.201100282).

37. Lu G., Li S., Guo Z., Farha O. K., Hauser B. G., Qi X., Huo F. (2012), Imparting functionality to a metal–organic framework material by controlled nanoparticle encapsulation, *Nat. Chem.*, 4, 310–316 (DOI.org/10.1038/nchem.1272).

38. (a) Tsukuda T., Tsunoyama H., & Sakurai H. (2011), Aerobic oxidations catalyzed by colloidal nanogold, *Chem. Asian. J.*, 6, 736–748 (DOI:10.1002/asia.201000611); (b) Mohapatra S., Kumar R. K., & Maji T. K. (2011), Green synthesis of catalytic and ferromagnetic gold nanoparticles, *Chemical Physics Letters*, 508, 76–79 (DOI:10.1016/j.cplett.2011.04.006); (c) Tsunoyama H., Tsukuda T., & Sakurai H. (2007), Synthetic Application of PVP-stabilized Au Nanocluster Catalyst to Aerobic Oxidation of Alcohols in Aqueous Solution under Ambient Conditions, *Chemistry Letts.*, 212-213 (DOI:10.1246/cl.2007.212).

39. (a) Tian J., Jin J., Zheng F., & Zhao H. (2010), Self-assembly of gold nanoparticles and polystyrene: A highly versatile approach to the preparation of colloidal particles with polystyrene cores and gold nanoparticle coronae, *Langmuir.*, 26, 8762–8768 (DOI:10.1021/la904519j); (b) Zhang Q., Xie J., Yu Y., & Lee J. Y. (2010), Monodispersity control in the synthesis of monometallic and bimetallic quasi-spherical gold and silver nanoparticles, *Nanoscale.*, 2, 1962–1975 (DOI:10.1039/c0nr00155d); (c) Shin J., Zhang X., & Liu J. (2012), DNA-Functionalized Gold Nanoparticles in Macromolecularly Crowded Polymer Solutions DNA-Functionalized Gold Nanoparticles in Macromolecularly Crowded Polymer Solutions. *J. Phys. Chem. B.,* 116, 13396-13402.

40 (a) Mandal T., Dasgupta C., & Maiti P. K. (2013), Engineering gold nanoparticle interaction by PAMAM dendrimer, *J. Phys. Chem. C*, 117, 13627–13636 (DOI:10.1021/jp401218t); (b) Lang N. J., Liu B., & Liu J. (2014), Characterization of glucose oxidation by gold nanoparticles using nanoceria, *Journal of Colloid and Interface Science*, 428, 78–83 (DOI:10.1016/j.jcis.2014.04.025); (c) Bai J., Li Y., Du J., Wang S., Zheng J., Yang Q., & Chen X. (2007), One-pot synthesis of polyacrylamide-gold nanocomposite, *Materials Chemistry and Physics*, 106, 412–415

(DOI:10.1016/j.matchemphys.2007.06.021); (d) Sharma B., Mandani S., & Sarma T. K. (2014), Enzymes as bionanoreactors: glucose oxidase for the synthesis of catalytic Au nanoparticles and Au nanoparticle–polyaniline nanocomposites, *J. Mater. Chem. B.*, 2, 4072 (DOI:10.1039/c4tb00218k).

41. (a) Singh A. K., & Xu Q. (2013), Synergistic Catalysis over Bimetallic Alloy Nanoparticles, *ChemCatChem.*, 5, 652–676 (DOI:10.1002/cctc.201200591). (b) Menezes W. G., Neumann B., Zielasek V., Thiel K., & Bäumer M. (2013), Bimetallic AuAg Nanoparticles: Enhancing the Catalytic Activity of Au for Reduction Reactions in the Liquid Phase by Addition of Ag, *ChemPhysChem.*, 14, 1577–1581 (DOI:10.1002/cphc.201201100). (c) Sankar M., Dimitratos N., Miedziak P. J., Wells P. P., Kiely C. J., & Hutchings, G. J. (2012), Designing bimetallic catalysts for a green and sustainable future, *Chem. Soc. Rev.*, 41, 8099–8139 (DOI:10.1039/C2CS35296F). (d) Zhang B., & Yan N. (2013), Towards Rational Design of Nanoparticle Catalysis in Ionic Liquids, *Catalysts*, 3, 543–562 (DOI:10.3390/catal3020543).

42. (a) Tao, F. (Feng), Zhang, S., Nguyen, L., & Zhang, X. (2012), Action of bimetallic nanocatalysts under reaction conditions and during catalysis: evolution of chemistry from high vacuum conditions to reaction conditions, *Chem. Rev.*, *41*, 7980-7993 (DOI:10.1039/c2cs35185d); (b) Tao, F. (2012), Synthesis, catalysis, surface chemistry and structure of bimetallic nanocatalysts, *Chem. Rev.*, *41*, 7977–7979 (DOI:10.1039/c2cs90093a);

43. (a) Ward, T., Delannoy, L., Hahn, R., Kendell, S., Pursell, C. J., Louis, C., & Chandler, B. D. (2013). Effects of Pd on catalysis by Au: CO adsorption, CO oxidation, and cyclohexene hydrogenation by supported Au and Pd-Au catalysts, *ACS Catalysis*, *3*, 2644–2653 (DOI:10.1021/cs400569v); (b) Ferrando, R., Jellinek, J., & Johnston, R. L. (2008), Nanoalloys: From Theory to Applications of Alloy Clusters and Nanoparticles, *Chem. Rev*, 108, 846–904 (DOI:10.1021/cr040090g); (c) Okum, H. Z. K. K. M. (2014), Colloidal Au single-atom catalysts embedded on Pd nanoclusters, *, J. Mater. Chem. A.,* 2, 13498–13508 (DOI:10.1039/c4ta01696c); (d) Tao F. (Feng) Zhang, S., Nguyen L., & Zhang X. (2012), Action of bimetallic nanocatalysts under

reaction conditions and during catalysis: evolution of chemistry from high vacuum conditions to reaction conditions, *Chem. Soc. Rev.,* 41 (DOI:10.1039/c2cs35185d).

44. (a) Sankar M., Dimitratos N., Miedziak P. J., Wells P. P., Kiely C. J., & Hutchings G. J. (2012), Designing bimetallic catalysts for a green and sustainable future, *Chem. Rev.,* 41, 8099–8139 (DOI:10.1039/c2cs35296f); (b) Ward, T., Delannoy, L., Hahn, R., Kendell, S., Pursell, C. J., Louis, C., & Chandler, B. D. (2013), Effects of Pd on catalysis by Au: CO adsorption, CO oxidation, and cyclohexene hydrogenation by supported Au and Pd-Au catalysts, *ACS Catalysis,* 3, 2644–2653 (DOI:10.1021/cs400569v).

45. (a) Han P., Axnanda S., Lyubinetsky I., & Goodman D. W. (2007), Atomic-Scale Assembly of a Heterogeneous Catalytic Site, *J. Am. Chem. Soc.*, 129, 14355–14361 (DOI:10.1021/ja074891n); (b) Villa A., Wang D., Su D. S., & Prati L. (2015), New challenges in gold catalysis: bimetallic systems, *Catal. Sci. Technol.*, 5, 55–68 (DOI:10.1039/C4CY00976B); (c) Chandler B. D., Schabel A. B., & Pignolet L. H. (2001), Ensemble size effects on toluene hydrogenation and hydrogen chemisorption by supported bimetallic particle catalysts, *J. Phys. Chem. B.*, 105, 149–155 (DOI:10.1021/jp002222p); (d) Gao F., & Goodman D. W. (2012), Pd–Au bimetallic catalysts: understanding alloy effects from planar models and (supported) nanoparticles, *Chem. Soc. Rev.*, 8009–8020 (DOI:10.1039/c2cs35160a).

46. (a) Zafeiratos S., Piccinin S., & Teschner D. (2012), Alloys in catalysis: phase separation and surface segregation phenomena in response to the reactive environment, *Catal. Sci. Technol.,* 2, 1787–1801 (DOI:10.1039/C2CY00487A); (b) Liu P., & Nørskov J. K. (2001), Ligand and ensemble effects in adsorption on alloy surfaces, *Phys. Chem. Chem. Phys.*, 3, 3814–3818 (DOI:10.1039/b103525h).

47. (a) Singh A. K., & Xu Q. (2013), Synergistic Catalysis over Bimetallic Alloy Nanoparticles, *ChemCatChem.*, 5, 652–676 (DOI:10.1002/cctc.201200591); (b) Menezes W. G., Neumann B., Zielasek V., Thiel K., & Bäumer M. (2013), Bimetallic AuAg Nanoparticles: Enhancing

the Catalytic Activity of Au for Reduction Reactions in the Liquid Phase by Addition of Ag, *ChemPhysChem.*, 14, 1577–1581 (DOI:10.1002/cphc.201201100); (c) Sankar M., Dimitratos N., Miedziak P. J., Wells P. P., Kiely C. J., & Hutchings, G. J. (2012), Designing bimetallic catalysts for a green and sustainable future, *Chem. Soc. Rev.*, 41, 8099–8139 (DOI:10.1039/C2CS35296F); (d) Zhang B., & Yan N. (2013), Towards Rational Design of Nanoparticle Catalysis in Ionic Liquids, *Catalysts*, 3, 543–562 (DOI:10.3390/catal3020543).

48. (a) Ward, T., Delannoy, L., Hahn, R., Kendell, S., Pursell, C. J., Louis, C., & Chandler, B. D. (2013), Effects of Pd on catalysis by Au: CO adsorption, CO oxidation, and cyclohexene hydrogenation by supported Au and Pd-Au catalysts, *ACS Catal.*, 3, 2644–2653 (DOI:10.1021/cs400569v); (b) Ferrando, R., Jellinek, J., & Johnston, R. L. (2008), Nanoalloys: From Theory to Applications of Alloy Clusters and Nanoparticles, *Chem. Rev*, 108, 846–904 (DOI:10.1021/cr040090g); (c) Okum, H. Z. K. K. M. (2014), Colloidal Au single-atom catalysts embedded on Pd nanoclusters, *J. Mater. Chem. A.,* 2, 13498–13508 (DOI:10.1039/c4ta01696c); (d) Tao F. (Feng) Zhang, S., Nguyen L., & Zhang X. (2012), Action of bimetallic nanocatalysts under reaction conditions and during catalysis: evolution of chemistry from high vacuum conditions to reaction conditions, *Chem. Soc. Rev.,* 41, 7980-7993 (DOI:10.1039/c2cs35185d).

49. Ferrando R., Jellinek J., & Johnston R. L. (2008), Nanoalloys: From Theory to Applications of Alloy Clusters and Nanoparticles, *Chem. Rev.*, 108, 845–910 (DOI:10.1021/cr040090g).

50. Sankar M., Dimitratos N., Miedziak P. J., Wells P. P., Kiely C. J., & Hutchings G. J. (2012), Designing bimetallic catalysts for a green and sustainable future, *Chem. Soc. Rev.*, 8099–8139 (DOI:10.1039/c2cs35296f).

51. (a) Zhou K., & Li Y. (2012), Catalysis based on nanocrystals with well-defined facets, *Angew. Chem. Int. Ed.*, 51, 602–613 (DOI:10.1002/anie.201102619); (b) Tsung C. (2009), Sub-10 nm Platinum Nanocrystals with Size and Shape Control : Catalytic Study for Ethylene and Pyrrole Hydrogenation Sub-10 nm Platinum Nanocrystals with Size and Shape

Control : Catalytic Study for Ethylene and Pyrrole Hydrogen, *J. Am. Chem. Soc.*,18, 5816–5822; (c) Wang F., Li C., Sun L. D., Wu H., Ming T., Wang J., Yan, C. H. (2011), Heteroepitaxial growth of high-index-faceted palladium nanoshells and their catalytic performance, *J. Am. Chem. Soc.*, 133, 1106–1111 (DOI:10.1021/ja1095733); (d) Xia Y., Xiong Y., Lim B., & Skrabalak S. E. (2009), Shape-Controlled Synthesis of Metal Nanocrystals : Simple Chemistry Meets Complex Physics *Angew. Chem. Int. Ed.,* 60–103 (DOI:10.1002/anie.200802248); (e) Wang J., Gong J., Xiong Y., Yang J., Gao Y., Liu Y., Tang Z. (2011), Shape-dependent electrocatalytic activity of monodispersed gold nanocrystals toward glucose oxidation. *Chem. Commun.*, 47, 6894–6896 (DOI:10.1039/c1cc11784j); (f) Grzelczak M., Pérez-Juste J., Mulvaney P., & Liz-Marzán L. M. (2008), Shape control in gold nanoparticle synthesis, *Chem. Soc. Rev.*, 37, 1783–1791 (DOI:10.1039/b711490g).

52. Gu J., Zhang Y.-W., & Tao F. (2012), Shape control of bimetallic nanocatalysts through well-designed colloidal chemistry approaches, *Chem. Soc. Rev.*, 8050–8065 (DOI:10.1039/c2cs35184f).

Chapter 2

Ultrasound mediated synthesis of α-aminophosphonates and 3, 4-dihydropyrimidin-2-ones using graphene oxide as a recyclable catalyst under solvent-free conditions

2.1 Introduction

With the advent of materials in the nanometer dimensions, there has been a tremendous effort towards the development of eco-friendly, more efficient and atom economic nanomaterial based heterogeneous catalytic systems for organic reactions. Nanomaterials offer manifold increase in the surface area to volume ratio that leads to enhancement of catalytic activity much higher compared to their bulk counterparts. With the focus on the development of green chemistry pathway for industrial applications, carbonaceous materials have taken center-stage in catalysis research because of their negligible toxicity, availability from natural resources and possibility of surface functionalization as desired. Carbonaceous materials, including mesoporous carbon, fullerenes and carbon nanotubes, in their pristine or doped states have been used as both supports and metal free catalysts for facilitating synthetic transformations.[1] After the report by Geim and co-workers,[2] graphene and related two dimensional sp^2 -hybridized materials have invoked incredible research interest owing to their inherent optical, electrochemical and mechanical properties.[3] The development of the wet chemical methods for chemically modifed graphene in substantial quantities has sparked great excitement, enabling the facile fabrication of carbon based functional materials.[4] Graphene oxide (GO), which is oxygenated graphene sheets covered with hydroxyl, epoxy and carboxyl groups (Figure 2.1), offers tremendous opportunities for functionalization, and it can be processed into a wide variety of novel materials. In the field of catalysis, GOs have been focused on primarily as supports for catalytically active metals. Taking advantage of the large nucleation or stabilization sites present on the GO surface, catalytically active nanoparticle–GO composite materials have been synthesized and demonstrated as versatile and recyclable heterogeneous catalysts in several important organic transformations.[5] Similarly, the activity of proteins and enzymes increased several fold while immobilized on graphene oxides.[6] On the other hand, with the help of the aromatic scaffold decorated with oxygenated functional groups, the inherent chemical properties of GO have been recently exploited as an effective carbocatalyst that might present a green alternative to metal catalysis. GO has been used as an oxidant

for the oxidation of sulphides, and other hydrocarbons.[7] Furthermore, the acidic nature of GO has been exploited for use as a solid acid for the hydration of various alkynes, Friedel–Crafts addition of indoles to *α,β*-unsaturated ketones, Aza-Michael addition of amines to activated alkenes, condensation and ring opening of epoxides under mild conditions.[8]
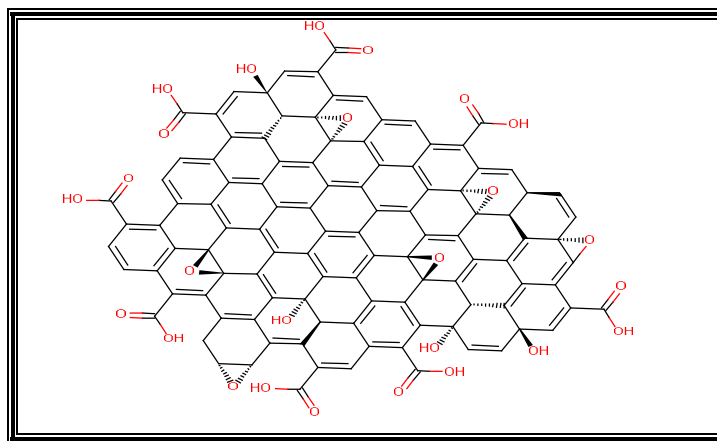
Figure 2.1 Schematic structure of a single layer graphene oxide.

Here, we report the exploitation of the acidic oxygenated groups on the GO sheets towards the applicability of GO as a potent catalyst for the three-component one-pot synthesis of *α*-aminophosphonates and 3,4-dihydropyrimidin-2-ones (DHPM),which are important classes of biologically active compounds. It is well known that multi-component reactions are more competent than multistep syntheses as they require minimal workup and desired products can be obtained in one pot, and often in quantitative yield.[9] Hence, there has been an intensified focus towards new heterogeneous catalysts for multicomponent reactions that would reinforce environmental benefits. The synthesis of *α*-aminophosphonates has gained considerable interest because of their structural analogy to α-amino acids and their action as peptide mimics, enzyme inhibitors, herbicides and pharmacological agents.[10] A number of methods have been developed using various Bronsted acids, Lewis acids, heteropolyacids and nanocatalysts to accomplish the synthesis of these compounds.[11] Similarly, intense synthetic investigations have been carried out on DHPM scaffolds due to their broad pharmacological profile as calcium channel modulator, antiviral, anti-inflammatory, antifungal and

antitumor agents.[12] The synthetic approach to DHPMs is based on ternary condensation of ethyl acetoacetate, aromatic aldehyde and urea under strong acidic conditions, which was first reported by Biginelli.[1]

R= OMe, Me, NO_2, Cl, Br
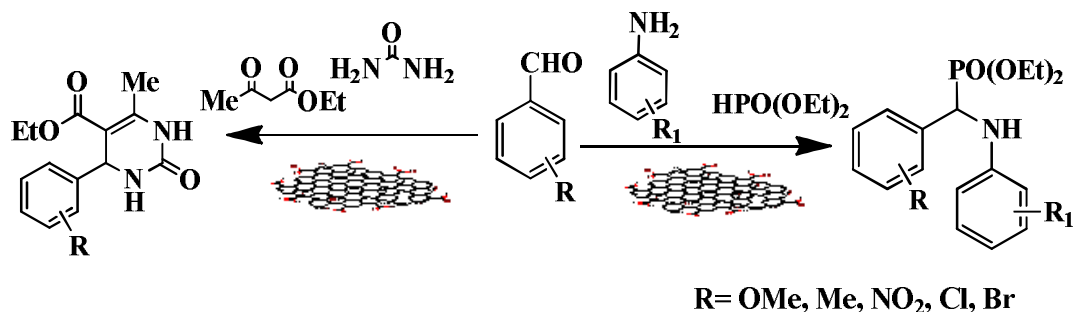
Figure 2.2 *Schematic representation of Syntheses of α-aminophosphonates and 3,4-dihydropyrimidin-2-ones using GO as a heterogeneous catalyst.*

Subsequently, a variety of procedures using homogeneous Lewis acids as well as protic acids or heterogeneous catalysts have been developed to accomplish this transformation.[14] However, in spite of their potential utility, many of these reported protocols suffer from various drawbacks such as the use of expensive and highly corrosive catalysts, tedious separation procedures and prolonged reaction times. Most of the existing methods use metal-based homogeneous catalysts, which are destroyed during the work-up procedure and their recovery and reusability is often impossible, limiting their use from the aspect of environmentally benign processes. Consequently, the design of a simple, efficient, metal-free and green catalyst would extend the scope of the synthesis of these important classes of biologically active molecules. The presence of bronsted acid sites over a large surface area of GO motivated us to test the activity of this non-toxic material as an acid catalyst for the three-component one-pot coupling reactions, leading to the formation of α-aminophosphonates and 3,4- dihydropyrimidin-2-ones (Figure 2.2). Further we used GO as a catalyst towards the synthesis of 3-substituted indoles through a multi-component coupling pathway. The use of metal-free catalysts such as GO follows the precepts of green chemistry, i.e. the reactions are carried out under solvent-free conditions and can be used in several cycles.

2.2 Results and discussion

2.2.1 Optimization for the synthesis of *α*-amino phosphonates with graphene oxide in different conditions

Table 2.1
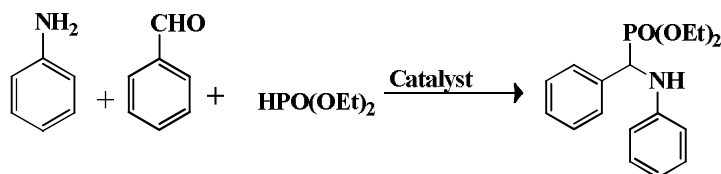
Entry	Catalyst (mg or mol%)	Reaction condition	Yield[b] (%)
1	None	[c]Water, 25°C, 3 h.	0
2	None	[c]No solvent, 25°C, 3 h.	0
3	GO (10)	[c]Water, 25°C, 4 h.	18
4	GO (10)	[c]1,4-dioxane, 25°C, 4 h.	0
5	GO (10)	[c]hexane, 25°C, 4 h.	1
6	GO (10)	[c]toluene, 25°C, 4 h.	1
7	GO (10)	[c]CH₃CN, 25°C, 4 h.	8
8	GO (10)	[c]THF, 25°C, 4 h.	12
9	GO (10)	[c]DMF, 25°C, 4 h.	8
10	GO (10)	[c]ethanol, 25°C, 4 h.	10
11	GO (10)	[c]methanol, 25°C, 4 h.	12
12	GO (10)	[c]water, 60°C, 4 h.	25
13	GO (10)	[c]water, 80°C, 4 h.	30
14	GO (10)	[c]No solvent, 25°C, 1 h.	79
15	GO (10)	[c]No solvent, 60°C, 1 h.	85
16	GO (10)	[c]No solvent, 80°C, 1 h.	92[e]
17	GO (2)	[c]No solvent, 25°C, 1 h.	41
18	GO (5)	[c]No solvent, 25°C, 1 h.	56
19	*p*TSA (10)	[c]No solvent, 25°C, 1 h.	58
20	AlCl₃ (10)	[c]No solvent, 25°C, 1 h.	29
21	CSA (10)	[c]No solvent, 25°C, 1 h.	77
22	GO (10)	[c]0.1 mL pyridine, 25°C, 1 h.	9
23	Amorphous carbon (10)	[c]No solvent, 25°C, 4 h.	13
24	Graphite (10)	[c]No solvent, 25°C, 1 h.	10
25	RGO (10)	[c]No solvent, 25°C, 1 h.	16
26	GO (2)	[d]No solvent, 25°C, 45 min.	82
27	GO (5)	[d]No solvent, 25°C, 15 min.	88
28	**GO (10)**	**[d]No solvent, 25°C, 5 min.**	**96**

[a]Unless otherwise specified, all the reactions were carried out with benzaldehyde (1.0 mmol), aniline (1.0 mmol) and diethylphosphite (2.0 mmol), [b]isolated yields, [c]under magnetic stirring, [d]under ultrasonic irradiation (50 Hz), [e]polyaniline formed as byproducts.

In order to test the efficacy of GO as a catalyst for the one pot multi-component reactions, we choose the model Kobachnik-Fields reaction between benzaldehyde (1.0 mmol), aniline (1.0 mmol) and diethylphosphite (2.0 mmol). The effect of reaction parameters, such as the influence of solvents, catalytic concentration, temperature and other reaction conditions, was evaluated to optimize the reaction conditions. It was noteworthy that, in the absence of GO, no significant product formation was observed under similar reaction conditions. In non-polar solvents such as 1,4-dioxane, n-hexane and toluene, the reaction did not take place in the presence of GO as a catalyst even after prolonged reaction time (entry 4–6, Table 2.1). Moreover, in the case of polar aprotic solvents, such as acetonitrile, THF and DMF, the yield of the reaction was found to be very low (entry 7– 9, Table 2.1). Furthermore, even in the case of polar protic solvents such as methanol and ethanol, the yield of the desired product was very low (Entry 10-11, Table 2.1). When we used water as the solvent for the reaction in presence of GO, the reaction did not progress well, we were able to isolate the coupling product with a moderate yield (18-30%) at various temperature (Entry 11-13, Table 2.1). Interestingly, there was a substantial enhancement in the yield when the coupling reaction was carried out under solvent free conditions with constant stirring. The desired coupling product (phenyl-phenylaminomethyl)-phosphonic acid diethyl ester was obtained in a 79% yield after reacting at room temperature for 4 hours (Entry 14, Table 2.1). The yield of the product increased to 92% when the reaction was carried out at elevated temperature (80 °C) (Entry 16, Table 2.1), however a small amount of green coloured byproduct was formed that could be attributed to the emeraldine form of polyaniline and was formed by the aerial oxidation under acidic condition. It is observed that the order of mixing the substrates did not influence the product yield. GO showed equivalent or superior catalytic behavior as an acid catalyst under solvent free conditions compared to other commonly used catalysts such as p-toluene sulfonic acid (pTSA), anhydrous AlCl₃ or camphor sulfonic acid (CSA), under similar reaction conditions (entry 19–21, Table 2.1). For comparison, we performed the synthesis in the presence of other carbon catalysts such as activated carbon, graphite and reduced graphene

oxide (RGO, GO reduced with hydrazine, entry 23–25, Table 2.1). The results suggested that the presence of acidic groups on the surface of GO played an essential role in the multi-component coupling reaction. To verify these results, the coupling reaction was performed in the presence of 0.1mL of pyridine, and the yield was only 9%, indicating the poisoning of the acid sites in GO (entry 22, Table 2.1).

Sonochemistry has been recognized to be an efficient technique in organic synthesis as ultrasound irradiation can accelerate chemical reactions to provide improved reaction yields, shortened reaction time and increased selectivity.[16] When we performed the model coupling reaction between benzaldehyde, aniline and diethylphosphite in an ultrasonicator bath (50 Hz) under solvent-free conditions using GO as a catalyst, the reaction yields improved to 96% in a significantly reduced reaction time (5 minutes, Table 2.1, entry 28). Hence, it was imperative for us to use ultrasonic irradiation for developing a synthetic methodology for the synthesis of α-aminophosphonates. It is worth mentioning here that the substrate to catalyst ratio played an important role in the rate of the coupling reaction. When the catalyst-substrate ratio was low (2 wt %), the reaction yield was 82% after 45 minutes under ultrasonic irradiation, whereas there was a drastic enhancement in the rate of the reaction when 10 mg (10 wt%) of the catalyst was used under similar reaction conditions (96% yield in 5 minutes, entry 26– 28, Table 2.1). From the various reaction conditions shown in Table 2.1, it is obvious that the superior result was obtained at conditions mentioned in entry 28 (96% yield).
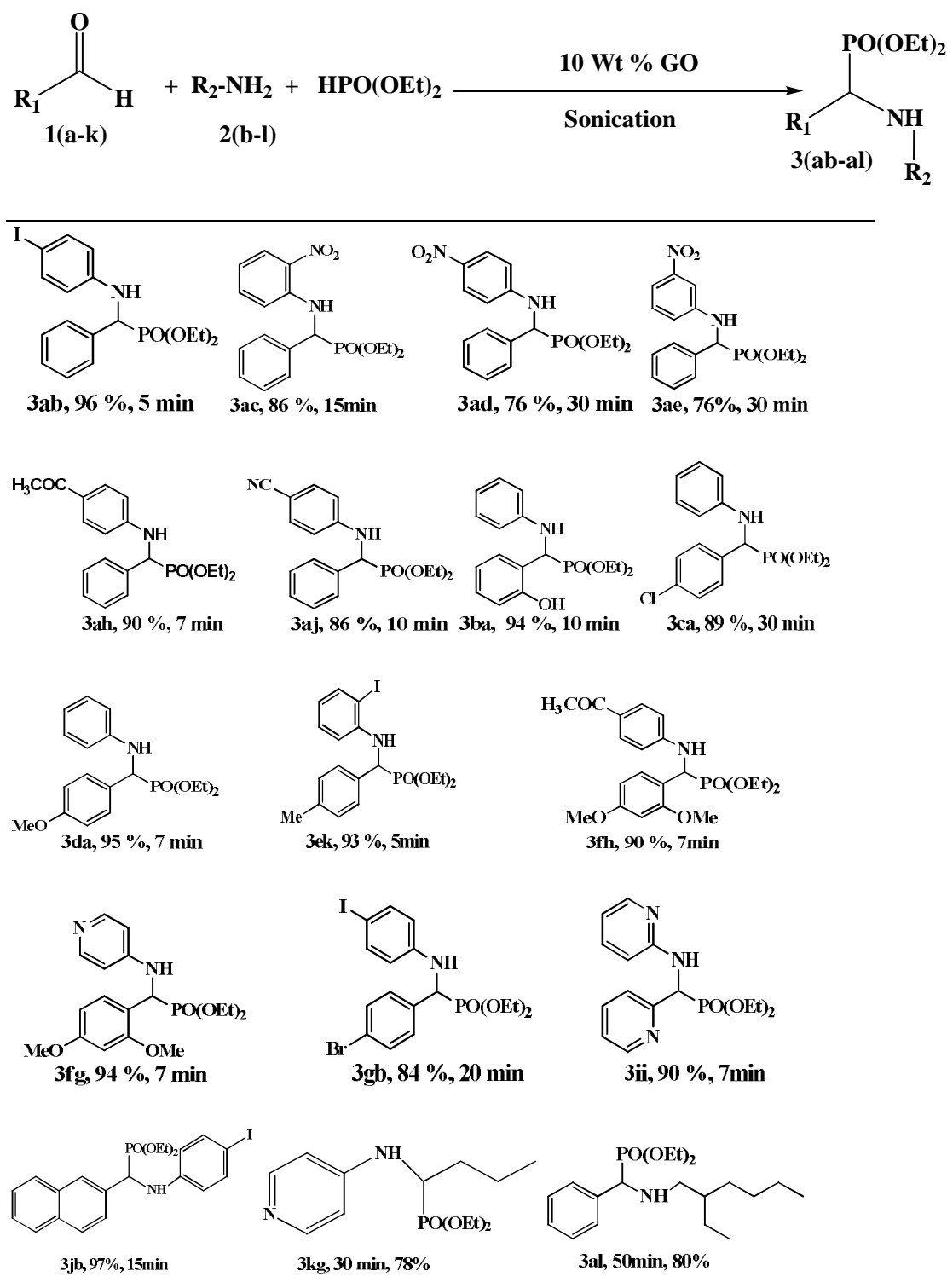
2.2.2 Screening with different amine and different aldehydes for the synthesis of   Aminophosphonates

Under optimal conditions, we examined the scope and generality of this multi-component coupling reaction using graphene oxide as a catalyst under standard reaction conditions, and the results are compiled in Table 2.2. It was observed that there was an insignificant electronic and position effects on the three-component coupling from aromatic amines, since anilines with p-, m- or o-substituents resulted in the corresponding α-aminophosphonates in excellent yield. The aromatic aldehydes having either electron-donating groups or even

electron-withdrawing groups gave excellent yield of products (Table 2.2, entry 1–21). However, the presence of electron-withdrawing groups as a substituent in the aryl moiety had considerable effect on the kinetics of the reaction, as we observed lesser yield with these substrates even a prolonged ultrasound irradiation.

Table 2.2 Synthesis of α-aminophosphonates (3aa-al)

3ab, 96 %, 5 min   3ac, 86 %, 15min   **3ad, 76 %, 30 min**   3ae, 76%, 30 min

3ah, 90 %, 7 min   **3aj, 86 %, 10 min** 3ba, 94 %, 10 min   **3ca, 89 %, 30 min**

3da, 95 %, 7 min   **3ek, 93 %, 5min**   3fh, 90 %, 7min

3fg, 94 %, 7 min   **3gb, 84 %, 20 min**   **3ii, 90 %, 7min**

3jb, 97%, 15min   3kg, 30 min, 78%   **3al, 50min, 80%**

Similar effects were observed when electron-withdrawing groups were present in the aniline moiety. The reaction was found to be compatible with various functional groups such as -Br, -Cl, -OMe, $-NO_2$, -OH and -CN, which do not interfere in the reaction by competitive complex formation with the catalyst or by nucleophile.

Encouraged by the electiveness of graphene oxide as a catalyst for multicomponent one-pot transformations such as the synthesis of α-aminophosphonates, we intended to study the versatility of the catalyst towards the rapid, automated and high throughput synthesis of biologically active 3,4-dihydropyrimidin-2-ones through a multicomponent reaction pathway. The one-pot cyclocondensation reaction of aromatic aldehydes, ethylacetoacetate and urea in the presence of GO in a solvent-free environment under ultrasonication gave the corresponding products. However, for better conversion, the reaction had to be carried out for prolonged time compared to that for synthesizing α-aminophosphonates. A wide range of aromatic aldehydes were investigated for their reaction with ethyl acetoacetate and urea in the presence of graphene oxide as a catalyst under the optimized reaction conditions, and the results are summarized in Table 2.3.

Table 2.3 Synthesis of active 3, 4-dihydropyrimidin-2-ones

5a, 95%, 2hr

5b, 92%, 2hr

5c, 90%, 2hr

5d, 87%, 2hr

5e, 88%, 4hr

5f, 76%, 4hr

5g, 88%, 3hr
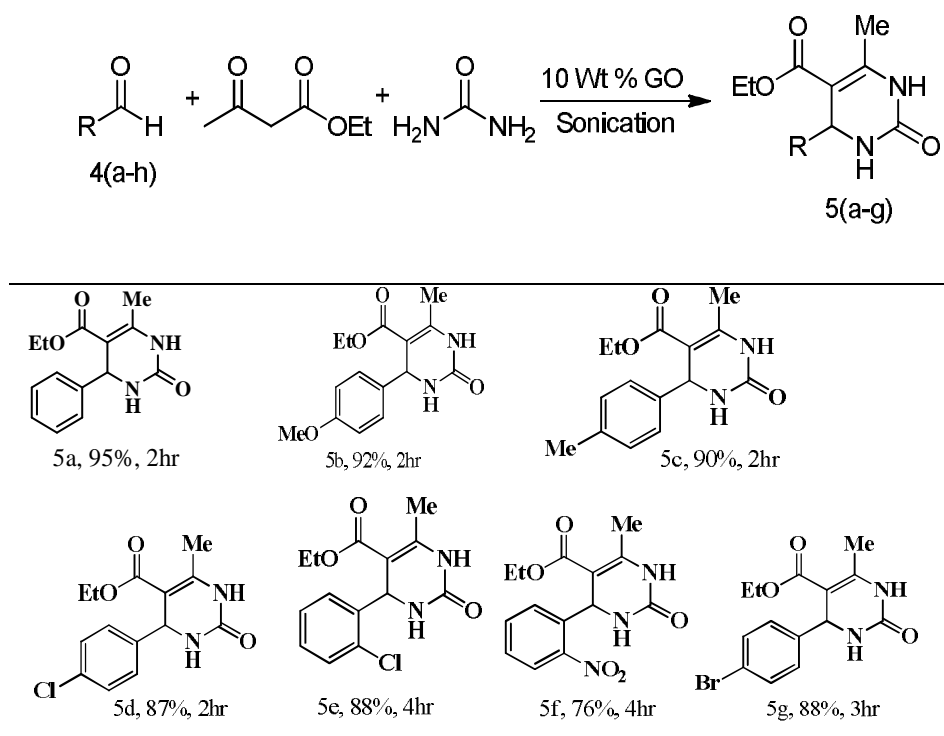
Aromatic aldehydes containing electron-releasing groups (Table 2.3-5b, 5c) in the para position afforded high yields of the products. Another important characteristic feature of this method is the tolerance and compatibility of various functional groups such as Cl and Br, to the reaction conditions, as we did not observe formation of any side product (Table 2.3, 5d, 5e, 5g). Notably, we have used low catalyst loading for this coupling reaction compared to the previous catalysis reactions using GO.[18] Therefore, with low catalyst loading, GO can be used as a model catalyst in a solvent-free and metal-free environment for practical application.

Table 2.4 Synthesis of 3-substituted indoles
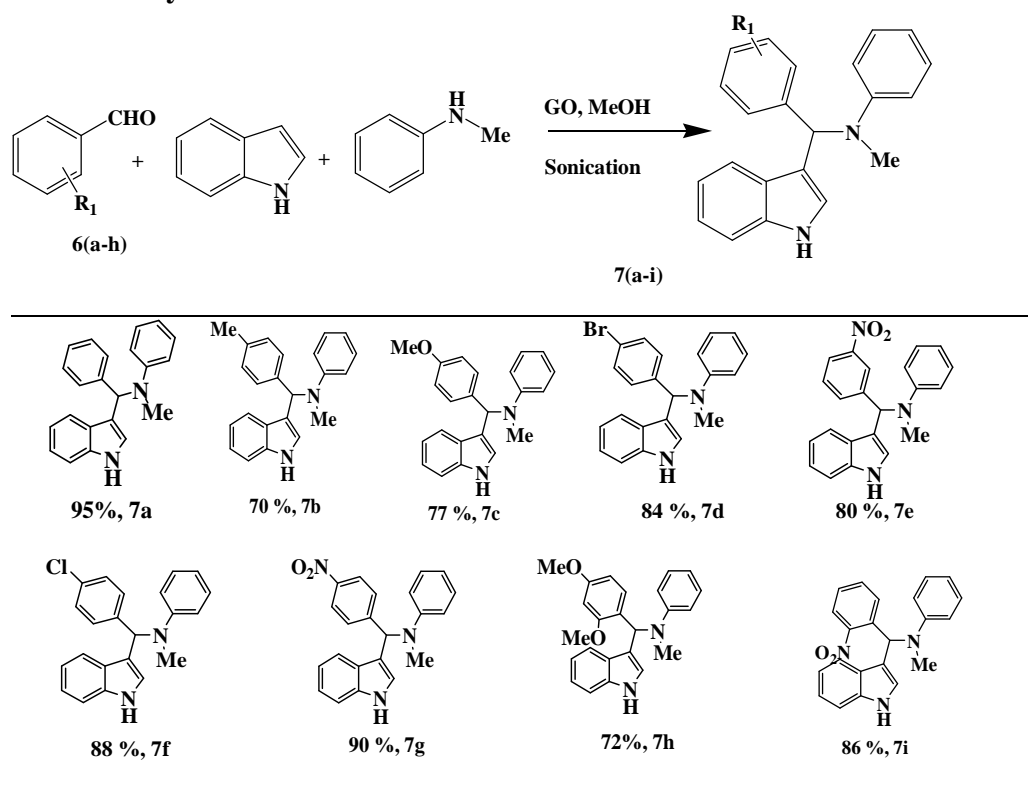
Further, we explored one-pot multicomponent condensation reaction of indole with aldehydes and N-methylaniline to synthesis a skeleton of 3-substituted indoles using graphene oxide as a catalyst under ultrasonic irradiation. In contrast to the earlier multicomponent reaction, higher yields for the formation of 3-substituted indoles were observed when the reactions were performed using MeOH as a solvent under ultrasonic irradiation. Several aromatic aldehydes with electron-donating and electron-withdrawing groups

were preceded to form the desired 3-substituted indole products. It was found that corresponding products formed in good yields after 2 hrs and which is summarized in this Table 2.4 The presence of electron withdrawing groups such as –NO_2, -Cl containing the aromatic aldehyde aromatic afforded better yield of corresponding products (7e, 7g, 7i, 7f in Table 2.4) compared to the presence of the electron donating groups such as -OMe, -Me as substituents (7b, 7c, 7h).

2.2.4 Recyclability of graphene oxide catalyst

Reusability without much loss of activity is a hallmark of a good heterogeneous catalyst. GO catalyst shows good recyclability and could be reused by simple filtration and rinsing with dilute HCl. For the model reaction between benzaldehyde (1.0 mmol), aniline (1.0 mmol) and diethylphosphite (2.0 mmol), the GO catalyst showed very good recyclable activity up to the seventh cycle tested figure 2.3. GO catalyst recovered even after the fifth cycle afforded 79% of the desired product, indicating that GO could be used as effective heterogeneous catalyst for these multi-component coupling reactions.
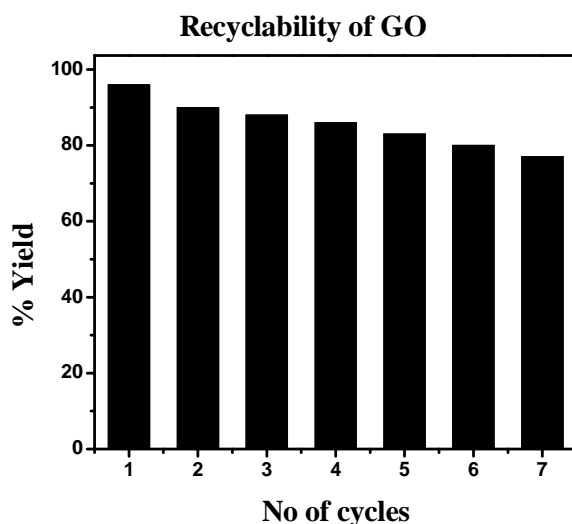
*Figure 2.3 Recyclability of graphene oxide catalysts.*

It is well known that primary amines such as aniline can function as a reducing agent, and it is imperative that the chemical nature of GO sheets is influenced during their participation as a catalyst. It was further confirmed by the fact that the catalytic activity of GO was reduced to some extent during the

subsequent cycle of coupling reaction. To study this, we compared the physicochemical properties of pristine GO and GO recovered after the 5th cycle of reaction.

2.3 Characterization of graphene oxide catalyst

2.3.1 UV-Vis study and Raman spectroscopic study

From the UV-visible studies shown in Figure 2.4 A, pristine GO exhibited two absorption peaks, a maximum at 230 nm corresponding to π -π* transitions of aromatic C–C bonds and a shoulder at 305 nm attributed to n -π* transitions of C-O bonds. In the case of GO recovered after 5th cycle of reaction, we observed shoulders at 222 nm, 256 nm and 309 nm, indicating that the electronic conjugation was slightly restored in the graphene sheet.[19]
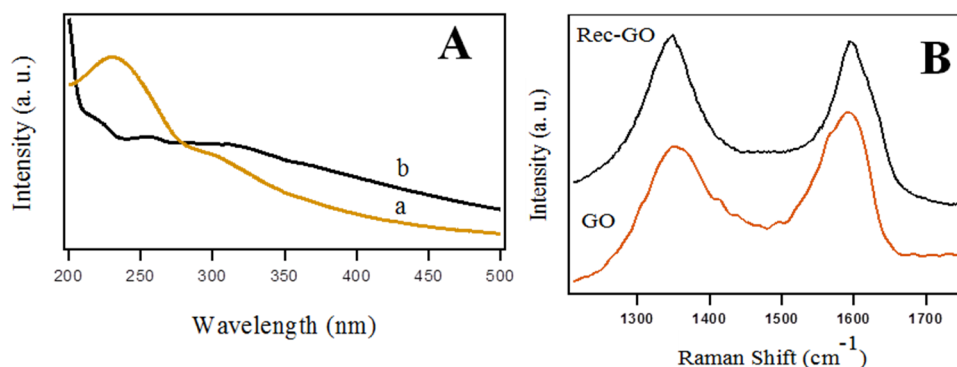

Figure 2.4 *A) UV Visible spectra of graphene oxide (a) and recovered graphene oxide (b) dispersed in EtOH with 0.03 gm/mL B) Raman spectra of graphene oxide and recovered graphene oxide.*

Furthermore, we performed Raman spectroscopy (Figure 2.4 B) in order to evaluate the crystal structure of carbon for pristine GO (red) and recovered GO (black). The D bands at 1350 cm^{-1} in both the samples in the Raman spectra confirmed the lattice distortions in the hexagonal graphitic layer. On the other hand, we did not observe any significant shift in the G peak (1592 cm^{-1}) in case of the recovered graphene oxide with respect to pristine graphene oxide. The G peak corresponds to the E_{2g} mode of graphite and is a signature to the sp^2 bonded carbon atoms in a two dimensional hexagonal lattice.[20] However, the I_D/I_G ratio of the recovered GO exhibited a significant increase as compared to pristine GO, demonstrating a partial reduction of GO after their participation as a catalyst in the multicomponent reaction.

**2.3.2 Thermal Gravimetric Analysis and X-Ray diffraction study**

Furthermore, the quality of the pristine GO and recovered GO after the 5th cycle of catalysis was examined by thermal gravimetric Study (TGA). As shown in Fig. 2.5A, pristine GO (red curve) showed major weight loss between 100 °C and 200 °C, indicating the release of oxygenated groups from the most labile functional groups during pyrolysis. At a temperature below 800 °C, the weight loss was observed to be about 69%. In the case of GO recovered after the 5th cycle (blue curve), we observed a similar pattern of weight loss. However, the weight loss was found to be 53% at a temperature below 800 °C. For comparison, we performed the TGA Study of reduced GO (black curve) formed by the reaction of GO with aniline in an ultrasonicator bath. The curve showed a completely different pattern, and the weight loss was found to be about 24% at a temperature below 800 °C, which can be attributed to the presence of polyaniline on the graphene oxide surface. From the results, it was concluded that although GO was partially reduced during its action as a catalyst, oxygen functional groups were not completely removed, which ascertains it's efficiency after repeated cycle. These results were further supported by ζ potential measurements in deionized water. Whereas in case of pristine GO dispersed in water, ζ was found to be -50.5 mV, the recovered GO after 5th cycle showed a ζ value of -44.3 mV, confirming that the GO surface was partially reduced during catalytic reactions.
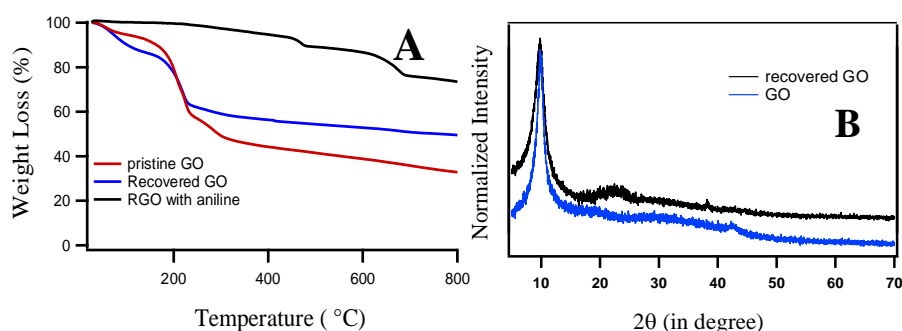
Figure 2.5 A) TGA diagram of pristine graphene oxide and recovered graphene oxide B) XRD of graphene oxide and recovered graphene oxide in solid form.

Powder x-ray diffraction studies on pristine GO and recovered GO were carried out in order to evaluate the structural modifications after their participation as catalysts. As shown in Figure 2.5 B, GO showed a broad band with 2θ maximum at 9.9. Whereas for the recovered GO after the 5th cycle of catalysis, along with the 2θ peak at 9.84, there was an additional broad peak with 2θ maxima at 22.8 with interlayer separation of 3.89 ´ (black curve). The results suggest the partial reduction of GO oxygenated groups during the catalytic reactions, which is consistent with other studies.[21]

2.3.3 FTIR Study
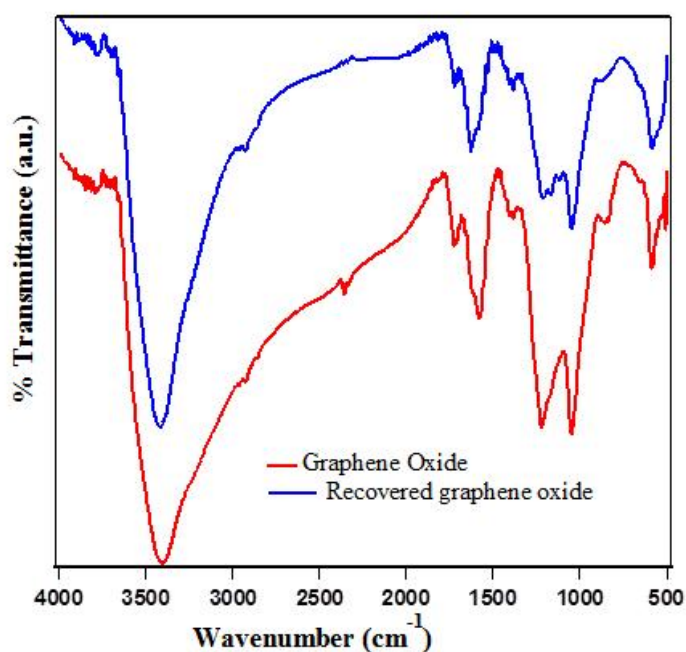
Figure 2.6 FTIR spectrum of graphene oxide (red line) and the graphene oxide recovered after 5th cycle of catalysis (blue line).

The FTIR spectra of both the pristine graphene oxide and the recovered graphene oxide exhibited broad and intense peaks centered at 3407 cm^{-1} attributed to the O-H stretching mode (Figure 2.6). Further peaks at 1703 cm^{-1} (C=O), 1557 cm^{-1} (C=C) and 1234 cm^{-1} (C-O) were observed in the FTIR spectrum indicating little changes in the bonding pattern of the graphene oxide before and after its participation as catalyst in the reaction.

2.3.5 Elemental Analysis

Elemental analysis of graphene oxide and graphene oxide recovered after 5th catalytic cycle of multicomponent reaction for the formation of α-amino

phosphonates have been compared in Table 2.4. The carbon content was found to increase from 31.4% (GO) to 33.7% (Recovered GO) while the oxygen content decreased from 43.2% (GO) to 41.2% (Recovered GO). The C/O ratio in the case of recovered GO after catalytic cycles was 1.09 compared to 0.97 in the case of pristine GO, signifying the partial reduction of GO after its participation in catalytic cycles. The detection of 1.8% nitrogen in the recovered GO suggested the adsorption of aniline on the GO surface during reaction.

Table 2.4 Elemental analysis of graphene oxide and graphene oxide recovered after 5th catalytic cycle of multicomponent reaction for the formation of α-amino phosphonates.

Element	C	H	O	N	S	Adsorbed Water	C/O Ratio
Wt% of Pristine graphene oxide	31.4	2.2	43.2	0	1.3	21.9	0.97
Atom ratio	2.62	1.1	2.7	------	0.04	1.22	
Wt % of recovered GO after 5th catalytic Cycle	33.7	2.1	41.2	1.8	0.9	20.3	1.09
Atom ratio	2.81	1.05	2.575	0.13	0.03	1.13	

2.3.6 Electron Microscopy Study

Transmission electron microscopy studies were carried out on a JEOL JEM-2100F microscope in order to observe if there was any morphological changes after graphene oxide participated as catalysts during the multicomponent reactions. For this purpose, GO and recovered GO after catalysis were transferred to a copper TEM grid. The TEM image in figure 2.7 showed the sheet like structure of graphene oxide having a wrinkled paper like morphology with the direct deposition on standard grids having the advantage of producing larger areas of GO. The HRTEM image of the GO sheet showed a monolayer structure (Figure 2.7b). Figure 2.7c depicts a selected area electron diffraction (SAED) pattern of GO that was taken using a selected area

from the GO sheet suspended above a micrometer-sized hole on a 200 mesh copper transmission electron microscopy (TEM) grid and clearly demonstrates that the GO had a crystalline structure. Similar results were obtained from the morphological studies by transmission electron microscopy (TEM), where both GO and recovered GO showed rippled paper-like structure. Selected area electron direction (SAED) pattern of both GO and recovered GO showed their high crystallinity (Figure 2.7c and 2.7e).
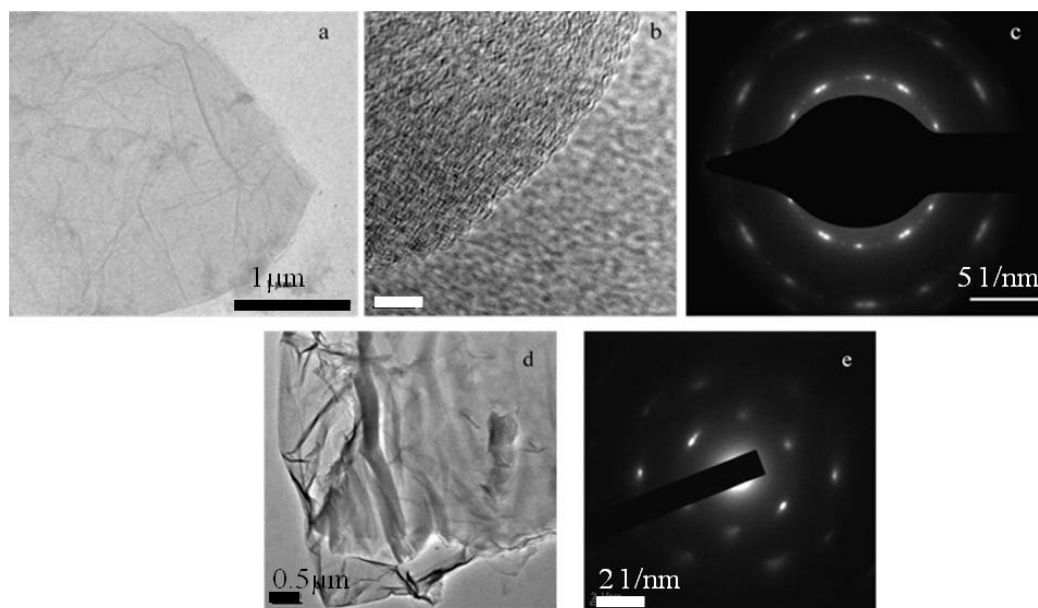

Figure 2.7 *(a) Transmission electron micrograph (scale bar 1 μm); (b) HRTEM image (scale bar 5 nm) and (c) SAED pattern of graphene oxide. (d) Transmission electron micrograph (scale bar 0.5 μm) and (e) SAED pattern of recovered GO after their participation in catalytic reactions.*

On the other hand, the recovered GO exhibited a typical rippled and crumpled morphology and paper-like structure with single or very thin multi layers. The recovered GO also showed highly crystalline structure. The inner six member ring came from the (1100) plane, while the six brilliant points were related to the [0001] diffractions and retained the hexagonal symmetry of the [0001] diffraction pattern. The diffraction pattern images showed that the resulting recovered GO has been somewhat restored into the hexagonal graphene framework.

2.4 Proposed Mechanism

Mechanistically, the formation of α-aminophosphonate progressed through the imine intermediate, similar to earlier reports[17] (Figure 2.8). The formation of imine was observed when benzaldehyde was reacted with aniline at room temperature under solvent-free conditions in the presence of GO as a catalyst, even without ultrasonication. The starting materials benzaldehyde and aniline exhibited peaks at 270 nm and 320 nm respectively, whereas the imine intermediate formed after catalysis by graphene oxide showed peak at 334 nm, confirming imine as the key intermediate in the product-forming pathway (Figure 2.8). The peak at 260 nm in the spectra of imine-graphene oxide conjugate is assigned to graphene oxide.
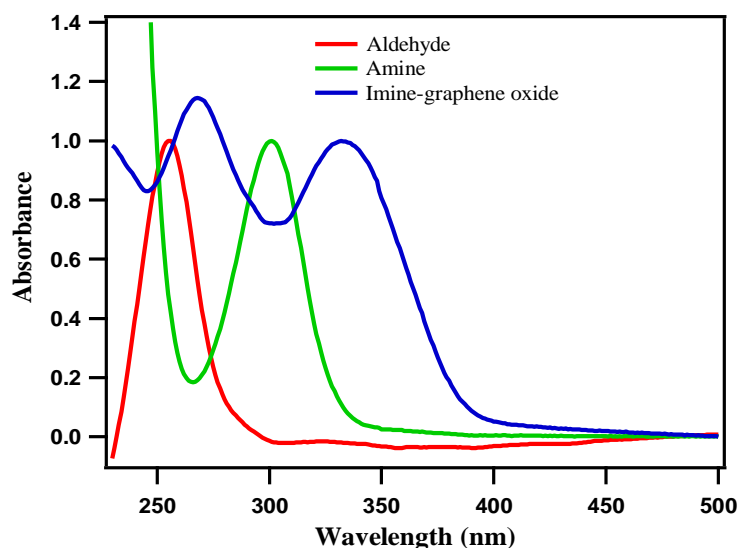
Figure 2.8 Normalized UV-Visible spectrum of benzaldehyde, aniline and imine intermediate formed catalyzed by graphene oxide.

Lewis acid-base interaction between the GO catalyst and the imine facilitates the reaction by shifting the equilibrium towards product formation in the coupling reaction. Based on the studies, a proposed mechanism is depicted in Figure 2.9. The presence of carboxylic acid groups on GO was primarily responsible for the activation. It was clearly evident from the observation that when the reaction was carried out in the presence of reduced GO (GO reduced with hydrazine), the reaction proceeded very slowly and required a prolonged reaction time (Table 2.1, entry 25).
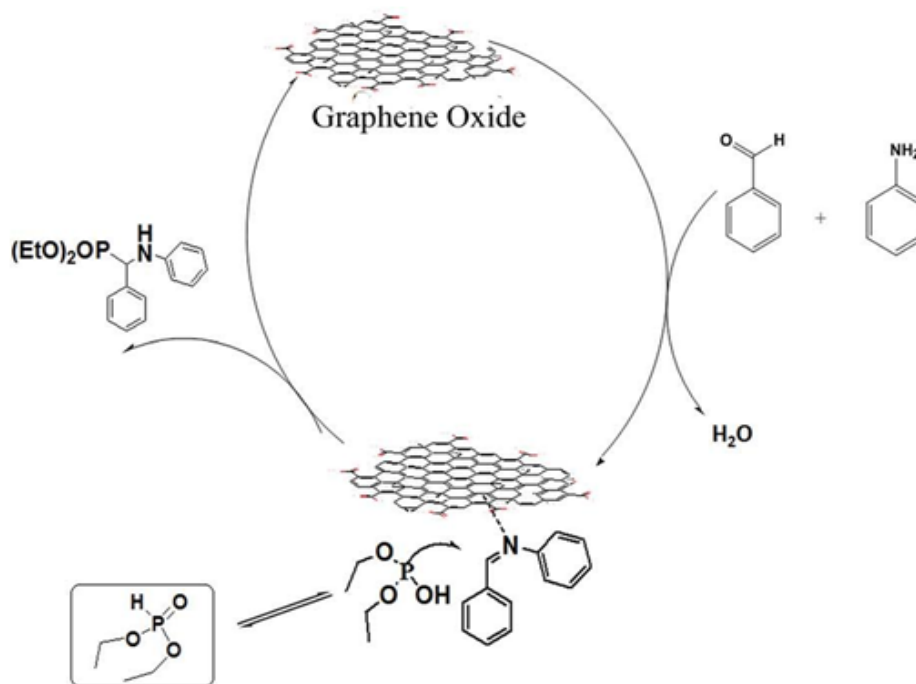
Figure 2.9 *Mechanistic proposal of synthesis of α-aminophosphonate.*

Recently, Su et al. reported the catalytic activity of porous graphene oxide, which was synthesized by a sequential base and acid treatment (ba-GO), for the oxidative coupling of amines to imines.[22] They reported that the oxidative coupling of various amines catalyzed by ba-GO involved molecular oxygen, and the reaction followed a free radical pathway with the generation of H_2O_2. In order to have further insight into the reaction mechanism for the multicomponent coupling reactions catalyzed by GO, we studied the generation of H_2O_2 spectrophotometrically using the FOX method. We did not observe any formation of H_2O_2 during the reaction, which thus eliminates the involvement of molecular oxygen during the reaction. Further conformation could be obtained from the fact that α-aminophosphonates, 3,4-dihydropyrimidin-2-ones and 3-substituted indoles were obtained as the sole products during the coupling reactions, and no formation of polyaniline as a byproduct was observed under the present reaction conditions.

If H_2O_2 would have been produced during the reaction, then significant amount of polyaniline should have been formed as a byproduct, as H_2O_2 is known to be a good oxidizing agent for the oxidation of aniline to form polyaniline. Moreover, when we carried out the coupling reaction of

benzaldehyde, aniline and diethylphosphite under argon environment instead of air, we obtained high yield of the coupling product. From these observations, it was clearly evident that molecular oxygen did not play any significant role in the reaction mechanism, and the reaction proceeded by the action of graphene oxide nanosheets, which only act as a facilitator for the stabilization of imine intermediate via acid–base interaction.

2.5 Conclusions

In conclusion, we have demonstrated for the first time that graphene oxide can be used as a mild, non-toxic and sustainable nanocatalyst for the multicomponent coupling reactions leading to biologically relevant α-aminophosphonates and 3,4-dihydropyrimidin-2-ones under solvent free conditions with low catalytic loading. Due to the acidic nature of GO, the method could be extended to other acid catalyzed one-pot multicomponent reactions. Carbocatalyst such as GO with minimal environmental footprints, low cost and possibility of scaling up in large quantities, with a multiplier effect of the surface area and presence of oxygen functionalities in the mesopores of nanostructured carbon could be used as an effective alternative to dwindling metal catalysts. Although the detailed mechanism of catalytic origin is not clearly understood, we believe that the presence of carboxylic groups at the edges of defect trap molecular oxygen and amine molecules and facilitate intermolecular arrangements. Taking advantage of oxygenated functional groups and possibility of incorporating functionality when necessitated, graphene oxide could be used as an ideal catalytic platform towards products of industrial interest through the multicomponent reaction.

2.6 Materials and Methods

2.6.1 Instrumentations

All reactions were carried out in air and monitored by TLC using Merck 60 F_{254} pre coated silica gel plates (0.25 mm thickness) and the products were visualized by UV detection. Flash chromatography was carried out with silica gel (200-300 mesh). FT-IR spectra were recorded on a Bruker Tensor-27 spectrometer. ^{1}H and ^{13}C NMR spectra were recorded on a Bruker Advance (III) 400 MHz spectrometer. Data for ^{1}H NMR are reported as a chemical shift

(δ ppm), multiplicity (s = singlet, d = doublet, q = quartet, m = multiplet), coupling constant J (Hz), integration, and assignment, data for ^{13}C are reported as a chemical shift. TMS was used an internal reference in the NMR spectra. Sample concentrations for NMR were in the range of 1-10 mmol in $(CD3)_2SO$ and $CDCl_3$. UV-visible spectra were recorded in a Varian Cary 100 Bio spectrophotometer, TEM images were recorded on a Tecnai G^2 20 Ultra- Twin microscope. Powder XRD spectra were recorded on a Bruker D8 Advance diffractometer using Cu Kα as the X-ray Source. Thermal gravimetric analysis (TGA) was performed in a Mettler-Toledo TGA-DSC/1 star system. Zeta potential measurements were carried out using a micromeritics NanoPlus 3 system.

2.6.2 Experimental section

Materials

Graphite, all the amines, aldehydes, diethylphosphite, ethyl acetoacetate, and urea were purchased from Aldrich Chemicals. Potassium permanganate ($KMnO4$), sulphuric acid (H_2SO_4) and hydrochloric acid (HCl) were purchased from Merck, India. All these chemicals were used without further purification. Milli Q water was used throughout the experiments.

2.6.3 Synthesis of graphene oxide by Modified Hummer's method

In a typical procedure, graphite powder (2.0 gm), $NaNO3$ (2.0 gm) and H_2SO_4 (100 ml) were mixed in reaction vessel. $KMnO4$ (20 gm) was added gradually with stirring on an ice bath. After addition of $KMnO4$, the reaction mixture was further stirred at room temperature for 24 hours. Subsequently, 200 ml water was added slowly and temperature of the reaction mixture was raised to 100 °C using an oil bath. After another 24 hours, 450 ml water was added, followed by addition of 30% H_2O_2 (40 ml). Finally, oxidation product was filtered and purified by rinsing with 110 ml of 5% HCl solution. The filtrate cake was repeatedly washed with HPLC grade water until the pH was about 6. This dark brown oxidized material was dried in oven at 90 °C. The dried product was grounded with a mortar and pestle to fine powder. The solid GO catalyst was recovered by collecting the non-sedimented supernatant solution after centrifugation at

15000 rpm followed by freeze-drying. The physico-chemical properties of GO were evaluated using various spectroscopic and microscopic technique.
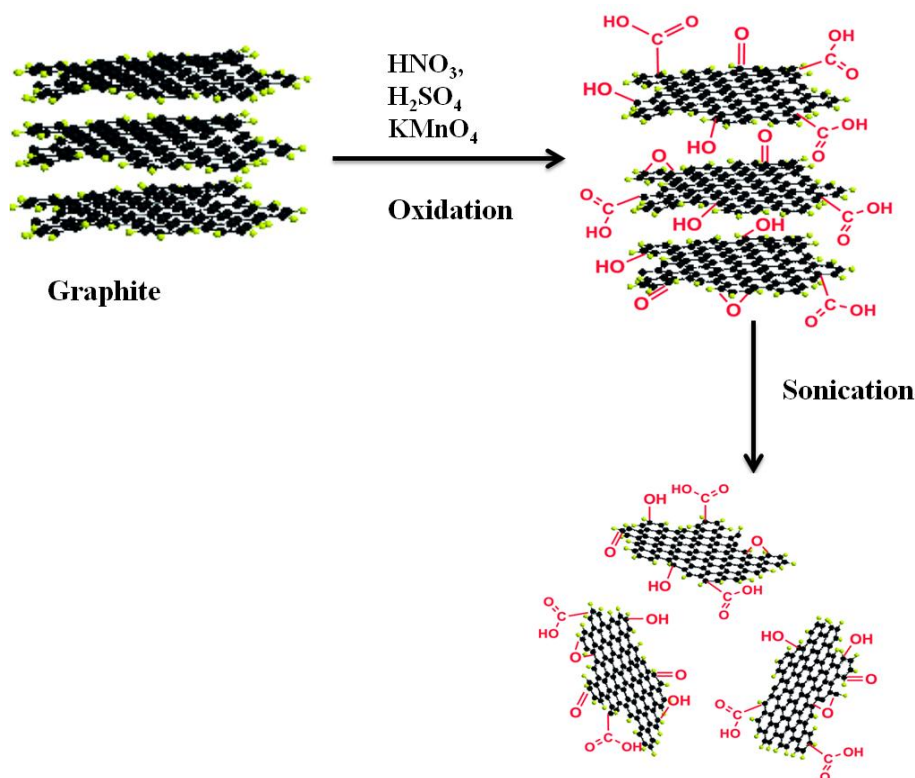
Figure 2.10 Schematic diagram of preparation of Graphene Oxide.

2.6.4 Synthesis of *α*-aminophosphonates

A mixture of aldehyde (1.0 mmol), amine (1.0 mmol), dialkyl phosphite (2.0 mmol) and graphene oxide (10 mg) was added in a test tube. The reaction mixture was sonicated at room temperature for the time indicated in Table 2 (progress of the reaction was monitored using TLC). The Product formed was extracted with ethyl acetate and water washing. The solid product was obtained after concentrating the combined ethyl acetate extracts on rotary evaporator. After extraction the water fraction was centrifuged and the catalyst was recovered which was reused for further reactions.

2.6.5 Synthesis of 3, 4-dihydropyrimidin-2-ones (DHPMs)

To a test tube, aldehyde (5.0 mmol), ethyl acetoacetate (5.0 mmol), and urea (10.0 mmol) were added and the mixture was sonicated at room temperature in the presence of prepared catalyst (graphene oxide) (50 mg) for 2.0–4.0 hours.

Completion of the reaction was monitored by TLC. The reaction mixture was extracted with DCM and water and the solid product was obtained after concentrating the combined DCM extracts on rotary evaporator. All the products were characterized by spectral (NMR) data.

2.6.6 Synthesis of 3-substituted Indoles

To a solution of N-methylaniline (114 mg, 1.2 mmol), Indole and a benzaldehyde (1.0 mmol) in methanol (2 mL) was added GO (30 mg) for 2 hrs. The progress of reaction was monitored by TLC. After completion of the reaction GO was removed by filtration and washed with ethyl acetate. The filtrate was dried over anhydrous sodium sulfate and concentrated to obtain the crude product, which was purified by column chromatography on silica gel (100–200 mesh) using ethyl acetate/hexane as eluents to yield a pure product. All the compounds were characterized by ESI-MS, ^{1}H NMR and ^{13}C NMR spectroscopic data.

NMR Data of α-amino phosphonates:

1.
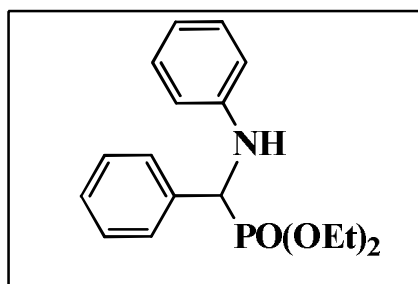
3aa (Table 2.2)

^{1}H NMR (CDCl$_3$, 400 MHz): δ_H 7.46-7.49 (m, 2H, C$_6$H$_5$), 7.33 (t, 2H, C$_6$H$_5$), 7.10 (t, 2H, C$_6$H$_5$), 6.69 (t, 2H, C$_6$H$_5$), 6.59 (d, 2H, C$_6$H$_5$), 4.71 (d, 1H, CH), 4.09-4.15 (m, 2H), 3.91-3.97 (m, 1H), 3.64-3.71 (m, 1H), 1.29 (t, 3H, -OCH$_2$CH$_3$), 1.12(t, 3H, -OCH$_2$CH$_3$); ^{13}C NMR (CDCl$_3$, 100 MHz) : 146.62, 146.47, 135.87, 129.13, 128.57, 127.80, 118.35, 113.82, 63.81, 55.28 (d, J=150 Hz, -CH), 16.43 (d, J=6 Hz, -OCH$_2$CH$_3$), 16.13 (d, J=6 Hz, -OCH$_2$CH$_3$).

2.

3ab (Table 2.2)

^{1}H NMR (CDCl$_3$, 400 MHz): δ$_H$ 7.49-7.46 (m, 2H, C$_6$H$_5$), 7.33 (t, 2H, C$_6$H$_5$), 7.12-7.08 (m, 2H, C$_6$H$_5$), 6.69 (t, 1H, C$_6$H$_5$), 6.61-6.59 (m, 2H, C$_6$H$_5$), 4.10 (d, 2H, -OCH$_2$CH$_3$), 3.97-3.91 (m, 1H, -OCH$_2$CH$_3$), 3.71-3.64 (m, 1H, -OCH$_2$CH$_3$), 1.29 (t, 3H, -OCH$_2$CH$_3$), 1.10 (t, 3H, -OCH$_2$CH$_3$); ^{13}C NMR (CDCl$_3$, 100M Hz) 146.54, 146.39, 136.06, 129.19, 128.60, 127.93, 118.37, 113.90, 63.34-63.28 (d, J=6 Hz), 56.85-55.36 (d, J=150 Hz), 16.47.
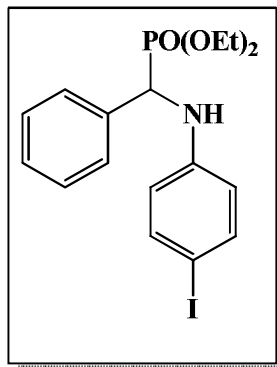
3.

3ac (Table 2.2)
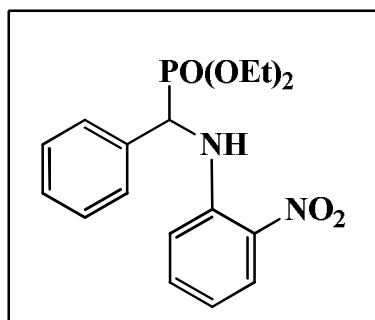
^{1}H NMR (CDCl$_3$, 400M Hz): δ$_H$ 8.98 (d, 1H, C$_6$H$_5$), 8.21 (d, 1H, C$_6$H$_5$), 7.50 (d, 2H, C$_6$H$_5$), 7.39-7.29 (m, 2H, C$_6$H$_5$), 6.72-6.67 (m, 3H, C$_6$H$_5$), 4.95 (d, 1H), 4.14-3.91 (m, 4H, -OCH$_2$CH$_3$), 1.29-1.25 (m, 6H, -OCH$_2$CH$_3$) ^{13}C NMR (CDCl$_3$, 100M Hz) 144.06, 143.93, 136.11, 134.59, 128.91, 128.42, 127.59, 126.88, 116.68, 114.68, 63.75-63.52, 56.28-54.78 (d, J=150 Hz), 16.38.

4.

3ad (Table 2.2)

^{1}H NMR (CDCl$_3$, 400M Hz): δ$_H$ 7.47-7.43 (m, 2H, C$_6$H$_5$), 7.39 (dd, 2H, C$_6$H$_5$), 7.27-7.20 (m, 1H, C$_6$H$_5$), 7.12-7.20 (m, 2H, C$_6$H$_5$), 7.10 (t, 1H, C$_6$H$_5$), 6.82(dd, 1H, C$_6$H$_5$), 4.76 (dd, 1H), 4.13-4.08 (m, 2H, -OCH$_2$CH$_3$), 3.91-3.85 (m, 1H), 1.23 (t, 3H, -OCH$_2$CH$_3$), 1.03 (t, 3H, -OCH$_2$CH$_3$); ^{13}C NMR
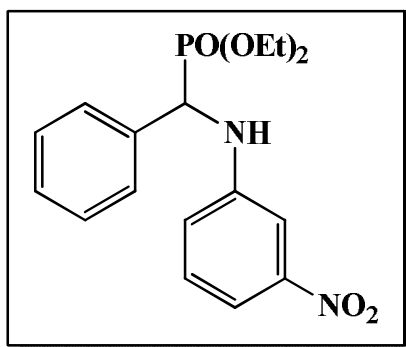
(CDCl$_3$, 100M Hz):148.79, 147.17, 134.63, 129.26, 128.39, 127.89, 127.64, 118.81, 112.21, 107.83, 63.40-62.92 (dd, J=46 Hz), 56.11-54.60 (d, J=151 Hz), 16.10-15.76 (dd, J=34 Hz).

5.

3ae (Table2.2)

^{1}H NMR (CDCl$_3$, 400M Hz): δ$_H$ 8.07-8.00 (m, 2H, C$_6$H$_5$), 7.49 (d, 2H, C$_6$H$_5$), 7.41-7.32 (m, 3H, C$_6$H$_5$), 6.69-6.62 (m, 2H, C$_6$H$_5$), 4.87 (d, 1H), 4.21-4.12 (m, 2H, -OCH$_2$CH$_3$), 3.96-3.90 (m, 1H, -OCH$_2$CH$_3$), 3.67-3.63 (m, 1H, -OCH$_2$CH$_3$), 1.33 (t, 3H, -OCH$_2$CH$_3$), 1.13 (t, 3H, -OCH$_2$CH$_3$); ^{13}C NMR (CDCl$_3$, 100 MHz): 152.15, 151.83, 138.51, 134.20, 128.54, 127.42, 125.72, 112.08, 63.54 63.06, 55.91 54.40-54.33 (d, J=150 Hz), 16.44-16.04(dd, J=20 Hz,).
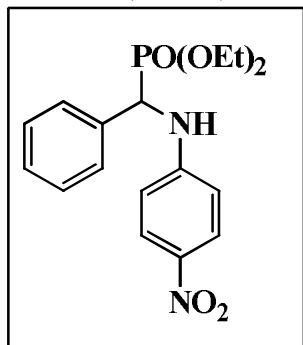
6.

3af (Table 2.2)

^{1}H NMR (CDCl$_3$, 400M Hz): δ$_H$ 8.02 (dd, 1H), 7.86 (dd, 1H), 7.29-7.22 (m, 3H), 6.99-6.91 (m, 2H), 6.82-6.80 (m, 1H), 5.36 (bs, 1H), 4.70 (dd, 1H), 4.10-4.05 (m, 2H), 3.91-3.85 (m, 1H), 3.65-3.59 (m, 1H), 1.23 (t, 3H, -OCH$_2$CH$_3$), 1.05 (t, 3H, -OCH$_2$CH$_3$); ^{13}C NMR (CDCl$_3$, 100M Hz): 161.56, 148.84, 147.23, 142.02, 136.01, 126.91, 124.81, 123.20, 121.42, 70.65-69.05 (d, J=160 Hz), 62.37-62.16 (d, J=21 Hz), 15.47.
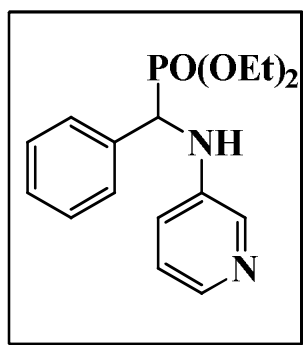
7.

3ag (Table 2.2)
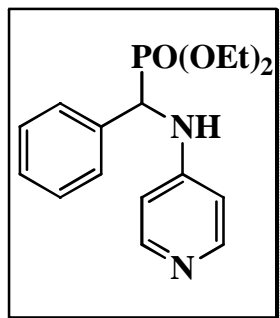
^{1}H NMR (CDCl$_3$, 400M Hz): δ_H 7.8 (d, 2H), 7.44-7.28 (m, 5H), 6.38 (d, 2H), 5.12 (bs, 1H), 5.10 (dd, 1H), 3.96-3.90 (m, 4H), 1.18-1.14 (m, 6H); ^{13}C NMR (CDCl$_3$, 100 MHz) :148.03, 137.62, 128.17, 127.89, 127.40, 127.34, 109.55, 71.41-69.80 (d, J=161 Hz), 63.24-63.06, 16.47.

8.

3ai (Table 2.2)
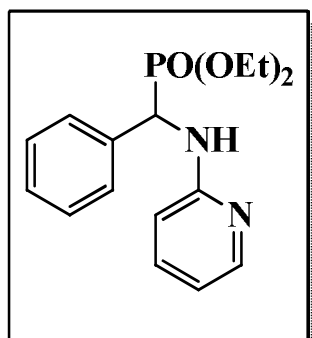
^{1}H NMR (CDCl$_3$, 400M Hz): 8.51 (d, 1H), 8.00 (t, 1H), 7.51-7.29 (m, 5H), 6.60 (d, 1H), 6.53-6.51 (m, 1H), 5.04 (d, 1H), 4.08-3.98 (m, 4H), 1.29-1.17 (m, 6H); ^{13}C NMR (CDCl$_3$, 100M Hz) 158.48, 134.74, 138.72, 137.38, 130.02, 129.27, 128.41, 127.44, 122.12, 71.68-70.09(d, J=159Hz), 63.61-63.21(dd, J=20 Hz), 16.60-16.14 (dd, J=23Hz).

9.

3aj (Table 2.2)
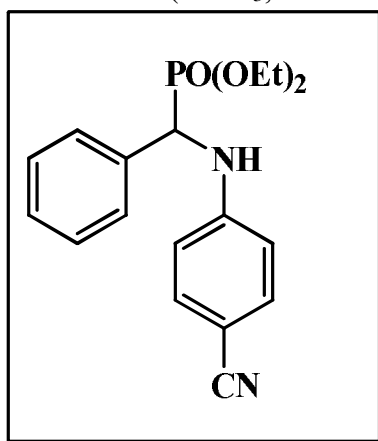
^{1}H NMR (CDCl$_3$, 400M Hz): δ_H 7.47 (d, 2H, C$_6$H$_5$), 7.36-7.28 (m, 5H, C$_6$H$_5$), 6.64 (d, 2H, C$_6$H$_5$), 4.80 (d, 1H, C$_6$H$_5$), 4.18-4.12 (m, 2H), 3.95-3.89 (m, 1H), 3.67-3.62 (m, 1H), 1.30 (t, 3H, -OCH$_2$CH$_3$), 1.10 (t, 3H, -OCH$_2$CH$_3$); ^{13}C NMR (CDCl$_3$, 100M Hz): 134.69, 133.42, 129.94, 128.71, 128.27, 127.74, 120.00, 113.35, 63.74-63.28 (d, J=46 Hz), 55.97-54.46 (d, J=151 Hz), 16.34-16.02.

10.

3ba (Table 2.2)
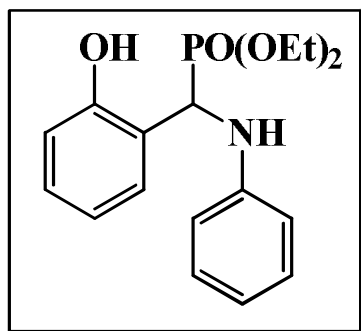
^{1}H NMR (CDCl$_3$, 400 MHz): δ_H 7.29 (d, 1H, C$_6$H$_5$), 7.15-7.11 (m, 2H, C$_6$H$_5$), 6.94 (d, 1H, C$_6$H$_5$), 6.85 (t, 1H, C$_6$H$_5$), 6.75 (t, 1H, C$_6$H$_5$), 6.70 (d, 2H, C$_6$H$_5$), 5.13 (d, 1H, C$_6$H$_5$), 4.83 (bs, 1H), 4.21-4.06 (m, 3H), 3.96-3.92 (m, 1H, -OCH$_2$CH$_3$), 1.29 (t, 3H, -OCH$_2$CH$_3$), 1.20 (t, 3H, -OCH$_2$CH$_3$); ^{13}C NMR (CDCl$_3$, 100M Hz) 155.58, 146.27, 129.12, 121.12, 121.42, 120.30, 119.02, 114.25, 63.94 (d, J=7 Hz), 63.55 (d, J=6 Hz), 53.71 (d, J=153 Hz), 16.33 (d, J=5 Hz), 16.16 (d, J=5 Hz).

11.

3da (Table 2.2)
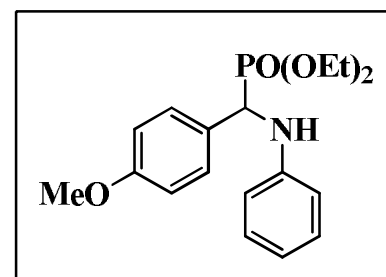
^{1}H NMR (CDCl$_3$, 400M Hz): δ_H 7.35 (dd, 2H, C$_6$H$_5$), 7.09 (t, 2H, C$_6$H$_5$), 6.86 (d, 2H, C$_6$H$_5$), 6.69 (d, 1H, C$_6$H$_5$), 6.59 (d, 2H, C$_6$H$_5$), 4.69 (d, 1H, CH), 4.17-4.07 (m, 2H), 3.97-3.91 (m, 1H), 3.77 (s, 3H, -OCH$_3$), 3.73-3.67 (m, 1H, -OCH$_2$CH$_3$), 1.29 (t, 3H, -OCH$_2$CH$_3$), 1.13 (t, 3H); ^{13}C NMR (CDCl$_3$,

100M Hz):167.34 ,150.35, 131.64, 128.01, 128.49, 128.09, 126.04, 113.01, 63.88 (d, J=7 Hz), 63.61 (d, J=7Hz), 55.55 (s, 1H), 16.73 (d, J=5 Hz), 16.48 (d, J=5 Hz).

12.

3ek (Table 2.2)
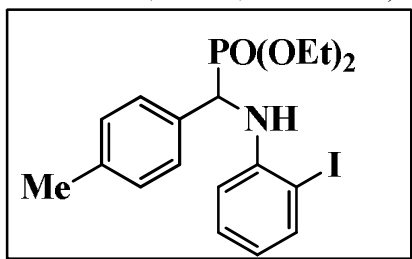
^{1}H NMR (CDCl$_3$, 400M Hz): δ_H 7.88 (d, 1H, C$_6$H$_5$), 7.55 (dd, 1H, C$_6$H$_5$), 7.25-7.22 (m, 2H, C$_6$H$_5$), 7.04 (d, 2H, C$_6$H$_5$), 6.94 (t, 1H, C$_6$H$_5$), 6.35-6.29 (m, 1H, C$_6$H$_5$), 5.91 (s, 1H), 4.66 (d, 1H), 4.06-3.92 (m, 3H, , -OCH$_2$CH$_3$), 3.80-3.73 (m, 1H, -

OCH$_2$CH$_3$), 2.21 (s, 3H,-CH$_3$), 1.20 (t, 3H, -OCH$_2$CH$_3$), 1.10 (t, 3H, -OCH$_2$CH$_3$); ^{13}C NMR (CDCl$_3$, 100M Hz) 145.93, 139.26, 130.33, 129.62, 129.49, 127.77, 120.03, 112.30, 64.11 (d, J=7 Hz), 63.87 (d, J=7 Hz), 57.13 (d, J=150 Hz), 21.36, 16.71(d, J=6 Hz), 16.55 (d, J=6 Hz).

13.

3fh (Entry 15, Table 2)

^{1}H NMR (CDCl$_3$, 400M Hz): δ$_H$ 7.73 (d, 2H), 7.01 (d, 1H), 6.84-6.77 (m, 2H), 6.60 (d, 2H), 5.38 (d, 2H), 4.15 (d, 2H), 3.90-3.78 (m, 1H), 3.65-3.62 (m, 1H), 3.89 (s, 3H), 3.67 (s, 3H), 2.42 (s, 3H), 1.30 (t, 3H), 1.05 (t, 3H); ^{13}C NMR (CDCl$_3$, 100MHz) : 196.41, 154.27, 154.18, 130.84, 127.86, 125.16, 125.07, 114.31, 112.67, 111.98, 63.78, 63.45, 56.59-55.90, 26.26, 16.66-16.36.
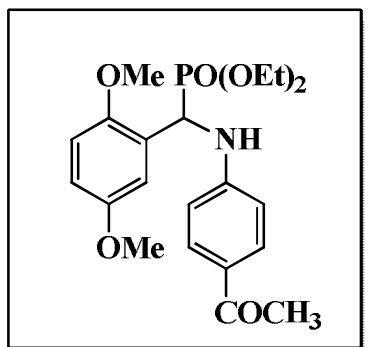
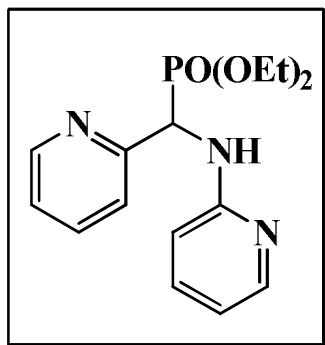14.

3fg (Entry 16, Table 2)

^{1}H NMR (CDCl$_3$, 400M Hz): δ$_H$ 7.87 (d, 2H), 6.77 (s, 2H), 6.47 (d, 1H), 6.04 (d, 1H), 5.53 (d, 2H), 4.14-4.07 (m, 2H), 4.05-3.97 (m, 1H), 3.96-3.91 (m, 1H), 3.74 (s, 3H), 3.72 (s, 3H), 1.25 (t, 3H), 1.17 (t, 3H); ^{13}C NMR (CDCl$_3$, 100M Hz): 155.26, 153.59, 150.63, 147.18, 127.05, 114.10, 111.5, 109.17, 64.58, 62.77, 55.94-55.43(d, J= 51Hz), 16.18.
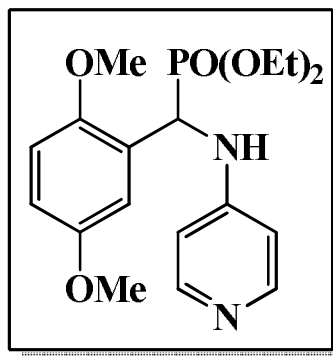
15.

3ii (Table 2.2)

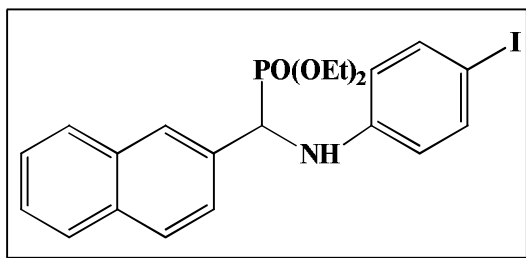^{1}H NMR (CDCl$_3$, 400M Hz): δ$_H$ 8.35 (d, 1H), 7.67 (d, 1H), 7.52 (d, 1H), 7.43 (d, 1H), 7.22 (s, 1H),7.05 (d, 1H), 6.48 (d, 1H), 6.34 (d, 1H), 6.01 (bs, NH), 5.02 (d, 1H), 4.00 (d, 2H), 3.97-3.94 (m, 1H), 3.68-3.64 (m,1H), 1.10 (t, 3H), 1.02 (t, 3H); ^{13}C NMR (CDCl$_3$, 100M Hz): 157.50, 155.19, 147.93, 143.00, 139.08, 136.08, 136.56, 122.82, 122.10, 112.13, 110.54, 71.21-69.62 (d, 150Hz), 16.30-16.12.

16.

3jb (Entry 21, Table 2)

^{1}H NMR (CDCl$_3$, 400M Hz): δ$_H$ 7.81 (s, 1H, C$_6$H$_5$), 7.72-7.67 (m, 3H, C$_6$H$_5$), 7.48 (dd, 1H, C$_6$H$_5$), 7.34 (dd, 2H, C$_6$H$_5$), 7.21 (d, 2H, C$_6$H$_5$), 6.34-6.32 (d, 2H, C$_6$H$_5$), 4.80 (dd, 1H), 4.06-4.01 (m, 2H, -OCH$_2$CH$_3$), 3.85-3.78 (m,1H), 3.58-3.51 (m,1H), 1.19

(t, 3H, -OCH$_2$CH$_3$), 0.97 (t, 3H, -OCH$_2$CH$_3$); ^{13}C NMR (CDCl$_3$, 100M Hz): 146.06, 133.15, 132.99, 132.88, 127.84, 127.58, 126.86-126.79 (d, J=7 Hz), 126.20-126.09 (d, J=7 Hz), 116.03, 79.33, 63.37-63.21 (dd, J=16 Hz), 56.81-55.31 (d, J=150 Hz), 16.39-16.08 (dd, J=31 Hz).

17.

3kg (Table 2.2)
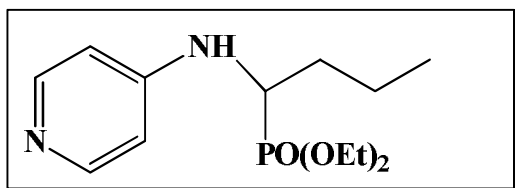
^{1}H NMR (CDCl$_3$, 400 MHz): δ$_H$ 8.06 (d, 2H), 6.45 (d, 2H), 4.60 (bs, NH), 4.13-4.05 (m, 4H), 3.83-3.78 (m, 2H), 1.68-1.55 (m, 3H), 1.39-1.33 (m, 1H), 1.26 (t, 3H), 0.88-0.85 (t, 3H,);
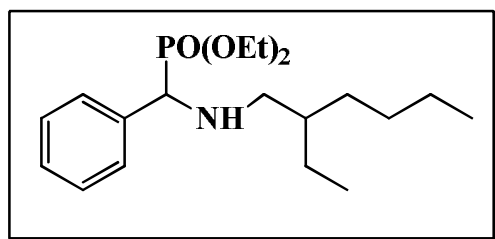
^{13}C NMR (CDCl$_3$, 100M Hz): 153.99, 148.31, 109.56, 68.36-66.77 (d, J=159 Hz), 62.60-62.48 (dd, J=12 Hz), 33.40, 19.01-18.87(d, J=14 Hz), 16.56-16.50 (d, J=6 Hz), 13.71.

18.

3al (Table 2.2)

^{1}H NMR (CDCl$_3$, 400M Hz): δ$_H$ 7.33 (d, 2H), 7.23 (t, 1H), 7.16 (d, 2H), 4.04-

3.97 (m, 2H), 3.90 (d, 1H), 3.91- 3.70 (m, 2H), 2.34-2.25 (m, 2H), 1.35-1.20(m, 8H), 1.18 (t, 3H), 1.07 (t, 3H), 0.79-.067 (m, 6H); ^{13}C NMR (CDCl$_3$, 100M Hz) :136.38, 132.31, 129.76, 128.46, 128.21, 127.64, 62.95-62.88 (d, J=7 Hz), 62.64-62.57 (d, J=7 Hz), 62.27-60.74 (dd, J=153 Hz), 51.16-50.99 (d, J=17 Hz), 39.48-39.35 (d, J=13 Hz), 28.96-28.76 (d, J=20 Hz), 24.45-24.29 (d, J=16 Hz), 23.01-22.96 (d, J=5 Hz), 16.37-16.31 (d, J=5 Hz), 16.37-16.31 (d, J=6 Hz), 16.17-16.11 (d, J=6 Hz), 13.99-13.96 (d, J=3 Hz), 10.95-10.88 (d, J=7 Hz).
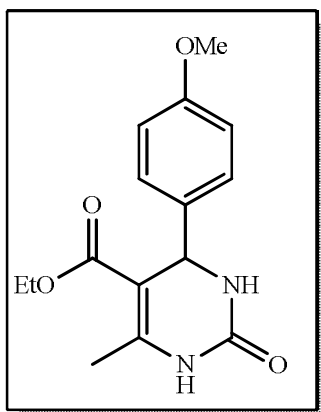
NMR data of 3,4-dihydropyrimidin-2-ones (DHPMs):

1.
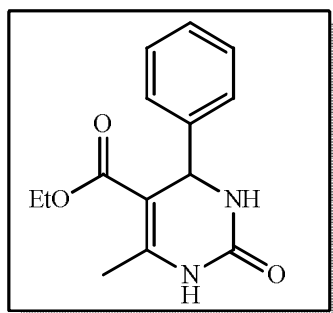
5a

^{1}H NMR (CDCl$_3$, 400M Hz): δ$_H$ 8.02 (s, 1H), 7.32-7.31 (m, 4H), 5.78 (s, 1H, NH), 5.40 (d, 1H), 4.08 (q, 2H), 2.35 (s, 3H), 1.15 (t, 3H).

2.

5b

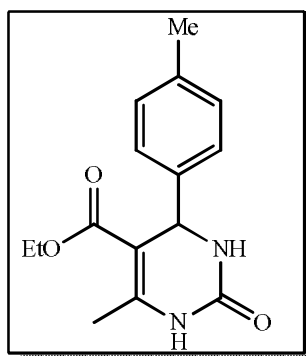^{1}H NMR (CDCl$_3$, 400M Hz): δ$_H$ 8.57 (s, 1H), 7.20 (d, 4H), 6.08 (s, 1H), 5.34 (d, 1H), 4.08 (q, 2H), 3.78 (s, 3H), 2.32 (s, 3H), 1.17 (t, 3H).
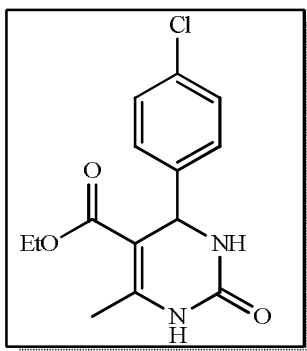
3.

5c

^{1}H NMR (CDCl$_3$, 400M Hz): 8.32 (s, 1H), 7.31-7.19 (m, 5H), 5.39 (s, 1H), 4.05 (q, 2H), 2.31 (s, 3H), 2.19 (s, 3H), 1.15 (t, 3H).
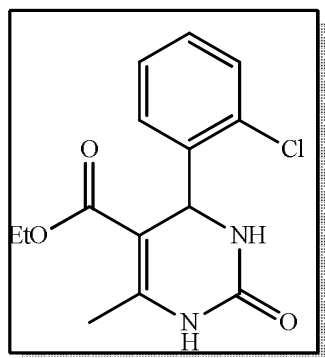
4.

5d

^{1}H NMR (CDCl$_3$, 400M Hz): δ$_H$ 8.00 (s, 1H), 7.44 (d, 2H), 7.20 (d, 2H), 5.83 (s, 1H), 5.37 (s, 1H), 4.10 (q, 2H), 2.34 (t, 3H), 1.17 (t, 3H).

5.

5e

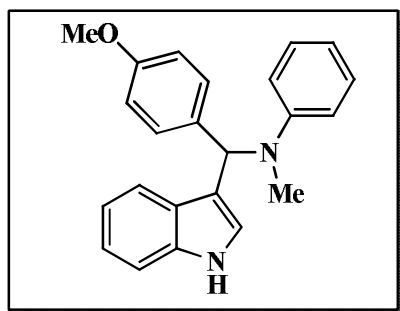^{1}H NMR (CDCl$_3$, 400M Hz): δ$_H$ 8.86 (s, 1H), 7.39 (d, 2H), 7.26-7.23 (m, 3H), 5.90 (s, 1H), 4.05 (q, 2H), 2.45 (s, 1H), 1.07 (t, 3H).

NMR of 3-substituted Indoles

1.

7c

^{1}H NMR (400 MHz, CDCl$_3$): δ 7.91(s, 1H), 7.36-7.08 (m, 11H), 6.60 (d, J = 8 Hz, 2H), 6.45- 6.48 (m, 2H), 5.45 (s, 1H), 3.71 (s, 3H), 2.81 (s, 3 H); ^{13}C NMR (100 MHz, CDCl$_3$): δ 39.66, 47.37, 50.88, 111.11, 112.32, 112.40, 119.05, 119.79, 122.06, 123.49, 123.82, 126.83, 129.62, 130.30, 131.31, 136.19, 143.08, 147.77.

2.7 References

1. (a) Zhang W., Zhang H., Xiao J., Zhao Z., Yu M. and Li Z. (2014), Carbon nanotube catalysts for oxidative desulfurization of a model diesel fuel using molecular oxygen, *Green. Chem.*, 16, 211 (DOI: 10.1039/C3GC41106K); (b) Gong K., Du F., Xia Z., Durstock M. and Dai L. (2009), Nitrogen-Doped Carbon Nanotube Arrays with High Electrocatalytic Activity for Oxygen Reduction, *Science*, 323, 760 (DOI: 10.1126/science.1168049); (c) Chung T. H., Won H. J.and Zeleney P. (2013), Active and stable carbon nanotube nanoparticle composite electrocatalyst for oxygen reduction, *Nat. Commun.*, 4, 1922 (DOI: 10.1038/ncomms2944); (d) Shanmugam S. and Osaka T. (2011), Efficient electrocatalytic oxygen reduction over metal free-nitrogen doped

carbon nanocapsules, *Chem. Commun.*, 47, 4463 (DOI: 10.1039/C1CC10361J); (e) Peng X., Chen J., Misewich A. J. and Wong S. S. (2009), Carbon nanotube–nanocrystal heterostructures, *Chem. Soc. Rev.,* 38, 1076 (DOI: 10.1039/B811424M); (f) Eder D.(2010), Carbon Nanotube-Inorganic Hybrids, *Chem. Rev.,* 110, 1348 (DOI: 10.1021/cr800433k); (g) Su S. D., Perathoner S. and Centi G. (2013), Nanocarbons for the Development of Advanced Catalysts, *Chem. Rev.,* 113, 5782 (DOI: 10.1021/cr300367d); (h) Wang J. Y., Wilkinson P. D. and Zhang J.(2011), Noncarbon Support Materials for Polymer Electrolyte Membrane Fuel Cell Electrocatalysts, *Chem. Rev.,* 111, 7625.(DOI: 10.1021/cr100060r); (i) Bitter H. J. (2010), Nanostructured carbons in catalysis a Janus material industrial applicability and fundamental insights, *J. Mater. Chem.,* 20, 7312 (DOI: 10.1039/C0JM00492H); (j) Dreyer R. D. and Bielawski W. C. (2011), Carbocatalysis: Heterogeneous carbons finding utility in synthetic chemistry, *Chem. Sci.,* 2, 1233 (DOI: 10.1039/c1sc00035g).

2. (a) Novoselov S. N., Geim K. A., Morozov V. S., Jiang D, Zhang Y, Dubonos V. S. , Grigorieva V. I. and Firsov A. A.(2004), Electric Field Effect In Atomically Thin Flims Science, 306, 666; (b) Geim K. A. and Novoselov S. K. (2007), The rise of graphene, *Nat. Mater.,* 6, 183 (DOI:10.1038/nmat1849).

3. (a) Geim K. A.(2009), Graphene: Status and Prospects, *Science,* 324, 1530 (DOI: 10.1126/science.115887); (b) Dreyer R. D., Ruoff S. R. and Bielawski W. C.(2010), From Conception to Realization: A Historial Account of Graphene and Some Perspectives for Its Future, *Angew. Chem. Int. Ed.*, 49, 9336 (DOI: 10.1002/anie.201003024); (c) Avouris P. (2010), Graphene: Electronic and Photonic Properties and Devices, *Nano Lett.,* 10, 4285 (DOI: 10.1021/nl102824h).

4. (a) Park S. and Ruoff S. R. (2009), Chemical methods for the production of graphenes, *Nat. Nanotechnol.,* 4, 217, (DOI:10.1038/nnano.2009.58); (b) Dreyer R. D., Park S., Bielawski W. C. and Ruoff S. R.(2010), The chemistry of graphene oxide, *Chem. Soc. Rev.,* 39, 228 (DOI: 10.1039/B917103G); (c) Guo S. and Dong S. (2011), Graphene nanosheet: synthesis, molecular

engineering, thin film, hybrids, and energy and analytical applications, *Chem. Soc. Rev.,* 40, 2644 (DOI: 10.1039/C0CS00079E); (d) Liu H., Liu Y. and Zhu D., Chemical doping of graphene, *J. Mater. Chem.,* 2011, 21, 3335 (DOI: 10.1039/c0jm02922j); (e) Georgakilas V., Otyepka M., Bourlinos B. A., Chandra V., Kim N., Kemp C. K., Hobza P., Zboril R. and Kim S. K. (2012), Functionalization of Graphene: Covalent and Non-Covalent Approaches, Derivatives and Applications, *Chem. Rev.,* 112, 6156 (DOI: 10.1021/cr3000412); (f) Chen D., Feng H. and Li J. (2012), Graphene Oxide: Preparation, Functionalization, and Electrochemical Applications, *Chem. Rev.,* 112, 6027 (DOI: 10.1021/cr300115g); (g) L. Rodr´ıguez-P´erez, M. ´A . Herranz and N. Mart´ın, The chemistry of pristine graphene, *Chem. Commun.,* 2013, 49, 3721 (DOI: 10.1039/C3CC38950B); (h) Jariwala D., V. K. Sangwan, L. J. Lauhon, T. J. Marks and M. C. Hersam, Carbon nanomaterials for electronics, optoelectronics, photovoltaics, and sensing, *Chem. Soc. Rev.,* 2013, 42, 2824 (DOI: 10.1039/c2cs35335k).

5. (a) An X. and Yu C. J. (2011), Graphene-based photocatalytic composites *RSC Adv.,* 1, 1426 (DOI: 10.1039/C1RA00382H); (b) Wang H. and Dai H. (2013), *Chem. Soc. Rev.,* 42, 3088 (DOI: 10.1039/c2cs35307e); (c) Huang C., Li C. and Shi G. (2012), Graphene based catalysts, *Energy Environ. Sci.,* 5, 8848 (DOI: 10.1039/C2EE22238H); (d) Machado F. B. and Serp P. (2012), Graphene-based materials for catalysis, *Catal. Sci. Technol.,* 2, 54 (DOI: 10.1039/C1CY00361E); (e) Han L., Wang P. and Dong S. (2012), Progress in graphene-based photoactive nanocomposites as a promising class of photocatalyst, *Nanoscale,* 4, 5814 (DOI: 10.1039/C2NR31699D); (f) Liang Y., Li Y., Wang H., Zhou J., Wang J., Regier T. and Dai H. (2011), Co_3O_4 nanocrystals on graphene as a synergistic catalyst for oxygen reduction reaction *Nat. Mater.,* 10, 780 (DOI:10.1038/nmat3087).

6. Zhang J., Zhang J., Zhang F., Yang H., Huang X., Liu, H., & Guo, S. (2010), Graphene oxide as a matrix for enzyme immobilization, *Langmuir,* 26, 6083–6085. (DOI:10.1021/la904014z).

7. (a) Dreyer R. D., Jia P.H., Todd D. A., Geng J. and Bielawski W. C. (2011), Graphite oxide: a selective and highly efficient oxidant of thiol and

sulfides, *Org. Biomol. Chem.,* 9, 7292 (DOI: 10.1039/C1OB06102J); (b) Dreyer R. D., Jia P. H. and Bielawski W. C.(2011), C−H oxidation using graphite oxide, *Tetrahedron,* 67, 4431 (DOI: 10.1016/j.tet.2011.02.065); (b) D. R. Dreyer, H. P. Jia and C. W. (2010), Bielawski, *Angew. Chem. Int. Ed.,* 122, 6965.

8. (a) Kumar V. A. and Rao R. K.(2011), Recyclable graphite oxide catalyzed Friedel−Crafts addition of indoles to *α,β*-unsaturated ketones, *Tetrahedron Lett.,* 52, 5188 (DOI: 10.1016/j.tetlet.2011.08.002); (b)Verma S., Mungse P. H., Kumar N., Choudhary S., Jain L. S., Sain B. and Khatri P. O.(2011), Graphene oxide: an efficient and reusable carbocatalyst for aza-Michael addition of amines to activated alkenes, *Chem. Commun.,* 47, 12673 (DOI: 10.1039/C1CC15230K); (c) Jia P. H., Dreyer R. D. and Bielawski W. C.(2011), Graphite Oxide as an Auto-Tandem Oxidation–Hydration–Aldol Coupling Catalyst, *Adv. Synth. Catal.,* 353, 528 (DOI: 10.1002/adsc.201000748); (d) Dhakshinamoorthy A., Alvaro M., Concepcio P., Forne V. and Garcia H.(2012), Graphene oxide as an acid catalyst for the room temperature ring opening of epoxides, *Chem. Commun.,* 48, 5443 (DOI: 10.1039/c2cc31385e).

9. (a) M. J. Climent, A. Corma and S. Iborra, Homogeneous and heterogeneous catalysts for multicomponent reactions, *RSC Adv.,* 2012, 2, 16 (DOI: 10.1039/C1RA00807B).

10. (a) Atherton F. R., Hassall C. H. and Lambert R. W.(1986), Synthesis and structure-activity relationships of antibacterial phosphonopeptides incorporating (1-aminoethyl) phosphonic acid and (aminomethyl)phosphonic acid, *J. Med. Chem.,* 29, 29 (DOI: 10.1021/jm00151a005); (b) Allen J. G., Atherton F. R., Hall M. J., Hassal C. H., Holmes S. W., Lambert R. W., Nisbet L. J. and Ringrose P. S.(1978), Phosphonopeptides, a new class of synthetic antibacterial agents, *Nature,* 272, 56. (DOI:10.1038/272056a0); (c) Giannousis P. P. and Bartlett P. A. (1987), Phosphorus amino acid analogs as inhibitors of leucine aminopeptidase, *J. Med. Chem.* 30, 1603 (DOI: 10.1021/jm00392a01); (d) Ren L., Lian L. X. and Gong Z. L. (2013), Brønsted Acid/Rhodium(II) Cooperative Catalytic Asymmetric Three-Component Aldol-Type Reaction

for the Synthesis of 3-Amino Oxindoles, *Chem. Eur. J.,* 19, 3315 (DOI: 10.1002/chem.201203993).

11. (a) Bhattacharya K. A. and Rana C. K.(2008), Amberlite-IR 120 catalyzed three-component synthesis of α-amino phosphonates in one-pot, *Tetrahedron Lett.,* 49, 2598 (DOI:10.1016/j.tetlet.2008.02.102); (b) Kidwai M., Bhardwaj S., Mishra K. N., Jain A., Kumar A. and Mozzumdar S., Application of mobilized Cu-nanoparticles as heterogeneous catalyst for the synthesis of *α-amino phosphonates via A^2 -P coupling, Catal. Sci. Technol.,* 2011, 1, 426 (DOI: 10.1039/c0cy00060d); (c) Yadav S. J., Reddy S. V. B. and Sreedhar P. (2002), An eco-friendly approach for the synthesis of α-aminophosphonates using ionic liquids, *Green Chem.,* 4, 436 (DOI: 10.1039/b203934f); (d) Disale T. S., Kale R. S., Kahandal S. S., Srinivasan G. T. and Jayaram V. R., Choline chloride $ZnCl_2$ ionic liquid: an efficient and reusable catalyst for the solvent free Kabachnik–Fields reaction, *Tetrahedron Lett.,* 2012, 53, 2277 (DOI: 10.1016/j.tetlet.2012.02.054); (e) Hosseini-Sarvari M. (2008), TiO_2 as a new and reusable catalyst for one-pot three-component syntheses of *α-aminophosphonates in solvent-free conditions, Tetrahedron*, 64, 5459 (DOI:10.1016/j.tet.2008.04.016).

12. (a) Snider B. B. and Shi J. Z.(1993), Biomimetic synthesis of (.+-.)-crambines A, B, C_1, and C_2. Revision of the structure of crambines B and C_1, *J. Org. Chem.*, 1993, 58, 382 (DOI: 10.1021/jo00067a014); (b) Kappe O. C. (2000), Biologically active dihydropyrimidones of the Biginelli-type a literature survey, *Eur. J. Med. Chem.,* 35, 1043 (DOI: 10.1016/S0223-5234(00)01189-2).

14. (a) Tamaddon F. and Moradi S. (2013), Controllable selectivity in Biginelli and Hantzsch reactions using nano ZnO as a structure base catalyst, *J. Mol. Catal. A: Chem.*, 370, 117 (DOI: 10.1016/j.molcata.2012.12.005); (b) Chitra S., and Pandiarajan K. (2009), Calcium fluoride: an efficient and reusable catalyst for the synthesis of 3,4-dihydropyrimidin-2(1*H*)-ones and their corresponding 2(1*H*)thione: an improved high yielding protocol for the Biginelli reaction, *Tetrahedron Lett.,* 50, 2222 (DOI: 10.1016/j.tetlet.2009.02.162); (c) Kappe O. C. (2000), Recent Advances in the

Biginelli Dihydropyrimidine Synthesis. New Tricks from an Old Dog, *Acc. Chem. Res*., 33, 879 (DOI: 10.1021/ar000048h); (d) Ma Y., Qian T. C., Wang M. L. and Yang M.(2000), Lanthanide Triflate Catalyzed Biginelli Reaction One-Pot Synthesis of Dihydropyrimidinones under Solvent-Free Conditions, *J. Org. Chem.,* 65, 3864 (DOI: 10.1021/jo9919052).

15. (a) Hummers S. W. and Offeman E. R. (1958), Preparation of Graphitic Oxide, *J. Am. Chem. Soc.,* 1958, 80, 1339 (DOI: 10.1021/ja01539a017); (b) Marcano C. D., Kosynkin V. D., Berlin M. J., Sinitskii A., Sun Z., Slesarev A., Alemany B. L., Lu W. and Tour M. J.(2010), Improved Synthesis of Graphene Oxide, *ACS Nano,* 4, 4806 (DOI: 10.1021/nn1006368).

16. (a) Cravotto G. and Cintas P., The Combined Use of Microwaves and Ultrasound: Improved Tools in Process Chemistry and Organic Synthesis, *Chem. Eur. J.,* 2007, 13, 1902 (DOI: 10.1002/chem.200601845); (b) Einhorn C., Einhorn J. and J. L. Luche, Sonochemistry The Use of Ultrasonic Waves in Synthetic Organic Chemistry, *Synthesis,* 1989, 11, 787 (DOI: 10.1055/s-1989-27398); (c) Lepore D. S. and He Y.(2003), Use of Sonication for the Coupling of Sterically Hindered Substrates in the Phenolic Mitsunobu Reaction, *J. Org. Chem.,* 68, 8261 (DOI: 10.1021/jo0345751); (d) Suslick S. K., Choe B. S., Cichowlas A. A. and Griinstaff W. M.(1991), Sonochemical synthesis of amorphous iron, *Nature,* 353, 414 (DOI:10.1038/353414a0).

17. Gallardo-Macias R. and Nakayama K. (2010), Tin (II) Compounds as Catalysts for the Kabachnik-Fields Reaction under Solvent-Free Conditions: Facile Synthesis of α-Aminophosphonates, *Synthesis,* 1, 57.

18. Xu Q. L., Liu L. Y., Neo G. K., E. T. Kang and G. D. Fu (2011), Reduction of Graphene Oxide by Aniline with Its Concomitant Oxidative Polymerization, *Macromol. Rapid Commun.,* 32, 684 (DOI: 10.1002/marc.201000765).

19. Lv X. and Weng J.(2013), Ternary Composite of Hemin, Gold Nanoparticles and Graphene for Highly Efficient Decomposition of Hydrogen Peroxide, *Sci. Rep.,* 3, 3285.

20. (a) Tuinstra F. and Koenig L. J.(1970), Ternary Composite of Hemin, Gold Nanoparticles and Graphene for Highly Efficient Decomposition of Hydrogen Peroxide, *J. Chem. Phys.*, 53, 1126 (DOI:10.1038/srep03285); (b) Cui P., Lee J., Hwang E. and Lee H.(2011), One-pot reduction of graphene oxide at subzero temperatures, *Chem. Commun.*, 2011, 47, 12370 (DOI: 10.1039/c1cc15569e).

21. Gao W., Alemany B. L., Ci L. and Ajayan M. P. (2009), New insights into the structure and reduction of graphite oxide, *Nat. Chem.,* 1, 403 (DOI: 10.1038/nchem.281).

22. Su C., Acik M., Takai K., Lu J., Hao J. S., Zheng Y., Wu P., Bao Q., Enoki T., Chabal J. Y. and Loh P. K.(2012), Probing the catalytic activity of porous graphene oxide and the origin of this behavior, *Nat. Commun.*, 3, 1298 (DOI:10.1038/ncomms2315).

Chapter 3

Self-assembled monolayer coated gold-nanoparticle catalyzed aerobic oxidation of α-hydroxy ketones in water: an efficient one-pot synthesis of quinoxaline derivative

3.1 Introduction

The exploration of gold nanoparticles (Au-NPs) as catalysts has attracted tremendous attention in recent years in the context of developing environmentally friendly and sustainable routes to a myriad of important organic transformations.[1] The high activity of Au in the nanometer dimension has led to several reports of catalytically active Au-NP systems prepared in the presence of supports, such as poly(N-vinyl-2-pyrrolidone), polyaniline, coordination polymers, dendrimers and solid oxide surfaces such as TiO_2, CeO_2, SiO_2, Al_2O_3 etc.[2] Although the catalytic activities of Au-NPs with various supports have been explored extensively, there are not much studies on the role of surface active groups (strongly or weakly bound) on the Au nanoparticle surfaces. Hence, there are no reports which study the catalytic properties of Au-NPs, governed mainly by the intrinsic surface properties of the nanoparticles, while stabilized with only a self-assembled monolayer, e.g. surface bound via the strong Au–S bond. Undoubtedly, understanding the catalytic behaviour of self-assembled monolayer-coated Au-NPs would be helpful in establishing the guiding principles for the rational design of active Au-NP-based catalytic systems.

Au nanoparticles functions as effective catalysts for oxidation reactions in presence of molecular oxygen. In this regard, developing a simple selfassembled monolayer-coated Au-NP-based catalytic system for the oxidation of α-hydroxy ketones and the synthesis of biologically significant quinoxaline derivatives in water has great significance. Aryl substituted 1,2-diketones and quinoxaline derivatives are utilized as intermediates in the synthesis of chiral ligands and biologically active compounds.[5,6] In addition to their medicinal use, these derivatives have also found technological importance in dyes, semiconductors, anticorrosion in mild steels, as photosensitive coatings in photocurable agents etc.[7] Investigations, such as oxalyl chloride with organostannanes,[8a] oxidation of alkynes,[8b] aldehyde condensation[8c] and oxidation of alcohols[8d,e,f] on the preparation of benzil derivatives have been reported. Similarly, for the preparation of quinoxaline derivatives, generally acid or transition metal (Mn, Ru, Pd, Cu, Ce etc.) catalyzed condensations of an aryl 1,2-dicarbonyl compound with a 1,2-diamine have been reported.[8,9]

There are several other approaches reported for the synthesis of quinoxaline compounds, e.g. the combination of phenyl epoxides or phenacyl bromides with o-phenylenediamines, using catalysts such as Bi(0), $HClO_4/SiO_2$, β-cyclodextrin (β-CD) and TMSCl.[10] Recently, a few reports of one pot syntheses of quinoxaline from α-hydroxy ketones using solid supports, such as KF/Al_2O_3, Ru/C in the presence of β–CD, manganese oxide octahedral molecular sieves (OMS-2), HgI_2, $RuCl_2(PPh_3)_3$–TEMPO, MnO_2 etc.[11] have been published. However, they often suffer from one or more disadvantages, such as the use of organic solvents, unsatisfactory product yields, tedious experimental procedures, non-catalytic, multistep, harsh reaction conditions, difficult operation etc. To overcome all these disadvantages, the development of an effective nanoparticle-based catalytic system is highly desirable for the synthesis of benzils and quinoxaline derivatives that leads to better yields under mild reaction conditions, specifically in water, which is very significant in the context of green chemistry. Herein, we demonstrate the activity of Au nanoparticles stabilized by 4-aminothiophenol towards the aerobic oxidation of aryl substituted α-hydroxy ketones to afford 1,2-diketones in water (Scheme 3.1) adopting a simple and green procedure. The method was extended for the one-pot direct synthesis of aryl substituted quinoxalines via in situ oxidation and condensation reactions between aryl substituted 1,2-diketones with aryl 1,2-diammines.
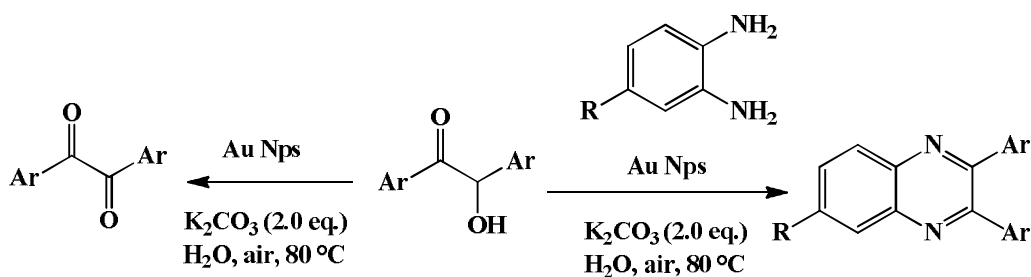
Scheme 3.1 *Syntheses of aryl 1, 2-diketones and quinoxaline derivatives.*

3.2 Characterization of 4-aminothiophenol monolayer-coated Au-NPs

The 4-aminothiophenol monolayer-coated Au-NPs (A) were prepared in a one-pot synthetic procedure using 4-aminothiophenol as both the reducing and

stabilizing agent, according to a literature procedure.[12] Briefly, a solution of 4-aminothiophenol in DMF was added to an aqueous solution of $HAuCl_4$ under continuous stirring (molar ratio of 4-aminothiophenol:$HAuCl_4$ was maintained at 3:1). The nanoparticle formation was confirmed by the optical changes in the solution from wine red initially to a brownish blue color. The Au-NPs were stabilized by thiolates adsorbed onto the surfaces of the nanoparticles.
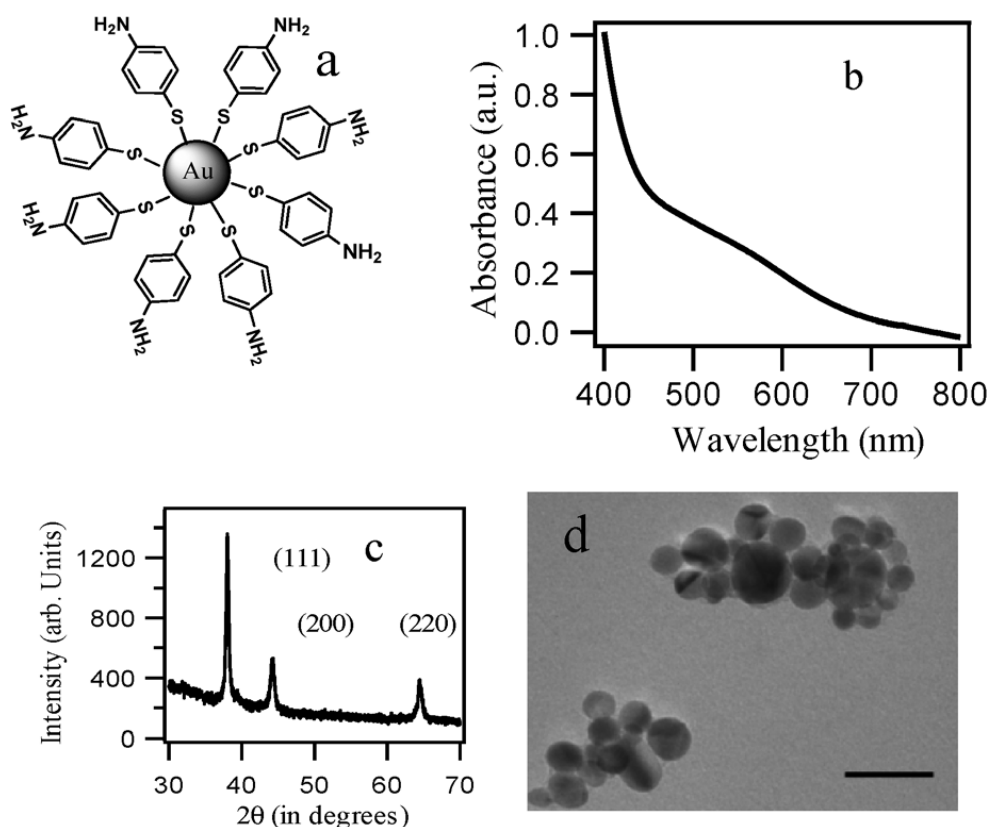

Figure 3.1 *a) Schematic representation of 4-aminothiophenol coated Au-NPs (Catalyst A). (b) UV-visible spectra of the Au-NPs formed using 4-aminothiophenol as both reducing and stabilizing agent in a DMF-water mixture. (c) XRD pattern of the Au-NPs, the corresponding lattice planes are marked. (d) TEM images of the Au-NPs in a DMF-water mixture Scale bar 20 nm.*

Figure 3.1a depicts a representation of the self-assembled monolayer formation of 4-aminothiophenol on the surfaces of the Au-NPs. The appearance of a plasmon resonance band at 530 nm (as shown in Figure 3.1b) confirmed the formation of Au-NPs. The formation of Au-NPs was further confirmed from

the powder X-ray diffraction (XRD) pattern, where the intense peaks corresponding to the (111), (200) and (220) Braggs' reflections are in good agreement with those reported for Au nanoparticles[4a] (Figure 3.1c). The TEM images taken of the synthesized Au-NPs from the DMF–water mixture (1 : 1), as shown in Fig 3.1d, indicated the formation of Au-NPs with an average diameter of 10 ± 3 nm. A closed-packed assembly of smaller Au-NPs was observed, whereas Au NPs were interconnected through hydrogen bonding between the amines and thiol groups or by covalent bonding.

We performed TGA experiment to evaluate the amount of Au in catalyst A. For this, the 4- aminothiophenol coated Au-NPs were dialyzed against water overnight to remove the unbound 4-aminothiophenol and DMF. Then the nanoparticles were dried using lyophilisation and the dried sample was evaluated for Au content using TGA. As shown in Figure 3.2, the typical thermogram showed the onset of desorption at around 150 °C and its completion around 300 °C. No significant mass loss was observed further. The total weight loss was approximately 76% and occurred predominantly through a single-step process.
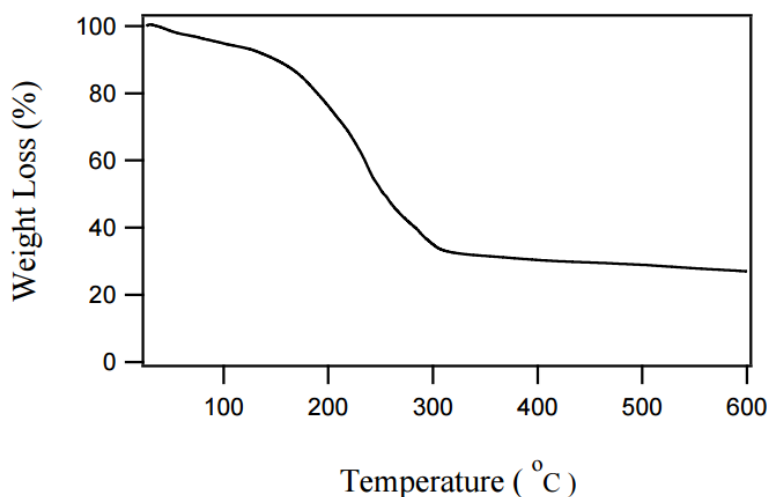
Figure 3.2 TGA graph for 4-aminothiophenol coated Au-NPs (catalyst A).

In order to compare the catalytic properties of the self-assembled monolayer systems which have terminal thiolate functional groups on the Au surface, we also synthesized undecanethiol-coated Au-NPs (catalyst B**).**
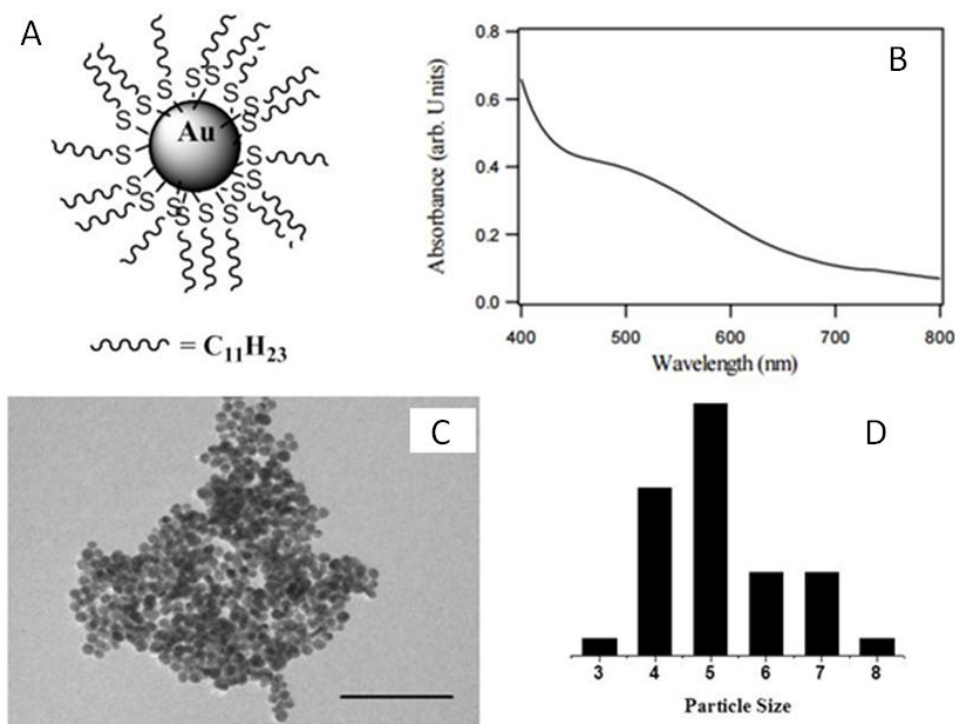
Figure 3.4 (A) Schematic representation for 1-undecanethiol coated Au-NPs (catalyst B) (B) UV-visible spectra of 1-undecanethiol coated Au-NPs in toluene (C) TEM image of Au-NPs coated with 1-undecanethiol, the nanoparticles were deposited from toluene solution. Scale bar 100 nm (D) particle size distribution.

3.3 Aerobic Oxidation of aryl-α-hydroxy ketones and aryl substituted quinoxalines

In order to evaluate the performance of Au nanoparticles capped with thiol containing monolayers, we optimized the oxidation of α-hydroxy ketone at different reaction conditions (temperature, catalyst loading and base) using two catalytic systems (4-aminothiophenol coated Au Nanoparticles and 1-undecathiol coated Au-nanoparticles).

Table 3.1 Optimization of reaction conditions for the aerobic oxidation of benzoin to benzyl.

Entry	Catalysts	Base	Temp (°C)	Yield[a] (%)
1	Nil	Nil	60	2
2	Nil	Na_2CO_3	60	-
3	Nil	K_2CO_3	60	-
4	A (4.00 atom %)	Nil	80	3
5	B (2.50 atom %)	K_2CO_3	60	15
6	A (2.50 atom %)	K_2CO_3	40	22
7	A (2.50 atom %)	K_2CO_3	60	38
8	A (2.50 atom %)	K_2CO_3	80	83
9	A (0.08 atom %)	K_2CO_3	80	40
10	A (1.6 atom %)	K_2CO_3	80	59
11	A (4.00 atom %)	K_2CO_3	80	91
12	A (4.00 atom %)	K_2CO_3	80	7[b]
13	**A (4.00 atom %)**	**K_2CO_3**	**80**	**92[c]**
14	A (4.00 atom %)	Na_2CO_3	80	27
15	A (4.00 atom %)	Cs_2CO_3	80	83

Unless otherwise specified, all reactions were carried out with benzoin (1.0 mmol), base (2.0 mmol) and water (10 mL) in the presence of air at the specified temperature and catalysts. [a]Isolated product after column chromatography. [b]Reaction was carried out in an argon atmosphere. [c]Reaction was carried out in an oxygen atmosphere.

We started optimization with this model oxidation reaction between benzoin (1.0 mmol), K_2CO_3 (2.0 mmol) and water (10 mL) in the presence of catalyst B (2.5 atom %) at 60 °C for 4 h under air. Although the reaction did not progress well, we were able to isolate the oxidized product in a 15% yield (Table 3.1, entry 5). As a consequence, this significant result prompted us to investigate the aerobic oxidation of benzoin. It was observed that the reaction proceeded very slowly in the absence of base, catalyst and air (entries 1–3 and 12, Table 3.1).

To improve the catalytic activity of this reaction, catalyst A was examined with different catalytic loading. As shown in Table 3.1, with a 2.5 atom% loading of catalyst A, the desired oxidized product benzil was obtained in a 22% yield after reacting at 40 °C for 4 h (entry 6). For this catalyst, on further increasing the reaction temperature to 80 °C, the yield improved dramatically

from 22% to 83% for the same reaction time (Table 3.1, entry 8). Among the bases, K_2CO_3 was the best choice compared to Na_2CO_3 and Cs_2CO_3 in terms of reactivity under similar reaction conditions (Table 3.1, entries 14 and 15). In particular, there was a substantial enhancement in the yield when the amount of catalyst was increased from 2.5 to 4 atom%. From various reaction conditions, as shown in Table 3.1, it is obvious that a superior result was obtained under the conditions mentioned in entry 11 (91% yield). In particular, there was no significant improvement in yield when the reaction was carried out in the presence of oxygen instead of air (Table 3.1, entry 13).

3.3.1 Synthesis of 1, 2 aryl diketones

To understand the scope and limitation of this novel aerobic oxidation reaction, we studied several aryl substituted α-hydroxy ketones using the self-assembled monolayer-coated Au-NPs, catalyst A (4 atom %), at standard reaction conditions and the results are compiled in Table 3.2. As is evident from Table 3.2, aryl α-hydroxy ketones with various substituents on the aromatic ring all produced the desired oxidized product in good to excellent yields (entries 2–4, Table 3.2). It should be pointed out that electron withdrawing substituents (entry 4, Table 3.2) on the aromatic ring increased the yield when compared to electron donating groups (entries 2 and 3, Table 3.2). Hetero-aryl groups also afforded the desired oxidized products in good yields at 60 °C. The reaction conditions were mild enough to tolerate furan, thiophene and pyridine rings (Table 3.2, entry 5-8). The isolated products were fully characterized from their spectral data and by direct comparison with the reported data. The catalytic loading was much lower than the earlier reported methods.

Table 3.2 Substrate scope of synthesis of 1,2 diketones

En-1, 91 %, 4 hr

Me

En-2, 71 %, 5 hr

OMe

MeO

En-3, 70 %, 5 hr

F

F

En-4, 95 %, 3.5 hr

N

N
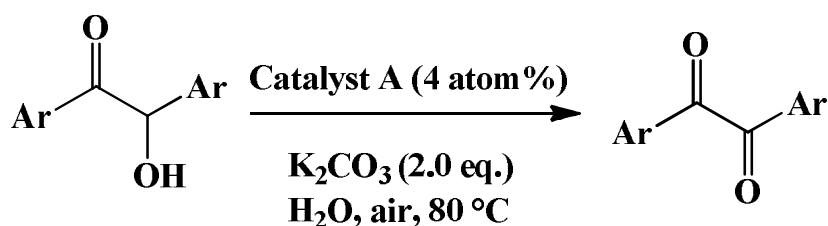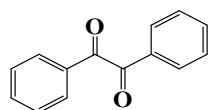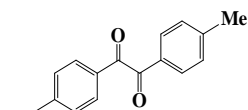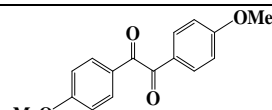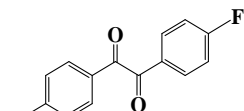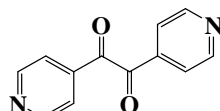
En-5, 90 %, 4 hr

En-6, 66 %, 6 hr
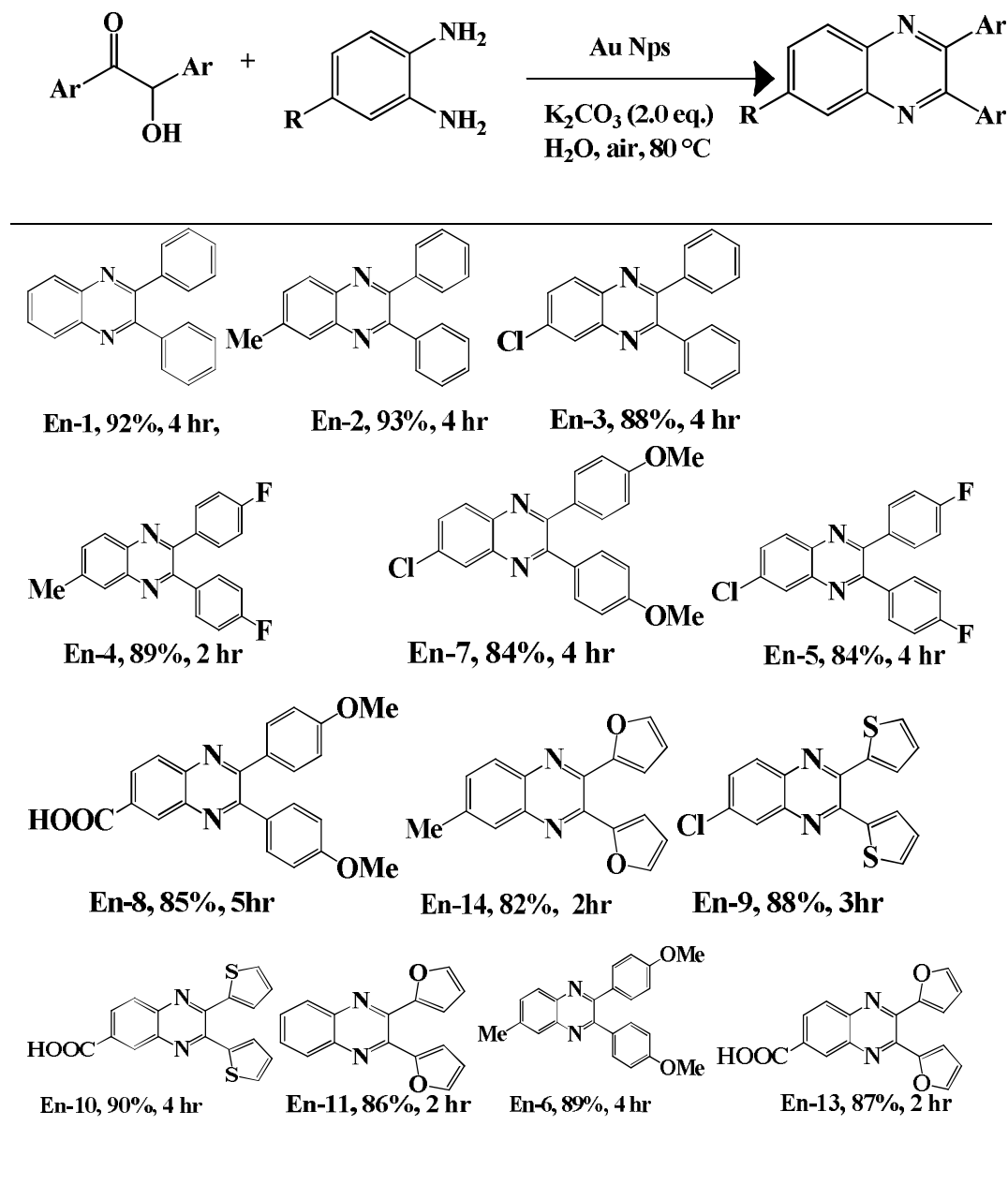
S

S
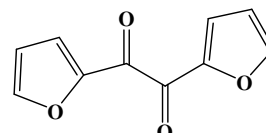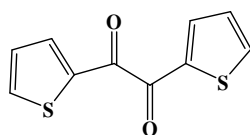
En-7, 93 %, 5 hr
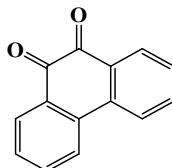
En-8, 82 %, 4 hr

3.3.2 Synthesis of quinoxaline

After successfully developing a simple, green and efficient catalytic system for the aerobic oxidation of α-hydroxy ketones to aryl 1,2-diketones, catalyzed by Au-NPs, we then applied the same procedure to a one-pot tandem oxidation and subsequent condensation reactions of aryl α-hydroxy ketones with aryl 1,2-diamines for the synthesis of functionalized quinoxaline derivatives using catalyst A in water. As shown in Table 3.3, wide range of structurally varied aryl substituted and un-substituted α-hydroxy ketones with aryl 1,2-diamine worked very well in this procedure to provide the corresponding quinoxaline derivatives in high to excellent yields. The synthesistic procedure for quinoloxine is given bellow. Several sensitive functional groups, such as -OMe, -Cl, -F and -CO$_2$H, remained unaffected under the present reaction conditions (Table 3.3). It is noteworthy that for the first time, 3,4-diaminobenzoic acid has been successfully used for this condensation reaction, providing excellent yields (entries 8, 10, and 13, Table 3.3). Our Au-NP catalytic system is very efficient for the synthesis of quinoxaline derivatives when compared to established procedures. In addition, the bench-scale preparation of the oxidized product of benzoin under our conditions was investigated. Catalyst A (80 atom %) was added to a stirred reaction mixture containing benzoin (20 mmol), K$_2$CO$_3$ (40 mmol) and water (200 mL) and

heated at 80 °C for 6 h. The benzil product was isolated with a 79% yield. This exciting result reveals that our present conditions can be applied for milligram to gram scale syntheses.

Table 3.3 Substrate scopes of quinoxaline

En-1, 92%, 4 hr,   En-2, 93%, 4 hr   En-3, 88%, 4 hr

En-4, 89%, 2 hr   En-7, 84%, 4 hr   En-5, 84%, 4 hr

En-8, 85%, 5hr   En-14, 82%, 2hr   En-9, 88%, 3hr

En-10, 90%, 4 hr   En-11, 86%, 2 hr   En-6, 89%, 4 hr   En-13, 87%, 2 hr

3.4 Recyclability of Au nanocatalyst

The reusability of the Au-NPs catalysts was investigated. As the 4-aminothiophenol coated Au-nanoparticles were acting as heterogeneous

catalysts for the oxidation of α-hydroxy ketones, we have performed the reusability study of catalyst A for the same condition of model reaction up to 3 cycles (figure 3.5). The recyclability of catalyst A was examined for the aerobic oxidation of benzoin. After completion of reaction, the organic compounds were extracted with diethyl ether (3×10 mL). The aqueous phase was isolated that was used for the next run. The activity of the nanoparticle catalysts decreased in a sequence of cycles while applied for the aerobic oxidation of benzoin to benzyl. The desired products were obtained in 71% for the Au nanoparticles recovered after 1st run and 53% after the 2nd run (Figure 3.5).
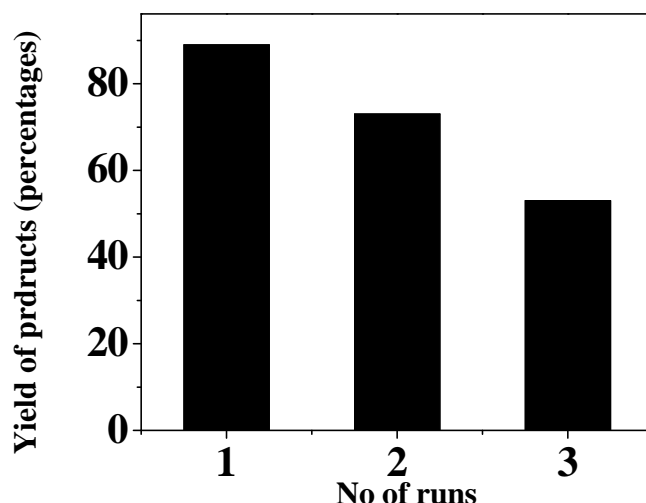
Figure 3.5 Recyclability study of 4-amino thiophenol coated Au-nanoparticles.

It was observed visually that the nanoparticles were agglomerated after successive runs and precipitations were observed after reactions. The catalytic activity of Au nanoparticles The recovered nanoparticles after the 1st and 2nd oxidations were examined by TEM measurements, which showed substantial agglomeration of the particles after the 2nd run. The TEM images were recorded from a concentrated aqueous solution and are shown in Figure 3.6. The agglomeration might be due to several factors, such as interactions among self-assemble monolayers, effect of salt (base) and temperature.[12,13] With the increase in size of the nanoparticles, the effective surface area decreased considerably, which resulted in decrease of catalytic activities of the Au-NPs.
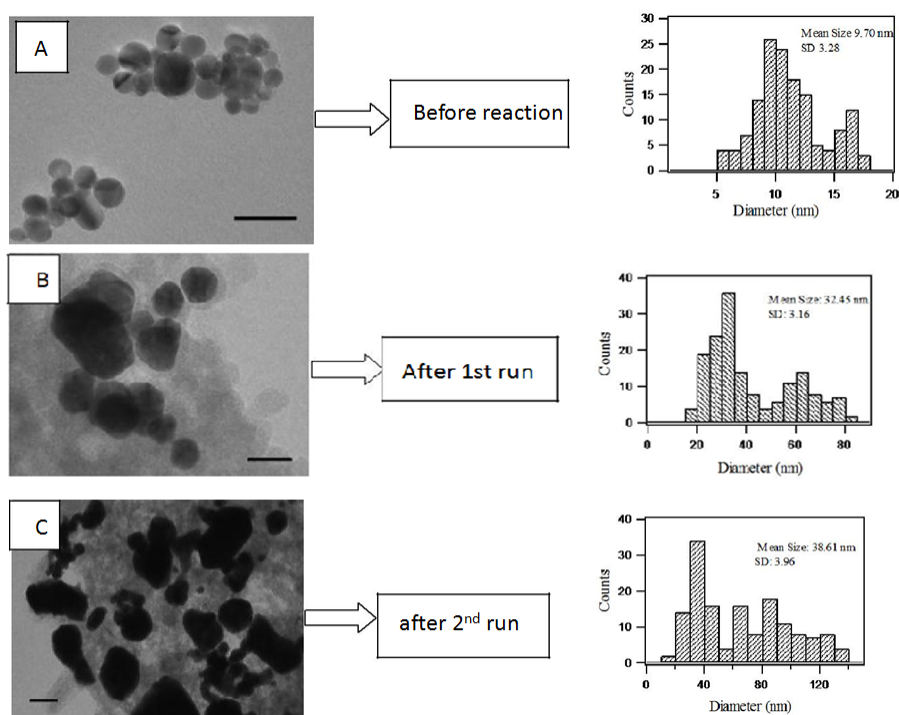
Figure 3.6 *Transmission electron micrograph and corresponding particle size distribution of catalyst A as synthesized (a) after the first oxidation (b) after the 2nd oxidation (c). The nanoparticles were deposited from water. Scale bar 50 nm.*

3.5 Proposed mechanism

We propose that the probable mechanism of this reaction follows a similar path to that reported earlier for the Au-NP-catalyzed aerobic oxidation reactions of alcohol. At first, the absorption of the oxygen onto the Au surface enhanced the electron density that facilitated the absorption of oxy aninon of alcohol. The ketone is formed due to the abstraction of hydrogen by the O_2^- species. From the reaction mechanism, the lower catalytic efficiency of the 1-undecanethiol-protected Au-NPs when compared to the 4-aminothiophenol-coated Au-NPs was not surprising. The formation of a highly dense monolayer in the case of the 1-undecanethiol-coated Au-NPs[14] probably retarded the absorption of bulky molecules onto the Au surface.
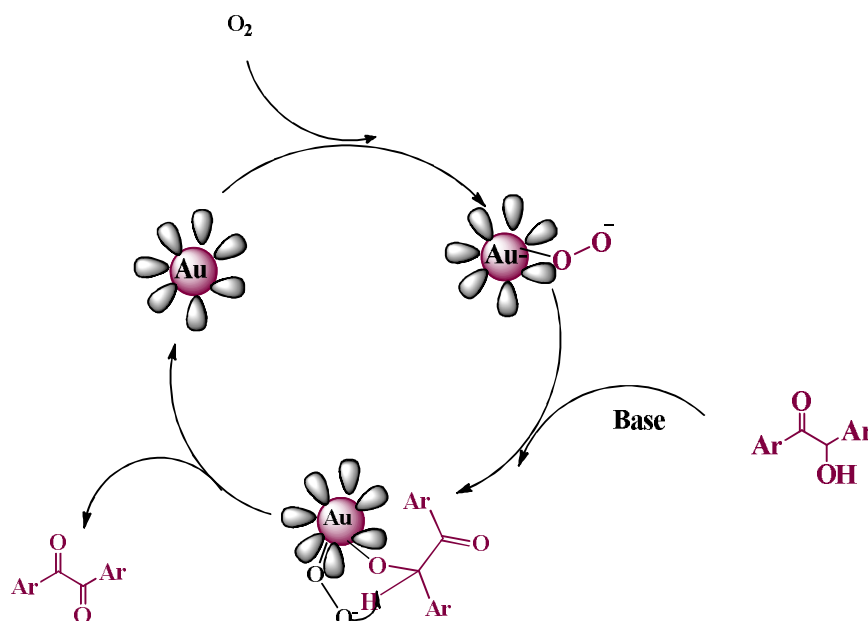
Figure 3.7 *Proposed mechanism for the aerobic oxidation of a-*hydroxy *ketones by the self-assembled monolayer-protected Au-NPs.*

3.6 Conclusion

In this chapter, we have investigated the catalytic activity of self-assembled monolayer-coated Au-NPs for the aerobic oxidation of aryl substituted α-hydroxy ketones to aryl 1,2-diketones and extended this reaction for a one-pot synthesis of highly biologically significant quinoxaline derivatives in water. Our current methods avoid the use of acid, highly toxic reagents, hazardous organic solvents, multisteps etc. In addition, the simplistic synthesis of the catalyst, operational simplicity, high yields, catalytic and environmentally friendly reaction conditions make them attractive. This result should encourage new applications for self-assembled monolayer-coated Au-NPs in organic syntheses as efficient catalysts. In the present system, the reusability of the catalyst was limited after few cycles of oxidation due to agglomeration of the nanoparticles. However, the development of suitable stabilizers to prevent agglomeration as well as enhance the catalytic efficiency of the nanoparticles would offer significant applications for self-assembled monolayer-coated nanoparticles in organic syntheses.

3.7 Materials and methods

Hydrogen tetrachloroaurate(III) hydrate, 4-aminothiophenol and 1-undecanethiol were purchased from Aldrich Chemicals. N, N-Dimethylformamide (DMF), hydrochloric acid (HCl) were purchased from Merck India. All these chemicals were used without further purification. Milli Q water was used throughout the experiment. The starting materials were either purchased from commercial sources or synthesized by known literature procedures.

3.7.1 Synthesis of 4-aminothiophenol coated Au-nanoparticles

To a stirred solution of 4-aminothiophenol (375 mg, 3.0 mmol) in DMF (20 mL) was added 20 mL of an aqueous solution of $HAuCl_4$ (394 mg, 1.0 mmol). The stirring was continued for 30 minutes at room temperature. The solution turned wine red immediately and finally became brownish blue indicating the formation of Au-NPs. For a 3:1 ratio of 4-aminothiophenol and $HAuCl_4$ the nanoparticles are stable for much longer time without any visible agglomeration at room temperature. The nanoparticles were precipitated by centrifugation at 10000 rpm, purified by washing with water and ether. Dialysis was performed against water to remove any excess unbound 4-aminothiophenol. The catalyst was finally freeze-dried using lyophilizer for characterization.
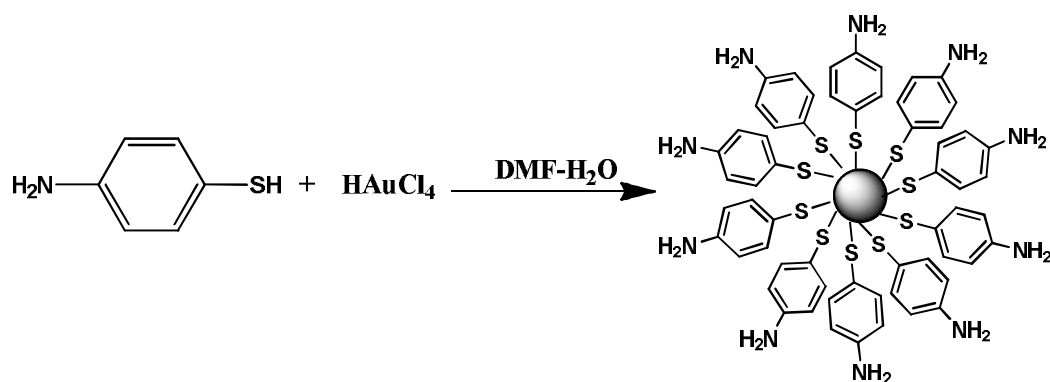
Figure 3.8 *Schematic presentation of synthesis 4-aminothiophenol-coated Au-NPs (catalyst A).*

3.7.2 Synthesis of 1-undecanthiol coated Au-nanoparticles

$$RSH \quad + \quad HAuCl_4 \xrightarrow[\substack{CHCl_3}]{\substack{NaBH_4,\ TOAB}}$$

TOAB= tetra octyl ammonium bromide

$\sim\sim\sim = C_{11}H_{23}$
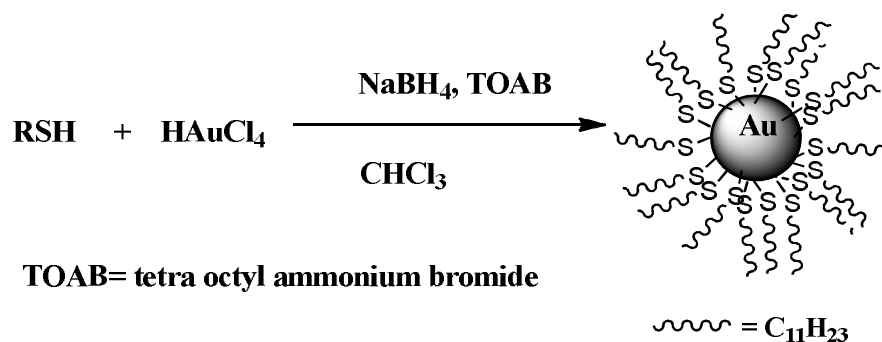
Figure 3.9 Schematic diagram of synthesis of 1-undecathiol capped Au-nanoparticles.

The 1-undecanethiol capped Au-NPs were prepared by well-known Brust method. To a stirred solution of tetraoctylammonium bromide (2.18 g, 4.0 mmol) in toluene was added an aqueous solution of HAuCl$_4$ (394 mg, 1.0 mmol) at RT. After vigorous stirring, the toluene solution turned violet indicating the transfer of AuCl$_4$ to the organic phase. After removing the aqueous phase, 1-undecanethiol (564 mg, 3.0 mmol) was added to the toluene solution and was stirred for 30 minutes. Then NaBH$_4$ (190 mg, 5.0 mmol) was added and the reaction mixture turned brownish indicating the formation of Au-NPs. The stirring was continued for overnight. Finally the catalyst was isolated by evaporating the organic solvents, followed by washing with ethanol, acetone and dried under vacuum

3.7.3 Synthesis of 1, 2 diketones

To a stirred of heterogeneous mixture of (1.0 mmol) in water (10 mL) were added K$_2$CO$_3$ (276 mg, 2.0 mmol) and 4-aminothiophenol capped Au-NPs (28 mg, 4 atom %) at RT. Then reaction mixture was heated at specified temperature and time under air. The progress of the reaction was monitored by TLC. After completion of reaction, the mixture was extracted with ethyl acetate (3 × 10 mL), washed with water and brine. The organic phase was evaporated by rotary evaporator under reduced pressure to give the crude product which was further purified by flash column chromatography over silica gel to furnish the pure product. All the products were characterized by

corresponding spectroscopic data which were in good agreement with the reported data.

3.7.4 Synthesis of quinoxaline

A mixture containing benzoin (212 mg, 1.0 mmol), o-phenylenediamine (108 mg, 1.0 mmol), K_2CO_3 (276 mg, 2.0 mmol) and catalyst A (28 mg, 4.0 atom%) in 10 ml of water was stirred and heated at 80 °C under air. After completion of the reaction (monitored by TLC), the reaction mixture was extracted with ethyl acetate. The organic layer was dried over anhydrous Na_2SO_4, followed by evaporation of the solvent to obtain the crude product which was purified by column chromatography over silica gel to give the pure product (259 mg, 92% yield). The product was characterized by the corresponding spectroscopic data, which was in good agreement.

NMR data of Quinoxalines

1.

En-1
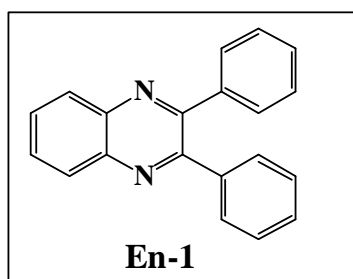
^{1}H NMR (400 MHz, CDCl$_3$) δ (ppm): 8.10 (q, 2H), 7.68 (q, 2H), 7.43 (dd, 4H), 7.23 (m, 6H); ^{13}C NMR (100 MHz, CDCl$_3$) δ (ppm): 153.5, 141.2, 139.1, 130, 129.9, 129.2, 128.8, 128.3.

2.

En-9
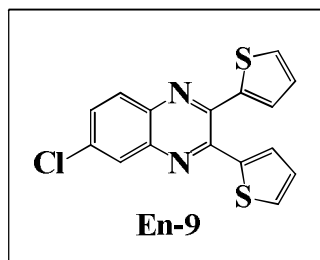
^{1}H NMR (CDCl$_3$, 400 MHz): δ 7.98 (d, J = 8.8 Hz, 1H), 7.92(d, J = 8 Hz, 1H), 7.57 (d, J = 4Hz, 1H), 7.43(d, J = 2 Hz, 2H), 7.20-7.18 (m, 2H), 6.96 (q, J = 2 Hz, 2H); ^{13}C NMR (CDCl$_3$, 100 MHz): δ 147.50, 146.75, 141.17, 140.08,

139.03, 131.05, 130.03, 129.71, 129.54, 129.16, 127.70, 127.64, 117.54, 116.25.

3.

En-2
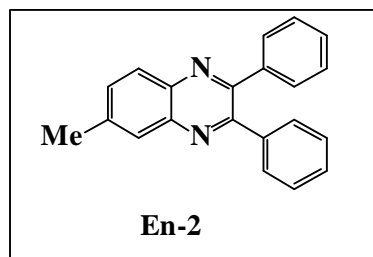
^{1}H NMR (CDCl$_3$, 400 MHz): δ 7.97 (d, J = 8 Hz, 1H), 7.8(s, 1H), 7.50 (dd, J = 4 Hz, 1H), 7.41 (d, J = 2 Hz, 4H), 7.24-7.21 (m, 7H); ^{13}C NMR (CDCl$_3$, 100 MHz): δ 153.33, 152.58, 141.30, 140.48, 139.72, 139.23, 132.29, 129.83, 128.71, 128.68, 128.62, 128.38, 128.22, 128.03, 21.91.

4.

En-11
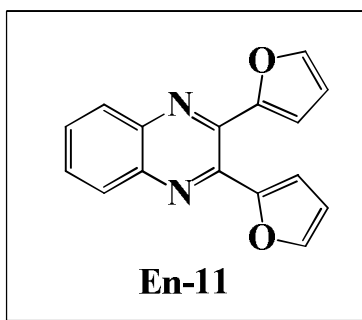
H NMR (CDCl$_3$, 400 MHz): δ 8.08-8.05(m, 2H), 7.69-7.67(m, 2H), 7.5(s, 1H), 6.64(s, 1H), 6.58 (d, J = 8.8 Hz, 4H), 6.5 (s, 1H); ^{13}C NMR (CDCl$_3$, 100 MHz): δ 150.22, 144.23, 144.23, 142.67, 140.65, 130.41, 129.13, 116.77, 113.00, 111.92.

5.

En-8
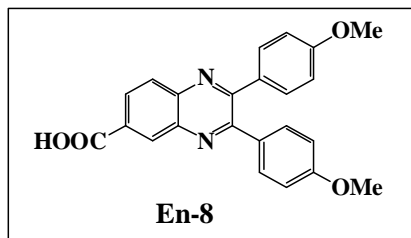
Yield: 328 mg, 85%; ^{1}H NMR (DMSO-d6, 400 MHz): δ 3.83 (s, 6H), 6.99 (d, J = 8.8 Hz, 4H), 7.52 (2d, J = 8.8 Hz, 4H), 8.20 (d, J = 8.8 Hz, 1H), 8.28-8.31(m, 1H), 8.64 (s, 1H); ^{13}C NMR (DMSO-d6, 100 MHz): δ 57.8, 57.9, 114.1, 129.5, 129.6, 131.0, 131.2, 131.3, 131.6, 131.7, 132.1, 139.9, 142.6, 154.0, 154.7, 160.4, 160.5, 167.1.

6.

En-10
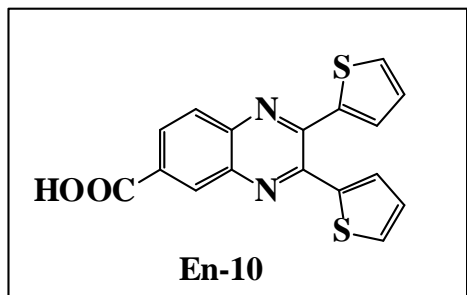
^{1}H NMR (400 MHz, DMSO-d^6): δ 7.15-7.19 (m, 2H), 7.31-7.34 (m, 2H), 7.86-7.89 (m, 2H), 8.15 (d, J = 8.8 Hz, 1H), 8.28 (d, J_1 = 10.4 Hz, 1H), 8.56 (s, 1H), 13.52 (s, 1H); ^{13}C NMR (DMSO-d6, 100 MHz): δ 126.5, 126.6, 127.5, 128.4, 128.5, 128.8, 128.9, 129.0, 129.4, 130.9, 137.7, 139.1, 139.3, 140.4, 145.9, 146.5, 165.1

7.

En-13
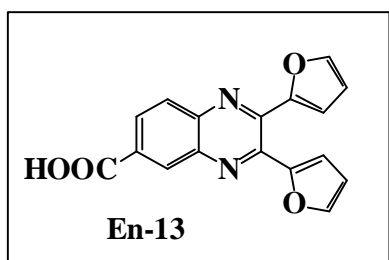
^{1}H NMR (400 MHz, DMSO-d6, ppm): δ 6.77-6.83(m, 4H), 7.93 (m, 2H), 8.15 (d, J = 8.8 Hz, 1H), 8.26 (d, J = 8.8 Hz, 1H), 8.55 (s, 1H); 13C NMR (100 MHz, DMSO-d6): δ 111.0, 111.1, 112.1, 112.7, 127.8, 128.7, 129.4, 131.1, 137.8, 140.5, 141.6, 142.1, 143.9, 144.3, 148.7, 148.7, 165.1.

8.

En-3
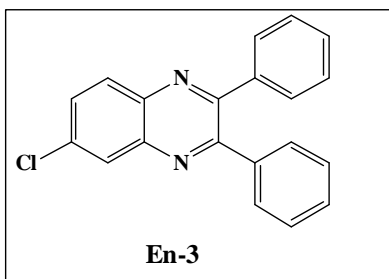
^{1}H NMR (400 MHz, DMSO-d^6, ppm): δ 8.06(d, J= 2Hz, 1H), 7.97 (d, J= 8Hz, 1H), 7.59(dd, J_1= 2Hz, J_2= 2Hz, 1H), 7.41(d, J= 8Hz, 5H), 7.27-7.21(m, 9H); 13C NMR (100 MHz, DMSO-d6): δ

154.3, 153.63, 141.49, 139.73, 138.73, 135.67, 130.96, 130.43, 129.86, 129.12, 129.12, 129.044, 128.46, , 128.33, 128.08, 127.78.

3.8 References

1. (a) Biella S., and Rossi M.(2003), Gas phase oxidation of alcohols to aldehydes or ketones catalysed by supported gold, *Chem. Commun.,* 378-379 (DOI: 10.1039/B210506C); (b) Milone C., Ingoglia R., Tropeano M., Neri G. and Galvango S. (2003), First example of selective hydrogenation of unconstrained *α, β*-unsaturated ketone to *α, β*-unsaturated alcohol by molecular hydrogen, *Chem. Commun.,* 868 (DOI: 10.1039/B212441F); (c) Haruta M. (2005), Catalysis: Gold rush *Nature*, 437, 1098 (DOI:10.1038/4371098a); (d) Pina D. C., Falletta E., Prati L. and Rossi M. (2008), Selective oxidation using gold, Chem. *Soc. Rev*., 37, 2077 (DOI: 10.1039/B707319B); (e) Hashmi K. S. A. and Hutchings J. G.(2006), Selective oxidation using gold, *Angew. Chem. Int. Ed.*, 45, 7896(DOI: 10.1039/b707319b); (f) Hashmi K. S. A. (2007), Gold-Catalyzed Organic Reactions, *Chem. Rev.,* 107, 3180 (DOI: 10.1021/cr000436x); (g) Jimenez-Nunez E. and Echavarren M. A. (2007), Molecular diversity through gold catalysis with alkynes, *Chem. Commun.,* 333 (DOI: 10.1039/b612008c).

2. (a) Haruta M. (1997), Size- and support-dependency in the catalysis of gold, *Catal. Today*., 36, 153 (DOI: 10.1016/S0920-5861(96)00208-8); (b) Ishida T. and Haruta M. (2007), Gold Catalysts: Towards Sustainable Chemistry, *Angew. Chem., Int. Ed.,* 46, 7154 (DOI: 10.1002/anie.200701622); (c) Min K. B., and Friend M. C. (2007), Heterogeneous Gold-Based Catalysis for Green Chemistry: Low-Temperature CO Oxidation and Propene Oxidation, *Chem. Rev*., 107, 2709 (DOI: 10.1021/cr050954d); (d) Hutchings J. G. and Brust H. (2008), Gold an introductory perspective, *Chem. Soc. Rev.,* 37, 1759 (DOI: 10.1039/B810747P); (e) Corma A., Garcia H (2008), Supported gold nanoparticles as catalysts for organic reactions, *Chem. Soc. Rev*., 37, 2096 (DOI: 10.1039/B707314N); (f) Chen S. M. and Goodman W. D. (2004), The Structure of Catalytically Active Gold on Titania, *Science,* 306, 252 (DOI: 10.1126/science.1102420); (g) Fang W., Chen J., Zhang Q., Deng W. and Wang Y. (2011), Hydrotalcite-Supported Gold Catalyst for the Oxidant-

Free Dehydrogenation of Benzyl Alcohol: Studies on Support and Gold Size Effects, *Chem. Eur. J.*, 17, 1247 (DOI: 10.1002/chem.201002469); (h) Tsunoyama, H., Ichikuni, N., Sakurai, H., & Tsukuda, T. (2009), Effect of electronic structures of au clusters stabilized by poly(N-vinyl-2-pyrrolidone) on aerobic oxidation catalysis, *J. Am. Chem. Soc.*, 131, 7086–7093 (DOI: 10.1021/ja810045y); (j) Liu H., Liu Y., Li Y., Tang Z., & Jiang H. (2010), Metal−Organic Framework Supported Gold Nanoparticles as a Highly Active Heterogeneous Catalyst for Aerobic Oxidation of Alcohols, *J. Phys. Chem. C.*, 114, 13362–13369 (DOI: 10.1021/jp105666f); (k) Ishida T., Nagaoka M., Akita T., & Haruta M. (2008), Deposition of gold clusters on porous coordination polymers by solid grinding and their catalytic activity in aerobic oxidation of alcohols, *Chemistry.*, 14, 8456–8460 (DOI:10.1002/chem.200800980); (l) Tsukuda, T., Tsunoyama, H., & Sakurai, H. (2011), Aerobic oxidations catalyzed by colloidal nanogold, *Chem. Asian. J.*, 6, 736–748 (DOI:10.1002/asia.201000611).

3. (a) Ranu, B. C., Samanta, S., & Guchhait, S. K. (2001), Stereoselective reduction of aryl-substituted gem dibromides to vinyl bromides by indium metal, *J. Org. Chem.,* 66, 4102–4103 (DOI:10.1021/jo0102314); (b) Ranu, B. C., Samanta, S., & Guchhait, S. K. (2002), Zinc tetrafluoroborate catalyzed Mannich-type reaction of aldimines and silyl enol ethers in aqueous medium, *Tetrahedron.*, 58, 983–988 (DOI:10.1016/S0040-4020(01)01177-2); (c) Hayashi Y., Samanta S., Gotoh H., & Ishikawa H. (2008), Asymmetric diels-alder reactions of α,β-unsaturated aldehydes catalyzed by a diarylprolinol silyl ether salt in the presence of water, *Angew. Chem. Int. Ed,* 47, 6634–6637 (DOI:10.1002/anie.200801408).

4. (a) Sarma T. K., Chowdhury D., Paul, A., & Chattopadhyay A. (2002), Synthesis of Au nanoparticle-conductive polyaniline composite using H_2O_2 as oxidizing as well as reducing agent, *Chem. Commun.,* 111, 1048–1049. (DOI:10.1039/b201014c); (b) Majumdar G., Goswami M., Sarma T. K., Paul A., & Chattopadhyay A. (2005), Au nanoparticles and polyaniline coated resin beads for simultaneous catalytic oxidation of glucose and colorimetric detection of the product, *Langmuir*, 21, 1663–1667 (DOI:10.1021/la047440e); c) Sarma T. K., & Chattopadhyay A. (2004), Reversible encapsulation of

nanometer-size polyaniline and polyaniline Au-nanoparticle composite in starch, *Langmuir.*, 20, 4733–4737 (DOI:10.1021/la0495884).

5. Ryoda A., Yajima, N., Haga, T., Kumamoto, T., Nakanishi, W., Kawahata, M. Ishikawa, T. (2008), Optical resolution of (±)-1,2-bis(2-methylphenyl)ethylene-1,2- diamine as a chiral framework for 2-iminoimidazolidine with 2-methylphenyl pendant and the guanidine-catalyzed asymmetric michael reaction of tert-butyl diphenyliminoacetate and ethyl acrylate, *J. Org. Chem.,* 73, 133–141 (DOI:10.1021/jo701923z).

6. (a) He W., Myers M. R., Hanney B., Spada A. P., Bilder G., Galzcinski H., Perrone M. H. (2003), Potent quinoxaline-based inhibitors of PDGF receptor tyrosine kinase activity. Part 2: the synthesis and biological activities of RPR127963 an orally bioavailable inhibitor, *Bioorganic & Medicinal Chem. Letts.*, 13, 3097–3100 (DOI: 10.1016/S0960-894X(03)00655-3); (b) Gomtsyan A., Bayburt E. K., Schmidt R. G., Guo Z. Z., Perner R. J., Didomenico S., Lee C. H. (2005), Novel transient receptor potential vanilloid 1 receptor antagonists for the treatment of pain; Structure-activity relationships for ureas with quinoline, isoquinoline, quinazoline, phthalazine, quinoxaliue, and cinnoline moieties. *J. Med. Chem.*, *48*, 744–752 (DOI:10.1021/jm0492958); (c) Branch N. T. (2010), An efficient synthesis of quinoxalines catalyzed by monoammonium salt of 12-tungstophosphoric acid, *Chem. Eur. J.,* 1, 291–293(DOI:10.5155/eurjchem.1.4.291).

7. (a) Dailey, S., Feast, W. J., Peace, R. J., Sage, I. C., Till, S., & Wood, E. L. (2001), Synthesis and device characterisation of side-chain polymer electron transport materials for organic semiconductor applications, *J. Mater. Chem.,* 11, 2238–2243 (DOI:10.1039/b104674h); (b) Rincón C. D., Hernández E., Alonso M. I., Garriga M., Wasim S. M., Rincón C., & León M. (2001), Optical transitions near the band edge in bulk $CuIn_x Ga_{1-x}Se_2$ from ellipsometric measurements, *Mater. Chem. Phys..*, 70, 300–304 (DOI:10.1016/S0254-0584(00)00518-6).

8. (a) Giraud, A., Provot, O., Peyrat, J. F., Alami, M., & Brion, J. D. (2006), Microwave-assisted efficient synthesis of 1,2-diaryldiketones: a novel oxidation reaction of diarylalkynes with DMSO promoted by $FeBr_3$,

Tetrahedron., 62, 7667–7673 (DOI:10.1016/j.tet.2006.05.072); (b) Shimakawa Y., Morikawa T., & Sakaguchi S. (2010) Facile route to benzils from aldehydes via NHC-catalyzed benzoin condensation under metal-free conditions, *Tetrahedron Lett.*, 51, 1786–1789 (DOI:10.1016/j.tetlet.2010.01.103); (c) Joo. C., Kang S., Kim S. M., Han H., & Yang J. W. (2010), Oxidation of benzoins to benzils using sodium hydride, *Tetrahedron Lett.*, 51, 6006–6007 (DOI:10.1016/j.tetlet.2010.09.028); (d) Kashiwabara T., & Tanaka M. (2009), Synthesis of 1, 2-Diketones by the Transition Metal-Catalyst-Free Reaction of *α*-Oxo Acid Chlorides or Oxalyl Chloride with Organostannanes, *J. Org. Chem.*, *74*, 3958–3961 (DOI:10.1021/jo802814r); e) Saio D., Amaya T., & Hirao T. (2010), Redox-active catalyst based on poly(anilinesulfonic acid)supported gold nanoparticles for aerobic alcohol oxidation in water, *Adv. Synth. Catal.*, *352*, 2177–2182 (DOI:10.1002/adsc.201000451).

9. (a) Bhosale R. S., Sarda S. R., Ardhapure S. S., Jadhav W. N., Bhusare S. R., & Pawar R. P. (2005), An efficient protocol for the synthesis of quinoxaline derivatives at room temperature using molecular iodine as the catalyst, *Tetrahedron Lett.*, 46, 7183–7186 (DOI:10.1016/j.tetlet.2005.08.080); (b) More V. S., Sastry V. N. M., Wang C.C. and Yao F. C.(2005), Synthesis of 1-, 2-, and 6-Azulenethiols, *Tetrahedron Lett.,* 46, 6345 (DOI:10.1016/S0040-4039(01)93890-0); (c) Darabi R. H., Mohandessi S., Aghapoor S. and Mohsenzadeh F.(2007), A recyclable and highly effective sulfamic acid/MeOH catalytic system for the synthesis of quinoxalines at room temperature, *Catal. Commun.,* 8, 389; (d) Heravi M., Taheri S., Bakhtiari K. and Oskooie A. H.(2007), On Water: A practical and efficient synthesis of quinoxaline derivatives catalyzed by $CuSO_4$:$5H_2O$**,** *Catal. Commun.,* 8, 211; (e) Huang K. T., Wang R., Shi L., and Lu X. X.(2008), Montmorillonite K-10: An efficient and reusable catalyst for the synthesis of quinoxaline derivatives in water, *Catal. Commun.,* 9, 1143; (f) Alinezhad H., Tajbakhsh M., Salehian F., & Biparva P. (2011), Nanoparticles as an Efficient and Recyclable Catalyst, *Bull. Korean Chem. Soc.,* 32, 3720–3725 (DOI:10.5012/bkcs.2011.32.10.3720).

10. (a) Ghosh P., & Mandal A. (2012), Sodium dodecyl sulfate in water: greener approach for the synthesis of quinoxaline derivatives, *Green. Chem. Letts. Revs.*, 6, 45–54 (DOI:10.1080/17518253.2012.703245); (b) Das B., Venkateswarlu K., Suneel K., & Majhi A. (2007), An efficient and convenient protocol for the synthesis of quinoxalines and dihydropyrazines via cyclization – oxidation processes using HClO$_4$. SiO$_2$ as a heterogeneous recyclable catalyst, *Tetrahedron Lett.,* 48, 5371–5374 (DOI:10.1016/j.tetlet.2007.06.036); (c) Madhav B., Narayana Murthy S., Prakash Reddy V., Rama Rao, K., & Nageswar, Y. V. D. (2009), Biomimetic synthesis of quinoxalines in water, *Tetrahedron Lett.*, 50, 6025–6028 (DOI:10.1016/j.tetlet.2009.08.033); (d) Wan J.-P., Gan S.-F., Wu J.-M., & Pan Y. (2009), Water mediated chemoselective synthesis of 1,2-disubstituted benzimidazoles using o-phenylenediamine and the extended synthesis of quinoxalines, *Green Chem.*, 11, 1633–1637 (DOI:10.1039/B914286J).

11. (a) Paul S., & Basu B. (2011), Synthesis of libraries of quinoxalines through eco-friendly tandem oxidation-condensation or condensation reactions, *Tetrahedron Lett.*, 52, 6597–6602 (DOI:10.1016/j.tetlet.2011.09.141); (b) Varela J. A., & Saá, C. (2008), Recent advances in the synthesis of pyridines by transition-metal-catalyzed [2+2+2] Cycloaddition, *Synlett.*, 17, 2571–2578 (DOI:10.1055/s-2008-1078275); (c) Kotharkar S. A., & Shinde D. B. (2006), Mercuric iodide (HgI2) as an oxidizing agent for the synthesis of quinoxaline, *Bull. Korean Chem. Soc.*, 27, 1466–1468 (DOI:10.5012/bkcs.2006.27.9.1466);

12. Sharma J., Mahima S., Kakade B. A., Pasricha R., Mandale A. B., & Vijayamohanan K. (2004), Solvent-Assisted One-Pot Synthesis and Self-Assembly of 4-Aminothiophenol-Capped Gold Nanoparticles, *J. Phys. Chem. B.*, 108, 13280–13286 (DOI:10.1021/jp0482013).

13. Mirkin C. A. (2000), Programming the Assembly of Two- and Three-Dimensional Architectures with DNA and Nanoscale Inorganic Building Blocks, *Inorg. Chem.*, 39, 2258–2272 (DOI:10.1021/ic991123r).

14. (a) Love J. C., Estroff L. A., Kriebel J. K., Nuzzo R. G., & Whitesides G. M. (2005), Self-Assembled Monolayers of Thiolates on Metals as a Form of Nanotechnology, *Chem. Rev.*, 105, 1103–1170 (DOI:10.1021/cr0300789); (b)

Samanta D., & Sarkar A. (2011), Immobilization of bio-macromolecules on self-assembled monolayers: methods and sensor applications, *Chem. Soc. Rev.*, 40, 2567–2592 (DOI:10.1039/C0CS00056F); (c) Daniel M.-C., & Astruc D. (2004), Gold Nanoparticles: Assembly, Supramolecular Chemistry, Quantum-Size-Related Properties, and Applications toward Biology, Catalysis, and Nanotechnology, *Chem. Rev.*, 104, 293–346 (DOI:10.1021/cr030698).

Chapter 4

Selective aerobic oxidation of α-hydroxy esters and α-hydroxy phosphonates using Au-Pd nanoparticles

4.1 Introduction:

Fascinating developments in the area of organic catalysis involving inorganic nanoparticles (NPs) as heterogeneous and reusable catalysts have led to exploration and design of a new generation of nanocatalysts to provide precise control over activity and selectivity of catalytic reactions.[1] The discovery that supported Au NPs show exceptionally effective size specific catalytic properties has initiated an explosion of interest in catalysis involving Au NPs to a myriad of organic transformations such as oxidation-reduction, cyclization, C-C bond formation and so on.[2] In particular, Au NPs have demonstrated effective catalysis for oxidation of alcohols with high selectivity and stability in presence of molecular oxygen. However, in most cases, high reaction temperature (above 100 °C) or the presence of a large excess of base additives (e.g. NaOH or K_2CO_3) are often indispensable to achieve high catalytic activity.[3] From a mechanistic point of view, high basic condition is essential to extract the alcoholic proton for promoting the oxidative transformation. However, excess base inevitably leads to severe problems such as undesirable side reactions and extra waste base treatment.

$$R = -COOEt, -PO(OEt)_2, -CH_2COOEt$$
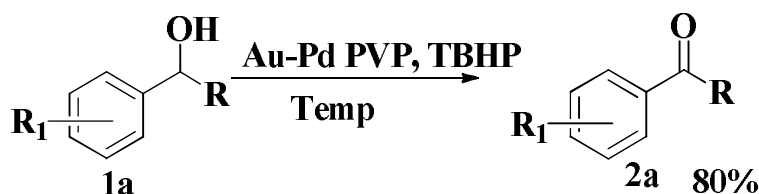
Scheme 4.1 *Oxidation of alcohols involving sensitive substrates (-COOEt, -PO(OEt)$_2$, -CH$_2$COOEt)*

Considering the usual drawbacks involving homogeneous catalysis such as separation and reuse of catalysts, the exploration of nanoparticle based heterogeneous catalysts for selective oxidation of alcohols involving sensitive substrates is highly demanding.[4]-Earlier, we reported the development of a self-assembled monolayer coated Au nanoparticle catalytic system for the aerobic oxidation of α-hydroxy ketones in basic aqueous medium and subsequent *in situ*

formation of quinoxaline derivatives.[5] However, the presence of base and water is not amicable for the oxidation of sensitive substrates such as α-hydroxy esters and α-hydroxy phosphonates. The presence of labile groups such as esters and phosphonates in these substrates discourages the use of base in the reaction medium, as under these conditions they are readily hydrolysed giving undesired carboxylic acid products.[6] α-keto esters and α-keto phosphonates are structural motifs of various natural products, pharmaceuticals and biologically active compounds and have been found at the core of numerous analgesic, non-steroidal anti-inflammatory drugs and phytohormonal growth regulators.[7] Hence, development of a nanoparticle based reusable catalyst that exhibits a wide range of substrate tolerance for the direct oxidation of α-hydroxy esters and α-hydroxy phosphonates to their keto counterparts is crucial from both synthetic and green chemistry point of view. Therefore it was imperative to focus on the development of a nanoparticle based catalytic system with activity and selectivity suitable for the title transformations under base free and solvent-free conditions. We envisioned that alloying Au with intrinsically active Pd might lead to a catalyst with fine-tuned activity for this specific reaction. It has been well established that bimetallic NPs offer greater reaction specificity, catalyst tunability and superior performance compared to their monometallic counterparts owing to the synergistic effect between two different metals.[8,9] Au-Pd bimetallic nanocomposites have generated special interest in heterogeneous catalyst for various reactions such as selective oxidation of C-H bonds and alcohols, direct synthesis of H_2O_2 from H_2 and O_2, C-C coupling, electrochemical reactions etc.[10,11]

In this chapter, we report the selectivity in oxidation of substrates having sensitive groups such as esters and phosphonates by controlling the Au:Pd ratio in a bimetallic nanoparticle catalyst under a base-free and solventless condition.

4.2 Characterization of Au-Pd PVP nanocomposites

We synthesized monometallic Au and Pd and a series of $Au_{1-x}Pd_x$ (x=0-1) NPs by co-reduction of $HAuCl_4$ and H_2PdCl_4 using $NaBH_4$ as a reducing agent and polyvinyl pyrrolidone (PVP) as a stabilizer following a reported method.[12]
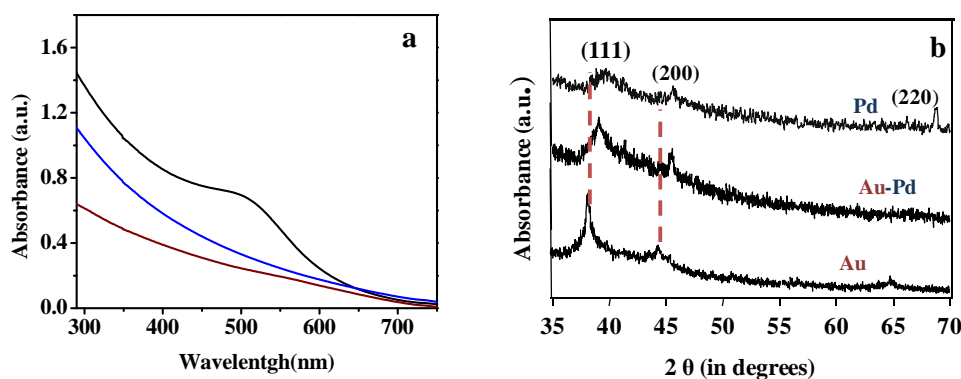
Figure 4.1 *(a) UV- visible spectrum of Au NPs (black line), Pd NPs (blue line) and Au- Pd alloy NPs (brown line),(b) XRD pattern Au-NP, Pd-NP and Au-Pd NPs; the corresponding lattice planes are marked.*

The composition of the bimetallic NPs was controlled by varying the ratios of Au and Pd metal salts. Au nanoparticles showed their characteristic plasmon resonance band at 528 nm, however, the plasmon resonance characteristics of Au disappeared in the UV-visible spectrum of Au-Pd nanoparticles (Figure 4.1a). The results confirmed the formation of bimetallic nanoalloys as the disappearance of the plasmon resonance characteristics could be attributed to changes in the band structure of Au nanoparticles due to alloying with Pd.[13] The XRD patterns of Au, Pd and bimetallic Au-Pd nanoparticles (Figure 4.1b) exhibit two major diffraction peaks in the region $30° < 2\theta < 70°$ that correspond to the (111) and (200) of the fcc structure of monometallic Au and Pd. The diffraction peaks of the bimetallic Au-Pd nanoparticles were observed in between the diffraction peaks of pure Au and Pd nanoparticles, signifying the formation of Au-Pd alloys. The d_{111} and d_{200} of Au (0.235 nm and 0.205 nm), Pd (0.224 nm and 0.195 nm) and $Au_{0.5}Pd_{0.5}$

(0.230 nm and 0.199 nm) were calculated following Bragg's equation (figure 4.1b).
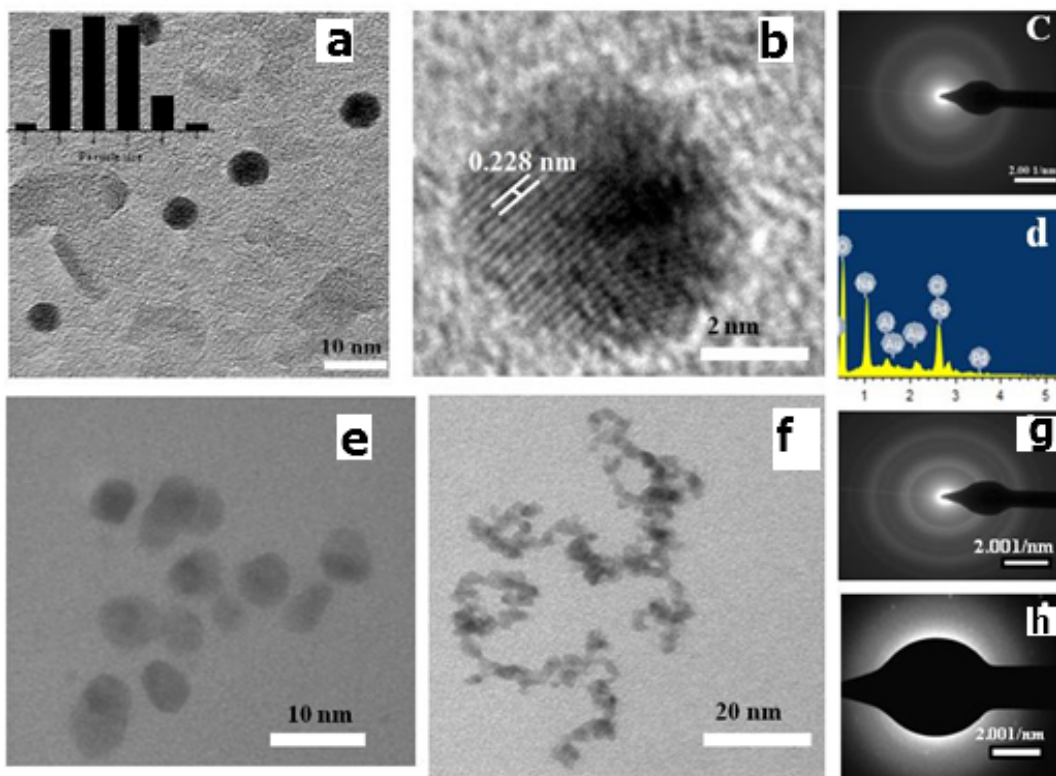
Figure 4.2 *TEM images of the Au-Pd nanoparticles stabilized with PVP in aqueous medium at scale bar a) 2 nm, b) 10 nm. c) corresponding SAED pattern. d) EDX spectrum of Au-Pd alloy nanoparticles. e) Au nanoparticles stabilized with PVP at scale bar 10 nm and f) Pd nanoparticles with PVP at scale bar 10nm. g) and h) SAED pattern of Au and Pd NPs.*

Transmission electron microscopy studies of the Au-Pd nanoparticles revealed the formation of very small spherical nanoparticles with an average diameter of 4.2 ± 1.4 nm (figure 4.2). High resolution TEM studies revealed the lattice fringe separation of 0.229 nm, which is close to the value as measured by XRD for Au-Pd (111) plane (figure 4.2 b). On the other hand, Au nanoparticles synthesized by

this method showed the formation of ultrasmall nanoparticles with an average diameter of 3.5 ± 0.9 nm, while Pd nanoparticles showed an agglomerate of

4.3 Optimization of Oxidation reaction

Table 4.1: Optimization of oxidation of α-hydroxy esters to α-keto esters
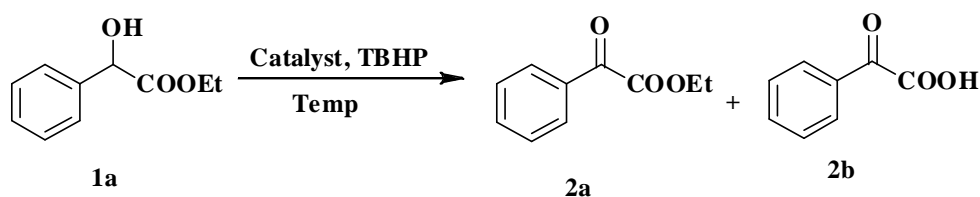
Entry	Catalyst	Reaction conditions (solvent/ temp/ oxidant)	Yield of 2a[b] (%)	Yield 2b (%)
1	No catalyst	Water, 80 °C, Air		-
2	PVP	Water, 80 °C, Air		-
3.	AuPVP/ K$_2$CO$_3$	Water, 80 °C, Air	-	Mandelic Acid
4.	AuPVP	Water, 80 °C, oxygen	5	-
5.	PdPVP	Water, 80 °C, oxygen	10	60
6.	Au-PdPVP (1:1)	Water, 40 °C, Air	15	-
7.	Au-PdPVP (1:1)	Solvent free, 40 °C, Air	15	trace
8.	Au-PdPVP (1:1)	Solvent free, 40 °C, oxygen	20	-
9.	Au-PdPVP (1:1)	Solvent free, 80 °C, oxygen	44	-
10.	Au-PdPVP (1:1)	Solvent free, 110 °C, oxygen	66	-
11.	Au-PdPVP (1:1)	Solvent free, 40, 5 mol % TBHP	33	-
12.	Au-PdPVP (1:1)	Solvent free, 40 °C,15 mol % TBHP	55	-
13.	**Au-PdPVP (1:1)**	**Solvent free, 40 °C, 25 mol % TBHP**	**88**	**-**
14.	No catalyst	Solvent free, 40 °C, 25 mol% TBHP	-	-
15.	Au-PdPVP (3:1)	Solvent free, 40 °C, 25 mol % TBHP	50	5
16.	Au-PdPVP (1:3)	Solvent free, 40 °C, 25 mol % TBHP	52	30
17.	Au-PdPVP (1:1)	Solvent free, 40 °C, Argon	10	-
18.	Au-PdPVP (1:1)	Solvent free, 40 °C, 25 mol % H$_2$O$_2$	40	

nanoparticles with reduced interparticle separation forming a chainlike structure. The Energy dispersive X-ray (EDX) spectroscopy of Au-Pd composite showed the presence of both Au and Pd in the composite (figure 4.2d).

Initially, oxidation of ethyl mandelate towards the formation of ethyl phenylglyoxylate was studied as a model reaction for obtaining the optimized condition by screening at various temperatures, solvent, oxidant and catalyst loading and the results are summarized in Table 4.1. When the usual pathway for oxidation reactions using Au NPs in presence of base such as K_2CO_3 was adopted in the present case, undesired mandelic acid was obtained as the sole product. The results indicated that α-hydroxy esters are highly unstable in presence of base. The presence of water in the reaction medium did not yield any significant product (Table 4.1, entry 3). In presence of oxygen as oxidant, use of monometallic Au NPs as catalysts did not result in significant conversion (Table 4.1, entry 4). On the other hand, Pd NPs showed high activity in the oxidation of hydroxyl groups although it was accompanied by hydrolysis of the ester leading to the formation of undesired phenylglyoxylic acid as the major product (Table 4.1, entry 5).
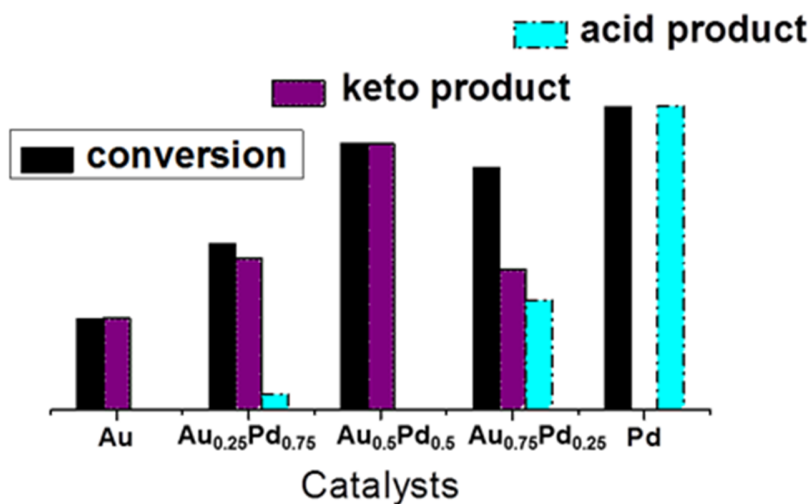
Figure 4.3 *Comparative study of oxidation of substrate α-hydroxy ester (1a) in the presence of various compositions of mono-/bimetallic nanoparticle catalysts. Condition: 1 mmol α-hydroxy ester, 0.05 mol% of Au-PdPVP, 25 % TBHP, 40 °C.*

In order to achieve high yield and better selectivity of our desired product ethyl phenylglyoxylate, we turned our attention towards using Au-Pd alloy NPs which are known to show superior performance compared to their monometallic counterparts owing to synergistic effect (Table 4.1, entry 9, 10, 13). It was observed that $Au_{0.5}Pd_{0.5}$ NPs showed the best activity among all the $Au_{0.5}Pd_{0.5}$ alloy compositions (Table 4.1, entry 13, 15, 16).

In comparison, using $Au_{0.7}Pd_{0.3}$ nanocatalysts resulted in 40 % of oxidized product with lower conversion, whereas $Au_{0.3}Pd_{0.7}$ NPs afforded phenylglyoxylic acid (yield 30 %) as a side product Table (4.1, entry 15,16). The yield of the oxidized product could be significantly enhanced upto 88% at lower temperature and shorter reaction time by using *tert*-butyl hydroperoxide (TBHP) as an additional oxygen donor (Table 4.1, entry 13). The best reaction conditions were achieved for our model reaction without any formation of byproducts at low temperature and solvent free conditions when $Au_{0.5}Pd_{0.5}$ NPs were used as catalysts in presence of 25 mol% of TBHP as an oxidant (Table 4.1, entry 13). It is worth mentioning that only TBHP is almost inactive, with a very negligible amount of the oxidized product being formed. Further, in absence of O_2, the model reaction using $Au_{0.5}Pd_{0.5}$ NPs as catalysts in presence of TBHP afforded 10 % of the oxidized product suggesting that the presence of oxygen was vital for this oxidation reaction (Table 4.1, entry 16). In order to verify the role of alloy NPs in selectivity of the oxidized product, we also performed the reaction under similar conditions using a mixture of monometallic Au and Pd NPs, that resulted in a mixture of ethyl phenylglyoxylate and phenylglyoxylic acid. With a clear understanding of the performance of various nanoparticle compositions on the activity and selectivity during the oxidation of α-hydroxy esters and optimized reaction conditions in hand, the generality of this novel nanoparticle catalyzed oxidation reaction was examined and the results are compiled in Table 4.1.

We first investigated the substrate scope of various substituted aryl hydroxy esters. A great variety of α-hydroxy esters were compatible with this protocol, leading to α-keto esters in moderate to high yield (93%).

Table 4.2: Oxidation of aryl α-hydroxy ester derivatives[ab]

Reaction scheme: **1a** (PhCH(OH)COOEt) → (0.10 mol%) AuPdPVP, 25 mol% TBHP, 40 °C, O$_2$ → **2a** (PhC(O)COOEt)

2a, 88%, 12hr

2b, 80 %, 16hr

2c, 91%, 16hr

2d, 90%, 16hr

2e, 72%, 12hr

2f, 59%, 28hr

2g, 78%, 16hr

2h, 83%, 17hr

2i, 80%, 16 hr

2j, 69%, 22hr

2k, 84%, 16hr

2l, 90%, 12hr

2m, 91%, 10hr

2n, 79%, 10hr

2o, 80%, 10hr

2p, 78 %, 16hr

2q, 82 %, 16hr

2r, 20%, 30hr

2s, trace, 30hr
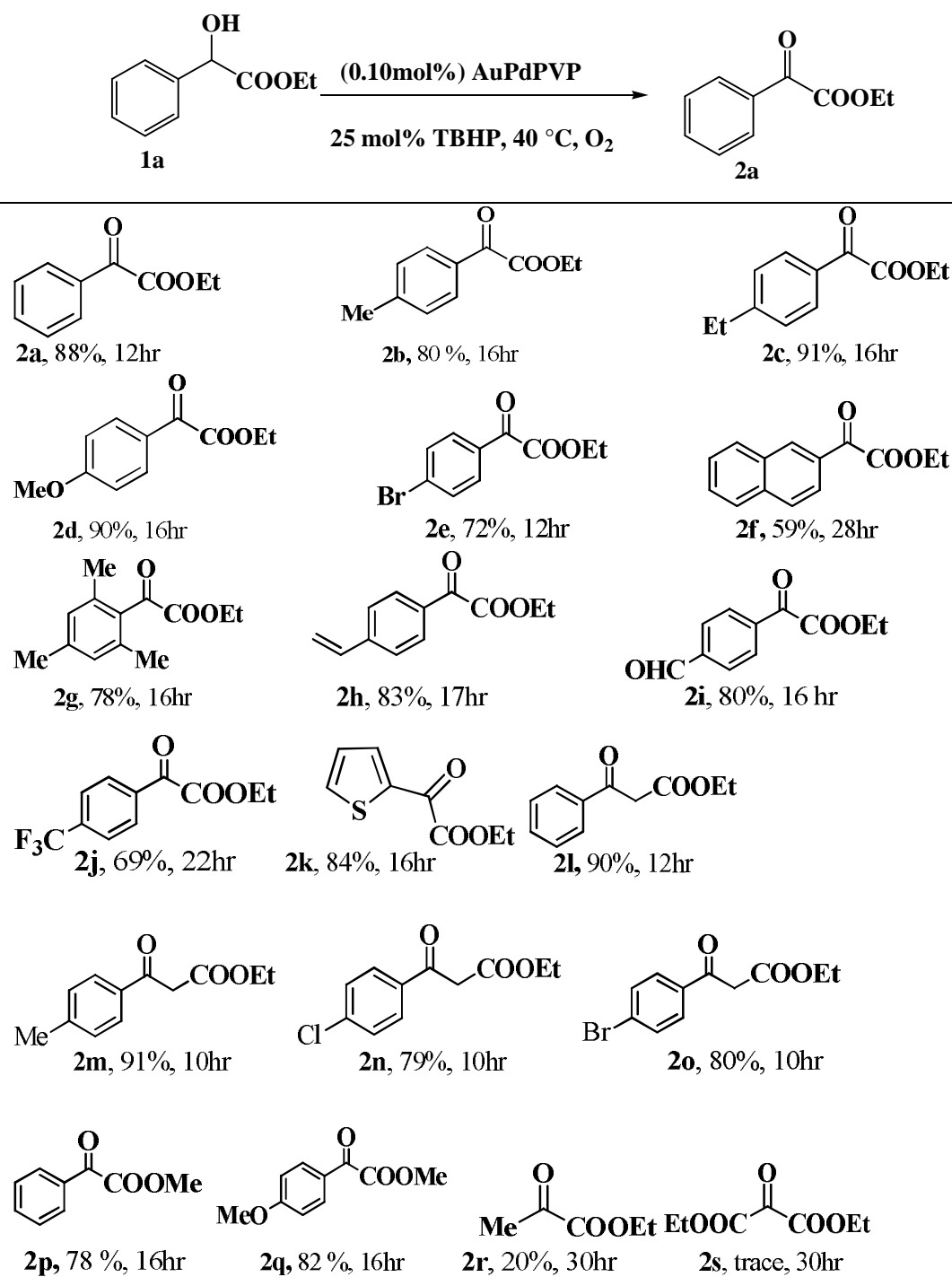
[a] Standard reaction conditions: 1mmol hydroxy ester, 0.10 mol % Au$_{0.5}$Pd$_{0.5}$ PVP NPs, 25 mol % TBHP (30 %). [b] isolated yields.

Both the electron-rich or electron-poor aryl substituents accommodated the reaction well and the functionalities such as –CH₃, -OMe, -Br, -vinyl, -CHO and –CF₃ on the aryl rings tolerated well during the reaction (2a-2j, Table 4.3). It should be pointed out that electron donating substituents on the aromatic ring enhanced the yield when compared to electron-withdrawing groups. The presence of fused ring substituents such as 1-napthyl afforded moderate yield (59%) although a longer reaction time was required. Hetero aryl groups such as 3-thienyl were also well suited and the corresponding oxidized product were obtained in good yields such as 84% (2k, Table-4.2). Interestingly, oxidation of methyl mandelate afforded high yield of the oxidized product at comparatively lesser reaction time, possibly due to less steric effect (yield 82%, 2q, Table 4.2).

However, employing alkyl-α-hydroxy esters such as ethyl lactate or diethylhydroxy malonate could not afford the desired product with any significant yield even at higher temperature (80 °C) and prolonged reaction time.
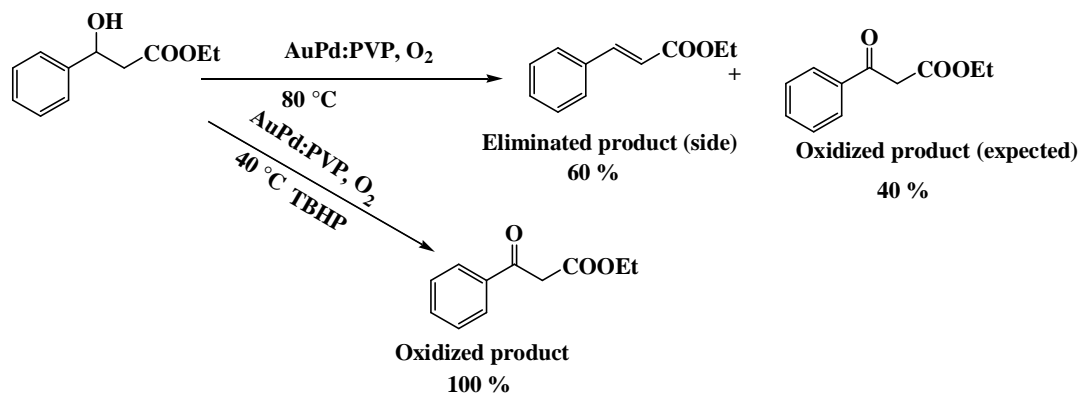
Scheme 4.2 *Selectivity of substrate β-hydroxy ester with Au₀.₅Pd₀.₅PVP alloy nanoparticle with presense of THBP and without TBHP. Condition: 1 mmol β-hydroxy ester, 0.05 mol% Au-PdPVP, 25 mol% TBHP, 40 °C.*

In case of aryl-β-hydroxy esters, the use of Au-Pd NPs in absence of TBHP led to a mixture of the desired oxidized product ethyl benzoylacetate (40%) and an

eliminated product ethyl cinnamate (60%). However, in presence of TBHP, $Au_{0.5}Pd_{0.5}PVP$ NPs afforded high yield of the desired oxidized products at lower reaction time with no side product formation (scheme 4.2).

Oxidation of α-hydroxy phosphonate to keto phosphonate:

Encouraged by the results for the selective oxidation of aryl α-hydroxy esters by Au-Pd alloy NPs in presence of TBHP as an oxidant under mild reaction conditions, we then applied the same methodology for the direct oxidation of aryl α-hydroxy phosphonates. Due to high sensitivity of the C(O)-P bonds in these compounds towards hydrolysis and acidic conditions, development of a nanocatalytic system for direct oxidation of α-hydroxy phosphonates to their corresponding keto products is tedious.
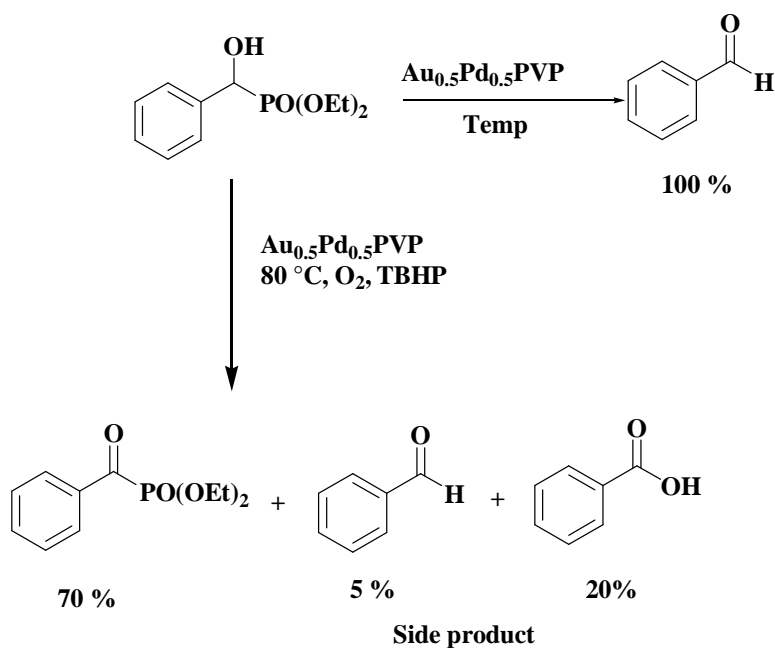
Scheme 4.3 *Selectivity of α-hydroxy phosphonate substrates with $Au_{0.5}Pd_{0.5}PVP$ alloy nanoparticle in presence of THBP and without TBHP. Condition: 1 mmol β-hydroxy ester, 0.10 mol% $Au_{0.5}Pd_{0.5}PVP$, 25 mol% TBHP, 40 °C.*

It was observed that using $Au_{0.5}Pd_{0.5}PVP$ nanoparticles in presence of O_2 as the sole oxidant led to the hydrolysis of the compounds giving their corresponding

aldehydes as the sole product. When TBHP was used along with O_2 as the oxidant, $Au_{0.5}Pd_{0.5}PVP$ NPs afforded the desired α-keto phosphonates as the major product at 80 °C under solventless conditions. Several substituents such as –Me, -OMe, -Cl, -Br on the aryl rings also afforded good yield of the oxidized product under the present reaction conditions (table-4.3, 4a-4e).

Table 4.3: Oxidation of α-hydroxy phosphonate 3 to keto phosphonate 4

Reaction condition:1 mmol α-hydroxy phosphonate, 0.10 mol % $Au_{0.5}Pd_{0.5}PVP$, 30 mol % TBHP

4.4 Reusability of $Au_{0.5}Pd_{0.5}PVP$ alloy nanocatalyst:

The reusability of the $Au_{0.5}Pd_{0.5}PVP$ alloy nanocatalysts in presence of TBHP was evaluated by studying the reaction yield over two cycles during the oxidation of ethyl mandelate. Although there was no marked change in the selectivity of the product, the conversion was found to be gradually decreasing over the cycles (recovery amount of ethyl phenylglyoxylate was 81% after the first run and 77%
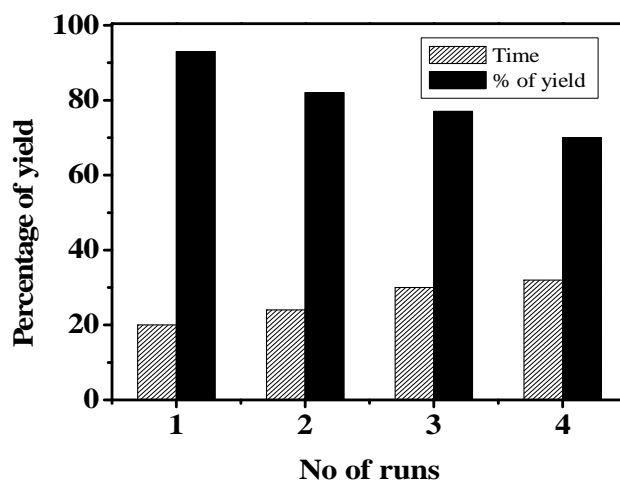
Figure 4.4 *Recyclability of Au$_{0.5}$Pd$_{0.5}$PVP alloy nanocatalysts*
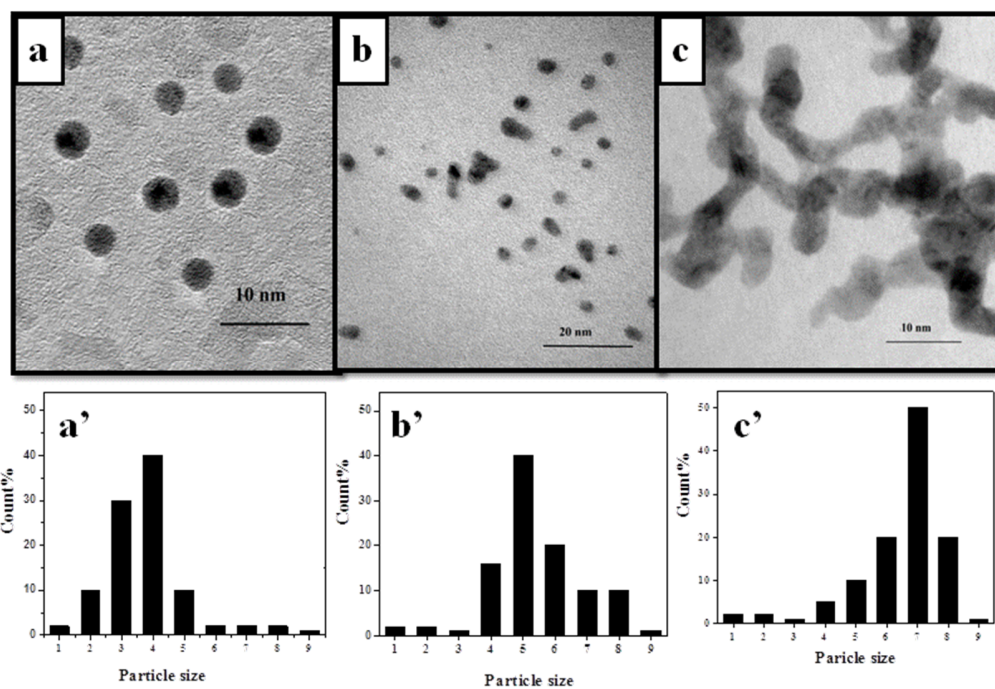
Figure 4.5 *TEM images and particle size distribution of a) Au$_{0.5}$Pd$_{0.5}$PVP nanoparticles; scale bar 10 nm and average particle size 3±2 nm. b) after addition of 25 mol% tetrabutyl hydrogen peroxide (TBHP) into reaction medium before the oxidation; scale bar 20 nm and the average particle size 5±2 nm c) after oxidation reaction; scale bar 10 nm and average particle size 7±3 nm.*

after the 2nd run (Figure 4.4). This could be attributed to the agglomeration of the nanoparticles upon interaction with TBHP as observed by TEM studies (Figure 4.5).

4.5 Proposed mechanism

For the mechanistic investigation of the reaction, we performed a few studies under various conditions. In presence of a free radical scavenger such as TEMPO ((2,2,6,6-Tetramethylpiperidin-1-yl)oxyl), when we performed our model reaction for the oxidation of ethyl mandelate using $Au_{0.5}Pd_{0.5}PVP$ NPs in presence of O_2, but in absence of TBHP as an additional oxidizer, the desired product was obtained with 15% yield.
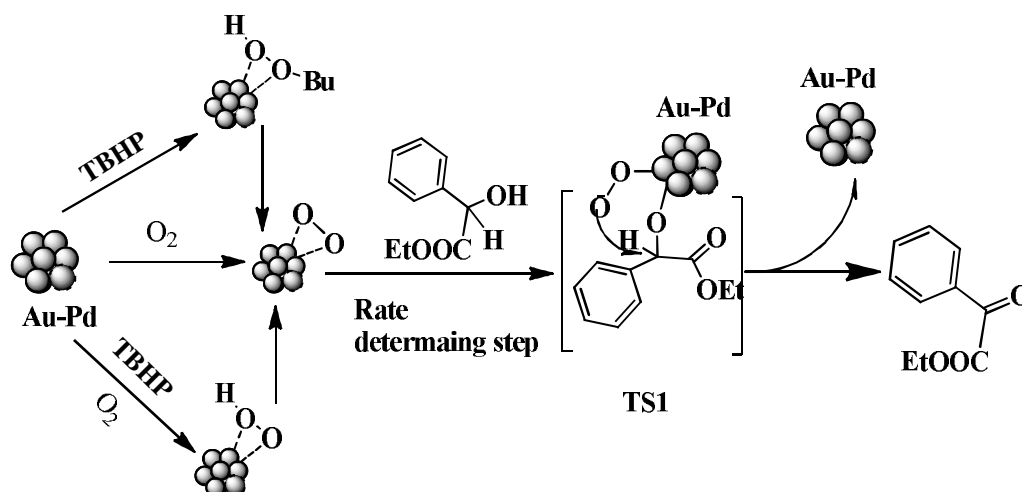
Figure 4.6 *Mechanistic proposal of oxidation of aryl α-hydoxy ester*

As the reaction was not affected by the presence of TEMPO, this suggested that the reaction did not proceed through the free radical mechanism. On the other hand, when the reaction was carried out in presence of TBHP, O_2 and TEMPO, we obtained 50% yield of the product. In this case, possibly, the reaction followed a free radical pathway. When the model reaction was carried out in presence of TBHP in argon atmosphere, the desired product was obtained with 15% yield. The

results suggest that O_2 is the primary oxidant for these oxidation reactions. From these studies and taking a cue from the earlier reports, we propose a mechanism for the selective oxidation of α-hydroxy esters. The three different oxidant systems can undergo different reaction pathways to activate the oxidants and generate a common peroxyformate intermediate Au-Pd-O_2. In case of O_2 as the sole oxidant, O_2 directly adsorbs on the Au-Pd surface to a superoxo species. In case of TBHP as an oxidant, interaction of TBHP and anionic $Au_{0.5}Pd_{0.5}$PVP forms a hydroperoxy species followed by loss of a H_2O molecule to give Au-Pd-O_2 species. In case of TBHP/O_2, initiation of TBHP forms species BuO$^-$/$^\cdot$OH which activates dioxygen to form superoxolike $O_2^\cdot$ species which is adsorbed on the NP surface. The peroxo-like intermediate is transformed to Au-Pd-O_2 species. The superoxo- or peroxo- like species generated on the cluster surface eliminates β-hydrogen from the alcohol to generate the keto product.[13]

4.6 Conclusion:

We developed an efficient, extraordinary, recyclable and selective Au-Pd alloy nanocatalyst for oxidation of α-hydroxy ester and α-hydroxy phosphonate compounds with high substrate scope in solventless heterogenous pathway. Au-Pd alloy nanoparticle were shown as exceptional superior catalyst compared to Au and Pd mononanoparticle catalyst alone due to the synergistic effect of both metals. We have also shown here that the catalytic property of Au-Pd alloy depends on the composition of metal precursors.

4.7 Instrumentation

All reactions were carried out in air and monitored by TLC using Merck 60 F_{254} pre coated silica gel plates (0.25 mm thickness) and the products were visualized by UV detection. Flash chromatography was carried out with silica gel (200-300 mesh). FT-IR spectra were recorded on a Bruker Tensor-27 spectrometer. ^{1}H and ^{13}C NMR spectra were recorded on a Bruker Advance (III) 400 MHz spectrometer. Data for ^{1}H NMR are reported as a chemical shift (δ ppm), multiplicity (s = singlet, d = doublet, q = quartet, m = multiplet), coupling constant

J (Hz), integration, and assignment, data for ^{13}C are reported as a chemical shift. High resolution mass spectral analyses (HRMS) were carried out using ESI-TOF-MS. UV-visible spectra were recorded in a Varian Cary 100 Bio spectrophotometer, TEM images were recorded on a Tecnai G^2 20 Ultra- Twin microscope. Thermal gravimetric analysis (TGA) was performed in a Mettler-Toledo TGA-DSC/1 star system.

PXRD measurements

Powder XRD spectra were recorded on a Bruker D8 Advance diffractometer using Cu Kα as the X-ray Source. X-ray diffraction patterns of bimetallic Au–Pd nanoclusters before and after reaction were recorded in thin film mode. The catalyst was centrifuged and washed with Millipore water and deposited on the glass slide followed by air-drying. The same method was applied for the preparation of samples of fresh monometallic and bimetallic catalysts and the XRD was performed. The crystallite size of the Au–Pd core was estimated from the peak width of the diffraction peak of the alloy Au–Pd (111) plane by fitting with a single Gaussian function. Finally, the core diameter was estimated from Scherrer's formula $D = \kappa\lambda/\beta \cos\Theta$, where κ, λ and β are Scherrer's constants.

4.8 Materials and Methods

 Hydrogen tetrachloroaurate (III) hydrate ($HAuCl_4, H_2O$, purum, -52% Au basis), palladium (II) chloride ($PdCl_2$, 99.9%), Poly(vinylpyrrolidone) (PVP, Mw = 300,000), Sodium Borohydride ($NaBH_4$), Boronic acids, Aldehydes, ethyl glyoxylate, $Pd_2(dba)_3$·$CHCl_3$, 2-di-tert-butylphosphanylbiphenyl were purchased from Sigma Aldrich. All these chemicals were used without further purification. MilliQ water was used throughout the experiment.

4.8.1 Preparation of PVP-Stabilized Au NPs

To an aqueous solution of $HAuCl_4$ (1 mM, 40 mL) was added 555.5 mg of PVP so that the molar ratio of $AuCl_4^-$ and monomer unit of PVP was kept at 1:100. The mixture was further stirred for 30 min in a bath kept at 0 °C.[14] Then, an aqueous solution of $NaBH_4$ (100 mM, 5 mL) was rapidly sprayed into the mixture under

vigorous stirring. The color of the mixture immediately turned from pale yellow to dark brown, indicating the formation of small Au NPs. The AuPVP NPs were subsequently dialyzed overnight to remove inorganic impurities such as Na^+ and Cl^-. The dialyzed hydrosol of the AuPVP NPs was diluted to 100 mL and stored at 2 °C. The water used in the present study was of MilliQ grade.

4.8.2 Preparation of PVP-Stabilized Pd NPs

For the synthesis of Pd nanoparticles, an aqueous solution of H_2PdCl_4 (50 mM) was prepared by completely dissolving 177.3 mg $PdCl_2$ in 100 mL of 20 mM HCl in a boiling water bath. To an aqueous solution of H_2PdCl_4 (1 mM, 30 mL) was added 555.5 mg of PVP. The mixture was further stirred for 30 min in a bath kept at 0 °C.[15] Then, an aqueous solution of $NaBH_4$ (100 mM, 5 mL) was rapidly sprayed into the mixture under vigorous stirring. The color of the mixture immediately turned from pale yellow to dark black, indicating the formation of small Pd NPs. The dialyzed hydrosol of the PdPVP NPs was diluted to 100 mL and stored at 2 °C. The water used in the present study was of MilliQ grade.

4.8.3 Synthesis of $Au_{0.5}Pd_{0.5}$PVP alloy nanoparticle

555.5 mg of PVP (K-30) was dissolved in 44 mL of MilliQ water and to the solution was added quantitative amount of $HAuCl_4$ (30 mM) and $PdCl_2$ (30 mM) and monomer unit of PVP was kept at 1:100. The resulting solution was stirred for 30 min at 0 °C. The solution was maintained at 4 °C before reduction, and an aqueous solution (5 mL) of NaBH4 (20 mg, 0.52 mmol) was added rapidly under vigorous stirring. The color of the mixture turned from pale yellow to brown, indicating the formation of Au–Pd bimetallic clusters. Thus obtained $Au_{0.5}Pd_{0.5}$PVP clusters were subsequently dialyzed through the membrane filter to remove the inorganic impurities such Na^+ and Cl^-. The dialyzed hydrosol of AuPdPVP was diluted to 25 mL and stored in refrigerator for catalytic reactions and characterizations.

4.8.4 Synthesis of α-hydroxy ester (starting alcohols):

To a suspension of aryl boronic acids (1.5 mmol) and Cs_2CO_3 (1 mmol, 326 mg) in dry toluene (3 mL) was added $Pd_2(dba)_3 \cdot CHCl_3$ (0.0125 mmol, 13 mg), 2-di-

tert-butylphosphino)biphenyl (0.05 mmol, 15 mg) and ethyl glyoxylate (1 mmol) under an atmosphere of argon at room temperature. The temperature was increased to 80 °C, and the mixture was stirred for 7–24 h. The reaction was quenched with water (10 mL), and the resulting mixture was extracted with dichloromethane (315 mL).[16] The combined organic phase was dried with sodium sulfate, filtered, and concentrated under vacuum. The resulting crude mixture was purified by flash chromatography with unmetalated silica (cyclohexane/ EtOAc).
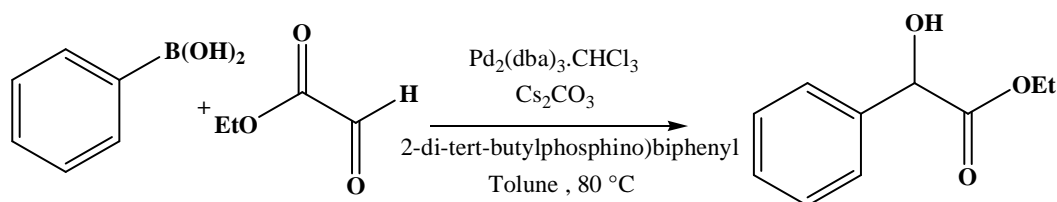
Figure 4.7 *Synthesis of α-hydroxyl ester.*

4.8.5 Synthesis of α-hydroxy phosphonates:

A mixture of benzaldehyde (1 mmol), triethyl phosphite (1 mmol) and CSA (0.1 mmol) under neat conditions was subjected to ultrasound irradiation for 30 min. Reaction progress was monitored by TLC (ethyl acetate/n-hexane: 1:9). After 30 min, 10 mL water was added to the reaction vessel and irradiated again for 10 min to obtain the solid product. Reaction mass containing product was poured on crushed ice and product was collected by simple filtration, washed with water and dried. The crude product was recrystallized from ethanol to obtain pure product.[17]
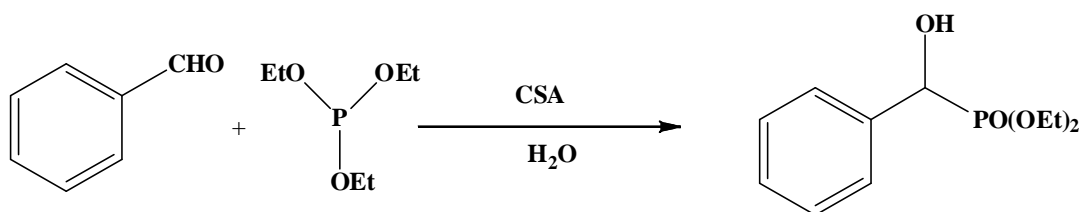
Figure 4.8 *Synthesis of α-hydroxyl phosphonates*

4.8.6 Oxidation of alcohols to keto compounds

 In a typical synthesis, 1mmol alcohol (hydroxyl ester, β-hydroxy ester, α-hydroxy phosphonate), 30 mg (0.05 mol %) $Au_{0.5}Pd_{0.5}PVP$, 25 mol% tert-butyl hydrogen peroxide were taken in a round bottom flask. The reaction mixture was then heated at specified temperature and time under air. The progress of the reaction was monitored by TLC. After completion of reaction, the mixture was extracted with ethyl acetate (3×10 mL), washed with water and brine. The organic phase was evaporated by rotary evaporator under reduced pressure to give the crude product which was further purified by flash column chromatography.

 NMR data of α-keto esters and α-keto phosphonates

 1.

ethyl 2-oxo-2-phenylacetate
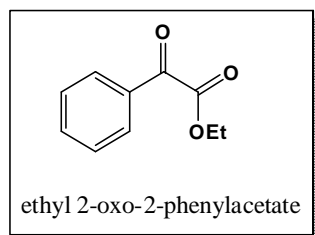
Colorless oil; R*f* 0.69; (hexanes: ethyl acetate, 80:20 v/v): ^{1}H NMR (400 MHz, CDCl$_3$, ppm): 7.99-7.97 (m, 2H), 7.63 (t, *J*= 12 Hz, 1H), 7.48 (t, *J*= 8Hz, 2H), 4.42 (q, *J$_1$*= 8 Hz *J$_2$*=8 Hz, 2H), 1.39 (t, *J*= 16 Hz, 3H) ^{13}C NMR (100 MHz, CDCl3): 186.03, 163.44, 134.49, 132.05, 129.58, 128.48, 61.91, 13.7.

2.

ethyl 2-oxo-2-*p*-tolylacetate
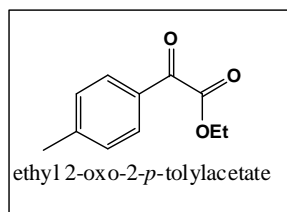
yellow oil; R*f* 0.59; (hexanes: ethyl acetate, 80:20 v/v) NMR (400 MHz, CDCl$_3$, ppm) 7.88-7.84 (dd, *J*= 8Hz, 2H), 7.28-7.24 (dd, *J$_1$*= 8 Hz, *J$_2$*= 8 Hz, 2H), 4.35 (m, 2H), 2.40 (S, 3H), 1.33(t, 3H), ^{13}C NMR (100 MHz, CDCl$_3$): 185.99, 163.95, 146.12, 129.51, 127.02, 62.08, 13.99.

3.

ethyl 2-(4-ethylphenyl)-2-oxoacetate
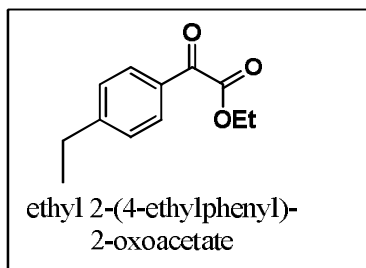
Greenish oil; Rf 0.79; (hexanes: ethyl acetate, 80:20 v/v) NMR (400 MHz, CDCl$_3$, ppm): 7.99-7.81 (d, J = 8 Hz, 2H), 7.30-7.28 (d, J = 8 Hz, 2H), 4.42(q, J_1 = 8 Hz, J_2 = 8 Hz, 2H), 2.69 (q, J_1 = 4 Hz, J_2 = 4 Hz, 2H), 1.38 (t, 3H), 1.22 (t, 3H), ^{13}C NMR (100 MHz, CDCl$_3$):186.03, 163.98, 152.21, 130.13, 128.35, 126.42, 62.07, 29.03, 14.91, 14.00

4.

ethyl 2-mesityl-2-oxoacetate
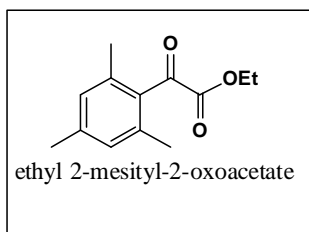
Colorless oil; R$_f$ 0.78; (hexanes: ethyl acetate, 80:20 v/v) NMR (400 MHz, CDCl$_3$, ppm): 6.88 (s, 2H), 4.34-4.39 (q, 2H), 2.30 (s, 3H), 2.25 (s, 6H), 1.35-1.39, (t, 3H) ^{13}C NMR (100 MHz, CDCl$_3$): 191.71, 162.49, 140.64, 135.93, 132.86, 128.75, 62.22, 20.91, 19.33, 13.64.

5.

ethyl 2-(4-methoxyphenyl)-2-oxoacetate
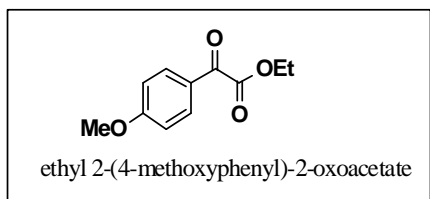
Colorless oil; R$_f$ 0.67; (hexanes: ethyl acetate, 80:20 v/v) NMR (400 MHz, CDCl$_3$, ppm): 8.01-7.99 (d, J = 8 Hz, 2H), 6.98-6.96 (d, J = 8 Hz, 2H), 4.40-4.46(q, 2H), 3.89 (s, 3H), 1.40-1.43, (t, 3H), ^{13}C NMR (100 MHz, CDCl$_3$): 184.91, 165.05, 164.19, 132.62, 125.60, 114.28, 62.19, 55.68, 14.17.

7.

ethyl 2-(4-bromophenyl)-2-oxoacetate
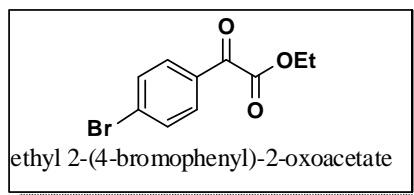
Colorless oil; R$_f$ 0.68; (hexanes: ethyl acetate, 60:40 v/v) 8.03-8.01 (d, 2H), 7.54-7.52 (d, 2H), 4.48-4.43 (q, 2H), 1.42-1.40 (t, 3H). ^{13}C NMR (100 MHz, CDCl$_3$): 207.35, 168.40, 149.35, 130.33, 129.15, 127.96, 53.76, 14.46.

8.

ethyl 2-oxo-2-(4-vinylphenyl)acetate
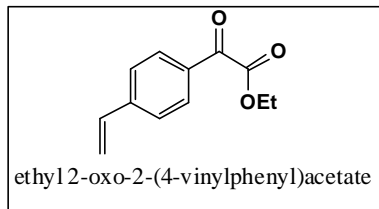
Greenish oil; R$_f$ 0.88; (hexanes: ethyl acetate, 60:40 v/v) NMR (400 MHz, CDCl$_3$, ppm): 8.01-7.98 (dd, $J = 8$ Hz, 2H), 7.54-7.52 (d, $J = 8$ Hz, 2H), 6.73-6.83 (q, 1H), 5.91-5.95 (d, 1H), 4.42-4.48 (q, ,-OCH$_2$, 2H), 1.42-1.44 (t, $J = 8$ Hz, 3H) ^{13}C NMR (100 MHz, CDCl$_3$: 185.76, 163.53, 146.12, 135.42, 130.18, 127.79, 127.09, 126.27, 117.67, 62.02, 13.83

9.

ethyl 2-(naphthalen-1-yl)-2-oxoacetate
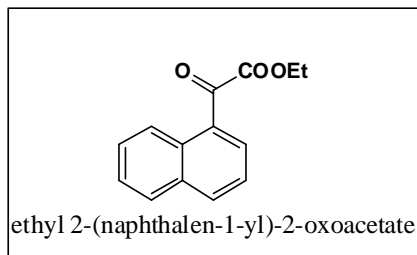
Colorless oil; R$_f$ 0.65; (hexanes: ethyl acetate, 80:20 v/v). NMR (400 MHz, CDCl$_3$, ppm): 9.05-9.03 (d, $J = 8$ Hz, 1H), 8.14-7.90 (m, 4H), 7.66-7.56 (m, 2H), 4.42-4.54 (m, 2H) ^{13}C NMR (100 MHz, CDCl$_3$: 185.76, 163.53, 146.12, 135.42, 130.18, 129.79, 127.09, 126.27, 117.67, 62.02, 13.83.

10.

ethyl 3-oxo-3-phenylpropanoate
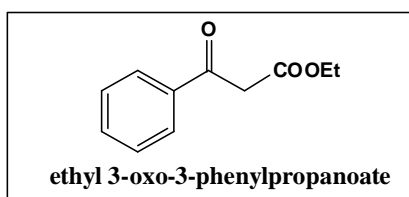
Colorless oil; R$_f$ 0.79; (hexanes: ethyl acetate, 80:20 v/v) NMR (400 MHz, CDCl$_3$, ppm) δ : 7.94-7.92 (d, $J = 8$ Hz, 2H), 7.60-7.56 (t, $J = 6$ Hz, 1H), 7.45-7.48 (t, $J = 6$ Hz, 2H), 4.54-4.42 (m, 2H), 1.18-1.15 (t, 3H) ^{13}C NMR (100 MHz, CDCl$_3$:192.60, 167.74, 136.27, 134.03, 133.96, 129.04, 128.73, 61.74, 52.70, 46.23, 14.30.

11.

ethyl 3-oxo-3-*p*-tolylpropanoate
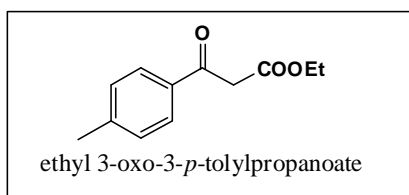
Colorless oil; R$_f$ 0.89; (hexanes: ethyl acetate, 80:20 v/v) NMR (400 MHz, CDCl$_3$, ppm) δ :

7.781-7.761 (d, J = 8 Hz, 2H), 7.212-7.189 (d, J = 8 Hz, 2H), 4.16-4.11 (q, 2H), 3.89 (s, 2H), 2.34 (s, 3H), 1.20-1.10 (t, 3H) .

12.
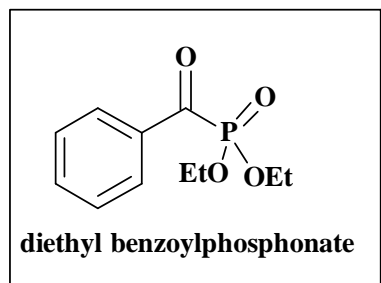
diethyl benzoylphosphonate	White solid; NMR (400 MHz, CDCl$_3$, ppm): 8.06-8.26 (m, 2H), 7.40-7.63 (m, 2H), 4.02-4.30 (dq,-OCH$_2$, 4H), 1.29-1.39 (t, J = 8 Hz, 6H) ^{13}C NMR (100 MHz, CDCl$_3$: 199.36, 134.43, 129.75, 129.49, 128.04, 63.80, 15.80

13.
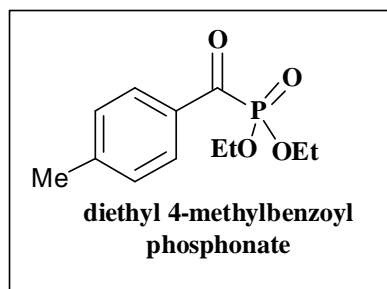
diethyl 4-methylbenzoyl phosphonate	Colorless oil; R$_f$ 0.88; (hexanes: ethyl acetate, 80:20 v/v) NMR (400 MHz, CDCl$_3$, ppm):8.08-8.10 (d, J = 8 Hz, 2H), 7.20-7.22 (d, J = 8 Hz, 2H), 4.16-4.23 (m,-OCH$_2$, 4H), 1.27-1.31 (t, J = 8 Hz,-CH$_3$, 6H) ^{13}C NMR (100 MHz, CDCl$_3$: 198.52, 145.63, 132.47, 129.52, 63.53, 21.42.

14.
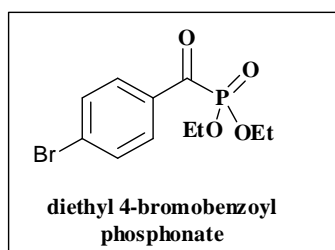
diethyl 4-bromobenzoyl phosphonate	Colorless oil; R$_f$ 0.67; (hexanes: ethyl acetate, 60:40 v/v) NMR (400 MHz, CDCl$_3$, ppm): 8.15-8.13 (d, J = 8 Hz, 2H), 7.67-7.65 (d, J = 8 Hz, 2H), 4.31-4.24 (m, 4H), 1.33-1.30 (t, 3H) ^{13}C NMR (100 MHz, CDCl$_3$: 189.35, 131.97, 131.29, 130.94, 128.20, 63.94, 63.89,

13.62.

15.
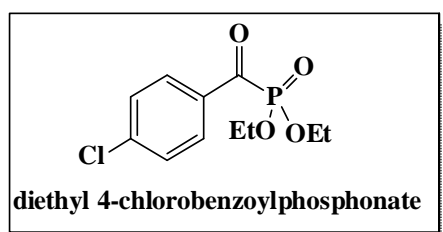
diethyl 4-chlorobenzoylphosphonate	Yellow oil; R$_f$ 0.68; (hexanes: ethyl acetate, 60:40 v/v) NMR (400 MHz, CDCl$_3$, ppm) : 8.15-8.13 (d, 2H), 7.42-7.39 (dd, 2H), 4.29-

4.20 (m, 2H), 1.27-1.23 (t, 6H). 198.17, 140.93, 133.03, 130.68, 128.75, 66.70, 14.56

4.9 References:

1. (a) Mallat T., & Baiker A. (2012), Potential of Gold Nanoparticles for Oxidation in Fine Chemical Synthesis, *Annual Review of Chemical and Biomolecular Engineering*, 3, 11–28 (DOI:10.1146/annurev-chembioeng-062011-081046); (b) Yamazoe S., Koyasu K., & Tsukuda T. (2014), Nonscalable Oxidation Catalysis of Gold Clusters, *Accounts of Chemical Research*, 47, 816–824 (DOI:10.1021/ar400209a); (c) Yan N., Xiao C., & Kou Y. (2010), Transition metal nanoparticle catalysis in green solvents, *Coordination Chemistry Reviews*, 254, 1179–1218 (DOI:10.1016/j.ccr.2010.02.015).

2. (a) Stratakis M., & Garcia H. (2012), Catalysis by Supported Gold Nanoparticles: Beyond Aerobic Oxidative Processes, *Chem. Rev.,* 112, 4469–4506 (DOI:10.1021/cr3000785); (b) Li G., & Jin R. (2013), Catalysis by gold nanoparticles: carbon-carbon coupling reactions, *Nanotechnology Reviews*, 2, 529–545 (DOI:10.1515/ntrev-2013-0020); (c) Corma A., & Garcia H. (2008), Supported gold nanoparticles as catalysts for organic reactions, *Chem. Soc. Rev.*, 37, 2096–2126 (DOI:10.1039/b707314n).

3. (a) Zheng N., & Stucky G. D. (2007), Promoting gold nanocatalysts in solvent-free selective aerobic oxidation of alcohols, *Chem. Commun.,* 1, 3862–3864 (DOI:10.1039/b706864f); (b) Tsunoyama H., Tsukuda T., & Sakurai H. (2007), Synthetic Application of PVP-stabilized Au Nanocluster Catalyst to Aerobic Oxidation of Alcohols in Aqueous Solution under Ambient Conditions, *Chem. Lett.*, (DOI:10.1246/cl.2007.212); (c) Tsukuda T., Tsunoyama H., & Sakurai H. (2011), Aerobic oxidations catalyzed by colloidal nanogold, *Chem. Asian. J.*, 6, 736–748 (DOI:10.1002/asia.201000611).

4. (a) Shei C. T., Chien H. L., & Sung K. (2008), $TiCl_4$/tert-butyl hydroperoxide: Chemioselective oxidation of secondary alcohols and suppression of sharpless

epoxidation, *Synlett.*, 7, 1021–1026, (DOI:10.1055/s-2008-1066997); (b) Heel J. P., & Jong C. L. (2009), Oxidation of benzylic alcohols with urea-hydrogen peroxide and catalytic magnesium bromide, *Synlett*, 1, 79–80 (DOI:10.1055/s-0028-1087391).

5. Bhattacharya T., Sarma T. K., & Samanta S. (2012), Self-assembled monolayer coated gold-nanoparticle catalyzed aerobic oxidation of α-hydroxy ketones in water: an efficient one-pot synthesis of quinoxaline derivatives, *Catal. Sci. Technol.*, 2, 2216 (DOI:10.1039/c2cy20438j).

6. (a) Leduc A. B., & Jamison T. F. (2012), Continuous flow oxidation of alcohols and aldehydes utilizing bleach and catalytic tetrabutylammonium bromide, *Organic Process Research and Development*, 16, 1082–1089 (DOI:10.1021/op200118h); (b) Zhang W., & Shi M. (2006), Reduction of activated carbonyl groups by alkyl phosphines: formation of alpha-hydroxy esters and ketones, *Chem. Commun.*, 11, 1218–1220 (DOI:10.1039/b516467b); (c) Verho O., Dilenstam M. D. V, Kärkäs M. D., Johnston E. V., Åkermark T., Bäckvall J. E., & Åkermark B. (2012), Application and mechanistic studies of a water-oxidation catalyst in alcohol oxidation by employing oxygen-transfer reagents, *Chem. Eur. J.*, 18, 16947–16954 (DOI:10.1002/chem.201202266); (d) Pawar V. D., Bettigeri S., Weng S.-S., Kao J.-Q., & Chen C.-T. (2006), Highly enantioselective aerobic oxidation of α-hydroxyphosphonates catalyzed by chiral vanadyl(V) methoxides bearing N-salicylidene-α-aminocarboxylates, *J. Am. Chem. Soc.*, 128, 6308–6309 (DOI:10.1021/ja060639o); (e) Shei C. T., Chien H. L., & Sung K. (2008), TiCl4/tert-butyl hydroperoxide: Chemioselective oxidation of secondary alcohols and suppression of sharpless epoxidation, *Synlett*, 7, 1021–1026 (DOI:10.1055/s-2008-1066997); (f) Salunke S. B., Babu N. S., & Chen C. T. (2011), Asymmetric aerobic oxidation of α-hydroxy acid derivatives catalyzed by reusable, polystyrene-supported chiral N-salicylidene oxidovanadium tert-leucinates, *Adv. Syn. Catal.*, 353, 1234–1240 (DOI:10.1002/adsc.201100062); (g) Radosevich A. T., Musich C., & Toste F. D. (2005), Vanadium-Catalyzed Asymmetric Oxidation of α-Hydroxy Esters Using Molecular Oxygen as

Stoichiometric Oxidant, *J. Am. Chem. Soc.*, 127, 1090-1091 (DOI: 10.1021/ja0433424); (h) Metz A. E., & Kozlowski M. C. (2013), 2‑Aryl-2-nitroacetates as Central Precursors to Aryl Nitromethanes , *α*‑Ketoesters , and *α*‑Amino Acids, *J. Org. Chem.,* 278, 717−722 (DOI.org/10.1021/jo302071s); (i) Su Y., Zhang L., & Jiao N. (2011), Utilization of natural sunlight and air in the aerobic oxidation of benzyl halides, *Org. Lett.,* 13, 2168–2171 (DOI:10.1021/ol2002013).

7. (a) Kategaonkar A. H., Pokalwar R. U., Sonar S. S., Gawali V. U., Shingate B. B., & Shingare M. S. (2010), Synthesis, in vitro antibacterial and antifungal evaluations of new α-hydroxyphosphonate and new *α*-acetoxyphosphonate derivatives of tetrazolo [1, 5-a] quinoline, *Eur. J. Med. Chem.*, 45, 1128–1132 (DOI:10.1016/j.ejmech.2009.12.013); (b) Suresh Kumar K., Bhupendra Reddy C., Veera Narayana Reddy M., Radha Rani C., & Suresh Reddy C. (2012), Green chemical synthesis of *α*-hydroxyphosphonates, *Organic Comm.*, 5, 50–57; (c) Verbrugghen T., Cos P., Maes L., & Van Calenbergh S. (2010), Synthesis and evaluation of *α*-halogenated analogues of 3-(acetylhydroxyamino)propylphosphonic acid (FR900098) as antimalarials, *J. Med. Chem.*, 53, 5342–5346 (DOI:10.1021/jm100211e); (d) Pokalwar R. U. (2006), Synthesis and antibacterial activities of α-hydroxyphosphonates and *α*-acetyloxyphosphonates derived from 2-chloroquinoline-3-carbaldehyde, *Arkivoc*, 196–204, (DOI:10.3998/ark.5550190.0007.b20); (e) Larsen R. D., Corley E. G., Davis P., Reider P. J., & Grabowski E. J. J. (1989), *α*-Hydroxy esters as chiral reagents: asymmetric synthesis of 2-arylpropionic acids, *J. Am. Chem. Soc.*, 111, 7650–7651 (DOI:10.1021/ja00201a075).

8.(a) Rossy C., Majimel J., Fouquet E., Delacôte C., Boujtita M., Labrugère C., Felpin F.-X. (2013), Stabilisation of carbon-supported palladium nanoparticles through the formation of an alloy with gold: application to the Sonogashira reaction, *Chem. Eur. J.* 19, 14024–14029 (DOI:10.1002/chem.201300347); (b) Peng X., Pan Q., & Rempel G. L. (2008), Bimetallic dendrimer-encapsulated nanoparticles as catalysts: a review of the research advances, *Chem. Soc. Rev.*, 37,

1619–1628 (DOI:10.1039/b716441f); (c) Ward T., Delannoy L., Hahn R., Kendell S., Pursell C. J., Louis C., & Chandler B. D. (2013), Effects of Pd on catalysis by Au: CO adsorption, CO oxidation, and cyclohexene hydrogenation by supported Au and Pd-Au catalysts, *ACS Catal.*, 3, 2644–2653 (DOI:10.1021/cs400569v).

9. (a) Wang D., Villa A., Porta F., Prati L., & Su D. (2008), Bimetallic gold/palladium catalysts: Correlation between nanostructure and synergistic effects, *J. Phys. Chem. C.*, 112, 8617–8622 (DOI:10.1021/jp800805e); (b) Singh A. K., & Xu Q. (2013), Synergistic Catalysis over Bimetallic Alloy Nanoparticles, *ChemCatChem*, 5, 652–676 (DOI:10.1002/cctc.201200591); (c) Jiang H. L., & Xu Q. (2011), Recent progress in synergistic catalysis over heterometallic nanoparticles, *J. Mater. Chem.*, 21, 13705 (DOI:10.1039/c1jm12020d); (d) Chen Q., Tanaka S., Fujita T., Chen, L., Minato T., Ishikawa Y., Jin T. (2014), The synergistic effect of nanoporous Au-Pd alloy catalysts on highly chemoselective 1,4-hydrosilylation of conjugated cyclic enones, *Chem. Commun.*, 50, 3344–3346 (DOI:10.1039/c3cc49524h).

10. (a) Song H. M., Moosa B. A., & Khashab, N. M. (2012), Water-dispersable hybrid Au–Pd nanoparticles as catalysts in ethanol oxidation, aqueous phase Suzuki–Miyaura and Heck reactions. *J. Mater. Chem.*, 22, 15953 (DOI:10.1039/c2jm32702c); (b) Sarina S., Zhu H., Jaatinen E., Xiao Q., Liu H., Jia J., & Chen C. (2013), Enhancing Catalytic Performance of Palladium in Gold and Palladium Alloy Nanoparticles for Organic Synthesis Reactions through Visible Light Irradiation at Ambient Temperatures, *J. Am. Chem. Soc.,* 135, 5793−5801.

11. (a) Raula, M., Rashid, M. H., Lai, S., Roy, M., & Mandal, T. K. (2012). Solvent-adoptable polymer Ni/Ni-Co alloy nanochains: Highly active and versatile catalysts for various organic reactions in both aqueous and nonaqueous media. *ACS Appl. Mater. Interfaces*, 4, 878–889 (DOI:10.1021/am201549a); (b) Li L., Niu Z., Cai S., Zhi Y., Li H., Rong H., Li Y. (2013), A Pd-Ag bimetallic nanocatalyst for selective reductive amination of nitroarenes, *Chem. Commun.*, 49, 6843–5 (DOI:10.1039/c3cc00249g); (c) Yu W., Porosoff M. D., & Chen J. G.

(2012), Review of Pt-based bimetallic catalysis: From model surfaces to supported catalysts, *Chem. Rev.*, 112, 5780–5817 (DOI:10.1021/cr300096b); (d) Peng X., Pan Q., & Rempel G. L. (2008), Bimetallic dendrimer-encapsulated nanoparticles as catalysts: a review of the research advances, *Chem. Soc. Rev.*, 37, 1619–1628 (DOI:10.1039/b716441f).

12. Lee Y. W., Kim N. H., Lee K. Y., Kwon K., Kim M., & Han S. W. (2008), Synthesis and characterization of flower-shaped porous Au-Pd alloy nanoparticles, *J. Phys. Chem. C.*, 112, 6717–6722 (DOI:10.1021/jp710933d).

13. Zhu Y., Qian H., & Jin R. (2010), An atomic-level strategy for unraveling gold nanocatalysis from the perspective of $Au_n(SR)_m$ nanoclusters, *Chem. Euro. J.*, 16, 11455–11462 (DOI:10.1002/chem.201001086).

14. Tsunoyama H., Sakurai H., Ichikuni N., Negishi Y., & Tsukuda T. (2004), Colloidal gold nanoparticles as catalyst for carbon-carbon bond formation: Application to aerobic homocoupling of phenylboronic acid in water, *Langmuir*, 20, 11293–11296 (DOI:10.1021/la0478189).

15. (a) Hei H., Wang R., Liu X., & Zhang G. (2012), Controlled Synthesis and Characterization of Noble Metal Nanoparticles, 34–40 (DOI:10.4236/snl.2012.23007); (b) Dhital R. N., Kamonsatikul C., Somsook E., & Sakurai H. (2013), Bimetallic gold–palladium alloy nanoclusters: an effective catalyst for Ullmann coupling of chloropyridines under ambient conditions, *Catal. Sci. Technol.*, 3, 3030 (DOI:10.1039/c3cy00303e).

16. Francesco I. N., Wagner A., & Colobert F. (2008), Suzuki-Miyaura coupling reaction of boronic acids and ethyl glyoxylate: Synthetic access to mandelate derivatives, *Eur. J. Org. Chem.*, 3, 5692–5695 (DOI:10.1002/ejoc.200800881).

17. Samanta S., Perera S., & Zhao C. G. (2010), Organocatalytic enantioselective synthesis of both diastereomers of α-hydroxyphosphinates, *J. Org. Chem.*, 75, 1101–1106 (DOI:10.1021/jo9022099).

Chapter 5

Aerobic oxidative cross- dehydrogenative coupling reactions catalyzed by heterogeneous spherical Au-Pd bimetallic nanoparticles: synthesis of α-ketoamide

5.1 Introduction

α-ketoamides are a well-known structural motif in a wide range of pharmaceuticals, drugs and natural products. α-ketoamide based compounds have been reported to act as anticancer agents, HIV inhibitors, FIV protease inhibitors, cyctokine inhibiter, epoxide hydrolase inhibiter, FK506, rapamycin, FKBP12 etc (Figure 5.1). The activities of transition state immunosuppressive drugs like tacrolimus and sirolimus are attributed to the presence of this moiety.[1] Apart from the biologically important application, they act as valuable precursors and synthetic intermediates in many functional group transformations. Due to the importance of the α-ketoamide scaffold, there has been a continuous effort towards the development of newer methods for the synthesis of these important molecules. The classical method involves the amidation of α-ketoacids with activating agents, however it is associated with several disadvantages such as use of strong oxidizing agents, limited substrate scope and harsh reaction conditions. Several other metal catalyzed methodologies have been developed and representative approaches are Pd catalyzed double carbonylation of aryl halides and amines using carbon monoxide,[2] Cu-catalyzed aerobic oxidative coupling of aryl acetaldehydes, Cu-catalyzed direct oxidative synthesis from aryl methyl ketones and Cu-catalyzed aerobic cross-dehydrogenative coupling of amine and α-oxoaldehyde etc.[3] However, most of the methods involve important drawbacks such as use of homogeneous catalysts, hazardous nature and sensitivity towards moisture and air.

Furthermore, most of the oxidative coupling reactions are highly exothermic, and since the reaction passes through transition state with high activation energy, harsh reaction conditions such as elevated temperatures and high pressure are required for significant conversion.[4] Towards the development of metal free approaches for the synthesis of α-ketoamides, carbonyl based starting materials such as aryl methyl ketones and oxoaldehydes under oxidative amidation condition with oxidants like *tert*-butyl hydrogen peroxide (TBHP) and selenium dioxide have been used.[5] Very recently, I_2 mediated formation of α-ketoamides in presence of TBHP from terminal alkenes/alkynes

or acetophenone have been reported.[6] One of the major drawbacks of this methodology is the selectivity of the products and formation of large fraction of undesired byproducts in the reaction. Vishwakarma *et.al.* recently reported a dimethyl sulfoxide (DMSO) promoted synthesis of ketoamide,[7] however this method is limited only to secondary amines. Although the reported methods have been moderate to highly successful towards the formation of *α*-ketoamides, the development of heterogeneous, recyclable catalysts for the amidation reaction is highly desired.
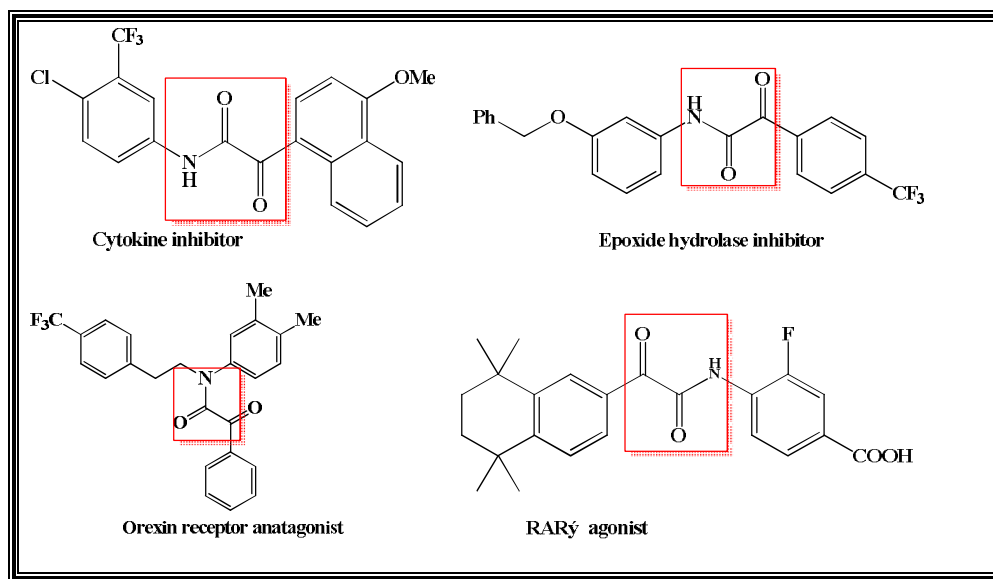
Figure 5.1 *A few examples of biologically active compounds containing α-ketoamide.*

In our pursuit towards the development of nanoparticle based catalysts for important organic transformations, we looked for the efficacy of noble metal based nanocatalytic systems for oxidative coupling reactions leading to the formation of *α*-ketoamides. Looking into the inherent advantages such as heterogeneity as well as recyclability, these nanocatalysts offer an alternative, convenient and efficient method for these important transformations. Although Au based catalytic systems have been reported for oxidation reactions as well as coupling reactions, development of a novel synthetic pathway with vast substrate scope under mild reaction conditions will bring forth a new impetus in organic chemistry.

Herein, we report the synthesis of α-ketoamides using 2-oxoaldehyde as a starting material that undergoes oxidative coupling with aniline derivatives using Au-Pd alloy nanoparticles as catalyst. Whereas monometallic Au or Pd nanoparticles could not sufficiently catalyze the reaction under mild conditions, the alloy nanoparticles of these two metals efficiently performed the reaction through their synergistic effect.[8,9] 2-oxoaldehydes were used as starting materials because of the higher reactivity of aldehyde in these groups in comparison to normal aldehydes owing to the existence of an electron-withdrawing ketone group. Interestingly, by this methodology, primary amines such as substituted anilines could be coupled, leading to the formation of α-ketoamides. To the best of our knowledge, this is the first report of any noble metal based nanocatalytic systems used as efficient catalyst for cross dehydrogenative coupling reactions.
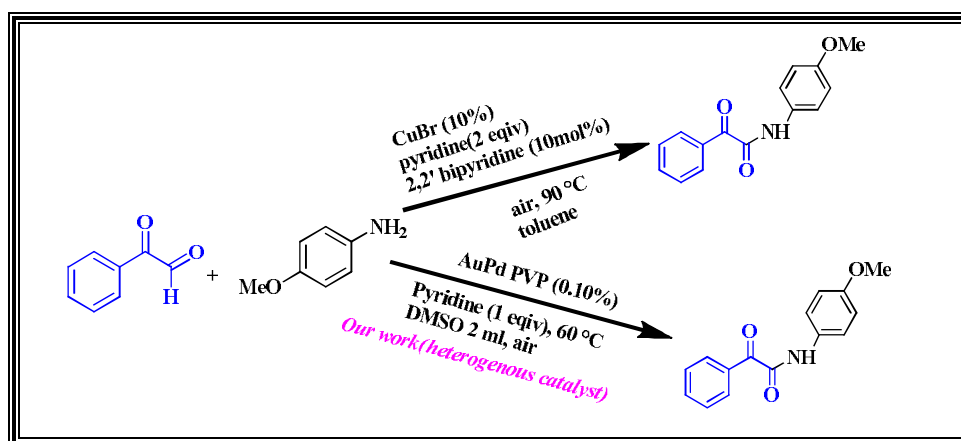
Figure 5.2 *Au-Pd alloy nanoparticles catalyzed oxidative cross-dehydrogenative coupling.*

5.2 Characterization of nanoparticles

The PVP stabilized Au, Pd and Au-Pd alloy nanoparticles with various compositions were prepared via the co-reduction method using $NaBH_4$ as a reducing agent in water as reported in the earlier chapter. As the physico-chemical properties of the nanoparticles evaluated by various spectroscopic and microscopic studies have been reported in the earlier chapter, the characterization is not repeated in this chapter.

5.3 Results and discussion

With the aim for the development of a nanocatalytic system towards the formation of α-ketoamides through the coupling of α-oxoaldehyde with a primary amine, we performed the reaction of phenylglyoxal and 4-methoxy phenylamine as a model reaction under various reaction conditions in order to explore the optimal reaction conditions. Various parameters such as temperature, solvent and base etc. were evaluated in order to study the performance of the various catalysts. The evaluation of the reaction parameters on the catalytic activity of the nanocatalysts were based on the criteria that the reaction could be carried out at low temperature using O_2 present in air as sole oxidizing agent (Table 5.1). The desired product 3aa was obtained with 20% yield using Au-PVP catalysts in DMSO with pyridine as a base at 50 °C after a reaction time of 24 hours. No products were formed in the absence of catalyst even at elevated temperature. Among all the solvents scrutinized, DMSO afforded the best results whereas other solvents such as DMF, acetonitrile and others afforded low yield. Further studies indicated that base promote this transformation and among the various bases studied pyridine afforded superior yield (entry 12, Table 5.1). The effect of reaction temperature on the yield of 3aa at different time intervals was subsequently examined. It was observed that increasing the reaction temperature to 80 °C and reaction time to 48 hours did not increase the yield of the product significantly. When monometallic Pd-PVP nanoparticles were used as a catalyst under similar reaction conditions in DMSO-pyridine, the desired product 3aa was obtained with 31% yield (entry 4, Table 5.1). Dramatic enhancement in the reaction yield was obtained when a bimetallic Au-Pd alloy nanoparticle was used as a catalyst. The best results were obtained with $Au_{0.5}Pd_{0.5}$PVP catalyst, where the desired product N-(4-Methoxy-phenyl)-2-oxo-2-phenyl-acetamide was achieved with 88% yield in DMSO-pyridine at 50 °C in 16 hours. Increasing the reaction temperature to 80 °C afforded slight enhancement in the product yield (entry 14, Table 5.1). Considering the relatively lower yield of the coupling product obtained using monometallic nanoparticles as catalysts, the efficiency of the bimetallic nanoparticles in catalyzing the oxidative cross-dehydrogenative reaction was pleasantly surprising.

Table 5.1 Optimization of oxidative reaction with phenyl glyoxal and 4-methoxy aniline
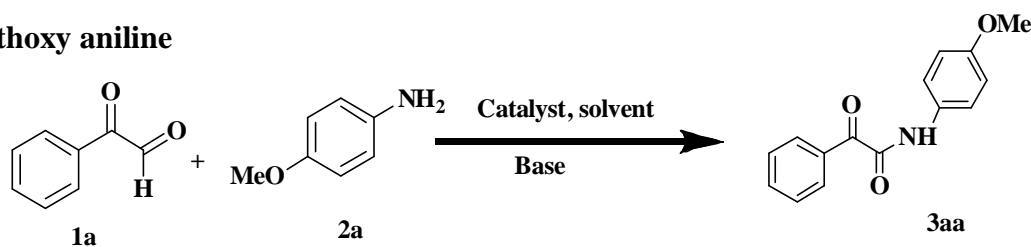
Entry	Catalyst	Solvent	Base	Temperature(°C)	Time	Yield %[ab]
1	None	DMSO	Pyridine	110	24h	No
2	AuPVP	DMSO	Pyridine	50	24h	20
3	AuPVP	DMSO	Pyridine	80	20h	28
4	PdPVP	DMSO	Pyridine	50	20h	31
5	$Au_{0.5}Pd_{0.5}PVP$	Water	Pyridine	50	20h	30
6	$Au_{0.5}Pd_{0.5}PVP$	MeOH	Pyridine	50	22h	47
7	$Au_{0.5}Pd_{0.5}PVP$	EtOH	Pyridine	50	20h	36
8	$Au_{0.5}Pd_{0.5}PVP$	DCM	Pyridine	50	20h	10
9	$Au_{0.5}Pd_{0.5}PVP$	DMF	Pyridine	50	20h	70
10	$Au_{0.5}Pd_{0.5}PVP$	Toluene	Pyridine	50	30h	50
11	$Au_{0.5}Pd_{0.5}PVP$	THF	Pyridine	50	30h	12
12	$Au_{0.5}Pd_{0.5}PVP$	**DMSO**	Pyridine	**50**	**16h**	**88**
13	$Au_{0.5}Pd_{0.5}PVP$	DMSO	Pyridine	RT	30h	60
14	$Au_{0.5}Pd_{0.5}PVP$	DMSO	Pyridine	80	16h	91
15	$Au_{0.5}Pd_{0.5}PVP$	DMSO	None	80	30h	None
16	$Au_{0.5}Pd_{0.5}PVP$	DMSO	K_2CO_3	50	24h	Trace
17	$Au_{0.5}Pd_{0.5}PVP$	DMSO	Cs_2CO_3	50	30h	Trace
18	$Au_{0.5}Pd_{0.5}PVP$	DMSO	Na_2CO_3	50	30h	Trace
19	$Au_{0.5}Pd_{0.5}PVP$	DMSO	DABCO	50	20h	45
20	$Au_{0.5}Pd_{0.5}PVP$	DMSO	Triethyl amine	50	30h	40

Reaction conditions: substrate phenylglyoxal 1a (1.0 mmol), p-anisidine 2a (1.0 mmol), 0.10 mol % catalyst, solvent (2ml), base (1 equivalent to phenylglyoxal) [a]Isolated yield, [b]NMR conversion compare to starting material aldehydes1a.

In order to have a better view of the catalysts, we performed the model reaction using alloy nanoparticles with varied composition of the metallic constituents. For this purpose, Au_xPd_{1-x} composites were prepared using PVP as the stabilizing agent using the same methodology except for varying the initial concentration of the metal precursors. As shown in the table 5.2, the nanocomposites showed almost equivalent composition of metals (measured by ICP-AES measurements) as the ratio of the $HAuCl_4$ and H_2PdCl_4 added initially. When the model oxidative dehydrogenative coupling reaction was performed at the optimized condition (DMSO-pyridine, 50 °C, 16 hours under

air) using various compositions of Au_xPd_{1-x}-PVP nanoparticles, the best results were obtained for $Au_{0.5}Pd_{0.5}$ (88% yield of the product) and $Au_{0.4}Pd_{0.6}$ (86% yield of the product). However for all future studies, we used $Au_{0.5}Pd_{0.5}$-PVP composites. The results are summarized in Table 5.3. The reaction kinetics was found to be highly dependent on the catalyst loading with increased reaction yield with higher catalyst loading.[10]

Table 5.2 Au/Pd ratio as measured by ICP-AES measurements for various Au-Pd compositions

Expected Designed compositions	$Au_{0.75}Pd_{0.25}$	$Au_{0.6}Pd_{0.4}$	$Au_{0.5}Pd_{0.5}$	$Au_{0.4}Pd_{0.6}$	$Au_{0.25}Pd_{0.75}$
The composition analysis by ICP-AES (Au/Pd)	70.28/29.34	65.12/34.41	53.34/46.15	37.24/62.7	22.24/77.62

Table 5.3 Catalytic performance of Au-PdPVP with varying the ratio of Au/Pd.
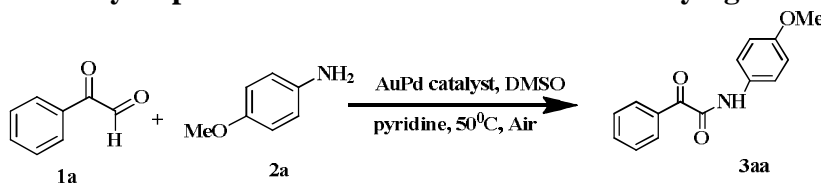
Entry	Catalyst	Catalyst loading	Yield (%)[ab]
1	Au PVP	0.10 mol%	20
2	$Au_{0.75}Pd_{0.25}$PVP	0.10 mol%	41
3	$Au_{0.6}Pd_{0.4}$PVP	0.10 mol%	68
4	**$Au_{0.5}Pd_{0.5}$PVP**	**0.10 mol%**	**88**
5	$Au_{0.4}Pd_{0.6}$PVP	0.10 mol%	86
6	$Au_{0.25}Pd_{0.75}$PVP	0.10 mol%	69
7	Pd PVP	0.10 mol%	30
8	$Au_{0.5}Pd_{0.5}$PVP	0.02 mol%	33
9	$Au_{0.5}Pd_{0.5}$PVP	0.05 mol%	63
10	$Au_{0.5}Pd_{0.5}$PVP	0.15 mol%	89

Reaction conditions: substrate phenylglyoxal 1a (1.0 mmol), p-anisidine **2a** (1.0 mmol), 2ml DMSO, pyridine (1 equiv. w.r.t. 1a), [a]Isolated yield, 50 °C. [b]NMR conversion compare to starting material aldehydes **1a**.

Following this optimized procedure, different sets of experiments were carried out to investigate the scope and limitation of the reaction. First the scope of substituted amines (2b) was investigated (Table 5.4). Both electron-rich and electron-deficient anilines could be smoothly transformed into the desired products (3ac-3af, Table 5.4). Halo-substituted aniline derivatives survived well leading to halo-substituted products (3ac, 3ad and 3ak Table 5.4). N-substituted anilines such as N-methylaniline and hetero-aryl amines could be smoothly transformed into the desired products (3ai, 3ag Table 5.4). The electron-donating substituents (3aj, 3ae, 3al) on the aromatic ring in anilines increased the yield when compared to electron withdrawing groups (3ah, 3ak, 3af).

Table 5.4 Oxidative coupling of phenyl glyoxal with substituted anilines[ab]
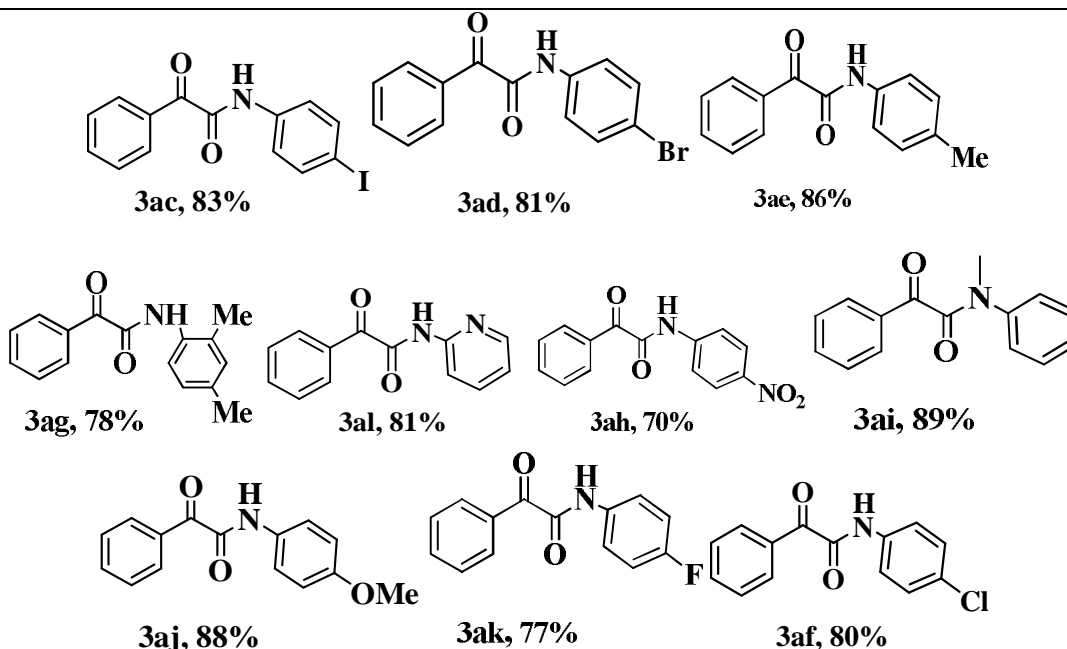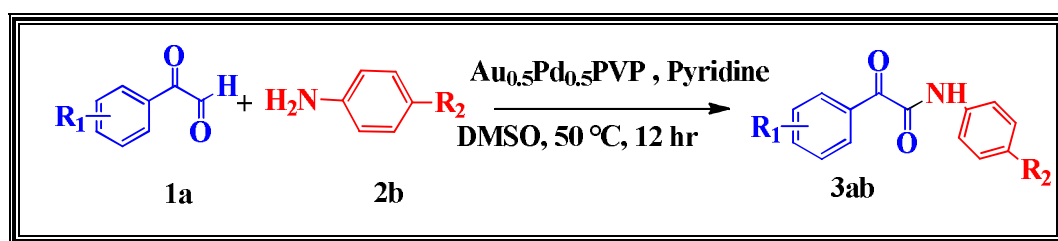
Reaction conditions: substrate 1a (1.0 mmol), aromatic amine 2a (1.0 mmol), 0.10 mol% Au$_{0.5}$Pd$_{0.5}$PVP. [a] Isolated yield. [b]NMR conversion compare to starting material aldehydes 1a.

The scope of the Au-Pd nanoparticle-catalyzed aerobic oxidative dehydrogenative functionalization was further expanded to a variety of substituted α-carbonyl aldehydes. Substituted anilines reacted with substituted aldehydes, leading to good to excellent yields of desired products (3be, 3ce, 3dj, 3ci and 3ei Table 5.5). Furthermore, aryl α-carbonyl aldehyde with both electron-donating and electron-withdrawing groups did not affect the efficiency of this transformation.

Table 5.5 Oxidation coupling substituted phenyl glyoxals with substituted anilines[ab]
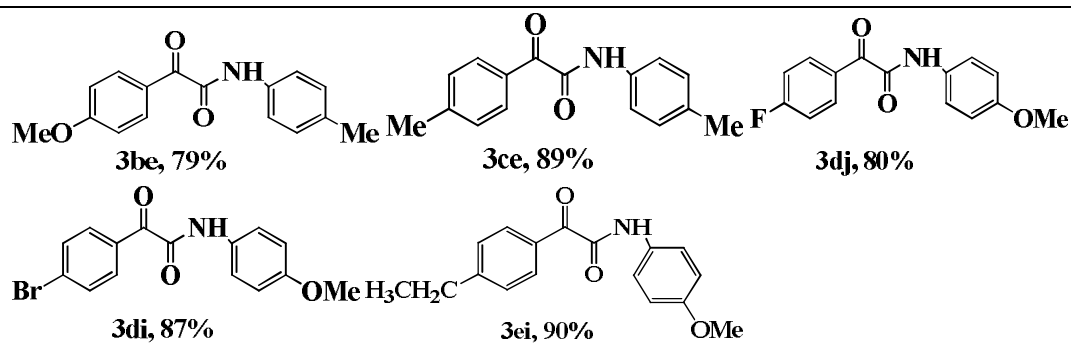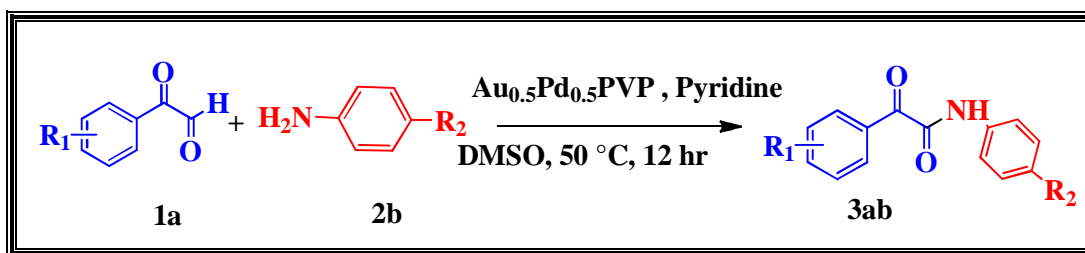
Reaction conditions: substrate **1a** (1.0 mmol), anilines **2b** (1.0 mmol), 0.10 mol% Au$_{0.5}$Pd$_{0.5}$PVP. [a]Isolated yield. [b]NMR conversion compare to starting material aldehydes 1a.

5.4 Proposed Mechanism for oxidative coupling with 2‑Oxoaldehydes and aromatic amine

Aldehydes are desirable starting materials in amide synthesis due to their ready availability and nontoxic nature. However, under the standard reaction conditions, 4-Methoxy phenylamine (1a) and benzaldehyde (4a) did not afford the desired product N-(4-Methoxy-phenyl)-2-oxo-2-phenyl-acetamide (scheme 6), which illustrates that this nanocatalytic system catalyzed the reaction through a different pathway in contrast to previous reported C-N

coupling of aldehydes.[11] Furthermore, the desired product was not detected when the reaction of 1a and 2a was carried out under Argon(scheme 5), even employing higher catalytic loading of Au-Pd nanoparticles (0.2 mol%). This result shows that molecular oxygen plays a role not only as the oxidant but also as an initiator to trigger this catalytic process. From the earlier literature, it is well-known that the adsorption of O_2 on metallic nanoparticle surface leads to the formation of a superoxide species. The nucleophilic attack of amines on phenylglyoxal leads to the formation of an anion, which is adsorbed onto the nanoparticle surface to give intermediate (II) Au-Pd-O_2^-, the superoxo- or peroxo- like species stabilized on the cluster surface eliminates β-hydrogen from the intermediate (II) to generate a hemiaminal intermediate (III) and finally to give the ketoamide product. From the mechanism it is evident that there is no possibility of amide byproduct formation as it will involve C-C bond cleavage.

5.5 Systematic study of the oxidative coupling reaction with different substrates

Scheme 4

3ab (0%)

Scheme 5:

3ab (0%)

Scheme 6:

3db (0%)
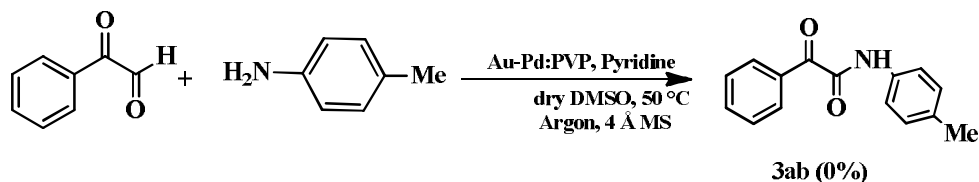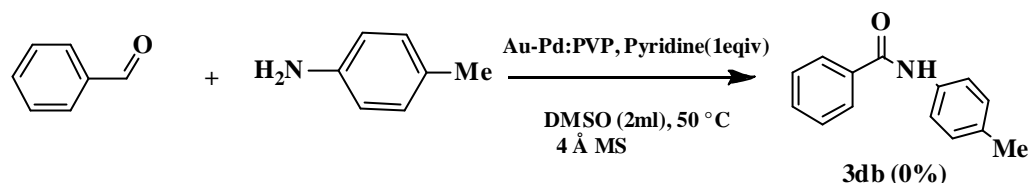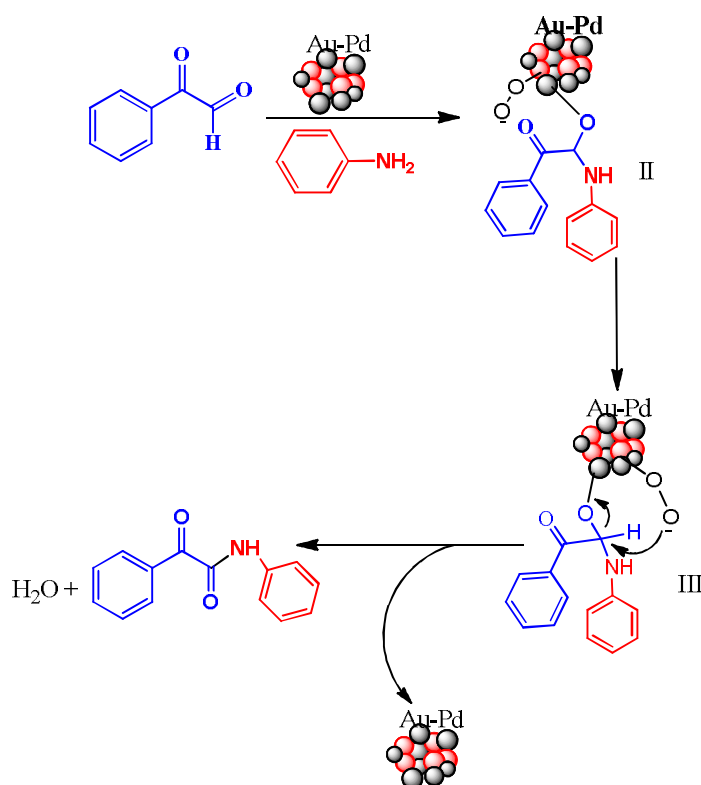
Figure 5.3 *Mechanistic proposal of Au$_{0.5}$Pd$_{0.5}$PVP nanoparticle catalyzed oxidative crossdehydrogenative coupling.*

5.6 Reusability test of Au$_{0.5}$Pd$_{0.5}$ -PVP alloy nanoparticles
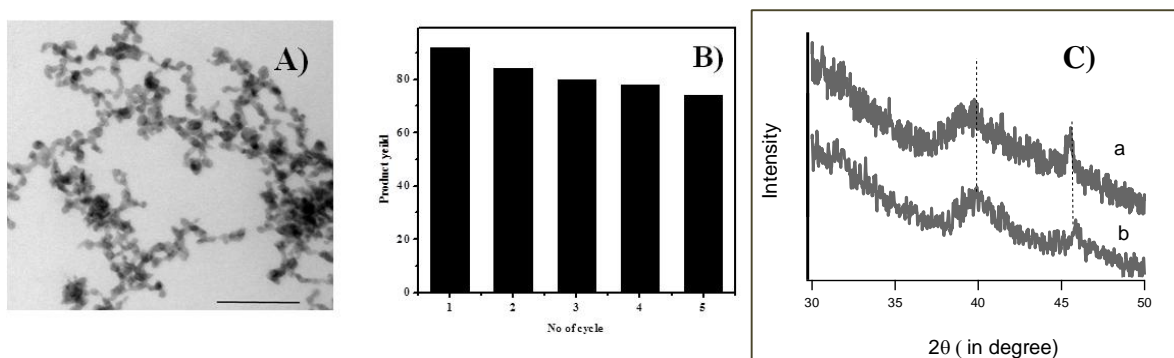
Figure 5.4 *A) Transmission electron microscopy of Au-Pd PVP nanoparticle after 3rd cycle; scale bar 50 nm, B) Recyclability test of Au-Pd-PVP alloy nanoparticles for the oxidative coupling reaction for the model reaction; C) PXRD pattern of Au-Pd-PVP alloy (a) before and (b) after participating in the model coupling reaction.*

Recyclability is an important criteria for studying the effectiveness of a heterogeneous catalyst. In order to study the efficiency of the $Au_{0.5}Pd_{0.5}$-PVP nanocatalysts, we performed the model catalytic reaction using the nanocatalysts recycled after consecutive cycles. Although the catalytic activity of the nanocatalysts decreased after every cycle, still we could obtain 69% yield of the desired coupled product after the fifth cycle, confirming high activity of the nanocatalysts. To ensure the reproducibility of the transformation, repeated typical experiments were carried out under identical reaction conditions. The alloy catalysts were recovered after subsequent run through high speed centrifugation, washed three times with water, dried in an oven at 80 °C for 10 h and tested in the subsequent run. The morphology of the nanoparticles recovered after the 3rd cycle was evaluated by TEM, which showed that the interparticle separation was reduced and clusters gathered to form a chain-like structure. X-ray diffraction studies did not show any considerable shift in the diffraction peak maxima for (111) and (200) planes of Au-Pd nanoparticles before and after participating in the catalytic reaction. Moreover no peaks corresponding to the formation of PdO was observed. The results clearly indicate that there was no major structural changes in the Au-Pd-PVP nanoparticles. Probably, PVP could not function as an effective stabilizer for the Au-Pd nanoparticles in the catalytic reaction environment (in presence of O_2 and amines), resulting in the agglomeration of the nanoparticles as revealed by TEM studies.

Leaching of Pd atoms during the oxidation reactions is a prominent phenomenon, where Pd leached in the oxidative environment functions in a pseudo-homogeneous way, leading to enhanced catalytic activity. This phenomenon is quite prominent in case of oxidative cross-coupling reactions such as Suzuki or Heck reactions, where the addition of halogenated substrates induces the leaching of small metal clusters from the alloy surface.[13] In order to gain an insight to the possibility of leaching in Au-Pd-PVP catalyst during catalytic reaction we performed the following experiment. The model reaction of phenylglyoxal and 4-methoxy phenylamine was performed in the presence of the $Au_{0.5}Pd_{0.5}$-PVP nanocatalyst (0.1 mol%) in DMSO-pyridine medium under optimized reaction conditions. The reaction was stopped after 8 hours of

continuous stirring, cooled to room temperature and the Au-Pd nanocatalysts were separated from the reaction mixture by high speed centrifugation. The supernant was separated into two fractions, one fraction was worked up to evaluate the reaction yield through ^{1}H NMR spectroscopy, whereas the other fraction was allowed to stir for another 12 hours under the standard reaction conditions (50 ^{0}C, air). The reaction yield was evaluated after workup followed by ^{1}H NMR spectroscopy. The ^{1}H NMR spectroscopic results revealed that there was no enhancement in the formation of the desired coupling product in the reaction for these two fractions. This experiment clearly demonstrated that there was no active catalyst remaining in the reaction mixture, after the Au-Pd nanocatalysts were separated from the reaction mixture. In order to further confirm any leaching of metals, we performed the inductively coupled plasma atomic emission spectroscopy (ICP-AES) of the $Au_{0.5}Pd_{0.5}$-PVP catalysts before and after their participation in the model coupling reaction between phenylglyoxal and 4-methoxy phenylamine. There was no significant leaching of Au or Pd during the participation of the nanocatalyst in the oxidative dehydrogenative coupling reaction (Table 5.6). The amount of Pd leached during (1.84 ppm) and after the completion (1.26 ppm) was well below the maximum acceptable range of Pd (3-5 ppm). On the other hand leaching of Au was not detected during or after the catalytic reaction.

The enhanced catalytic activity of AuPd alloy nanoparticles compared to the monometallic Au or Pd nanoparticles for the oxidative dehydrogenative coupling reactions towards the formation of α-ketoamides can be attributed to the synergistic effect between the two metallic counterparts. Au-PVP was unable to catalyze the coupling reaction, although small Au nanoclusters are known for their activity towards oxidation reactions (e.g. oxidation of alcohols) in presence of base. As shown in Chapter 3 and as reported in several earlier studies, the catalytic activity of Au nanoparticles proceeds through the adsorption of molecular oxygen leading to the formation of oxygen superoxide moiety on Au nanoparticle surface.

Table 5.6 Amount Au and Pd atoms in Au$_{0.5}$Pd$_{0.5}$-PVP nanocatalysts (before and after the catalytic reaction) and in the supernatant liquid from the catalytic reaction as detected by ICP-AES.

Entry	Reagents	Amount of Au/Pd ratio detected by ICP-AES
1	Au$_{0.5}$Pd$_{0.5}$-PVP catalyst before reaction	Au/Pd 53.3/46.7
2	Au$_{0.5}$Pd$_{0.5}$-PVP catalyst after reaction (after completion)	Au/Pd 52.1/47.9
3	Supernatant of reaction (after 8 hours of reaction)	Au (not detected) Pd (1.84 ppm)
4	Supernatant of reaction (after completion of reaction)	Au (not detected) Pd (1.26 ppm)

However using Au nanoparticles alone as a catalyst could not afford the synthesis of α-ketoamides under the present reaction conditions. On the other hand, Pd nanoparticles also could not afford higher yield of the product under the present reaction conditions. Pd (II) catalysts have shown high catalytic activities towards oxidative coupling reactions either under inert atmosphere or in presence of external oxidizers, whereas under aerial reaction environment they are easily converted to PdO nanoparticles.[14] However a combination of the two metals in a alloy composition could afford the synthesis of α-ketoamides under mild reaction conditions under aerial environment. This could be attributed to the synergistic effect between the two metallic constituents where charge transfer from Pd to Au leads to enhanced catalytic activity due to change in electronic structure.

5.7 Conclusion

In summary, we have shown that Au-Pd alloy nanoparticles function as efficient catalyst for the oxidative dehydrogenative coupling reactions towards the formation α-ketoamides under aerobic conditions. The reaction involved phenyl glyoxals and primary aromatic amines using DMSO as a solvent in presence of pyridine as a base under mild conditions. Although monometallic Au or Pd nanoparticles could not function as effective catalysts for this reaction, the alloy Au-Pd afforded the reaction with high yield of the desired product through remarkable synergistic effect that accounts for their high activity and stability. The use of nanocatalytic systems for the synthesis of important biologically important molecules through a heterogeneous pathway will be crucial for large scale synthesis. Although the deactivation of the nanocatalysts was observed during recyclability studies of the catalyst due to agglomeration of the nanoparticles, it could be envisioned that designing alloy nanocatalytic systems for important organic transformations will offer new opportunities for the application of heterogeneous catalysts for other related reactions.

5.8 Experimental sections

A) Instrumentation :

All reactions were carried out in air and monitored by TLC using Merck 60 F254 pre coated silica gel plates (0.25 mm thickness) and the products were visualized by UV detection. Flash chromatography was carried out with silica gel (200-300 mesh). FT-IR spectra were recorded on a Bruker Tensor-27 spectrometer. 1H and 13C NMR spectra were recorded on a Bruker Advance (III) 400 MHz spectrometer. Data for 1H NMR are reported as a chemical shift (δ ppm), multiplicity (s = singlet, d = doublet, q = quartet, m = multiplet), coupling constant J (Hz), integration, and assignment, data for 13C are reported as a chemical shift. UV-visible spectra were recorded in a Varian Cary 100 Bio spectrophotometer, TEM images were recorded on a Tecnai G2 20 Ultra- Twin microscope. Powder XRD spectra were recorded on a Bruker D8 Advance diffractometer using Cu Kα as the X-ray Source.

B) Materials:

Hydrogen tetrachloroaurate(III) hydrate ($HAuCl_4,H_2O$, purum, -52% Au basis), H_2PdCl_4 ($PdCl_2$ in HCl medium), Poly(vinylpyrrolidone) (PVP, Mw = 300,000), Sodium Borohydride ($NaBH_4$), Phenyl glyoxals were purchased from sigma aldrich. All these chemicals were used without further purification. MilliQ water was used throughout the experiment.

C) Synthesis of nanoparticles:

In a typical synthesis, 555.5 mg of PVP (K-30) was dissolved in 46 mL of MilliQ water and to the solution was added quantitative amount $HAuCl_4/H_2PdCl_4$ mixtures in molar ratios of 3:1, 1:1, 2.1, 1.2 and 1:3 and monomer unit of PVP was kept at 1:100. The resulting solutions were stirred for 30 mins at 0 °C. The solution was maintained at 4 °C before reduction, and an aqueous solution (5 mL) of $NaBH_4$ (20 mg, 0.52 mmol) was added rapidly under vigorous stirring. The color of the mixture was turned from pale yellow to brown, indicating the formation of Au–Pd bimetallic clusters. Thus obtained $Au_{0.5}Pd_{0.5}PVP$ clusters were subsequently dialyzed to remove the inorganic impurities such Na^+ and Cl. The dialyzed hydrosol of AuPdPVP was diluted to 25 mL and stored in refrigerator for catalytic reactions and characterizations. For comparison, Au and Pd monometallic nanoparticles were prepared in the same way by substituting aqueous solutions of $HAuCl_4/K_2PdCl_4$ mixtures by $HAuCl_4$ and H_2PdCl_4 solutions, respectively.
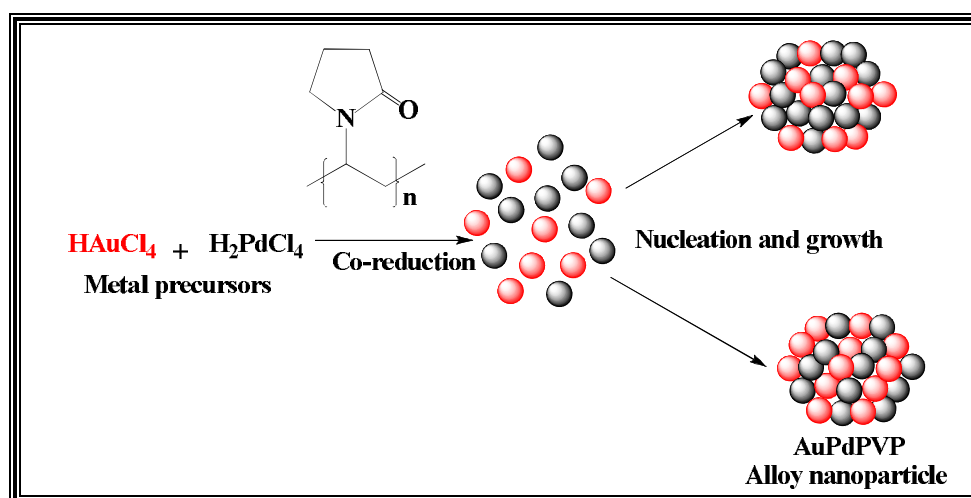
Figure 5.5 *Synthesis of AuPd alloy nanoparticles with co reduction process.*

D) Synthesis of α-ketoamides:

2-Oxo-2-phenylacetaldehyde monohydrate 1a (1.0 mmol), 4-methoxy aniline 2a (1.0 mmol), pyridine (1.0 mmol) was mixed properly in DMSO (2mL) solvent medium using Au-Pd:PVP (0.10 mol %) under aerobic condition. The reaction was continued with heating in temperature 60 °C for 12-18 hr. After cooling down to room temperature, the

reaction mixture was extracted with di-ethyl ether after adding water, and the combined organic phase was dried with sodium sulfate, filtered, and concentrated under vacuum. The resulting crude mixture was purified by flash chromatography with unmetalated silica (cyclohexane/ EtOAc).
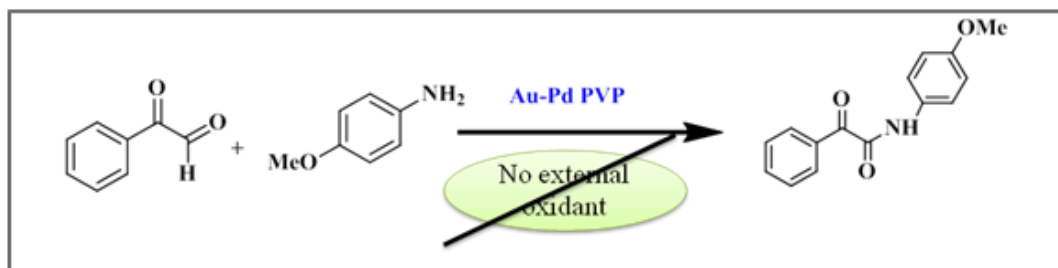
Figure 5.6 *Synthesis of α-ketoamides catalyzed with Aupd alloy nanoparticles.*

NMR data

1. **3aaf (Table 5.4)**
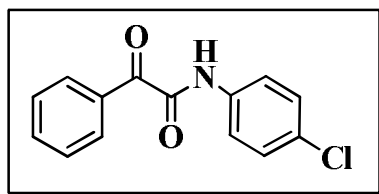
^{1}H NMR (CDCl$_3$, 400M Hz): δ_H = 8.97 (s, bs, NH), 8.44 (dd, J = 4Hz, 2H), 7.69-7.65 (m, 3H), 7.52 (t, J = 8 Hz, 2H), 7.37 (tt, J = 4Hz, 2H); ^{13}C NMR (CDCl$_3$, 100M Hz): δ 187.03, 158.73, 135.21, 134.80, 132.94, 130.42, 129.32, 128.63, 121.13.

2. **3aaj (Table 5.4)**
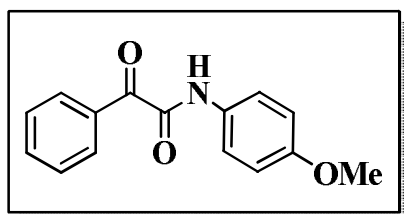
^{1}H NMR (CDCl$_3$, 400M Hz): δ_H = 8.86 (bs, NH), 8.42 (d, J = 8 Hz, 2H), 7.66 (t, J = 12 Hz, 3H), 6.93 (d, J = 8 Hz, 2H), 3.63 (s, 3H); ^{13}C NMR (CDCl$_3$, 100M Hz): δ 187.59,

158.63, 157.08, 139.31, 135.41, 134.59, 133.22, 131.48, 130.23, 129.11, 128.58, 125.62, 125.62, 123.14, 121.51, 114.40, 114.08, 55.53.

3. 3aag (Table 5.4)
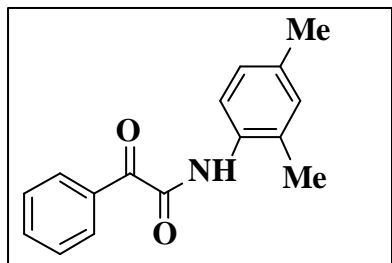
^{1}H NMR (CDCl$_3$, 400M Hz): δ_H = 8.24 (d, J = 1.6 Hz, 2H), 8.12 (s, 1H), 7.50 (d, J = 7.2 Hz, 1H), 7.40 (t, J = 8 Hz, 2H), 7.00 (s, 1H), 2.30 (s, 3H), 2.24 (s, 3H); ^{13}C NMR (CDCl$_3$, 100M Hz): δ 190.60, 155.09, 145.24, 138.27, 135.03, 133.77, 133.02, 127.16, 116.37, 20.74, 7.76.

4. 3aal (Table 5.4)
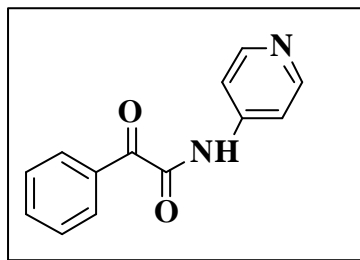
^{1}H NMR (CDCl$_3$, 400M Hz): δ_H = 9.13 (s, NH), 8.52 (s, 2H), 8.331 (d, J = 4 Hz, 2H), 7.81-7.57 (m, 3H), 7.45 (t, J = 8 Hz, 2H); ^{13}C NMR (CDCl$_3$, 100M Hz): δ186.33, 159.53, 150.87, 143.72, 135.03, 132.57, 131.46, 126.71, 113.86.

5. 3aad (Table 5.4)
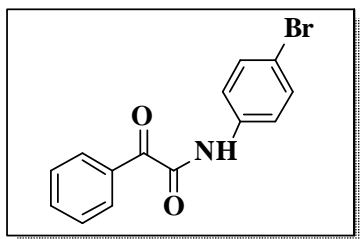
^{1}H NMR (CDCl$_3$, 400M Hz): δ_H = 8.41 (d, J = 8 Hz, 2H), 7.67 (d, J = 8Hz, 1H), 7.61 (d, J = 12 Hz, 1H), 7.52 (t, J = 6 Hz, 4H); ^{13}C NMR (CDCl$_3$, 100M Hz): δ 190.35, 157.38, 134.96, 133.83, 132.62, 123.51, 121.45, 116.14.

6. 3aae (Table 5.4)
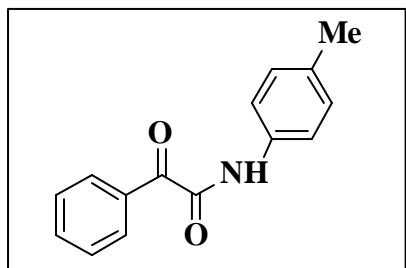
^{1}H NMR (CDCl$_3$, 400M Hz): δ_H = 8.91 (s, NH), 8.42(d, J = 1.6Hz, 1H), 7.63(t, J = 4 Hz, 1H), 7.58 (d, J = 12 Hz, 2H), 7.51 (t, J = 8 Hz, 3H), 7.20 (d, J = 8 Hz, 2H); ^{13}C NMR (CDCl$_3$, 100M Hz): δ 187.53, 158.75,

135.08, 134.60, 131.48, 129.75, 128.73, 128.56, 128.21, 119.88, 20.99.

7. 3aak (Table 5.4)
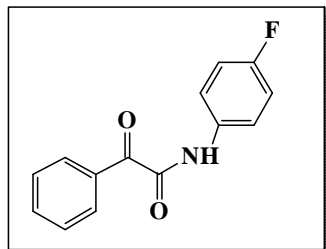
^{1}H NMR (CDCl$_3$, 400M Hz): δ$_H$ = 8.29 (d, J = 8 Hz, 2H), 7.62 (d, J = 8 Hz, 2H), 7.50 (t, J = 8 Hz, 2H), 7.35 (d, J = 4 Hz, 2H), 7.13 (t, J = 4 Hz, 2H); ^{13}C NMR (CDCl$_3$, 100M Hz): 190.48, 164.06, 161. 59, 156.52, 142.06, 135.06, 133.69, 130.69, 128.44, 123.29, 116.47.

8. 3di (Table 5.5)
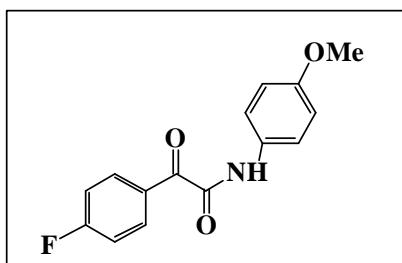
^{1}H NMR (CDCl$_3$, 400M Hz): δ$_H$ = 9.13 (s, NH), 8.39 (d, J = 8 Hz, 2H), 7.40 (d, J = 8 Hz, 2H), 7.17 (d, J = 12 Hz 2H), 6.98 (d, J = 4 Hz 2H), 3.86(s, 3H); ^{13}C NMR (CDCl$_3$, 100M Hz): δ189.35, 160.70, 141.41, 139.31, 133.45, 123.61, 115.4, 114.69, 55.59.

9. 3ei (Table 5.5)
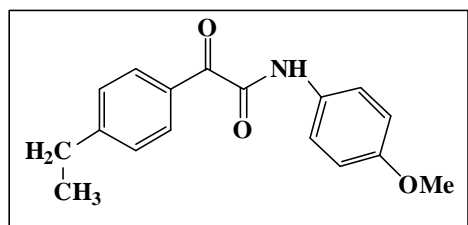
^{1}H NMR (CDCl$_3$, 400M Hz): δ$_H$ = 8.27 (s, NH), 8.15(d, J = 8 Hz, 2H), 7.32(d, J = 8 Hz, 2H), 7.25(d, J = 8 Hz, 2H), 6.88 (d, J = 12 Hz, 2H), 3.77(s, 3H), 2.65(q, J = 4 Hz, 2H), 1.20(t, J = 8 Hz, 3H); ^{13}C NMR (CDCl$_3$, 100M Hz): δ 190.43, 160.44, 154.54, 150.54, 141.79, 133.15, 130.81, 127.94, 123.47, 114.60, 55.53, 29.69, 24.06, 15.05.

5.8 References

1. (a) Zhang Y., Cui X., Shi F., & Deng Y. (2012), Nano-gold catalysis in fine chemical synthesis, *Chem. Rev.*, 112, 2467–2505 (DOI:10.1021/cr200260m); b) Hutchings G. J. (2013), Au–Pd nanoalloys supported on Mg–Al mixed metal oxides as a multifunctional catalyst for solvent-free oxidation of benzyl alcohol *Dalton Transactions*, 14498–14508 (DOI:10.1039/c3dt51855h); (c)

Catalysts A. T., Enache D. I., Catalysts A. T., Enache D. I., Edwards J. K., Landon P., Hutchings G. J. (2011) Solvent-Free Oxidation of Primary Alcohols to Aldehydes Using Au-Pd/TiO$_2$ Catalysts, *Science 362* (DOI:10.1126/science.1120560); (d) A. T., Enache D. I., Catalysts A. T., Enache D. I., Edwards J. K., Landon P., Hutchings G. J. (2011), Solvent-Free Oxidation of Primary Alcohols to Aldehydes Using Au-Pd/TiO$_2$ Catalysts, *Science,* 311, 362 (DOI:10.1126/science.1120560); (e) Chem J. M., Song H. M., Moosa A., & Khashab N. M. (2012), Water-dispersable hybrid Au – Pd nanoparticles as catalysts in ethanol oxidation , aqueous phase Suzuki – Miyaura and Heck reactions, *J. Mater. Chem.,* 22, 15953–15959 (DOI:10.1039/c2jm32702c); (f) Balcha T., Strobl J. R., Fowler C., Dash P., & Scott R. W. J. (2011), Selective Aerobic Oxidation of Crotyl Alcohol Using AuPd Core-Shell Nanoparticles, *ACS. Catal*., 1, 425–436 (DOI.org/10.1021/cs200040a); (g) Tongsakul D., Nishimura S., & Ebitani K. (2013), Platinum / Gold Alloy Nanoparticles-Supported Hydrotalcite Catalyst for Selective Aerobic Oxidation of Polyols in Base-Free Aqueous Solution at Room Temperature, *ACS Catal.,* 3, 2199−2207 (DOI:org/10.1021/cs400458k).

 2. Guin S., Rout S. K., Gogoi A., Ali W., & Patel B. K. (2014), A Palladium(II)-Catalyzed Synthesis of α-Ketoamides via Chemoselective Aroyl Addition to Cyanamides, *Adv. Syn. Catal.*, (DOI:10.1002/adsc.201400011).

3. (a) Mai W.-P., Wang H.-H., Li Z.-C., Yuan J.-W., Xiao Y.-M., Yang L.-R., Qu L.-B. (2012), nBu4NI-catalyzed direct synthesis of α-ketoamides from aryl methyl ketones with dialkylformamides in water using TBHP as oxidant, *Chem. Commun.*, 48, 10117 (DOI:10.1039/c2cc35279f); (b) Propiophenones A., Lamani M., & Ramaiah K. (2012), NIS-Catalyzed Reactions : Amidation of Acetophenones and Oxidative, *Chem. Eur. J.,* 18, 14638–14642 (DOI:10.1002/chem.201202703); (c) Deshidi R., Kumar M., Devari S., & Shah B. A. (2014), A general metal free approach to *α*-ketoamides via oxidative amidation-diketonization of terminal alkynes, *Chem. Commun.*, 50, 9533–9535 (DOI:10.1039/C4CC03783aa).

4. (a) Wang H., Guo L. N., & Duan X. H. (2013), Copper-catalyzed oxidative condensation of α-oxocarboxylic acids with formamides: synthesis of *α*-

ketoamides, *Org. Biomol. Chem.*, 11, 4573–6 (DOI:10.1039/c3ob40787j); (b) Mamillapalli N. C., & Sekar G. (2014), Chemoselective reduction of α-keto amides using nickel catalysts, *Chem. Comm.*, 50, 7881–4 (DOI:10.1039/c4cc02744b); (c) Zhang C., Zong X., Zhang L., & Jiao N. (2012), Copper-catalyzed aerobic oxidative cross-dehydrogenative coupling of amine and α-carbonyl aldehyde: A practical and efficient approach to α-ketoamides with wide substrate scope, *Org. Lett.*, 14, 3280–3283 (DOI:10.1021/ol301130u).

5. Padala A. K., Mupparapu N., Singh D., Vishwakarma R. a., & Ahmed Q. N. (2015), α-Carbonylimine to α-Carbonylamide: An Efficient Oxidative Amidation Approach, *Eur. J. Org. Chem.*, (DOI:10.1002/ejoc.201500251).

6. Dutta S., Kotha S. S., & Sekar G. (2015), Metal free one-pot synthesis of α-ketoamides from terminal alkenes, *RSC Adv.*, 5, 47265–47269 (DOI:10.1039/C5RA05671C).

7. Mupparapu N., Khan S., Battula S., Kushwaha M., Gupta A. P., Ahmed Q. N., & Vishwakarma R. A. (2014), Metal-free oxidative amidation of 2-oxoaldehydes: A facile access to α-ketoamides, *Org. Lett.*, 16, 1152–1155 (DOI:10.1021/ol5000204).

8. (a) Liu C.-H., Liu R.-H., Sun Q.-J., Chang J.-B., Gao X., Liu Y., Wang, S. D. (2015), Controlled synthesis and synergistic effects of graphene-supported PdAu bimetallic nanoparticles with tunable catalytic properties, *Nanoscale*, 7, 6356–6362 (DOI:10.1039/C4NR06855F); (b)Villa A., Wang D., Su D. S., & Prati L. (2015), New challenges in gold catalysis: bimetallic systems, *Catal. Sci. Technol.*, 5, 55–68 (DOI:10.1039/C4CY00976B); (c) Choo G. C. Y., Miyamura H., & Kobayashi S. (2015), Synergistic cascade catalysis by metal nanoparticles and Lewis acids in hydrogen autotransfer, *Chem. Sci.,* 6, 1719–1727 (DOI:10.1039/C4SC03627A).

9. Sankar M., Dimitratos N., Miedziak P. J., Wells P. P., Kiely C. J., & Hutchings G. J. (2012), Designing bimetallic catalysts for a green and sustainable future, *Chem. Soc. Rev.*, 8099–8139 (DOI:10.1039/c2cs35296f).

10. (a) Chem J. M., Song H. M., Moosa A., & Khashab N. M. (2012), Water-dispersable hybrid Au – Pd nanoparticles as catalysts in ethanol oxidation, aqueous phase Suzuki – Miyaura and Heck reactions, *J. Mater. Chem.*, 15953–15959 (DOI:10.1039/c2jm32702c); (b) Hutchings G. J. (2013), Au–Pd nanoalloys supported on Mg–Al mixed metal oxides as a multifunctional catalyst for solvent-free oxidation of benzyl alcohol, *Dalton Trans.,* 14498–14508 (DOI:10.1039/c3dt51855h); (c) Enache D. I., Edwards J. K., Landon P., Hutchings G. J. (2011), Solvent-Free Oxidation of Primary Alcohols to Aldehydes Using Au-Pd/TiO$_2$ Catalysts, *Science,* 362 (DOI:10.1126/science.1120560); (d) Wang D., & Li Y. (2011), Bimetallic Nanocrystals : Liquid-Phase Synthesis and Catalytic Applications, *Adv. Mater.,* 1044–1060 (DOI:10.1002/adma.201003695).

11. Zhang C., Zong X., Zhang L., & Jiao N. (2012), Copper-catalyzed aerobic oxidative cross-dehydrogenative coupling of amine and *α*-carbonyl aldehyde: A practical and efficient approach to *α*-ketoamides with wide substrate scope, *Org. Lett.*, 14, 3280–3283 (DOI:10.1021/ol301130u).

13. (a) Dhital R. N., Kamonsatikul C., Somsook, E., & Sakurai H. (2013), Bimetallic gold–palladium alloy nanoclusters: an effective catalyst for Ullmann coupling of chloropyridines under ambient conditions, *Catal. Sci. Technol.*, 3, 3030 (DOI:10.1039/c3cy00303e); (b) Chem J. M., Song H. M., Moosa A., & Khashab N. M. (2012), Water-dispersable hybrid Au – Pd nanoparticles as catalysts in ethanol oxidation , aqueous phase Suzuki – Miyaura and Heck reactions, *J. Mater. Chem.,* 22, 15953–15959 (DOI:10.1039/c2jm32702c); (c) Long J., Liu H., Wu S., Liao S., & Li Y. (2013), Selective Oxidation of Saturated Hydrocarbons Using Au − Pd Alloy Nanoparticles Supported on Metal−Organic Frameworks, *ACS Catal.,* 3, 647−654 (DOI.org/10.1021/cs300754k); (d) Rai R. K., Gupta K., Behrens S., Li J., Xu Q., & Singh S. K. (2015), Highly Active Bimetallic Nickel-Palladium Alloy Nanoparticle Catalyzed Suzuki-Miyaura Reactions, *ChemCatChem*, 7, 1806–1812 (DOI:10.1002/cctc.201500145); (e) Niu Z., Peng Q., Zhuang Z., He W., & Li Y. (2012), Evidence of an oxidative-addition-promoted Pd-

leaching mechanism in the Suzuki reaction by using a Pd-nanostructure design, *Chem. Eur. J.,* 18, 9813–9817 (DOI:10.1002/chem.201201224).

14. (a) Beller M., Balanta A., Godard C., & Claver C. (2011), Cross coupling reactions in organic synthesis themed issue Pd nanoparticles for C – C coupling reactions, *Chem. Soc. Rev.,* 10 (DOI:10.1039/c1cs15195a); (b) Coppage R., Slocik J. M., Ramezani-Dakhel H., Bedford N. M., Heinz H., Naik R. R., & Knecht M. R. (2013), Exploiting localized surface binding effects to enhance the catalytic reactivity of peptide-capped nanoparticles, *J. Am. Chem. Soc.*, 135, 11048–11054 (DOI:10.1021/ja402215t); (c) Srimani D., Sawoo S., & Sarkar A. (2007), Convenient synthesis of palladium nanoparticles and catalysis of hiyama coupling reaction in water, *Org. Lett.*, 9, 3639–3642 (DOI:10.1021/ol7015143).

Chapter 6

Aerobic Oxidative Cross-Dehydrogenative C-C Coupling reaction catalyzed with shape controlled Au-Pd bimetallic Nanoparticles

6.1 Introduction

With the development of synthetic methodologies for the composition and morphology controlled synthesis of nanoclusters, there has been a continuous surge of applying these materials for various applications such as devices, sensing, biomedical imaging and therapy and catalysis.[1] Especially in the area of catalysis, as the activity of the nanoparticles is governed by the electronic structure of the nanoparticle surface, research activities have been directed towards finding a correlation between structure, composition and surface properties with performance. As the catalytic performance of nanocrystals could be tuned through the modulation of their morphology, size and composition, there has been continuous focus on the application of these nanomaterials as effective, heterogeneous and reusable catalysts for important organic transformations in mild reaction conditions.[2] Most of the studies involving catalytic activity of nanoparticles are oriented around controlling the size (smaller size enhances catalytic activity due to larger surface area to volume ratio) or composition (bimetallic nanoparticles show better catalytic efficiency due to synergistic effect) of the nanoparticles.[3]

Controlled synthesis of nanocrystals with well-defined morphologies is an important subject in the field of nanotechnology because intrinsic physicochemical properties of nanostructures strongly depend on their shapes.[4] In particular, fine-tuning of the optical and electronic characteristics of noble metal nanocrystals by tailoring their morphologies has been extensively studied because of their promising applications in plasmonics, nanoelectronics, and surface-enhanced Raman scattering (SERS)-based diagnosis.[5] Furthermore, the shape of metal nanoparticles has a profound influence on their catalytic activity and selectivity in a variety of chemical reactions.[6] The enhanced catalytic activity of these shape-selective nanoparticles can be attributed to the different types of exposed crystallographic planes (facets) on their surfaces, which can determine the overall catalytic properties of the NCs. Since, the growth in non-spherical particles takes place along a particular crystallographic plane, hence different selectivity and

activity with different catalytic conversion on distinct planes of particles are expected.[7] In case of bimetallic nanoparticles, as different shaped nanoparticles have different number of facets, step edges or kinks and different ratio of number of atoms in those facets, the catalytic properties can be tuned tremendously. Furthermore, since the relative amount of each constituent metal in the bimetallic nanocrystals could modify the electronic state of the primary catalytic component and tune the binding properties for intermediate species during the reaction, the composition of shape-controlled bimetallic nanocrystals (alloy or core-shell structures) also has a great influence on their catalytic properties.[8]
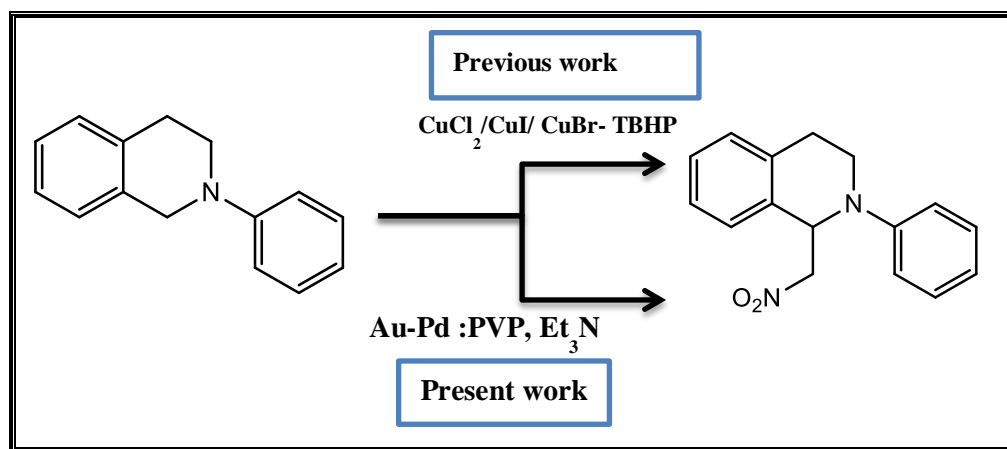
Scheme 6.1 *Schematic diagram oxidative coupling in comparison between our work and pervious work.*

In recent years, there has been tremendous growth in research activities with respect to wet-chemical methods for shape controlled synthesis of nanocrystals for both monometallic and bimetallic compositions. Following this, there has been a great deal of focus towards applying these nanocatalytic systems for organic transformations. The structure sensitivity of enantioselective hydrogenations on chirally modified metals was investigated using Pt nanoparticles of different shapes.[9] Similarly shape controlled Pt based alloy nanocatalysts have shown enhanced oxygen reduction.[10] In case of Au-Pd nanoalloys, recently Wang et. al. have demonstrated the higher catalytic activity of icosahedral Au-Pd alloy

nanocrystals over octahedrons in aerobic oxidation of cyclohexane.[11] Catalytic properties of Au-Pd nanoflowers for Suzuki coupling reactions as reported by Xu et. al. showed the involvement of leached Pd ions in catalyzing the reaction .[12]

Herein, we focused on the development of shape-selective Au-Pd nanocatalysts for direct conversion of two C-H bonds for the construction of C-C bond through cross-dehydrogenative coupling (CDC) reaction in presence of air as an oxidant. Among the many substrates that can be utilized in such reactions, amines and most notably N-aryl tetrahydroisoquinolines stand out because they have seen the development of a large number of methods for their oxidative coupling with other substrates, mostly reactive nucleophiles. Various homogeneous pathways have been developed for the oxidative cross-dehydrogenative coupling of tertiary amines with a variety of nucleophiles with different transition metal catalysts like Cu, Ru, Au (III), Pt etc.[13] In this regard, development of a heterogeneous catalyst and understanding the mechanism will be crucial for sustainable chemistry.

In this chapter, we report the cross-dehydrogenative coupling of N-phenyl 1,2,3,4-tetrahydroisoquinoline(1a) with nitromethane using urchin like Au-Pd bimetallic nanoparticles as heterogeneous catalysts without any external oxidant. The advantage of this synthetic methodology is that it has excellent selectivity with higher of desired coupled product under controlled temperature conditions (scheme 6.1). Mechanistically, it was observed that the Au-Pd nanoparticles catalyzed the reaction in a pseudo homogeneous pathway.[14]

6.2 Synthesis and characterization of bimetallic nanoparticles

It is well known that bimetallic nanoparticles show better catalytic activity compared to their monometallic counterparts. However the activities of these bimetallic nanocrystals depend on the morphology of the nanoparticles such as alloy or core-shell structures. As the catalytic activity of the nanocrystals depends on the atomic level distribution of the active species on the surface, therefore a precise control of composition and morphology is very important for tuning the catalytic properties. For shape-controlled synthesis of nanoparticles, along with

thermodynamic and kinetic control, the role of surface capping agents and shape directing agents are crucial. For our earlier studies involving Au based nanocatalysts, we have used polyvinyl pyrrolidone (PVP) as the surface capping agent for the growth and stabilization of nanoparticles. In order to have a fair comparison of the catalytic activity of the nanoparticles, we have used PVP in this work also for the synthesis of urchin shaped Au-Pd bimetallic nanoparticles. We used Br$^-$ ions as the oxidative etching agent for controlling the shape of the nanoparticles. Oxidative etching leads to manipulation of the distribution of single crystal vs twinned seeds during the nucleation and growth process through a process where the zero-valent metal atoms are reverted back to the metal ions. Halide ions (Cl$^-$, Br$^-$, I$^-$) show high etching activity under aerial conditions. Further, halide ions influence the generation of different facets of nanoparticles by adsorbing strongly on the metal nanoparticle surface, the chemisorption ability of halide increases in order Cl$^-$ <Br$^-$ <I$^-$. Further morphological evolution of the bimetallic nanoparticles depends on the kinetic parameters. Whereas use of a strong reducing agent leads to alloy structure with random atomic distribution of the metals, a weak reducing agent leads to the formation of core-shell nanostructures. In the present study, the Au-Pd bimetallic nanoparticles were synthesized by reduction of an aqueous mixture of H_2PdCl_4 and $HAuCl_4$ using ethylene glycol (EG) as a reducing agent in presence of KBr as a shape controlling/directing agent and PVP as a capping agent (modified polyol method). The reduction of both the metals using a weak reducing agent such as EG at 80 ^{0}C led to the formation of Au-Pd bimetallic nanostructures. Further Au and Pd monometallic nanoparticles were synthesized using the same methodology except for use of a single metal source.[15]

UV-visible spectra of Au-Br nanoparticles (nanoparticles produced by the reduction of $HAuCl_4$ using EG as reducing agent, PVP as surface capping agent and KBr and shape directing agent) showed their characteristic plasmon resonance band at 560 nm along with a band close to 400 nm which could be ascribed to $AuBr_4^-$ (Figure 6.1A). The results suggested that Br$^-$ is adsorbed on the Au surface. Pd-Br nanoparticles and Au-Pd-Br bimetallic nanoparticles did not show any band

similar to earlier reports. Powder X-ray diffraction (XRD) studies (Figure 6.1B) of Au-Br showed sharp peaks at 2θ values around 38.3, 44 and 65 degree corresponding to (111), (200) and (220) Bragg's reflection. In case of Pd-Br, a weak peak at 2θ value 40.1 was observed, which could be assigned to (111) reflection of Pd. On the other hand Au-Pd-Br showed reflection peaks at 2θ values 38.3, 44 and 65 degree, similar to Au-Br, however the peaks were broadened. Energy dispersive X-ray (EDX) studies of Au-Pd-Br showed the presence of Au, Pd and Br in the composite, which clearly showed that Br⁻ was present in the composite and could not be removed, even after extensive purification by centrifugation and dialysis(Figure 6.1C).[16]
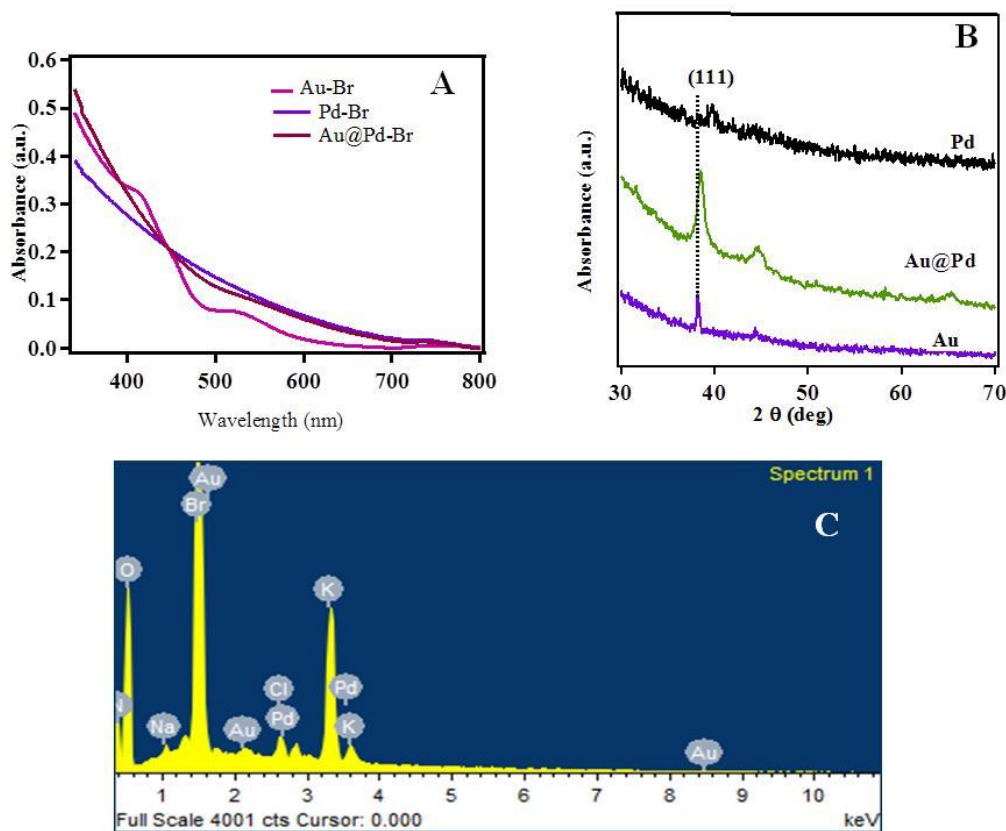
Figure 6.1 *A) UV-visible spectrum of Au-Br NPs, Pd-Br NPs and Au@Pd-Br NPs B) XRD pattern Au-Br NPs, Pd-Br NPs and Au@Pd-Br NPs; C) EDX spectra of Au@Pd-Br NPs.*

Transmission electron microscopy (TEM) characterization of Au-Br nanoparticles showed the formation of multiply twinned icosahedral structure of Au nanoparticles that look spherical at low resolution. HRTEM studies showed 5-fold twinned nanostructures and the presence of clear crystal lattice fringes (Figure 6.2). On the other hand, Au-Pd-Br showed the formation of Au-Pd core shell nanoparticles with an average particle size of 22.5 ± 4.5 nm. The formation of the core-shell structure was expected as it is well known using a weak reducing agent such as EG, Au will be reduced first forming the core whereas Pd forms the shell structure.[19]
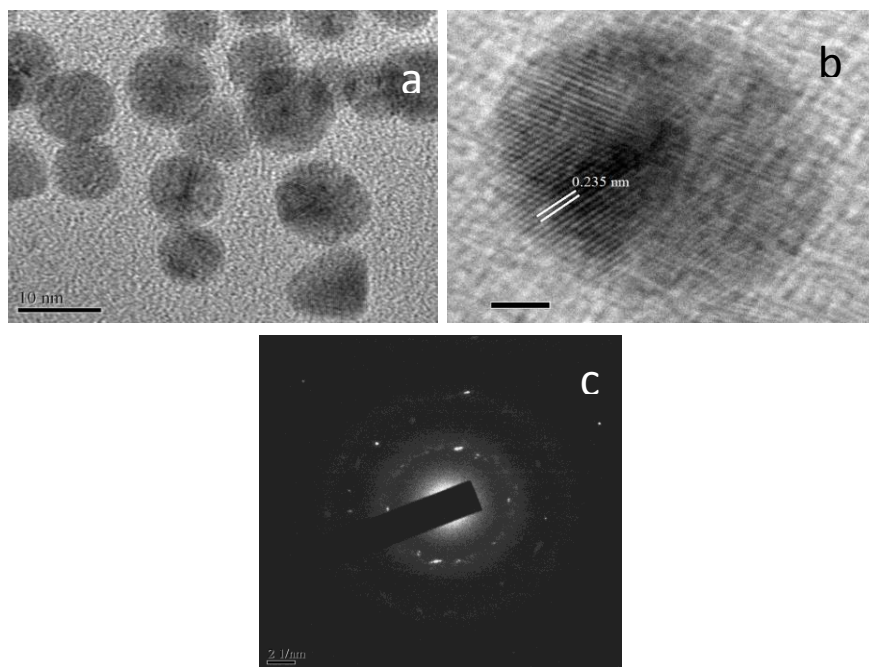
Figure 6.2 *(a) TEM (scale bar 10 nm); (b) HRTEM image (scale bar 5 nm) of Au nanoparticles using ethylene glycol as a reducing agent in presence of PVP and KBr; (c) SAED pattern of Au-Br.*
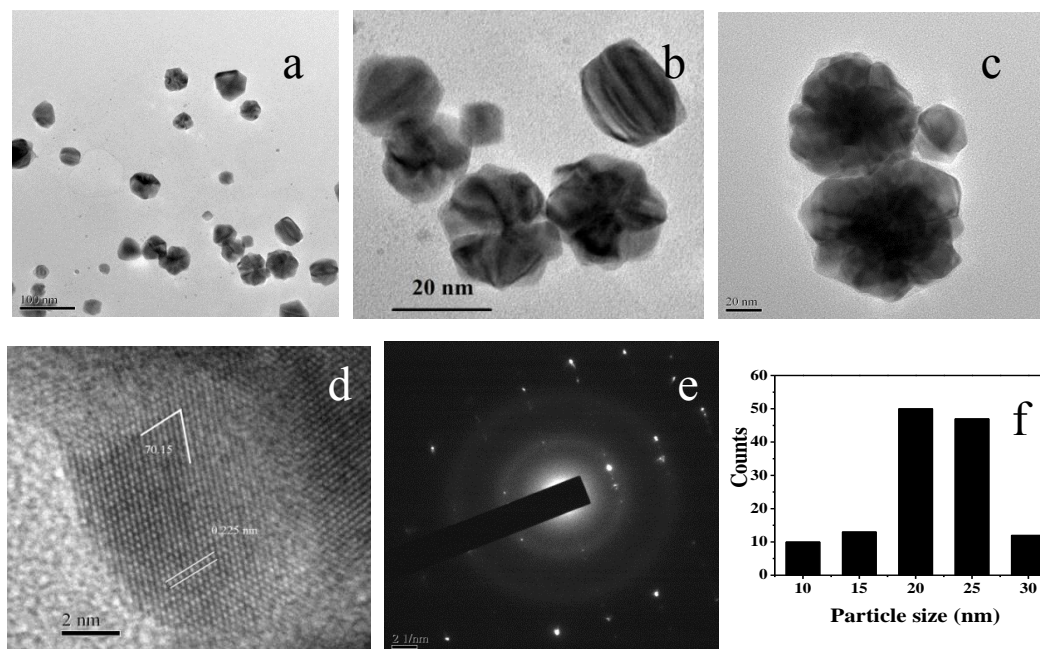
Figure 6.3 *(a) TEM image of AuPd-Br nanoparticles (scale bar 100 nm); (b,c) Image showing core-shell structure (scale bar 20 nm) (d) HRTEM image on the edge of the nanoparticle (scale bar 2 nm) (e) SAED pattern (f) Particle size distribution.*

Due to the presence of KBr, the nanoparticles formed were non-spherical and as observed from TEM images urchin kind of nanostructures were formed. HRTEM images on the edge of the nanocrystals showed a lattice fringe of 0.225 nm and dihedral angle of 70°. The values match well with Pd(111) Miller plane spacing and the corresponding angle. For comparison, we also synthesized Au-Pd alloy nanoparticles in presence of KI and PVP, using the same methodology except for using KI instead of KBr. The nanoparticles showed spherical shaped nanoparticles at low resolution, however at high resolution 5-fold twinned structures were observed. SAED pattern showed the crystalline nature of the particles with the *fcc* structure.
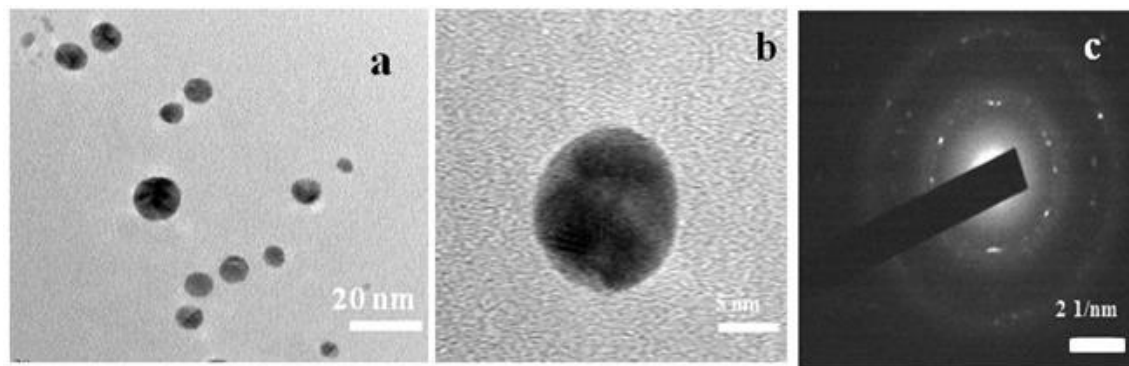
Figure 6.4 *(a) Low resolution (scale bar 20 nm) and (b) High resolution (scale bar 2 nm) TEM image of Au@Pd nanoparticles formed in presence of PVP and KI using EG as reducing agent; (c) SAED pattern of Au-Pd nanoparticles in presence of KI.*

It is a well-known fact that a weak reducing agent such as ethylene glycol favors the formation of a core-shell structure over randomly distributed alloy structure, although both the metal precursors were added simultaneously. As the reduction potential for Au^{3+} to Au^0 is higher compared to Pd^{2+}, they will be reduced first and form the core of the nanoparticle. The Pd shells will be grown on the Au seeds forming the core-shell structure. It was observed that the addition of Br^- led to the formation of urchin shaped Au@Pd nanoparticles, however another halide such as I^- led to the formation of spherical nanoparticles with twinned structure.

6.3 Catalytic studies:

In order to develop a heterogeneous catalytic system for the cross dehydrogenative C-C coupling (CDC) reaction, we first evaluated the catalytic activity of various Au based nanocatalytic systems under aerial conditions. For these studies, we opted for the coupling of N-phenyl tetrahydroisoquinoline (1a) and nitromethane as a model reaction. First we studied the activity of various nanocatalysts for this coupling reaction in DMSO as a solvent and triethylamine as a base. It was observed that spherical Au-Br, Pd-Br (synthesized according to protocols discussed in chapter 4 and 5, using $NaBH_4$ as a reducing agent) were unable to

catalyze the reaction and there was no product formation even after 30 hours of reaction. In presence of Au-PdPVP catalysts (synthesized using NaBH$_4$ as a reducing agent) under aerial conditions we obtained the desired coupling product 1-Nitromethyl-2-phenyl-1,2,3,4-tetrahydroisoquinoline (**3a**) with 31% yield along with the formation of undesired byproduct 2-phenyl-1,2,3,4-tetrahydroisoquinoline-1-ol (**3b**) with 12% yield (Table-6.1, entry-3). In presence of TBHP (t-butyl hydrogen peroxide) as an additional oxidizer, Au-Pd alloy nanocatalysts yielded a mixture of byproducts. On the other hand, using the Au-Pd bimetallic nanoparticles (synthesized using PVP and ethylene glycol without KBr) we could obtain the coupled product **3a** with 18 % yield (Table-6.1, entry-10). Therefore we turned out attention towards the shape-controlled nanoparticles as catalysts for this reaction. As shown in table 6.1, Au nanoparticles synthesized in presence of PVP and KBr (**Au-Br**) could not catalyze the reaction sufficiently resulting in 5% yield of the desired coupling product **3a** (Table-6.1, entry-6). On the other hand, when **Pd-Br** (Pd nanoparticles synthesized in presence of PVP and KBr) was used as a catalyst, the yield of the desired product **3a** was 12% (Table-6.1, entry-7). A dramatic enhancement in reaction yield was observed when Au@Pd urchin shaped nanoparticles (**Au@Pd-Br**) were used as a catalyst. The desired coupling product **3a** was obtained with 84% yield without any byproduct formation (Table-6.1, entry-8). When the reaction was performed in presence of spherical **Au@Pd-I** (AuPd nanoparticles synthesized in presence of PVP, KI and EG), we obtained 20% of the desired product **3a** along with 10% of the byproduct **3b** (Table-6.1, entry-9). From these results, it is clearly evident that shape-selective synthesis of the bimetallic nanoparticles had a definitive influence in catalyzing the coupling reaction.

The optimized condition with respect to conditions such as solvents, temperature and additives (base and oxidizer) were evaluated and are summarized in Table 6.2. It was observed that the best coupling product formation took place using DMSO as a solvent, triethylamine as a base and air as an oxidizing agent. Lesser yield of coupled product (3ab) was found when DMF, THF or CH$_3$CN solvents were used. Using methanol or ethanol as solvent results in the formation of several

byproducts. We observed that using nitromethane as a solvent (in absence of other solvents) led to lower yield of the product (Table 6.2).

Table 6.1 Optimization of CDC coupling reaction of N-phenyl tetrahydroisoquinoline with nitro-methane in presence of different Au@Pd nanocatalysts
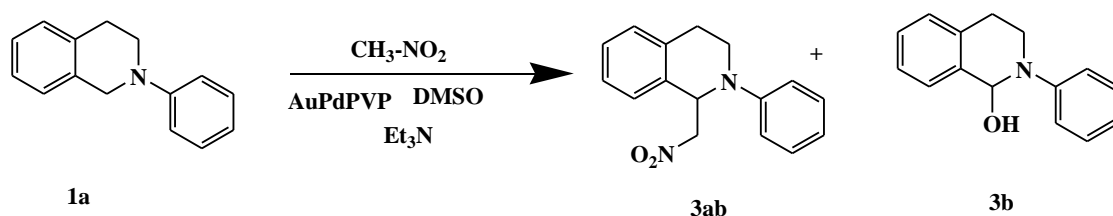
Entry[a]	Catalyst	Oxidant	Time(h)	Yield of 3ab[b] (%)	Yield of 3b (%)
1	Au PVP	Air	20	No	
2	Pd PVP	Air	20	No	
3	AuPd-PVP	Air	20	31	12
4	AuPd-PVP	Oxygen	22	34	16
5	AuPd-PVP	TBHP	20	20[c]	
6	Au-Br	Air	30	5	-
7	Pd-Br	Air	30	12	-
8	**Au@Pd-Br**	**Air**	**20**	**84**	-
9	Au@Pd-I	Air	30	20	10
10	AuPd (PVP-EG) (without KBr)	Air	30	18	-

[a]Standard reaction conditions, [b]isolated yields. 1mmol N-phenyl tetrahydroisoquinoline 1a, 5mmol nitromethane at 60° C. [c] peroxide compound.

Table 6.2 Optimization of coupling reaction with N-Phenyl tetrahydroisoquinoline with nitromethane
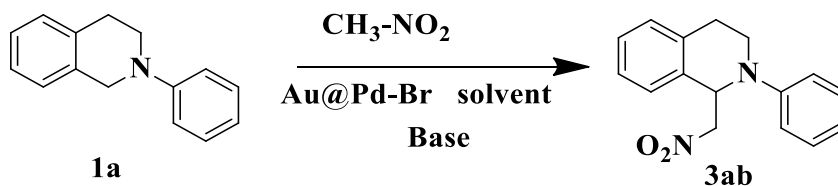
Entry	Catalyst	Oxidant (atom)	solvent	Base	temperature	Time	Yield %[ab]
1	No	no	DMSO	Et$_3$N	110	24h	No
2	No	Oxygen	DMSO	Et$_3$N	110	24h	No
3	Au@Pd-Br	Oxygen	water	Et$_3$N	60	20h	10
4	Au@Pd-Br	Oxygen	MeOH	Et$_3$N	60	22h	60[e]
5	Au@Pd-Br	Oxygen	THF	Et$_3$N	60	20h	50
6	Au@Pd-Br	Oxygen	EtOH	Et$_3$N	60	20h	43
7	**Au@Pd-Br**	**Oxygen**	**DMSO**	**Et$_3$N**	**60**	**20h**	**84**
8	Au@Pd-Br	Oxygen	DMSO	K$_2$CO$_3$	60	24h	15
9	Au@Pd-Br	oxygen	DMSO	Cs$_2$CO$_3$	60	30h	Trace[d]
10	Au@Pd-Br	oxygen	DMSO	KOAc	60	30h	Trace[d]
11	Au@Pd-Br	TBHP	DMSO	-	40	24h	Trace[cd]
12	Au@Pd-Br	Argon	DMSO	Et$_3$N	60	24h	No

[a] Standard reaction conditions, [b] isolated yields. 1mmol tetrahydroisoquinoline 1a, 5mmol nirtomethane at 60° C. [c] peroxide intermediate formation . [d] by-product formation. [e] methoxy-N-phenyl-isoquinoline formation.

To study the scope and generality of this heterogeneous bi-metallic catalyst, various 1,2,3,4-tetrahydroisoquinoline were coupled with a series of nucleophiles like nitromethane, dialkyl malonates and indole which gave excellent yields under optimized condition and the results are shown in Table-6.3. When N-phenyl tetrahydroisoquinoline (1a) or its derivatives were coupled with nitromethane or nitroethane as a nucleophile under basic conditions in DMSO medium, the coupled product 3ab-3an were obtained with yield of 80-83%. Due to the high regioselectivity of the Au@Pd urchin shaped nanocatalyst, no oxidized byproduct formation was observed during any of these coupling reactions. Other nucleophiles such as dialkyl malonates and manalonitriles showed with high

efficiency for the reaction using the nanocatalytic system without any external oxidant (3af, 3ah, 3al, 3am).[17]

Table 6.3 Oxidative coupling of N-Phenyl tetrahydroisoquinoline with nucleophiles

3ab, 84%

3ae, 80%

3db, 69%

3af, 74%

3ah, 72%

3al, 78%

3am, 68%

3ac, 81%

3ad, 74%

3aj, 57%

3bc, 68%

3ag, 70%

3cb, 76%

3cc, 71%

3ak, 69%

3ai, 71%

3an, 79%
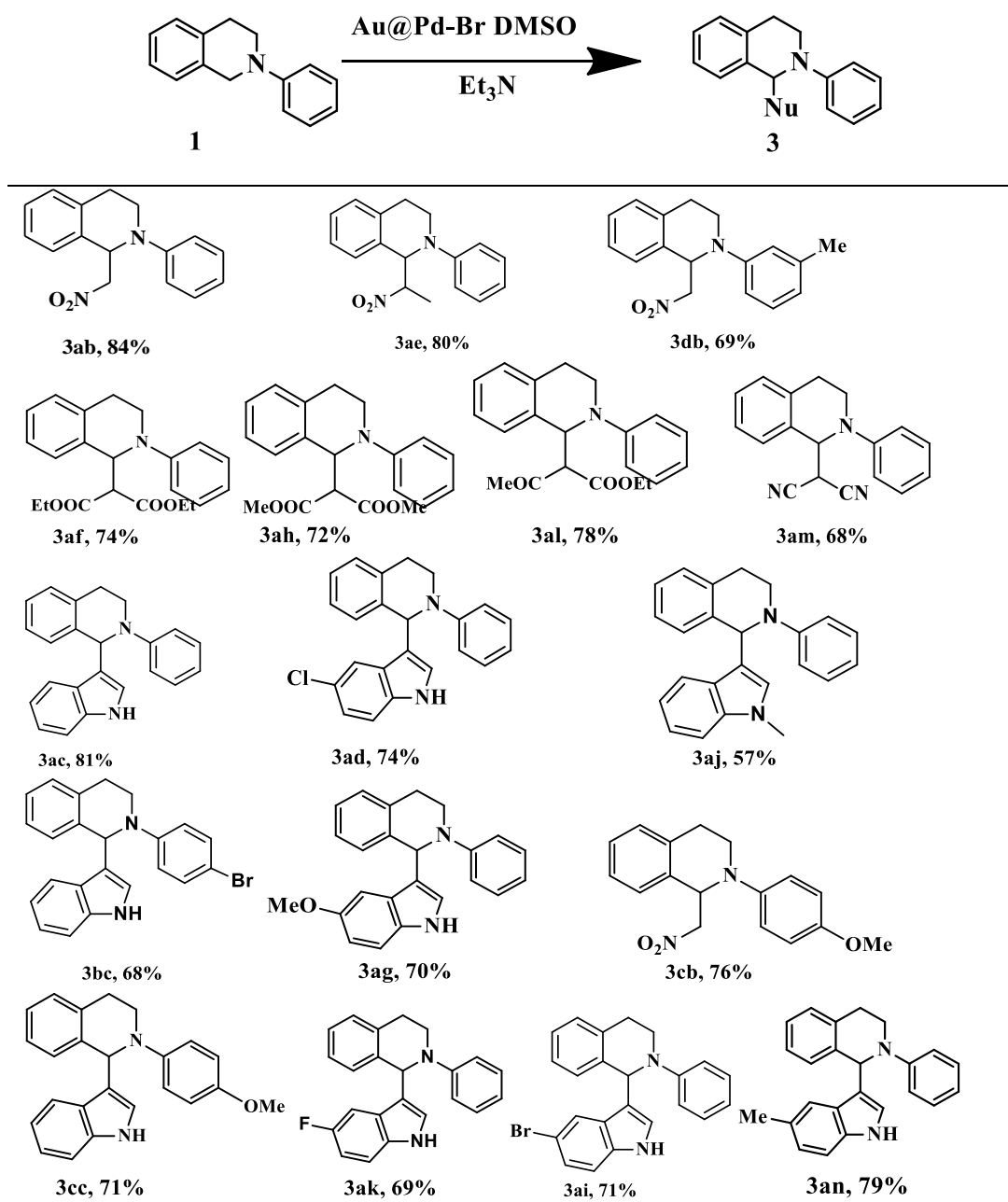
Standard reaction conditions: 1.0 mmol tetrahydroisoquinoline **1a**, 2-5 mmol nucleophile, Temp. 60° C, 2.0 ml DMSO, 0.10 mol% Au@Pd-Br NPs.

Furthermore, the coupling reaction also proceeds effortlessly using a variety of indole derivatives with substituents at the 1 and 5 position of indole without any protection of N-H bond (3ac, 3ad, 3aj, 3ag, 3ak, 3ai, 3an). These coupled products are important as precursors for synthesis of biologically active compounds and in pharmaceutical chemistry. The coupling reaction with electron donating groups containing indole derivatives such as 5-methoxyindole and 5-methylindole (3ag, 3an) and indole derivatives containing electron withdrawing groups such as 5-chloroindole and 5-bromoindole afforded the corresponding coupled products (3ad, 3ai, 3ak) in good yield. In order to analyze the electronic effect of N-H in indole, N-phenyl tetrahydroisoquinoline substrate (1a) reacted with 1-methylindole. The coupled product was obtained with lower yield of 57% after prolonged reaction time (30 hours) (3aj). Furthermore, paramethoxyphenyl tetrahydroisoquinoline and parabromophenyl tetrahydroisoquinoline underwent a favorable coupling with indole to produce the desired coupled products 3bc, 3cb, and 3cc with good yields.[18]

Also to check electronic effect of different position of indole, we tried the CDC reaction of N-phenyl tertrahydroisoquinoline with 7-methyl indole which gave less amount of coupled product (reaction yield 20%) under the optimized condition after 30 hours (scheme 6.2).
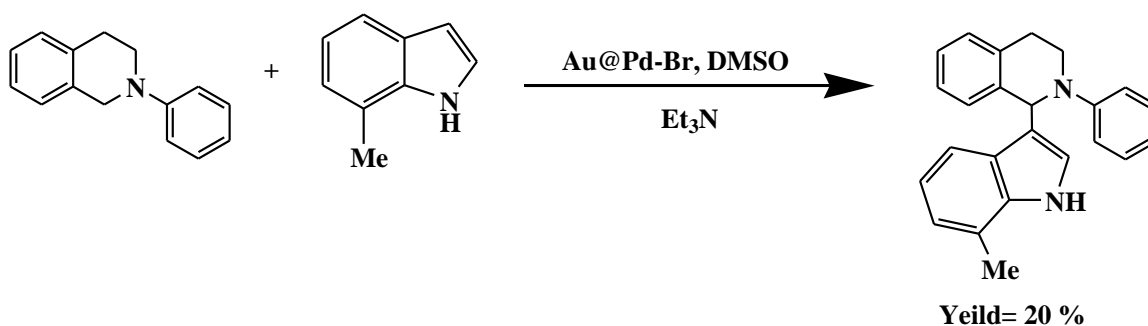
Scheme 6.2 *Oxidative coupling of N-phenyl tetrahydroisoquinoline with 7-methyl indole.*

6.4 Proposed mechanism

In order to have an insight to the possible reaction mechanism, we performed a few control reactions. It was observed that the presence of a free-radical scavenger such as TEMPO did not have any effect on the product yield in the model coupling reaction between N-phenyl tetrahydroisoquinoline and nitromethane. Further, we conducted the CDC reaction between BOC-protected tetrahydroisoquinoline and nitromethane under optimized conditions where no coupled product formation was observed.

Yeild= 0 %
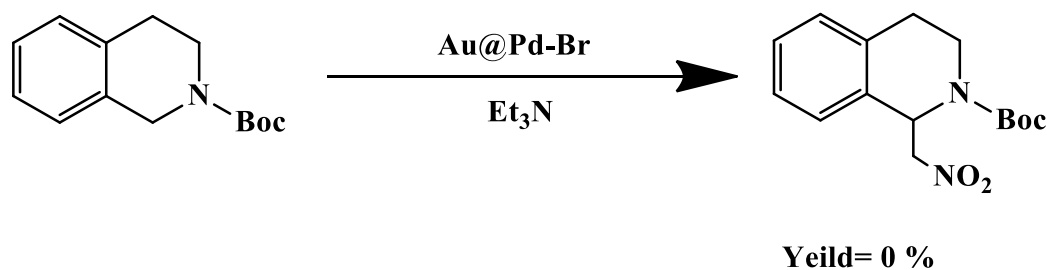
Scheme 6.3 Oxidative coupling N-Boc-tetraisoquinoline with nitromethane.
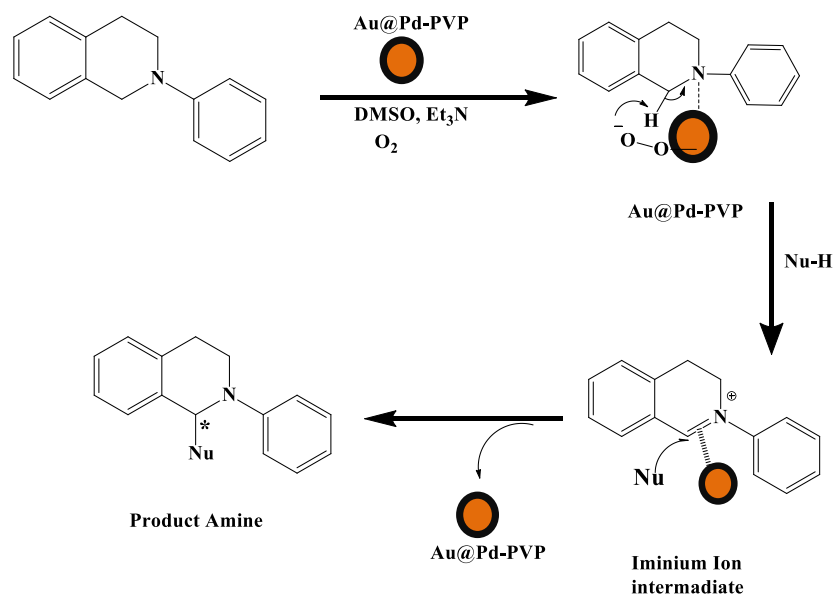
Figure 6.5 Mechanistic proposal of CDC reaction with Au@Pd-Br nanoparticles.

From these studies and based on earlier mechanistic studies, a probable mechanistic pathway as shown in Figure 6.5 involves two intermediate stages. The adsorption of tertiary amine on the Au@Pd surface takes place through electron donation by nitrogen atom. This activates the C-H bond alpha to nitrogen atom of tertiary amine. The superoxo species formed on the nanoparticle surface (formed by the interaction of nanoparticle with O_2) abstracts the hydrogen followed by the formation of iminium-type intermediate. The CDC product is formed following the attack of the nucleophile.[20]

6.5 Recyclability of alloy nanoparticle catalyst towards the cross dehydrogenative coupling
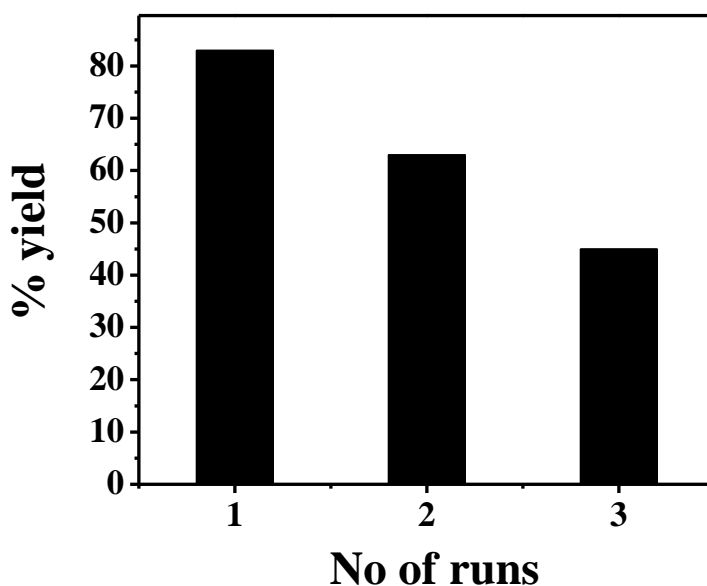
Figure 6.6 *Recyclability of alloy nanoparticle catalyst.*

We also explored the recyclability of the Au@Pd-Br nanocomposites for the model coupling reaction between N-phenyl tetrahydroisoquinoline and nitromethane under optimized reaction condition. The AuPd-Br could be recovered from the reaction mixture by centrifugation, washing with water and drying. It was observed that the AuPd-Br lost their catalytic activity considerably during their participation in the coupling reaction. The desired coupling products were obtained with 59% yield after the 1st cycle and 44% after the 2nd cycle. The

reduced catalytic activity of the nanoparticles could be due to the agglomeration of the nanoparticles at elevated temperature during the reaction. The TEM studies of the AuPd-Br nanoparticles recovered after the 1st cycle showed considerable agglomeration resulting in increase in particle size (Figure 6.7). Another very important observation was that the shape of the particle changed considerably from urchin-shape to spherical with a more distinct core-shell morphology. The SAED pattern showed high crystallinity of the recovered Au-Pd-Br nanocatalysts. The dynamic nature of the Au-Pd-Br nanoparticles as observed by the structural changes after their involvement in the catalytic cycle prompted us to perform the leaching experiment to find out the active species in the reaction. For this we performed the model reaction of N-phenyl-tetrahydro isoquiniloine and nitromethene in presence of the Au@Pd-Br nanocatalyst (0.1 mol%) in DMSO-triethyl amine medium under optimized reaction conditions. The coupling reaction was allowed to take place for 4 hours, after which the reaction was cooled down to room temperature and the nanoparticles were separated from the reaction mixture by
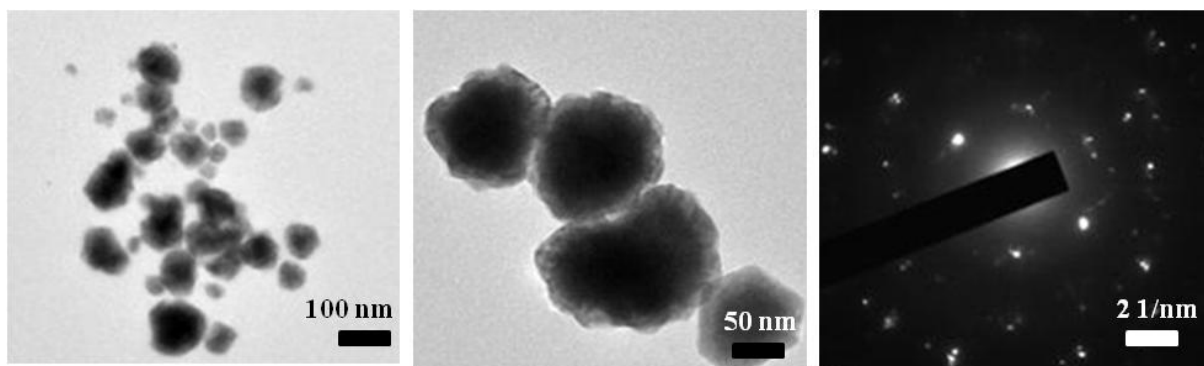
Figure 6.7 Transmission electron micrograph of Au@Pd-Br nanoparticles recovered after 1st cycle of catalytic reaction; (a) low resolution, scale bar 100 nm; (b) high resolution, scale bar 50 nm; (c) SAED pattern.

high speed centrifugation. The supernatant was separated into two fractions, one fraction was worked up for evaluating the yield of the coupling product. From ^{1}H NMR spectroscopy analysis of the crude product, the yield of the coupling product

was found to be 36%. The other fraction, without nanoparticle catalyst, was allowed to be stirred for another 20 hours under standard reaction conditions (60 °C, air). After the reaction was stopped this fraction was worked up and the yield of the coupling product from the crude mixture was evaluated by ^{1}H NMR spectroscopy, which showed a yield of 49% of the coupling product. In presence of Au-Pd-Br catalysts, the coupling product yield for this reaction was found to 84% (Table 6.3, entry 3ab). The results demonstrated that some active catalytic species remained in the solution which catalyzed the coupling reaction even after the removal of the Au-Pd-Br nanoparticles by centrifugation. In order to evaluate the active species, we performed the ICP-AES spectroscopy of the nanoparticles and supernatants. The results for Au and Pd are shown in Table 6.4. The Au:Pd ratio in the Au-Pd-Br nanocomposite increased before and after the catalytic reaction clearly suggesting that Pd leached during the catalytic reaction, suggesting that Pd(II) might act as the active species during the reaction. Further studies of the metal components in the supernatants showed that the level of Au ions was below the detection limit, whereas there was appreciable detection of Pd ions during and after the completion of the reaction. Probably in the Au@Pd urchin shaped nanoparticles, Pd is present on the surface as Pd-Br. During their participation in the catalytic reaction, Pd was leached in the reaction medium and performed the catalytic reaction and again re-deposited on the nanoparticle surface after the catalytic reaction. The dynamic structural changes of the Au@Pd-Br nanoparticles after their participation in the catalytic reaction also suggested the continuous leaching and re-deposition of active species. The poor reusability of the nanocatalytic system also probably suggested the change of morphology of the structure during the reaction.

Table 6.4: ICP-AES studies of the Au and Pd components in Au-Pd-Br nanocomposite in the catalytic reaction.

Entry	Reagents	Amount of Au/Pd ratio detected by ICP-AES
1	Au-Pd-Br catalyst before reaction	Au/Pd 69.7/30.28
2	Au-Pd-PVP catalyst after reaction (after completion)	Au/Pd 73.7/26.3
3	Supernatant of reaction (after 8 hours of reaction)	Au (not detected) Pd (38.84 ppm)
4	Supernatant of reaction (after completion of reaction)	Au (not detected) Pd (14.16 ppm)

6.5 Conclusion

In conclusion, urchin shaped Au-Pd core-shell bimetallic nanoparticles could be used as an efficient catalyst for the regioselective synthesis of coupling products during the cross-dehydrogenative coupling reaction of N-phenyl tetrahydroisoquinoline and nucleobases under mild reaction conditions using air as the sole oxidant. The resulting coupling products were obtained with high yield. While developing the first nanoparticle based catalyst for these important CDC reactions, we found that the reaction mechanism is quite complex and several factors such as shape selectivity, morphology of the nanoparticles, synergistic effect and leaching of metallic species from the nanoparticle surface, all played very crucial roles in determining the rate and selectivity of the reaction. We believe that the studies will open up new avenues for the use of shape-selective

nanoparticles and the role of shape-directing agents in catalytic reactions leading to important synthetic pathways for biologically active compounds.

6.6 Experimental section

6.6.1. Chemicals and Materials: Hydrogen tetrachloroaurate(III) hydrate, palladium chloride (PdCl$_2$), Ethylene glycol, potassium bromide (KBr) poly (vinyl pyrrolidone) (PVP, MW 55000), 1,2,3,4-tetrahyroisoquinoline, nitroalkanes and Indoles were purchased from Sigma Aldrich. Ethylene glycol and potassium bromide were purchased from SRL chemicals. All the reagents were of analytical grade and used without further purifications.

6.6.2. Synthesis of PVP capped shape controlled Au-Pd alloy nanoparticles
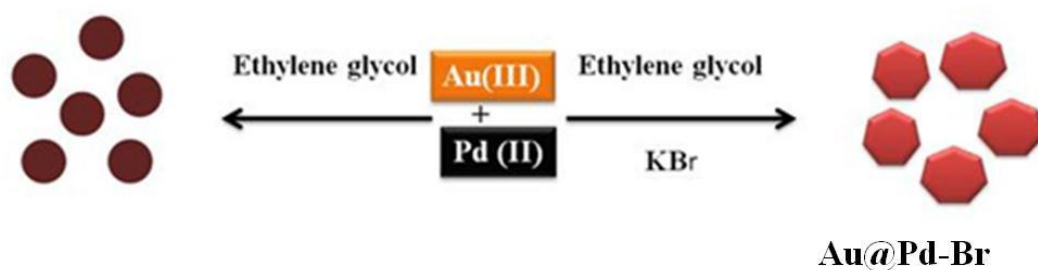
Figure 6.8 *Schematic diagram of synthesis of Au-Pd alloy in presence of facet capping agent KBr and without KBr in ethylene glycol medium.*

6.6.3 Synthesis of nanoparticle:
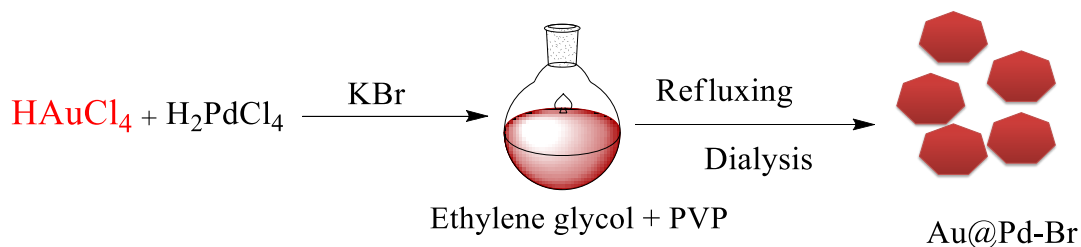
Figure 6.9 *Synthetic procedure of shape selective Au-Pd alloy nanoparticle in presence of KBr and PVP as capping agent.*

In a typical synthesis, 3 mL of EG was taken in a 25-mL, three-neck flask (equipped with a reflux condenser and a Teflon-coated magnetic stirring bar) and heated in air with magnetic stirring at 80 °C. Simultaneously two different solutions were prepared. One contained 100 µl of 0.03 M $HAuCl_4$ and 100 µl H_2PdCl_4 (0.03 M) together with 0.100 g of KBr in 2ml H_2O. The second solution comprised of 0.111g PVP in 3ml of ethylene glycol. Both these solutions were slowly added to the hot EG solutions at the same time. The reaction mixture was further heated at 80° C for 12hrs. After cooling down to room temperature, the final solution was dialyzed to remove excess EG and the inorganic impurities such Na^+, Br^- and Cl^- ions. The dialyzed hydrosol of Au@Pd was diluted to 25 ml and stored in refrigerator for catalytic reactions and characterizations. For comparison, Au and Pd monometallic nanoparticles were prepared in the same way by substituting aqueous solutions of $HAuCl_4/H_2PdCl_4$ mixtures by $HAuCl_4$ and H_2PdCl_4 solutions respectively. Also to see the effect of the halide ions on the catalytic activity of the nanocatalysts, we synthesized two different AuPd-PVP nanoparticles by replacing KBr with KCl and KI salt respectively. The as obtained samples were characterized by transmission electron microscopy (TEM), high-resolution TEM, energy-dispersive X-ray (EDX) analysis, powder X-ray diffraction (PXRD), and X-ray photoelectron spectroscopy (XPS).

6.6.4 Synthesis of N-Phenyl-tetrahydroisoquinoline:

Phenyl boronic acid (0.368 g, 2.00 mmol) and $Cu(OAc)_2·H_2O$ (20.0 mg, 0.100 mmol) in CH_2Cl_2 (8.00 mL) were stirred for 5 minutes at room temperature. To this stirring suspension 1,2,3,4 tetrahydroisoquinoline (0.072 g, 99.0 µL, 1.00 mmol) was added and stirred under an atmosphere of O_2 for 24h. The crude reaction mixture was extracted with water and excess DCM. The product (1a) was isolated by silica gel column chromatography (eluting with hexanes: EtOAc 9:1 ~ 3:1 gradient) as a pale yellow oil.

6.6.5 General procedure of aerobic oxidative coupling reaction of amine and nitroalkanes:

A mixture of N-Ar-1,2,3,4-tetrahydroisoquinoline (0.1 mmol), nitroalkanes (0.4 mL) and triethyl amine was added to DMSO (2 mL). The reaction mixture was then stirred at 60 ^{o} C under air for several hours. After the completion of the reaction, the reaction mixture was cooled to room temperature and the reaction was quenched using water (2.0 mL). The resulting mixture was extracted with EtOAc (3×10 mL) and washed with brine solution. The combined organic layers were dried over anhydrous Na_2SO_4. After removing the solvents under vacuum, the residue was purified by flash column chromatography on silica gel.

NMR data:

1.

3ab

Yellow oil, ^{1}H NMR (400 MHz, CDCl$_3$): δ 7.28-7.11 (m, 6H), 6.97 (d, 2H, *J*= 8
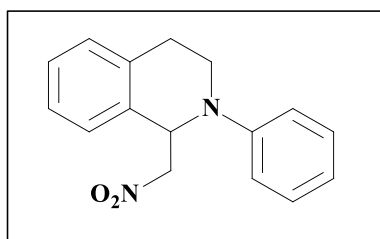
Hz), 6.84 (t, 1H, **J**=8Hz), 5.54 (t, 1H, *J* = 8Hz,), 4.84 (dd, 1H, J= 8Hz), 4.54(dd, 1H, J= 6.4Hz, J=6.8Hz), 3.67-3.60(m, 2H), 3.11-3.03(m, 1H), 2.77 (dt, 1H, *J*=4.8Hz); ^{13}C NMR (100 MHz, CDCl$_3$): 148.73, 135.58, 133.22, 129.81, 129.49, 128.42, 127.30, 126.99, 119.73, 115.42, 79.08, 58.5, 42.37, 26.75.

2. 3ac

Yellow solid, ^{1}H NMR (400 MHz, Acetone-d$_6$): δ 7.55 (d, 2H, *J*=8Hz), 7.36 (d,
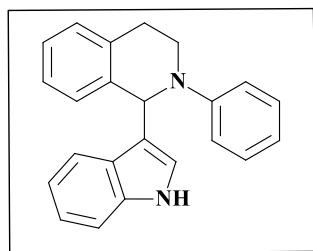
1H, *J*=8Hz), 7.21-7.16 (m, 5H), 7.08-7.05 (m, 3H), 6.96-6.94 (t, 1H, *J*=4Hz), 6.78(s, 1H), 6.71-6.67 (t, 1H),

6.28 (s, 1H), 3.67-3.63 (m, 2H), 3.10-3.03 (m, 1H), 2.95-2.85 (m, 1H); ^{13}C NMR (100 MHz, Acetone-d$_6$): 149.86, 138.05, 137.15, 135.45, 129.02, 128.63, 128.05, 126.63, 126.50, 124.52, 121.36, 119.67, 118.80, 118.41, 117.63, 115.37, 111.3, 56.31, 41.98, 26.55.

3.

3ad
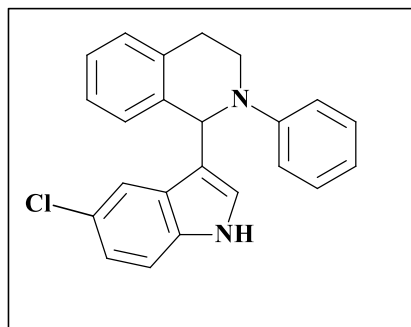
Yellow solid, ^{1}H NMR (400 MHz, Acetone-d$_6$): δ 7.47 (d, 1H, J=2Hz), 7.37(s, 1H), 7.35 (t, 1H, J=4Hz), 7.21-7.18 (m, 5H), 7.08 (d, 2H, J=8Hz), 7.04 (dd, 1H, J=2Hz), 6.83-6.82 (d, 1H, J=1.6Hz), 6.71 (tt, 1H, J=7.2Hz), 6.25 (s, 1H), 3.64-3.59 (m, 2H), 3.10-

3.02 (m, 1H), 2.90-2.87 (m, 1H); ^{13}C NMR (100 MHz, Acetone-d6): 149.92, 137.62, 135.57, 135.42, 129.07, 128.77, 128.51, 128.07, 126.66, 126.42, 125.65, 125.53, 121.45, 119.10, 118.32, 118.14, 115.88, 112.75, 56.23, 42.12, 26.48.

4.

3ae
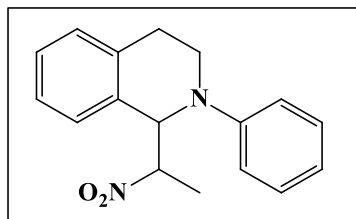
White liquid, ^{1}H NMR (400 MHz, CDCl$_3$): major isomer 5.27-5.25 (d, J 1H), 5.07-5.02 (m, 1H), 3.63-3.56 (m, 2H), 1.55 (d, 3H). minor isomer 5.25-5.23 (d, J-1H), 4.98-4.88 (m 1H), 3.88-3.81 (m 1H), 1.72-1.70 (d, 3H). 7.30-7.18 (m, 5H), 7.12-7.10(t, J=, 2H), 7.01-6.98 (m, 1), 3.10-3.04 (m 1H), 2.95-2.86 (m, 1H).

5.

3af

White liquid, ^{1}H NMR (400 MHz, CDCl$_3$): 7.26-7.09 (m, 6H), 6.88 (d, 2H, *J*=8Hz), 6.64 (t, 1H, *J*=7.2Hz), 5.64(d, 1H, *J*=12Hz), 4.11-3.96 (m, 4H), 3.90 (d, 1H, *J*=8Hz), 3.70-3.62 (m, 2H), 3.09-3.01(m, 1H), 2.77 (t, 1H, *J*=5.2Hz), 1.06 (t, 3H, *J*=4Hz), 0.98 (t, 3H, *J*=8Hz); ^{13}C NMR (100 MHz, CDCl$_3$): 167.52, 166.71, 148.44, 135.52, 134.39, 128.63, 127.10, 125.57, 118.03, 114.66, 61.13, 61.06, 59.12, 57.48, 41.87, 25.72, 13.64, 13.51.
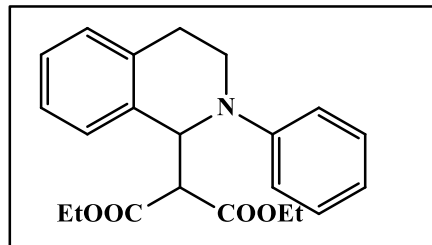
6.

3ag

^{1}H NMR (400 MHz, CDCl$_3$): 7.32-7.28 (m, 2H), 7.18-7.13 (m, 5H), 7.10-7.06 (m, 2H), 6.97 (d, 2H, J=8Hz), 6.76-6.69 (m, 2H), 3.89 (t, 1H, *J*=4Hz), 3.57 (s, 3H), 3.53(d, 2H, *J*=8Hz), 3.04 (t, 1H, *J*=12Hz), 2.82-2.74 (m, 1H); ^{13}C NMR (100 MHz, CDCl$_3$): 153.81, 142.97, 138.32, 132.16, 129.53, 129.19, 128.93, 128.74, 127.26, 126.99, 126.91, 125.73, 125.41, 120.99, 120.34, 112.19, 111.73, 55.84, 55.66, 49.49, 26.41.
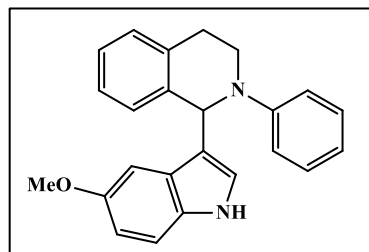
7.

3ah

^{1}H NMR (400 MHz, CDCl$_3$): 7.28-7.15 (m, 6H), 6.95 (d, 2H, *J*=8Hz), 6.82-6.78 (m, 1H), 5.42 (t, 1H, *J*=8Hz), 4.13 (q, 1H, *J*=8Hz), 3.69-3.63 (m, 2H), 3.35(d, 1H, *J*=1.76Hz), 3.09-3.04 (m, 1H), 2.94(dd, 1H, *J*=8Hz), [2.19 (s), 2.09 (s, 3H,)] [1.28 (t), 1.23 (t) 3H]. 13C NMR (125 MHz, CDCl3): 207.27, 201.40, 166.80, 148.82, 148.87, 138.27, 137.75, 134.48, 129.36, 129.33, 129.28, 129.73, 128.59, 126.93, 126.90, 126.86, 126.80, 126.34, 126.26, 118.56, 118.26, 115.03, 114.77, 61.37, 54.95, 54.79, 50.24, 50.21, 42.12, 42.06, 30.92, 29.69.
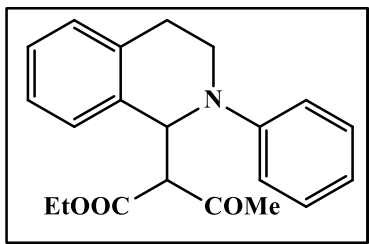
8.

3bc

^{1}H NMR (400 MHz, CDCl$_3$): 8.01 (s, 1H), 7.62 (d, 1H, 4Hz), 7.50 (d, 1H, *J*=8Hz), 7.29-7.25 (m, 3H), 7.17-7.12 (m, 3H), 7.01 (d, 2H, *J*=12Hz), 6.83 (t, 2H, *J*=8Hz), 6.60(d, 1H, *J*=4Hz), 6.06 (s, 1H), 3.59-3.51 (m, 2H), 3.01-2.97 (m, 1H), 2.80 (dt, 1H, *J*=4Hz); ^{13}C NMR (100 MHz, CDCl$_3$): 148.73, 136.63, 131.92, 131.65, 128.82, 127.99, 126.31, 125.87, 124.14, 122.22, 119.89, 119.75, 119.43, 117.30, 117.26, 111.17, 56.86, 42.54, 29.08, 26.65.
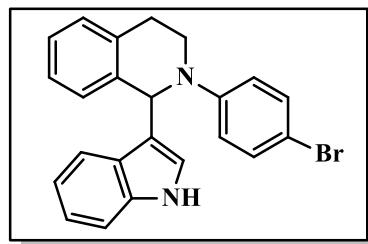
9.

3ai

¹H NMR (400 MHz, CDCl₃): 8.05 (s, 1H), 7.62 (d, 1H), 7.28-7.24 (m 3H), 7.23-7.22(d, 1H), 7.21-7.15 (m, 3H), 7.03-7.02 (d, 2H), 6.85-6.82 (t, 1H), 6.61 (d, 1H), 6.09 (s, 1H), 3.62-3.58 (m,2H), 3.14-3.01 (m, 1H), 2.84-2.78 (dt, 1H). ¹³C NMR (100 MHz, CDCl₃): 149.87, 137.04, 135.43, 135.20, 129.21, 128.98, 128.90, 128.14, 127.95, 126.81, 125.42, 124.97, 122.67, 118.97, 118.79, 116.53, 112.96, 56.73, 42.58, 26.64.
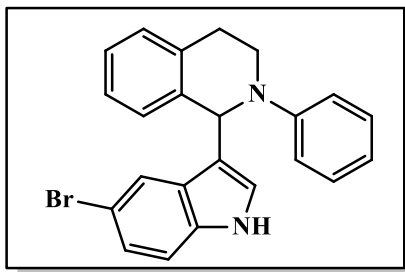
10.

3cc

¹H NMR (400 MHz, Acetone-d6): δ 7.35 (d, 1H), 7.21 (d, 1H, *J*=8Hz), 7.14 (d, 1H, *J*=8Hz), 7.04-6.95 (m, 6H), 6.90 (d, 2H, *J*=8Hz), 6.80 (t, 1H, *J*=12Hz), 6.52 (t, 1H, *J*=12Hz), 6.10 (s, 1H), 3.50 -3.42 (m, 5H), 2.93-2.87 (m, 1H), 2.74 (dt, 2H, *J*=4Hz); ¹³C NMR (100 MHz, Acetone-d6): 150.55, 142.47, 138.80, 138.31, 129.82, 129.64, 129.64, 129.48, 127.78, 127.31, 126.40, 122.14, 120.6, 119.77, 119.55, 118.39, 116.01, 112.90, 56.96, 42.74, 27.36.
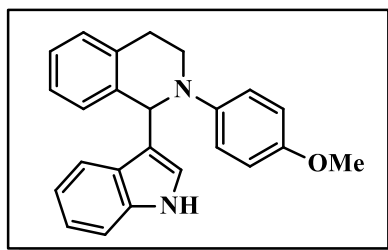
6.7 References

1. Sonström P., & Bäumer M. (2011), Supported colloidal nanoparticles in heterogeneous gas phase catalysis: on the way to tailored catalysts, *Phys. Chem. Chem. Phys.*, 13, 19270 (DOI:10.1039/c1cp22048a).

2. (a) Hutchings, G. J. (2008), Nanocrystalline gold and gold palladium alloy catalysts for chemical synthesis, *Chem. Comm.*,7345 (DOI:10.1039/b712305c); (b) Cheong, S., Watt, J. D., & Tilley, R. D. (2010), Shape control of platinum and palladium nanoparticles for catalysis, *Nanoscale.*, 2, 2045–2053 (DOI:10.1039/c0nr00276c); (c) Shao M., Yu T., Odell J. H., & Xia Y. (2011), Structural dependence of oxygen reduction reaction on palladium nanocrystals, *Chem. Comm.,* 47, 6566–6568 (DOI:10.1039/c1cc11004g); (d) Narayanan, R., & El-sayed, M. A. (2005), Catalysis with Transition Metal Nanoparticles in Colloidal Solution : Nanoparticle Shape, *J. Phy. Chem. B.*, 109, 12663–12676; (e) Narayanan R., El-sayed M. A. (2004), Changing Catalytic Activity during Colloidal Platinum Nanocatalysis Due to Shape Changes : Electron-Transfer Reaction, *J. Am. Chem. Soc.*, 126, 7194–7195; (f) Narayanan R., & El-Sayed, M. A. (2004), Effect of nanocatalysis in colloidal solution on the tetrahedral and cubic nanoparticle SHAPE: Electron-transfer reaction catalyzed by platinum nanoparticles, *J. Phy. Chem. B.*, 108, 5726–5733 (DOI:10.1021/jp0493780).

3. (a) Chiang W.-H., & Sankaran R. M. (2008), Synergistic Effects in Bimetallic Nanoparticles for Low Temperature Carbon Nanotube Growth, *Advanced Materials*, 20, 4857–4861 (DOI:10.1002/adma.200801006); (b) Choo G. C. Y., Miyamura H., & Kobayashi S. (2015), Synergistic cascade catalysis by metal nanoparticles and Lewis acids in hydrogen autotransfer, *Chem. Sci.*, 6, 1719–1727 (DOI:10.1039/C4SC03627A).

4. (a) Xu R., Wang D., Zhang J., & Li Y. (2006), Shape-Dependent Catalytic Activity of Silver Nanoparticles for the Oxidation of Styrene, *Chem. Asian J.,* 1, 888–893. DOI:10.1002/asia.200600260; (b) Canlas C. P., Lu J., Ray N. A.,

Grosso-giordano N. A., Lee, S., Elam J. W., Notestein J. M. (2012), Shape-selective sieving layers on an oxide catalyst surface. *Nature Chemistry*, 4, 1030–1036 (DOI:10.1038/nchem.1477); (c) Lee H., Kim C., Yang S., Woo J., & Jiyeon H. (2011), Shape-Controlled Nanocrystals for Catalytic Applications, *Catal Surv Asia.,* (DOI:10.1007/s10563-011-9130-z); (d) Xiong B. Y., & Xia Y. (2007), Shape-Controlled Synthesis of Metal Nanostructures : The Case of Palladium, *Adv. Mater.* 19, 3385–3391 (DOI:10.1002/adma.200701301); (e) Bratlie K. M., Lee H., Komvopoulos K., Yang P., & Somorjai G. A. (2007), Platinum nanoparticle shape effects on benzene hydrogenation selectivity, *Nano Letters,* 7, 3097–3101 (DOI:10.1021/nl0716000).

5. Lee Y. W., Kim M., Kang S. W., & Han S. W. (2011), Polyhedral Bimetallic Alloy Nanocrystals Exclusively Bound by {110} Facets: Au–Pd Rhombic Dodecahedra, *Angew. Chem. Inter. Ed.,* 50, 3466–3470 (DOI:10.1002/anie.201007220).

6. Xiong Y., Wiley B. J., & Xia Y. (2007), Nanocrystals with unconventional shapes - A class of promising catalysts *Angew. Chem. Inter. Ed.,* 46, 7157–7159, (DOI:10.1002/anie.200702473).

7. (a) Lee I., Morales R., Albiter M. A, & Zaera F. (2008), Synthesis of heterogeneous catalysts with well shaped platinum particles to control reaction selectivity, *PNAS*, 105, 15241–15246 (DOI:10.1073/pnas.0805691105); (b) Bratlie K. M., Lee H., Komvopoulos K., Yang P., & Somorjai G. a. (2007), Platinum nanoparticle shape effects on benzene hydrogenation selectivity, *Nano. Lett.,* 7, 3097–3101 (DOI:10.1021/nl0716000).

8. (a) Xiong Y., Cai H., Wiley B. J., Wang J., Kim M. J., & Xia Y. (2007), Synthesis and mechanistic study of palladium nanobars and nanorods, *J. Am. Chem. Soc.*, 129, 3665–3675 (DOI:10.1021/ja0688023); (b) Narayanan R., & El-Sayed M. A. (2005), Catalysis with Transition Metal Nanoparticles of Different Shapes, *J. Phy. Chem. B.,* 900, 12663–12676 (DOI:10.1557/PROC-0900-O10-02).

9. Schmidt E., Vargas, A., Mallat, T., & Baiker, A. (2009). Shape-selective enantioselective hydrogenation on Pt nanoparticles, *J. Am. Chem. Soc.*, 131, 12358–12367 (DOI:10.1021/ja9043328).

10. Zhang J., Yang H., Fang J., & Zou S. (2010), Synthesis and oxygen reduction activity of shape-controlled Pt(3)Ni nanopolyhedra, *Nano. Lett.*, 10, 638–644 (DOI:10.1021/nl903717z).

11. Wang L., Zhao S., Liu C., Li C., Li X., Li H., Zeng J. (2015), Aerobic Oxidation of Cyclohexane on Catalysts Based on Twinned and Single-Crystal $Au_{75}Pd_{25}$ Bimetallic Nanocrystals, *Nano Lett.*, (DOI:10.1021/nl5045132).

12. Xu J., Wilson A. R., Rathmell A. R., Howe J., Chi M., & Wiley B. J. (2011), Synthesis and catalytic properties of Au-Pd nanoflowers, *ACS Nano.*, 5, 6119–6127 (DOI:10.1021/nn201161m).

13. (a) Alagiri K., Devadig P., & Prabhu K. R. (2012), CDC Reactions of N-Aryl Tetrahydroisoquinolines Using Catalytic Amounts of DDQ: C-H Activation under Aerobic Conditions, *Chem. Eur. J.*, 18, 5160–5164 (DOI:10.1002/chem.201200100); (b) Li C.-J. (2009), Cross-Dehydrogenative Coupling (CDC): Exploring C−C Bond Formations beyond Functional Group Transformations, *Accounts of Chemical Research*, 42, 335–344 (DOI:10.1021/ar800164n); (c) Su W., Yu J., Li Z., & Jiang Z. (2011), Solvent-Free Cross-Dehydrogenative Coupling Reactions under High Speed Ball-Milling Conditions Applied to the Synthesis of Functionalized Tetrahydroisoquinolines, *J. Org. Chem.*, 76, 9144–9150 (DOI:10.1021/jo2015533); (d) Zhong J.-J., Meng Q.-Y., Liu B., Li X.-B., Gao X.-W., Lei T., Wu L.-Z. (2014), Cross-Coupling Hydrogen Evolution Reaction in Homogeneous Solution without Noble Metals, *Org. Lett.*, 16, 1988–1991 (DOI:10.1021/ol500534w); (e) Ghobrial M., Mihovilovic M. D., & Schnürch M. (2014), Exploration of C–H and N–H-bond functionalization towards 1-(1,2-diarylindol-3-yl) tetrahydroisoquinolines, *Beilstein J. Org. Chem.*, *10*, 2186–2199 (DOI:10.3762/bjoc.10.226); (f) Alagiri K., Kumara G. S. R., & Prabhu K. R. (2011), An oxidative cross-dehydrogenative-

coupling reaction in water using molecular oxygen as the oxidant: vanadium catalyzed indolation of tetrahydroisoquinolines, *Chem. Commun.*, 47, 11787 (DOI:10.1039/c1cc15050b); (g) Liu P., Zhou C.-Y., Xiang S., & Che C.-M. (2010), Highly efficient oxidative carbon-carbon coupling with SBA-15-support iron terpyridine catalyst, *Chem. Commun.*, 46, 2739–2741 (DOI:10.1039/c001209b); (h) Chu L., & Qing F.-L. (2010), Benzoyl peroxide (BPO)-promoted oxidative trifluoromethylation of tertiary amines with trimethyl(trifluoromethyl)silane, *Chem. Commun.*, 46, 6285–6287 (DOI:10.1039/c0cc01073a).

14. Eong H. H., Ishikawa Y., Asao N., Yamamoto Y., and Jin T. (2015), "Highly Efficient Heterogeneous Aerobic Cross-Dehydrogenative Coupling via C-H Functionalization of Tertiary Amines by Nanoporous Gold Skeleton Catalyst." *Chem. Commun.* 51, 12764–12767 (DOI: 10.1039/c5cc04856g).

15. (a) Tsuji M., Ikedo K., Matsunaga M., & Uto K. (2012), Epitaxial growth of Au@Pd core–shell nanocrystals prepared using a PVP-assisted polyol reduction method, *CrystEngComm.,* 14, 3411 (DOI:10.1039/c2ce00037g); (b) Harpeness R., & Gedanken A. (2004) Microwave synthesis of core-shell gold/palladium bimetallic nanoparticles, *Langmuir*, 20, 3431–3434 (DOI:10.1021/la035978z).

16. Samanta A., Rajesh T., & Devi R. N. (2014), Confined space synthesis of fully alloyed and sinter resistant Au-Pd nanoparticles encapsulated in porous silica, *J. Mater. Chem. A.,* 4398–4405 (DOI:10.1039/c3ta15194h).

17. (a) Serpell C. J., Cookson J., Ozkaya D., & Beer P. D. (2011), Core@shell bimetallic nanoparticle synthesis via anion coordination, *Nat. Chem.,* 3, 478–483 (DOI.org/10.1038/nchem.1030); (b) Sun D., Zhang G., Jiang X., Huang J., Jing X., Zheng Y., Li Q. (2014), Biogenic flower-shaped Au–Pd nanoparticles: synthesis, SERS detection and catalysis towards benzyl alcohol oxidation, *J. Mater. Chem. A*, 2, 1767 (DOI:10.1039/c3ta13922k).

18. (a) Alagiri K., Devadig P., & Prabhu K. R. (2012), CDC reactions of N-aryl tetrahydroisoquinolines using catalytic amounts of DDQ: C-H activation under

aerobic conditions, *Chem. Eur. J.*, 18, 5160–5164 (DOI:10.1002/chem.201200100); (b) Baslé O., & Li C. J. (2009), Copper-catalyzed aerobic phosphonation of *sp³* C-H bonds, *Chem. Comm.*, 27, 4124–4126 (DOI:10.1039/b905275e); (c) Shen Y., Li M., Wang S., Zhan T., Tan Z., & Guo C.-C. (2009), An efficient copper-catalyzed oxidative Mannich reaction between tertiary amines and methyl ketones, *Chem. Comm.*, (8), 953–955 (DOI:10.1039/b819657e).

19. (a) Xie J., Li H., Zhou J., Cheng Y., & Zhu C. (2012), A highly efficient gold-catalyzed oxidative C-C coupling from C-H bonds using air as oxidant, *Angew. Chem. Inter. Ed.*, 51, 1252–1255 (DOI:10.1002/anie.201107605); (b) Chu L., Zhang X., & Qing F. L. (2009) CuBr-catalyzed oxidative difluoromethylation of tertiary amines with difluoroenol silyl ethers, *Organic Lett.*, 11, 2197–2200 (DOI:10.1021/ol900541n).

20. (a) Boess E., Sureshkumar D., Sud, A. Wirtz, C., Far C., & Klussmann M. (2011), Mechanistic Studies on a Cu-Catalyzed Aerobic Oxidative Coupling Intermediates and the Role of Methanol As a Solvent, *J. Am. Chem. Soc.,* 133, 8106–8109 (DOI.org/10.1021/ja201610c); (b) Kumar R. A., Saidulu G., Prasad K. R., Kumar G. S., Sridhar B., & Reddy K. R. (2012), Transition metal-free *α*-C(sp³)-H bond functionalization of amines by oxidative cross dehydrogenative coupling reaction: Simple and direct access to C-4-alkylated 3,4-dihydroquinazoline derivatives, *Adv. Syn. Catal.*, 354, 2985–2991 (DOI:10.1002/adsc.201200679).

Chapter 7

Relevance and scope of work

In recent years, the area of nanochemistry has grown tremendously where control over the size, shape, morphology and composition through solution based methods have resulted in real-time application of these materials in various technologies. In the area of catalysis, nanoparticles offer an advantageous route compared to their bulk counterparts due to large surface area to volume ratio and possibility to reuse them over several cycles. With tremendous focus towards the development of greener routes in synthetic organic chemistry avoiding harmful organic solvents and harsh reaction conditions, the use of nanocatalysts is becoming significantly important in modern organic chemistry. However, the atomic level understanding for the various surface processes taking place on the nanoparticle surface is very difficult and therefore there is lots of scope of research for efficient and reproducible use of nanoparticles in synthetic organic chemistry.

In this thesis, we have demonstrated the activity of graphene oxide nanosheets as metal free carbocatalysts and Au nanoparticle based monometallic and alloy nanocatalytic systems for various important organic transformations. We have performed detailed spectroscopic and microscopic investigations towards understanding active species responsible for these catalytic reactions. The rationale for these studies is to exploit the structural and compositional intricacies of the nanoparticles for catalytic organic reactions with high activity, selectivity, atom-efficiency and step-efficiency.

In Chapter 2 we demonstrated that graphene oxide can be used as a mild, non-toxic and sustainable catalyst for the multicomponent coupling reactions, leading to biologically relevant α-aminophosphonates, 3,4-dihydropyrimidin-2-ones and 3-substituted indoles which are motif of biologically active compounds under solvent-free conditions with low catalytic loading. Due to the acidic nature of GO, the method can be extended to other acid catalyzed one-pot multicomponent reactions. Taking advantage of the oxygenated functional groups and the possibility of incorporating functionality when required, graphene oxide can be used as an ideal catalytic platform towards products of industrial interest through the multicomponent reaction pathway.

In Chapter 3, the catalytic activity of self-assembled monolayer-coated Au-NPs for the aerobic oxidation of aryl substituted α-hydroxy ketones to aryl 1,2-diketones is described and this reaction is extended for a one-pot synthesis of biologically significant quinoxaline derivatives in water. In this work, we looked into the role of thiol containing self-assembled monolayers on the catalytic activity of Au nanoparticles. It is well-known that thiols bind strongly on any metallic surface and hence it was expected that the composite nanomaterial might not show high catalytic activity for oxidation reactions as the self-assembled monolayer will prevent the access of the substrates towards the nanoparticle surface. However, the thiol containing monolayer protected Au nanoparticles showed high activity towards oxidations of hydroxyl to ketones. Our current methods avoid the use of acid, highly toxic reagents, hazardous organic solvents, multistep synthesis etc. In addition, the simplistic synthesis of the catalyst, operational simplicity, high yields, catalytic and environmentally friendly reaction conditions make them attractive. This result should encourage new applications for self-assembled monolayer-coated Au-NPs in organic syntheses as efficient catalysts.

In chapter 4, we have shown the activity of AuPd alloy nanoparticles towards direct oxidation of α-hydroxy esters and α-hydroxy phosphonates for the formation of their keto counterparts through synergistic effect between the two metals. It is worth mentioning that direct oxidation of these compounds often leads to the formation of carboxylic acids due to the presence of good leaving groups such as esters and phosphonates. With proper control of the composition between Au and Pd, it was possible to perform the oxidation reaction under mild reaction conditions without the formation of any side products.

In chapter 5, we have described the activity of AuPd nanoparticles towards the development of α-ketoamides, an important structural motif of biologically active compounds, through an oxidative dehydrogenative coupling process using molecular oxygen as the sole oxidizing agent under mild reaction conditions. Again the synergistic effect between the two metallic components was taken advantage of towards the synthesis of these important compounds.

In chapter 6, we have shown how a combination of synergistic effect, morphology, shape-selectivity and leaching process could lead to effective and regioselective synthesis of coupling products through aerobic oxidative dehydrogenative coupling (CDC). In all the Au based nanocatalytic systems we used polyvinylpyrrolidone (PVP) as the surface stabilizer for the growth of the nanomaterials. The obvious reason was to use a common surface coating in order to have a better understanding towards the molecular processes taking place during the catalytic reactions. However this had an impact on the stability of the catalysts during the catalytic reactions and the activity of the catalysts was reduced significantly during the recycled reactions. This can be improvised by immobilizing these nanoparticles on other heterogeneous supports such as mesoporous carbon, metal oxides or mesoporous materials.

However our aim was to have an understanding on the correlation between the intrinsic surface properties of the nanoparticles and the catalytic activity of various important transformations. Although we have fairly achieved towards our goal, more studies involving sophisticated surface characterization techniques such as X-ray photoelectron spectroscopy, high angle annular dark field electron microscopy etc. will be crucial in better understanding of the atomic processes involved in these nanocatalytic systems. Unfortunately, due to lack of facilities we could not perform these studies.

Appendix A

Chapter 2

Characterization NMR Data α-amino phosphonates, 3 substituted Indole (Table 2.2 and Table 2.4)

¹H NMR of compound 3aa (CDCl₃, 400 MHz)
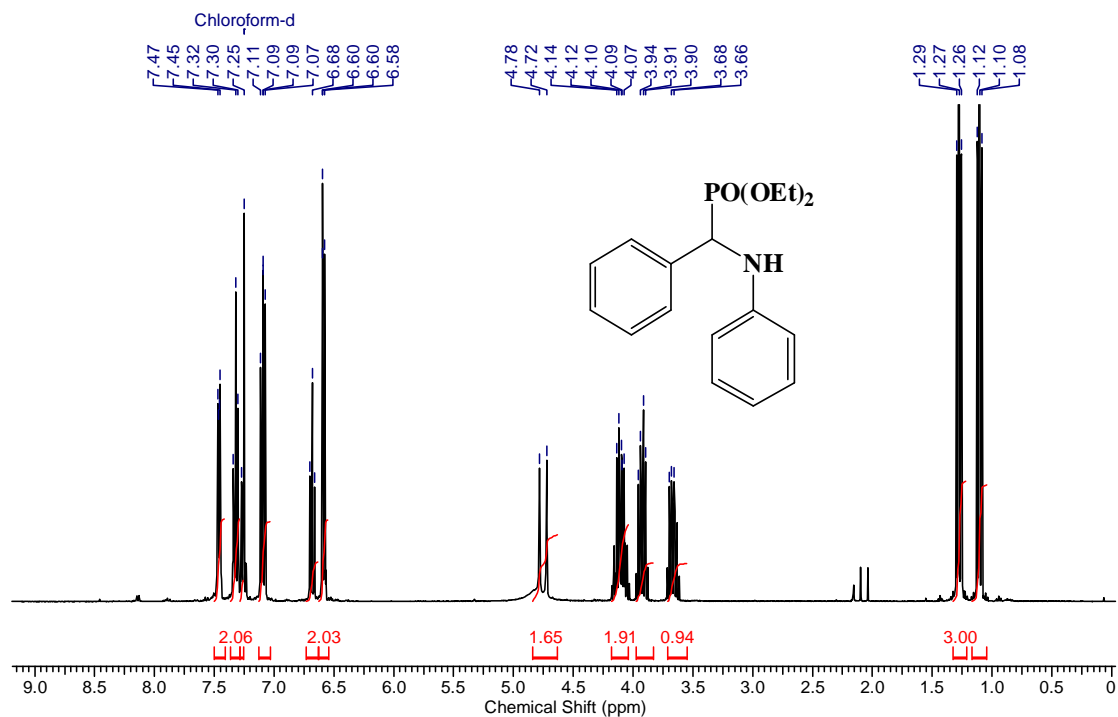
^{1}H NMR of compound 3aa (CDCl$_3$, 400 MHz)
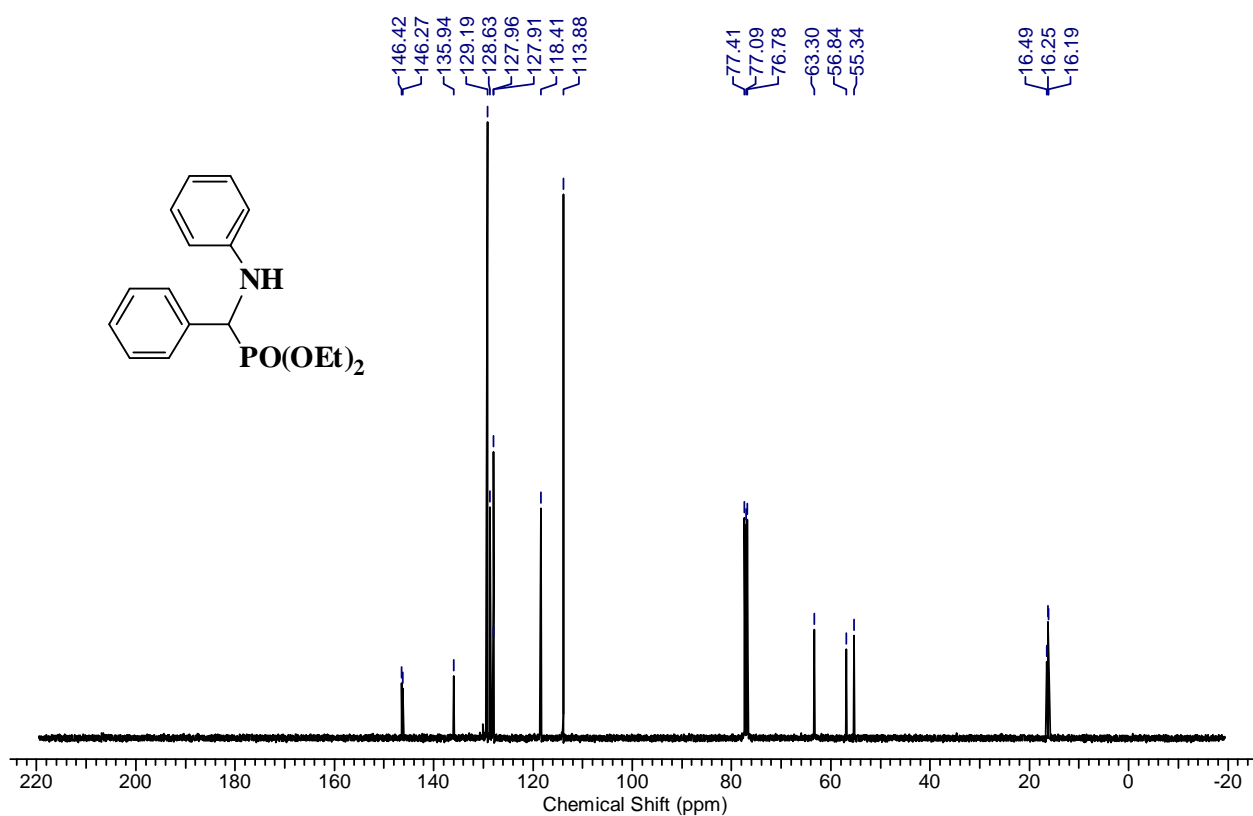
^{13}C NMR of compound 3aa (CDCl$_3$, 100 MHz)
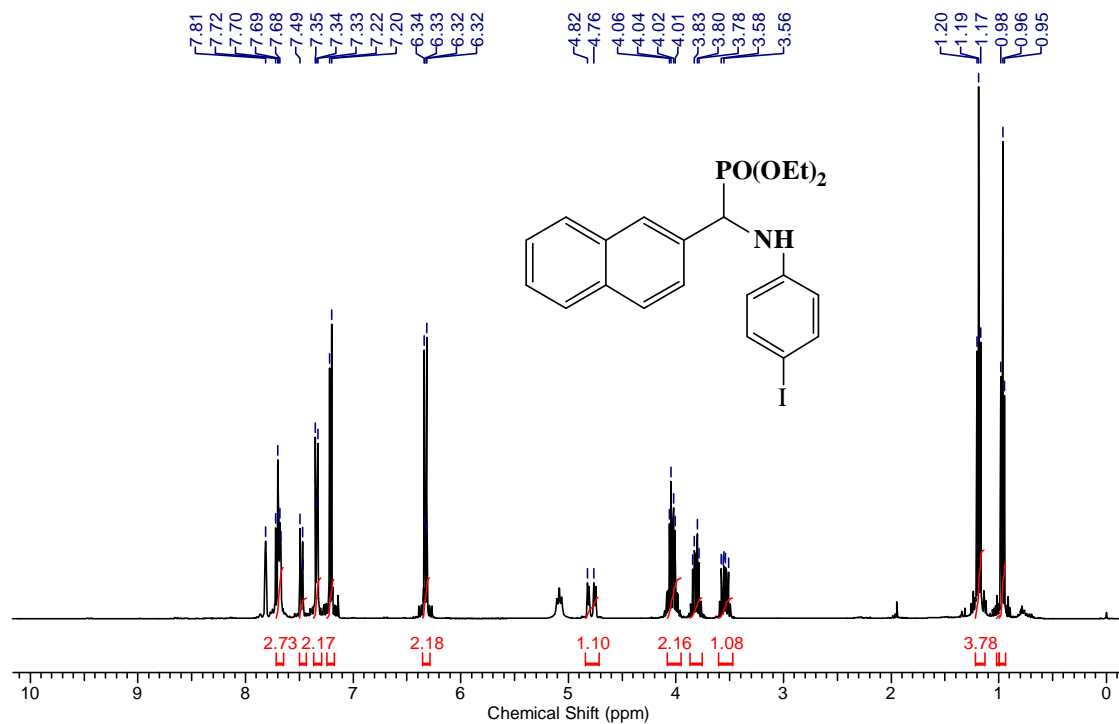
¹H NMR of compound 3ab (CDCl₃, 400 MHz)
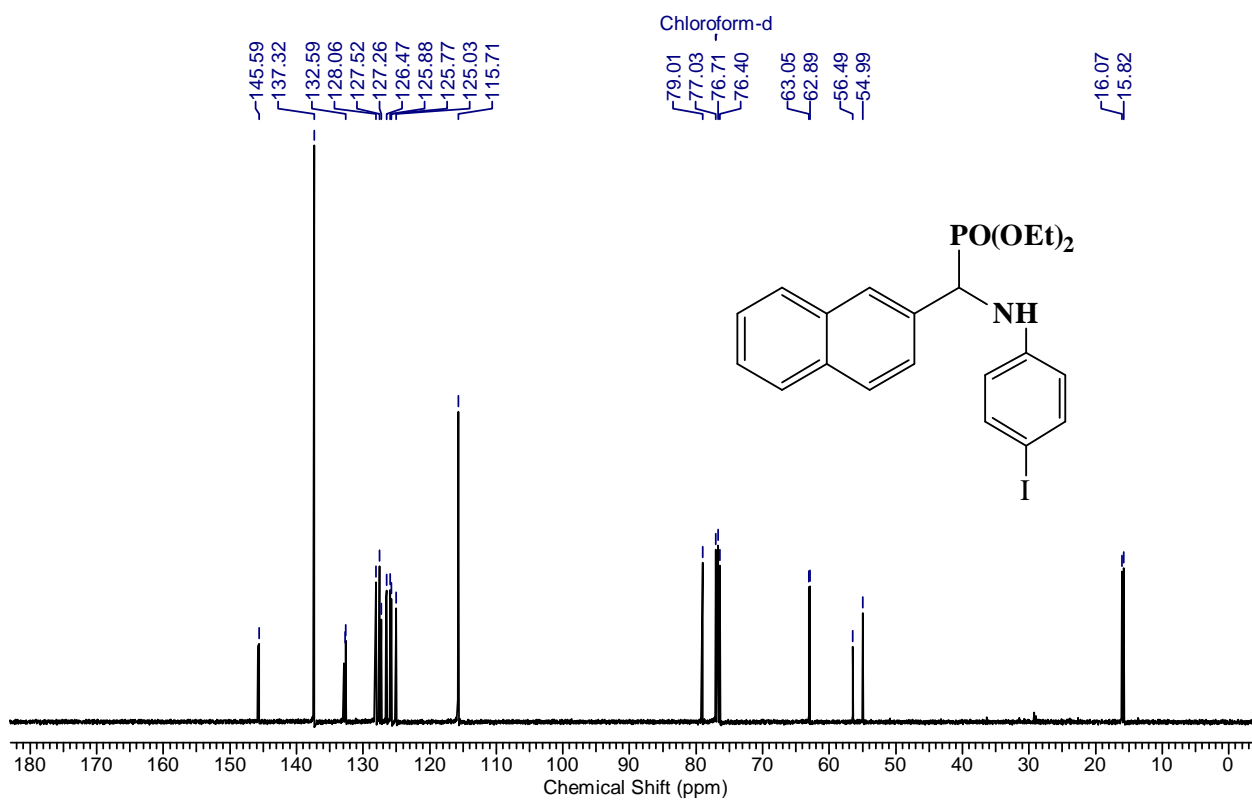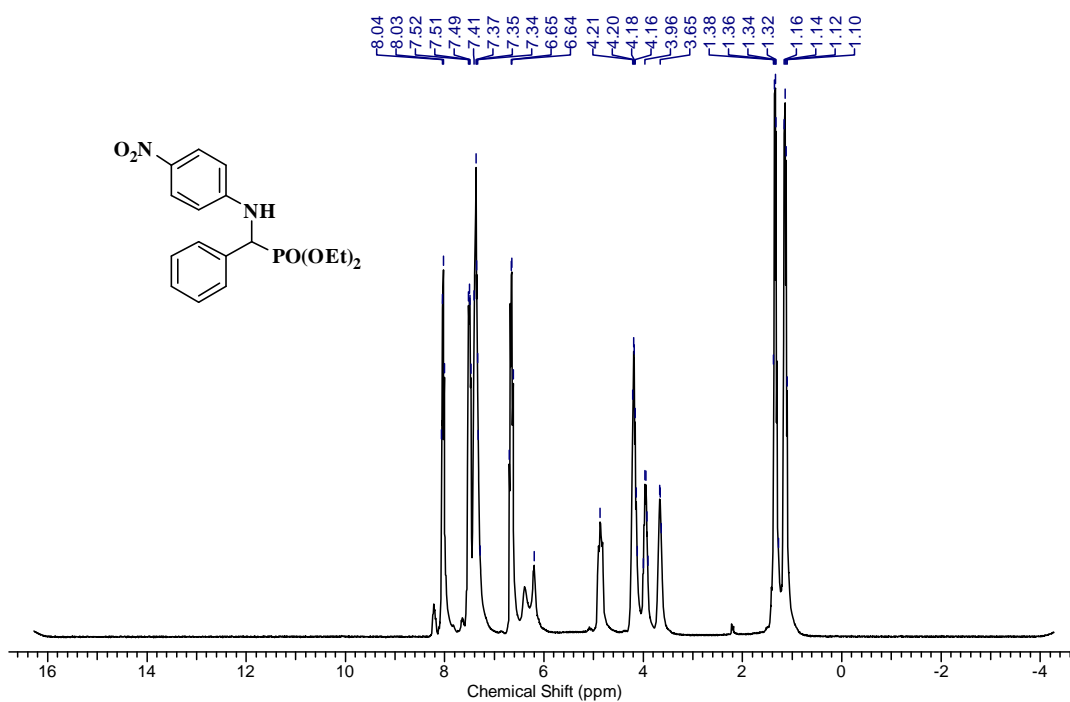
¹³C NMR of compound 3ab (CDCl₃, 100

¹H NMR of compound 3ae (CDCl₃, 400 MHz)
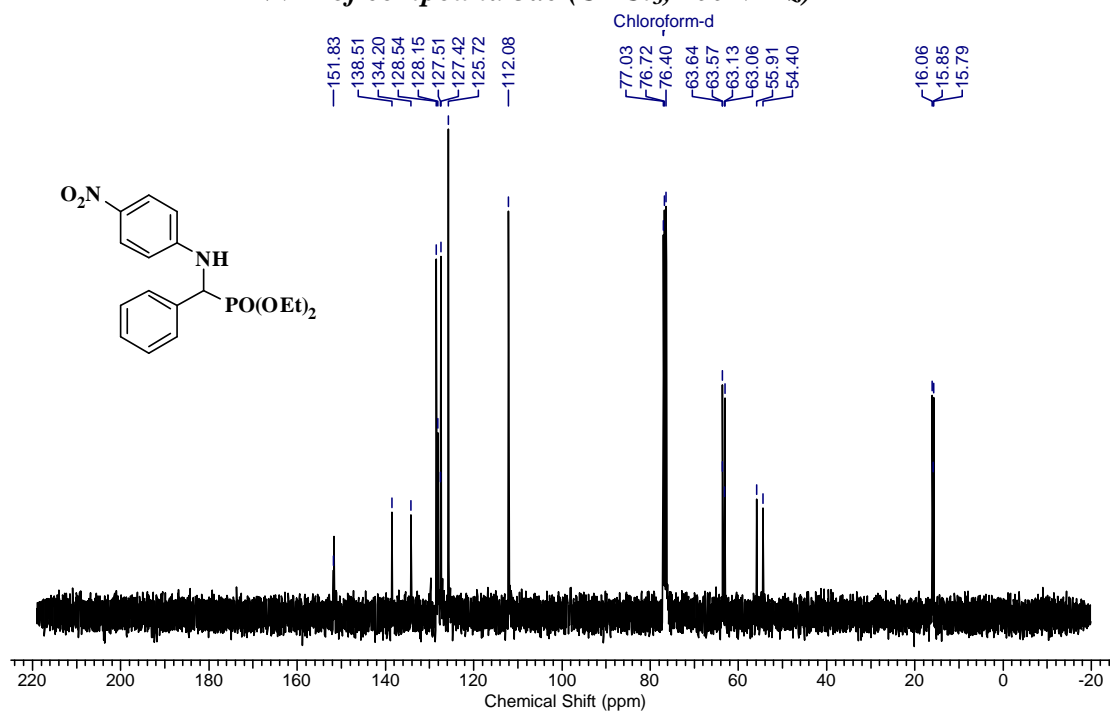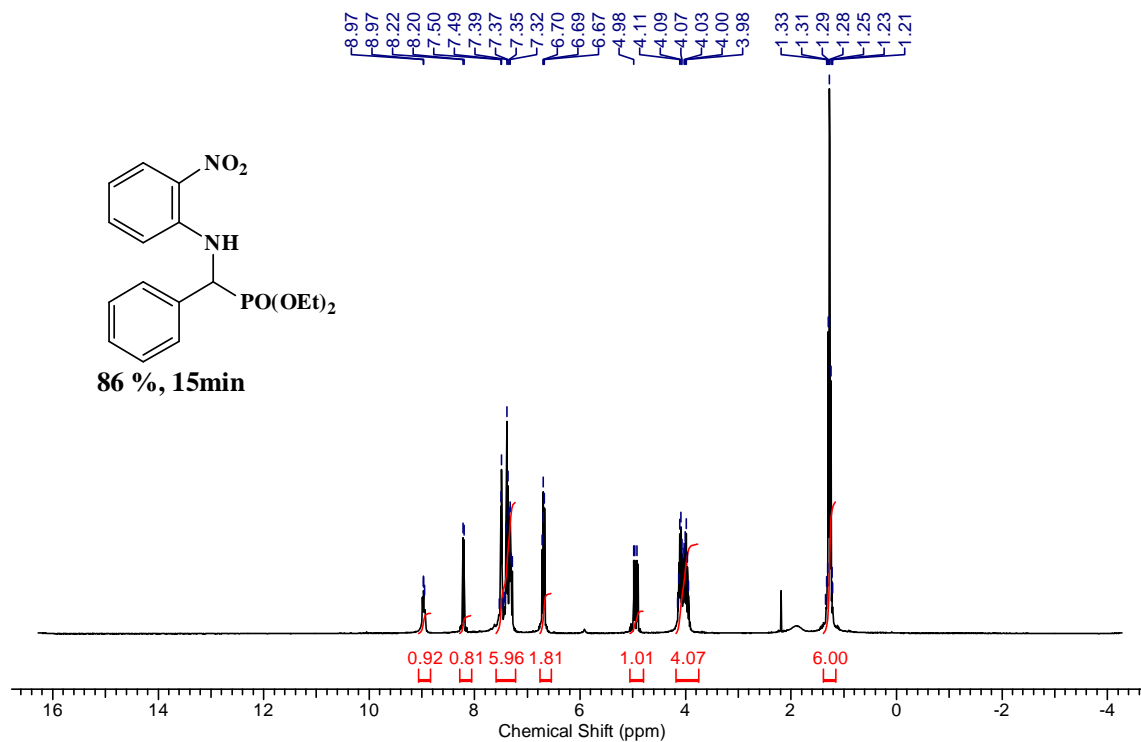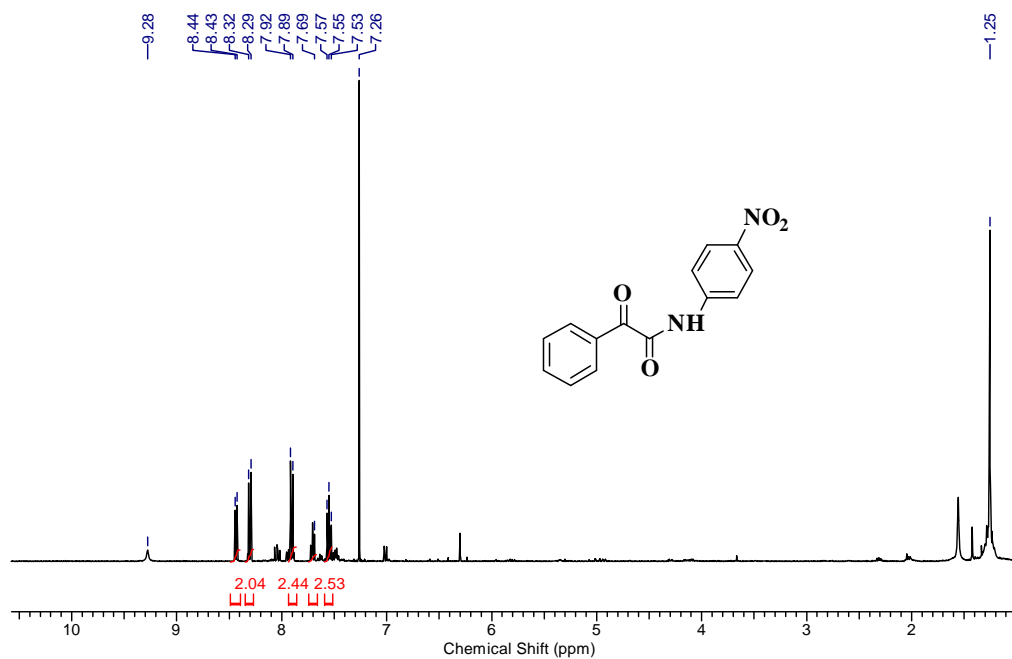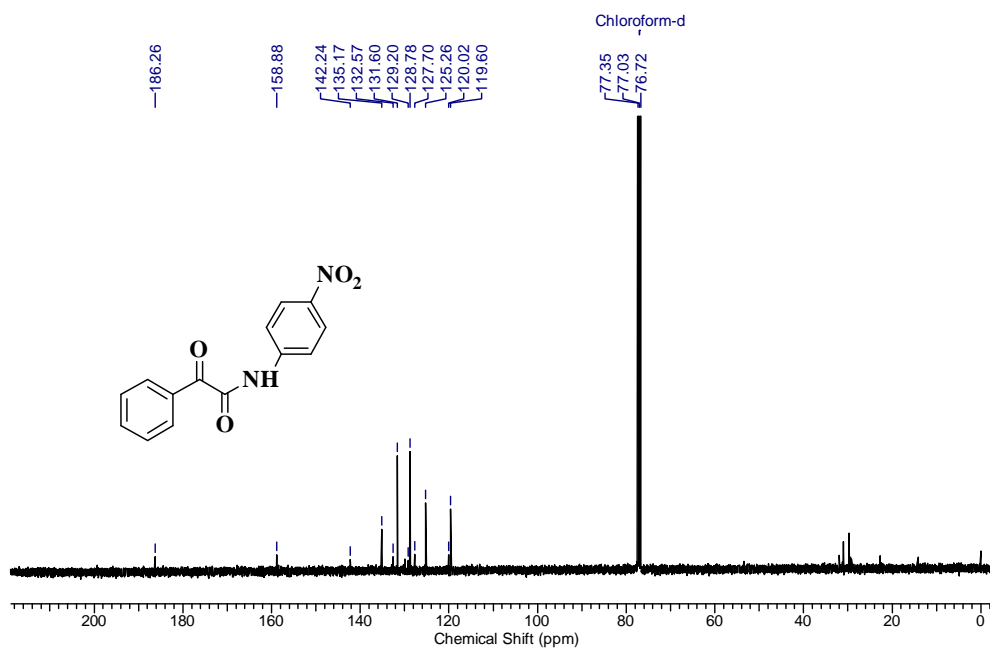

¹³C NMR of compound 3ae (CDCl₃, 100 MHz)

¹H NMR of compound 3ac (CDCl₃, 400 MHz)

¹³C NMR of compound 3ac (CDCl₃, 100 MHz)

¹H NMR of compound 3ad (CDCl₃, 400 MHz)

¹³C NMR of compound 3ad (CDCl₃, 100 MHz)

188
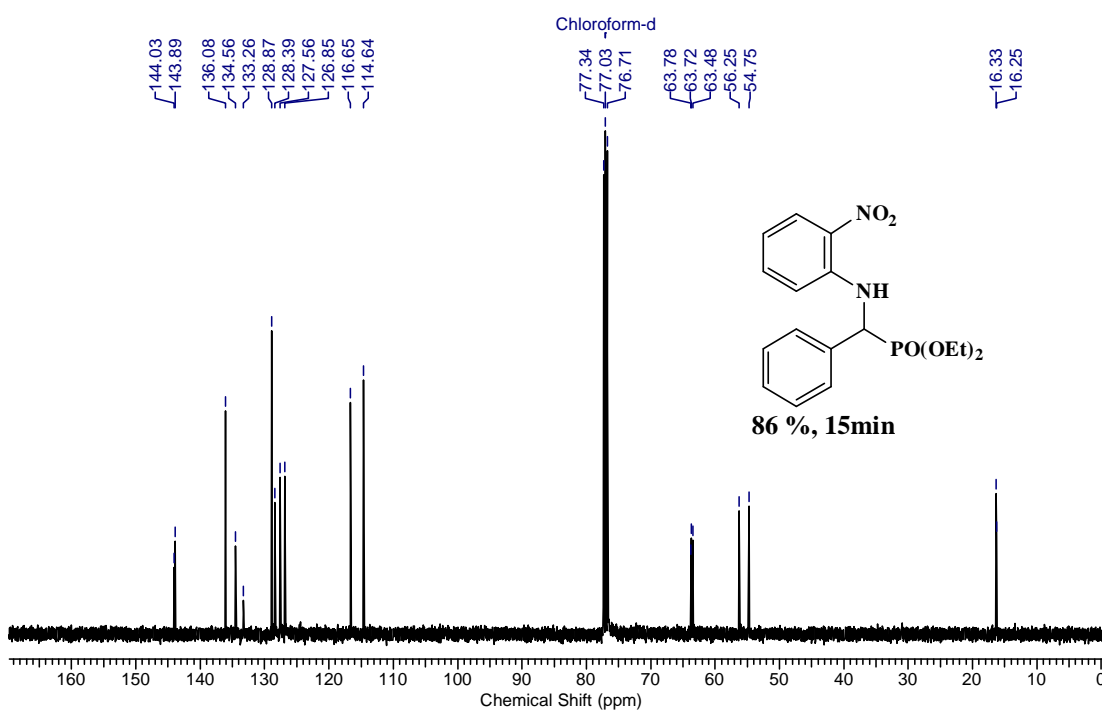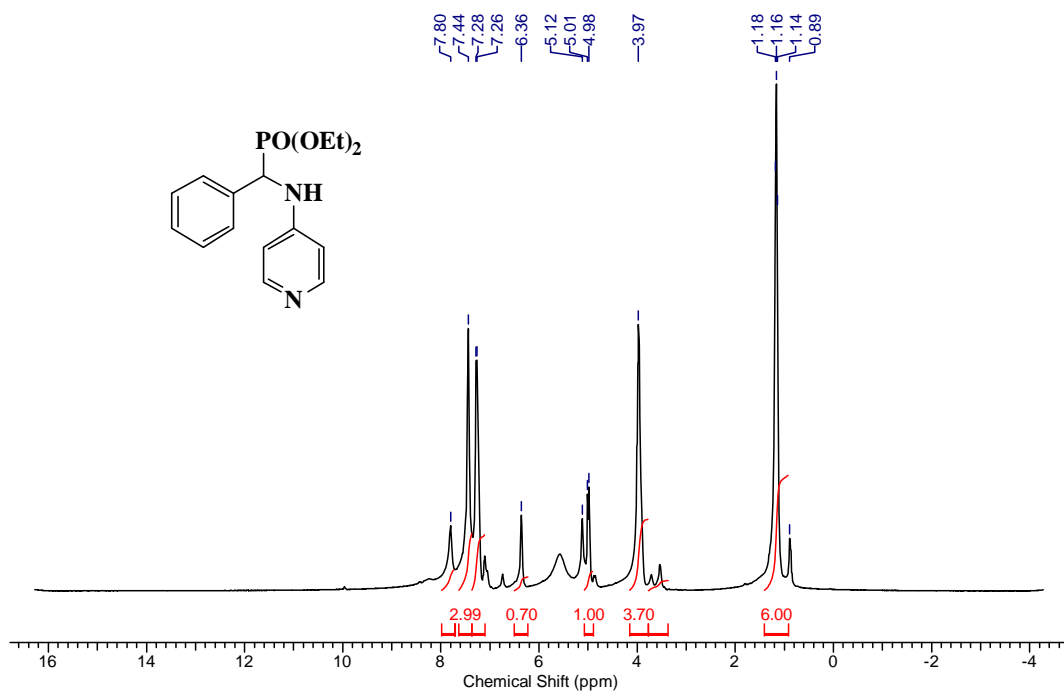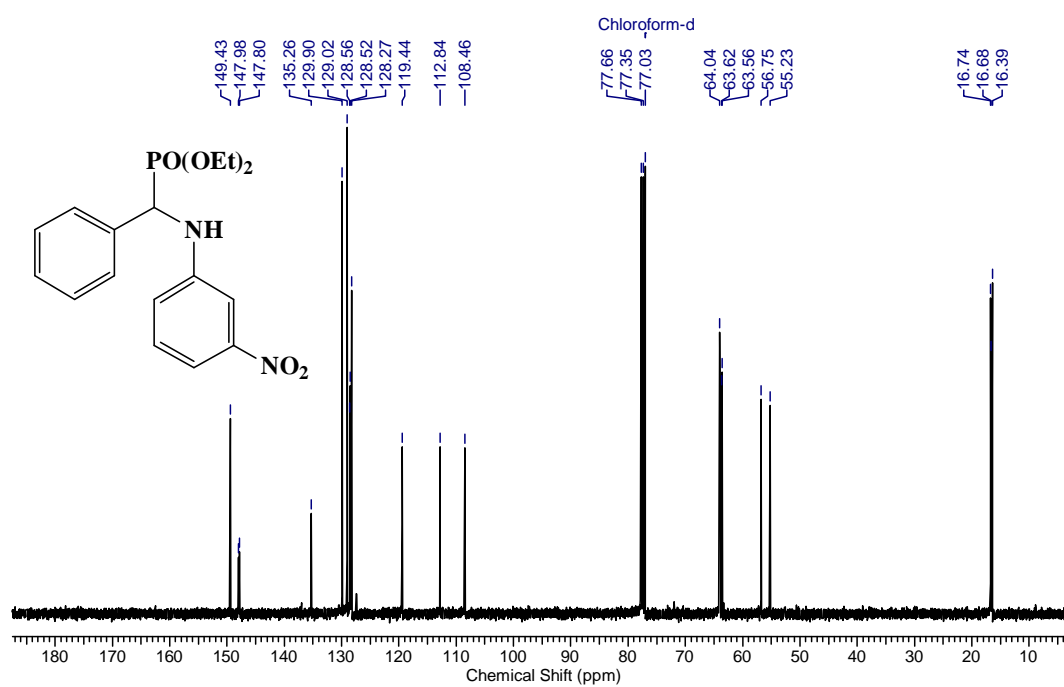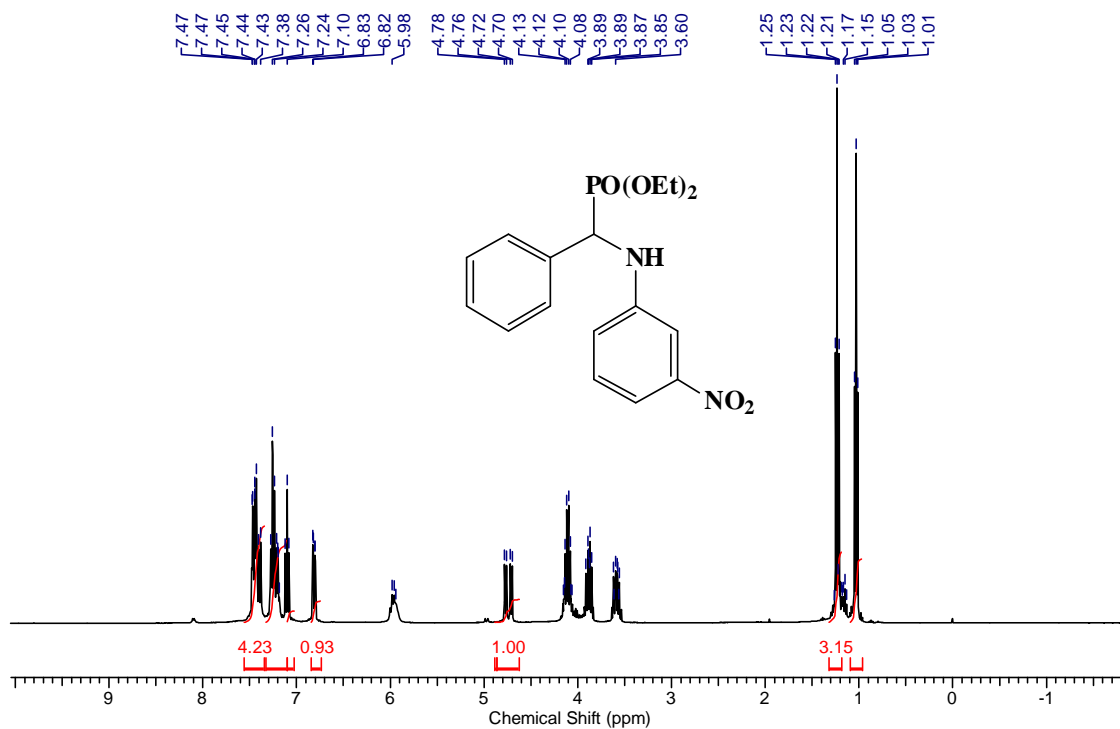
¹H NMR of compound 3ag (CDCl₃, 400 MHz)
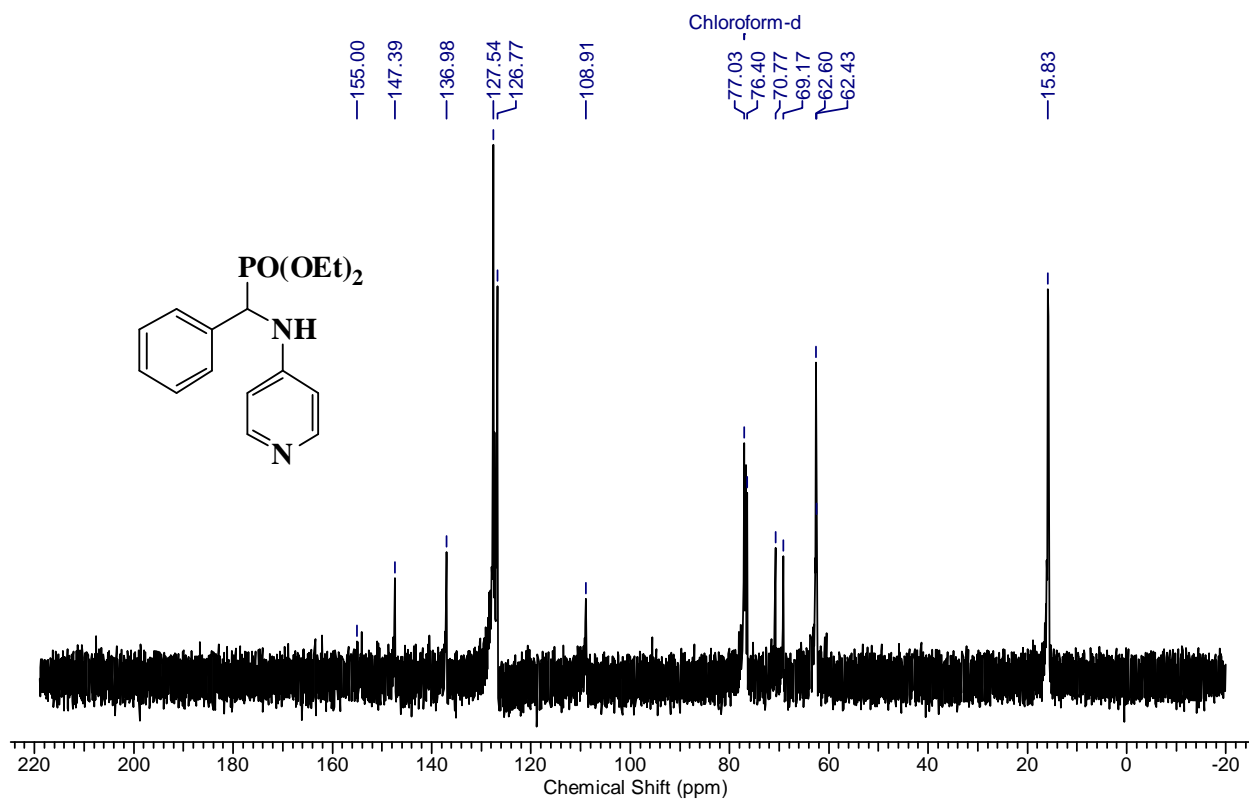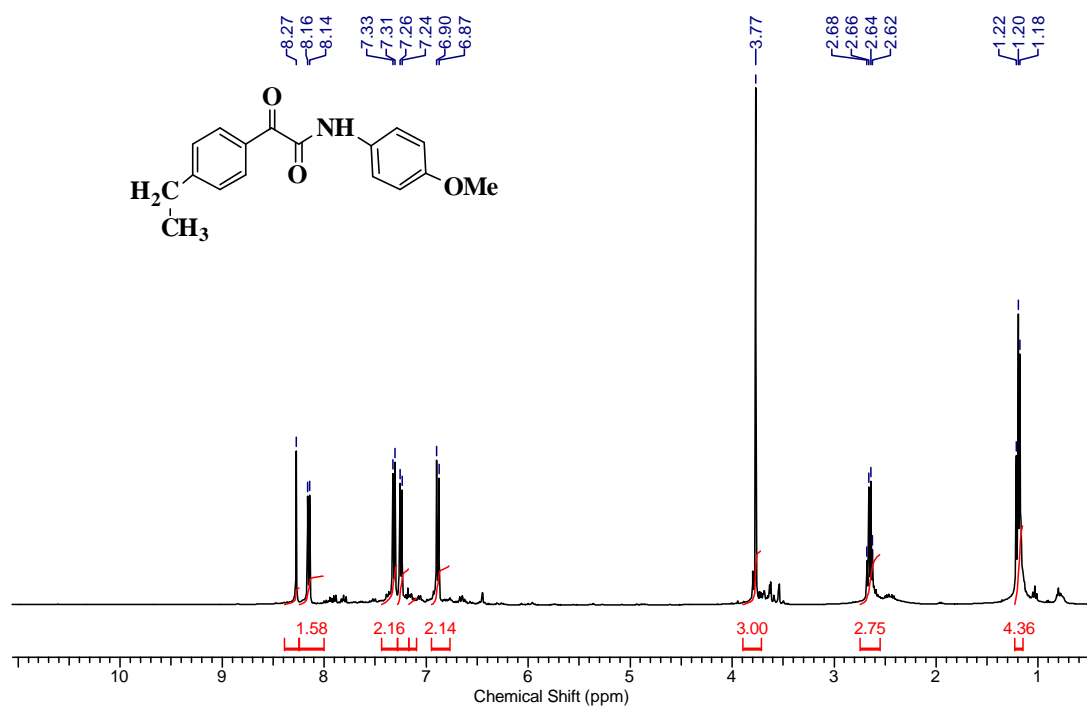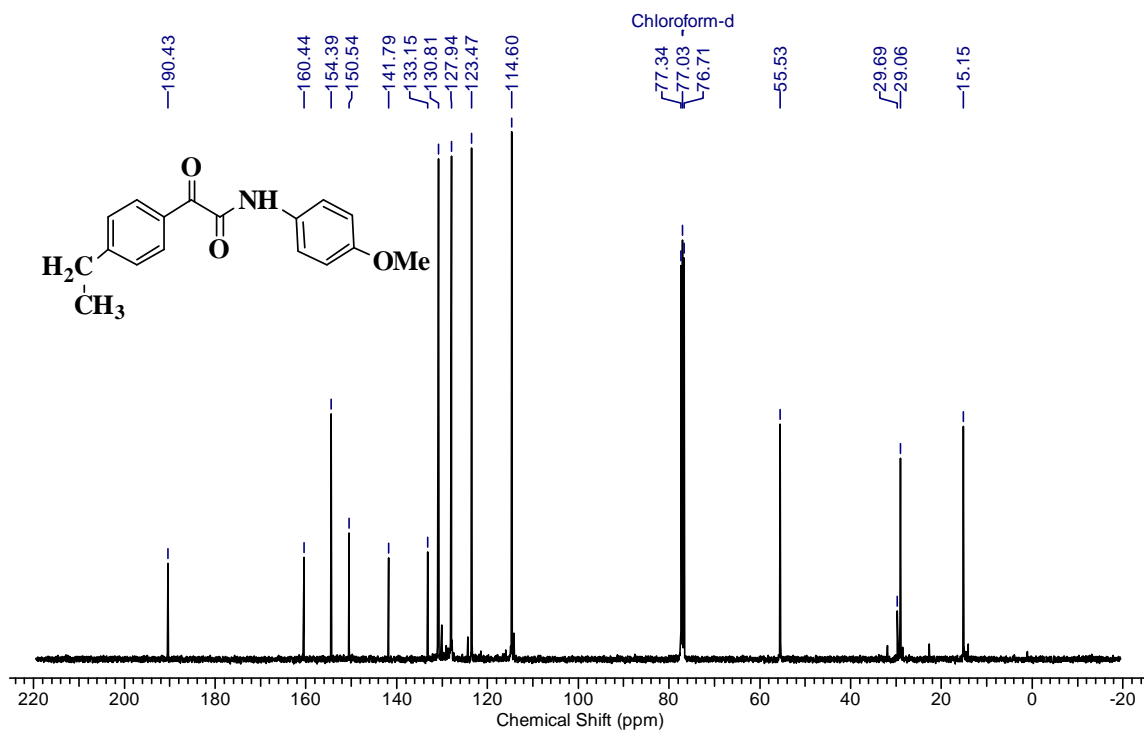

¹³C NMR of compound 3ag (CDCl₃, 100 MHz)
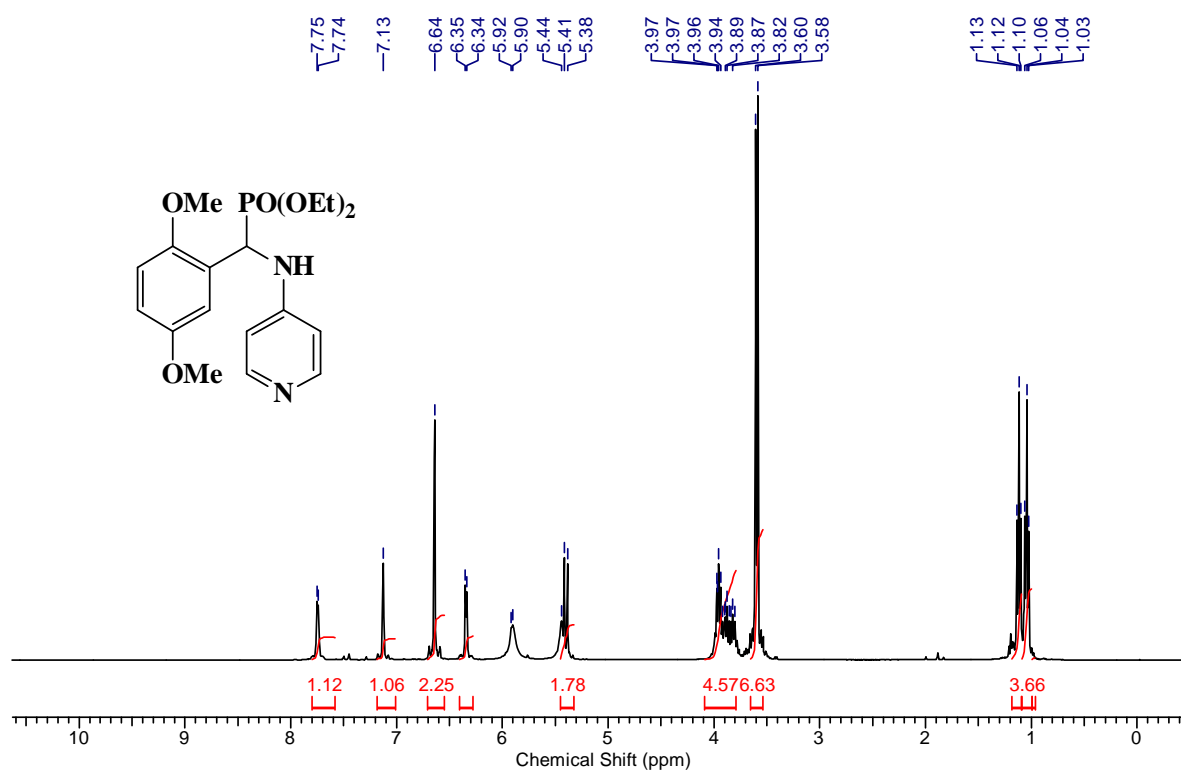
^1H NMR of compound 3fg (CDCl₃, 400 MHz)
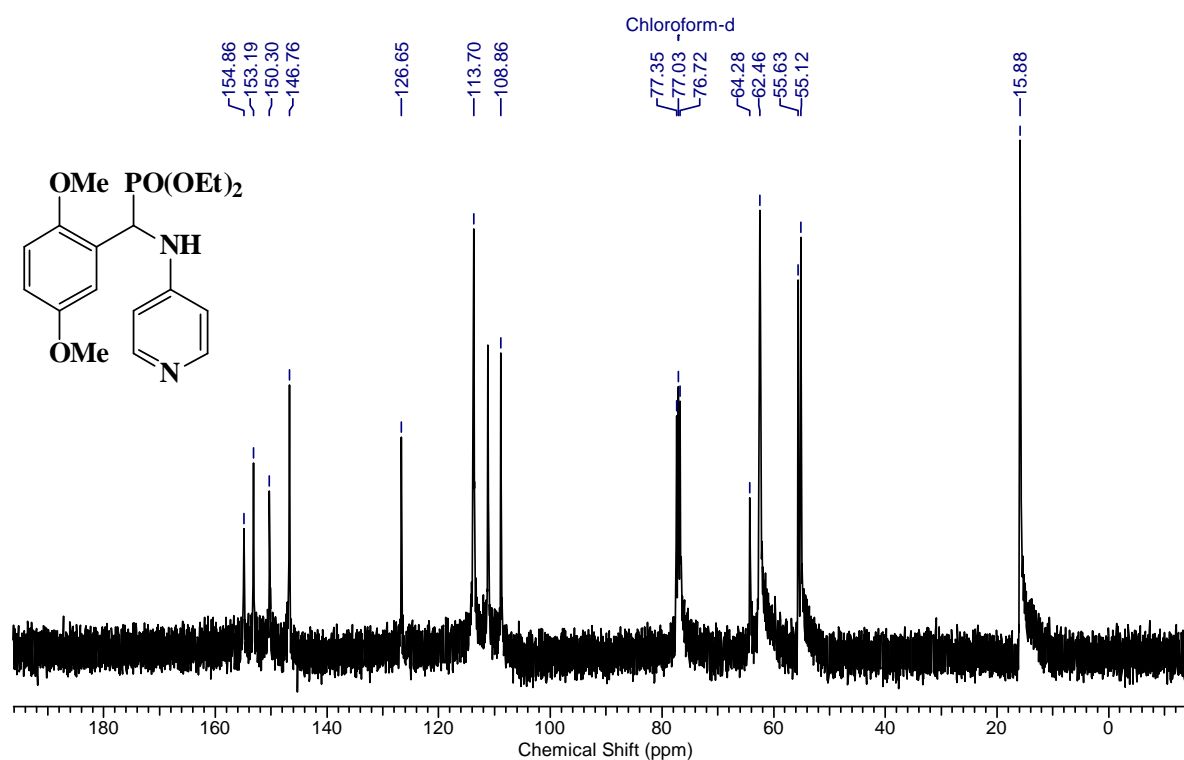
^{13}C NMR of compound 3fg (CDCl₃, 100 MHz)
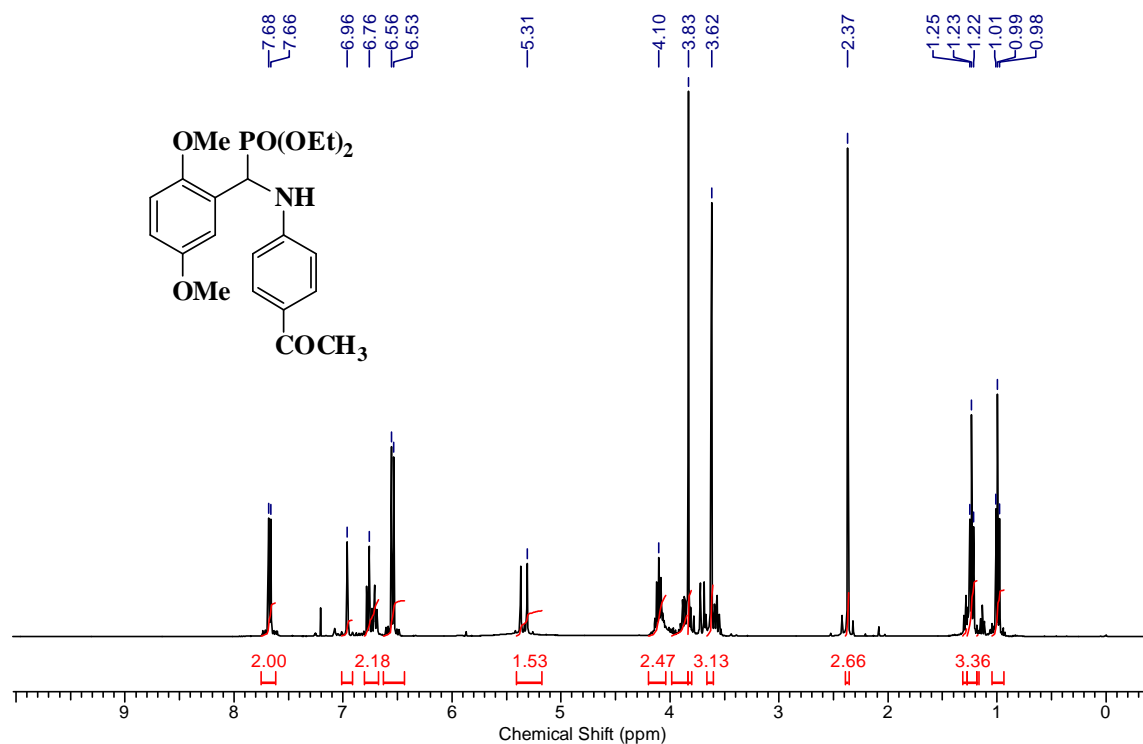
¹H NMR of compound 3fh (CDCl₃, 400 MHz)
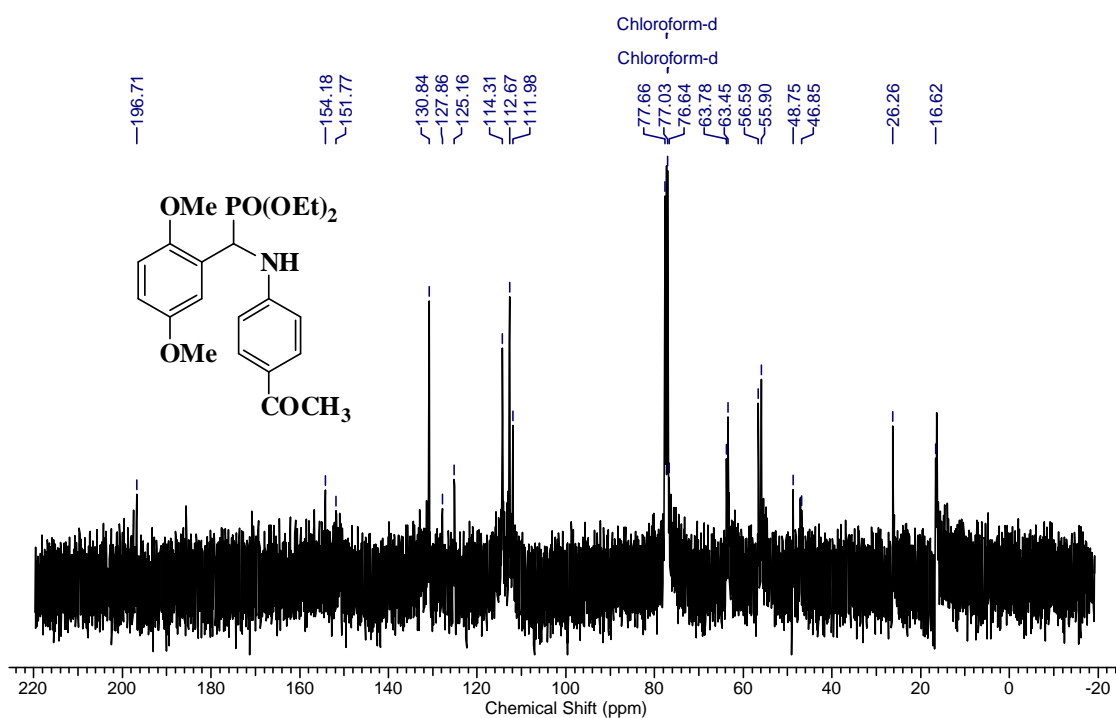
¹³C NMR of compound 3fh (CDCl₃, 100 MHz)
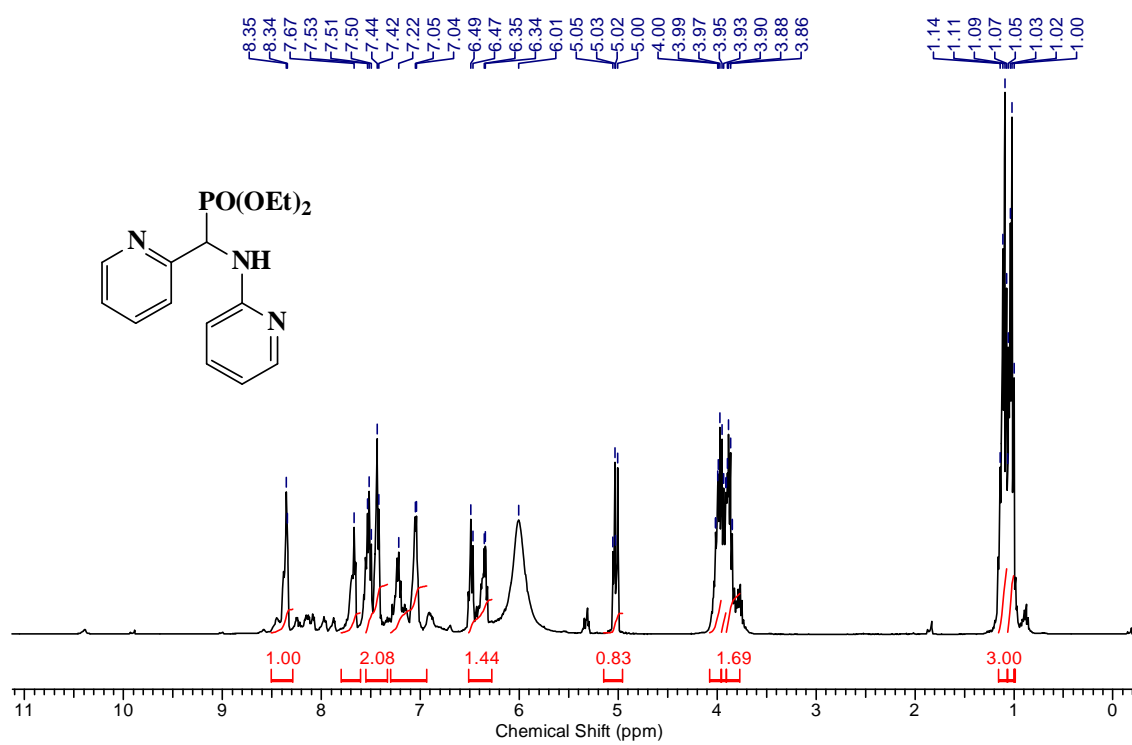
¹H NMR of compound 3ii (CDCl₃, 400 MHz)
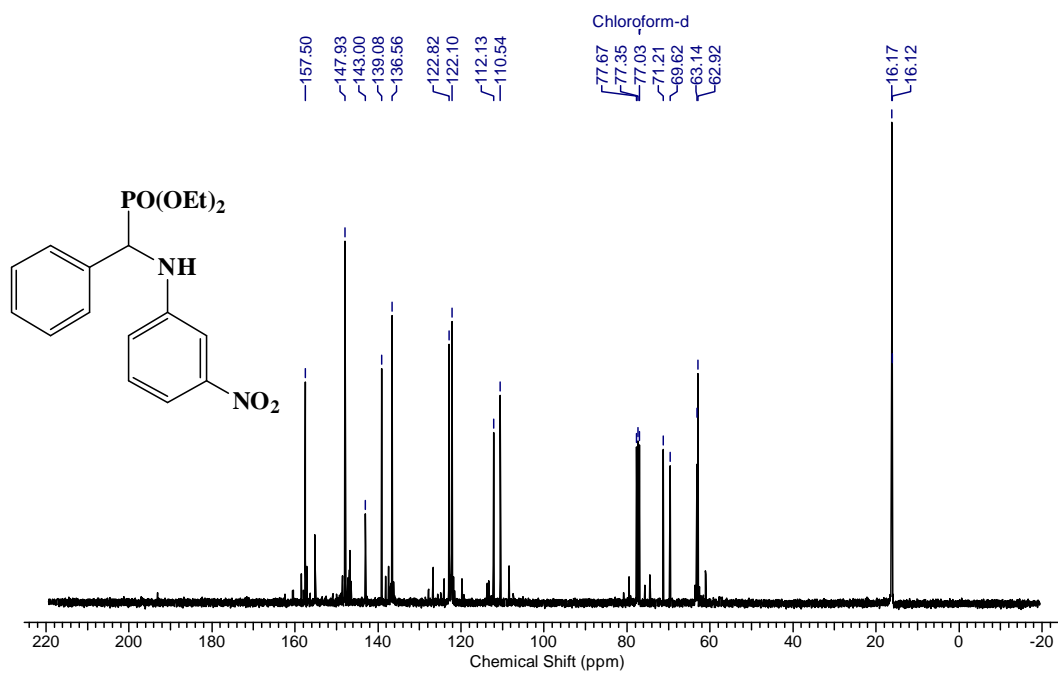
¹³C NMR of compound 3ii (CDCl₃, 100 MHz)
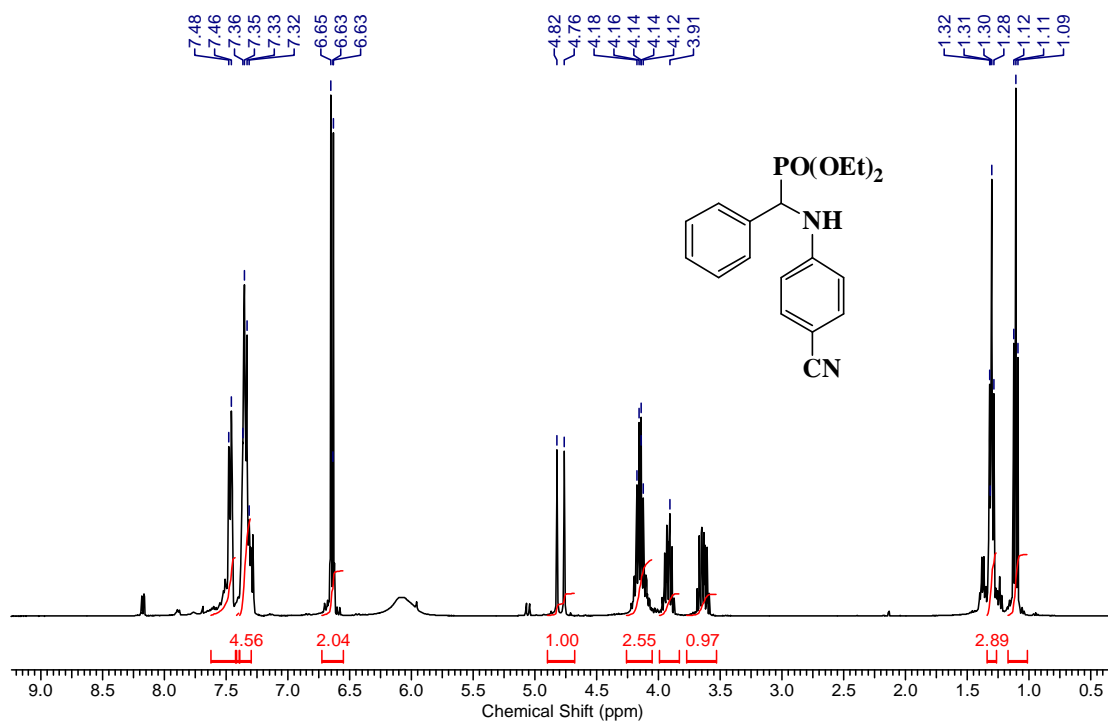
¹H NMR of compound 3aj (CDCl₃, 400 MHz)
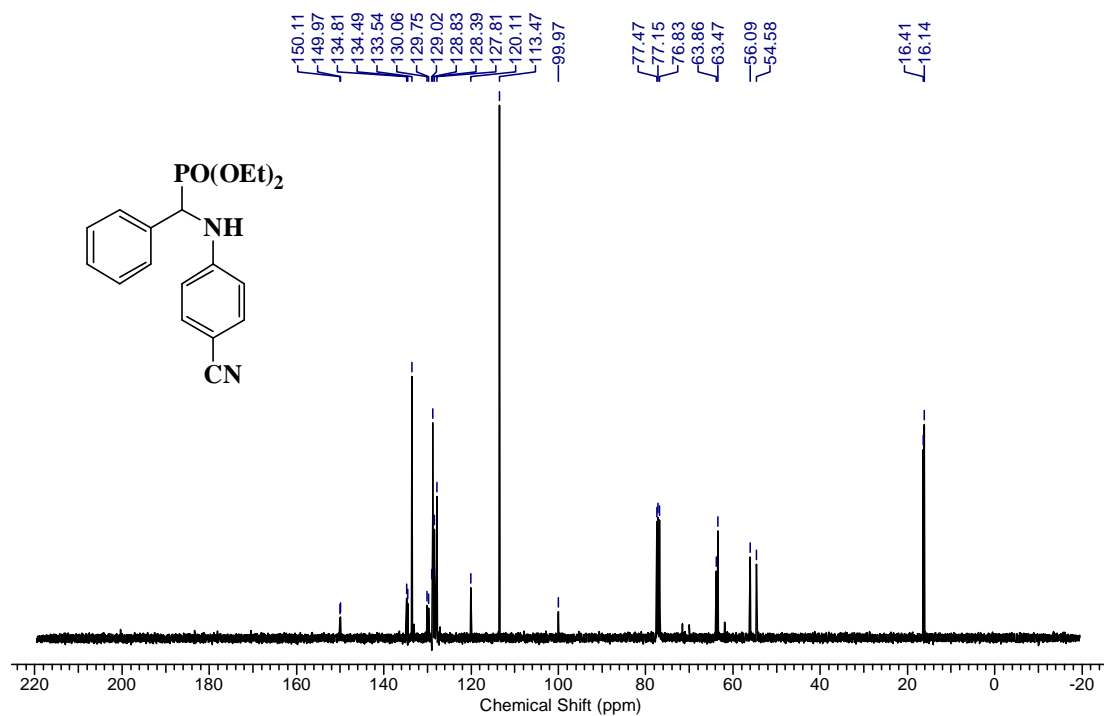
¹³C NMR of compound 3aj (CDCl₃, 100 MHz)
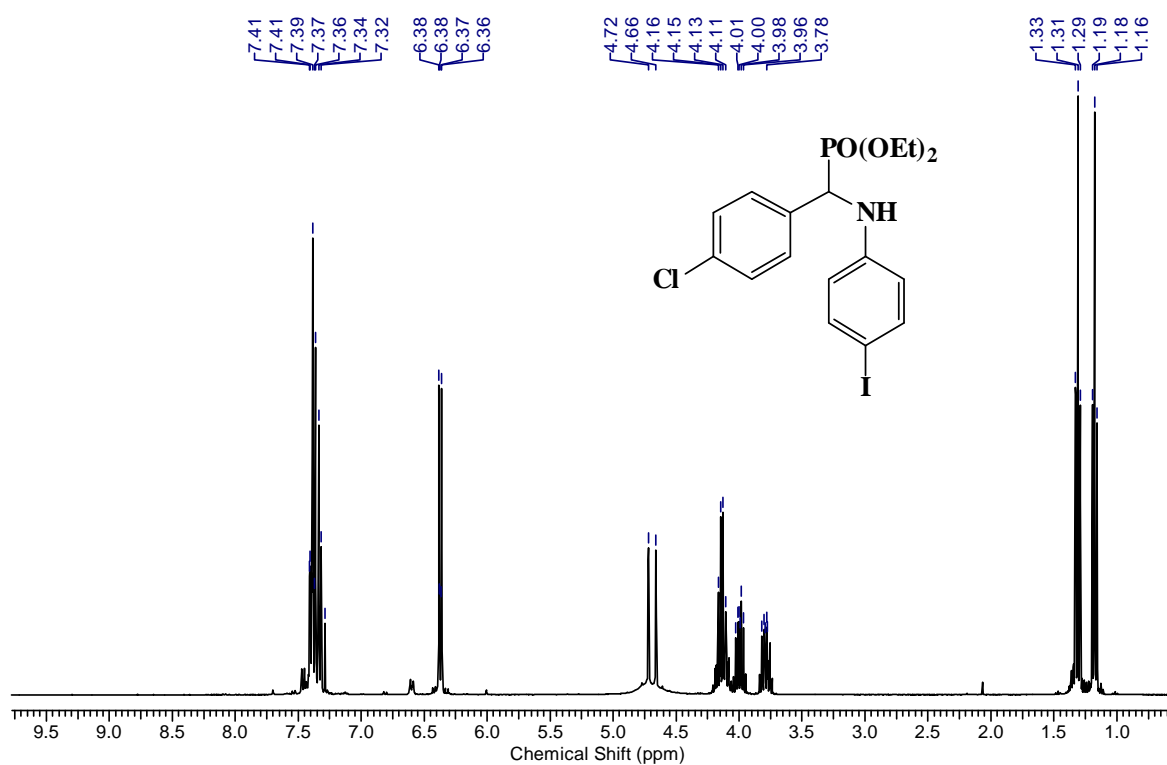
^1H NMR of compound 3al (CDCl$_3$, 400 MHz)
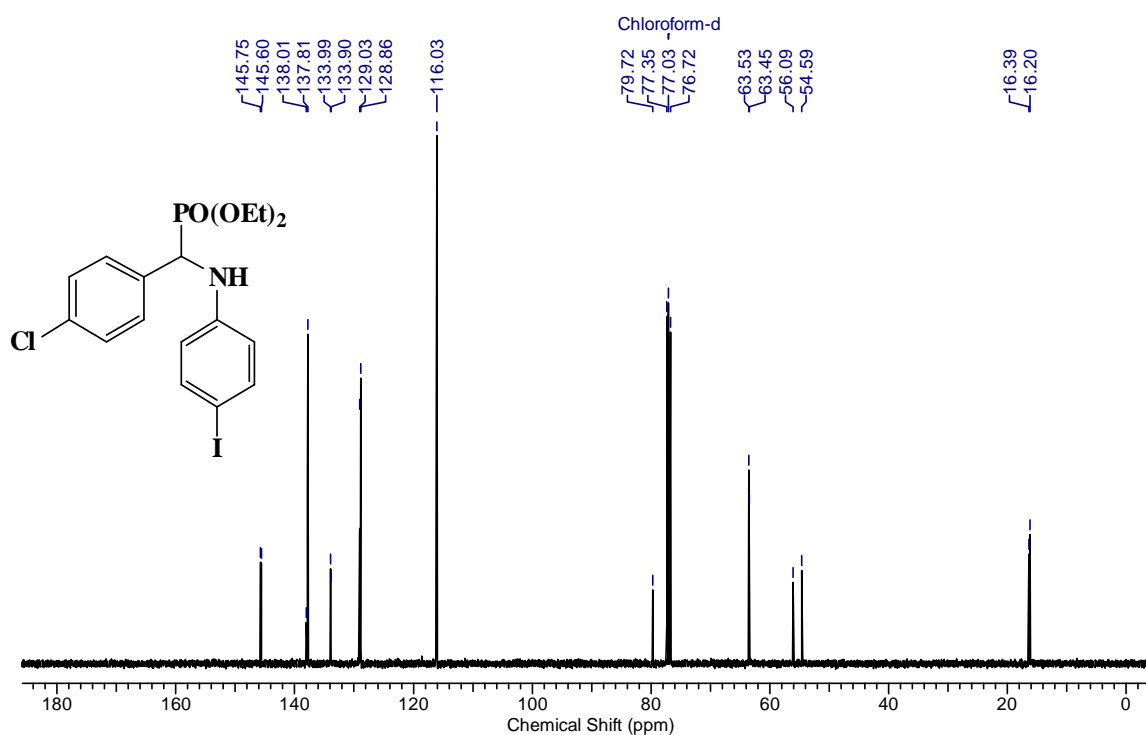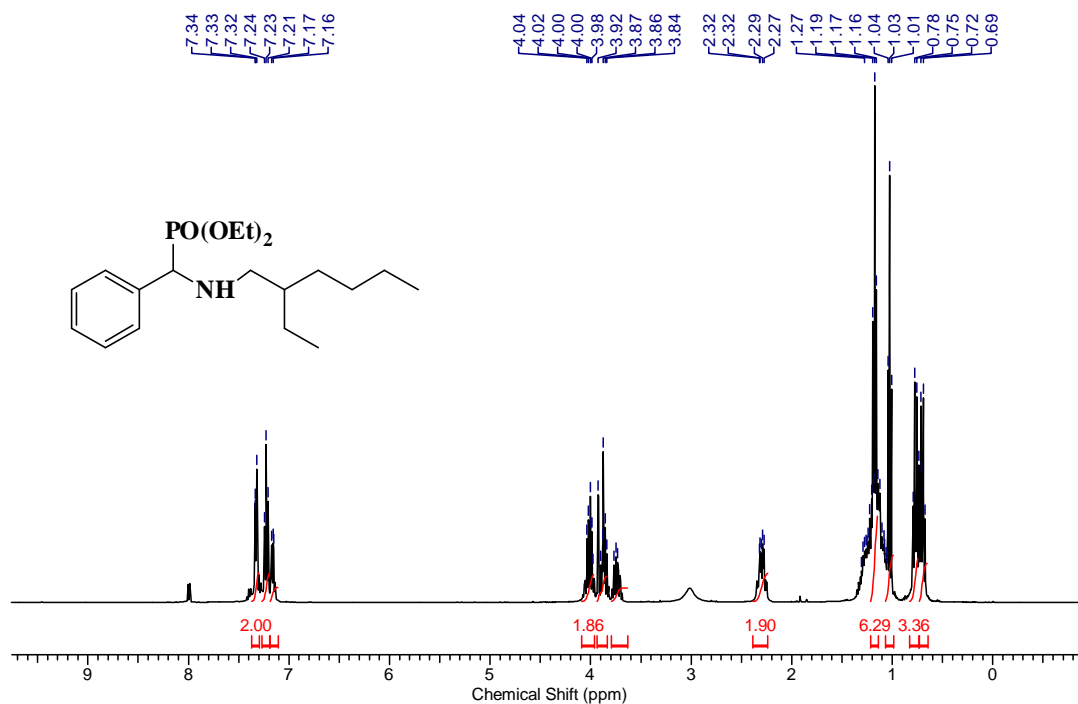
^{13}C NMR of compound 3al (CDCl$_3$, 100 MHz)

¹H NMR of compound 3al (CDCl₃, 400 MHz)
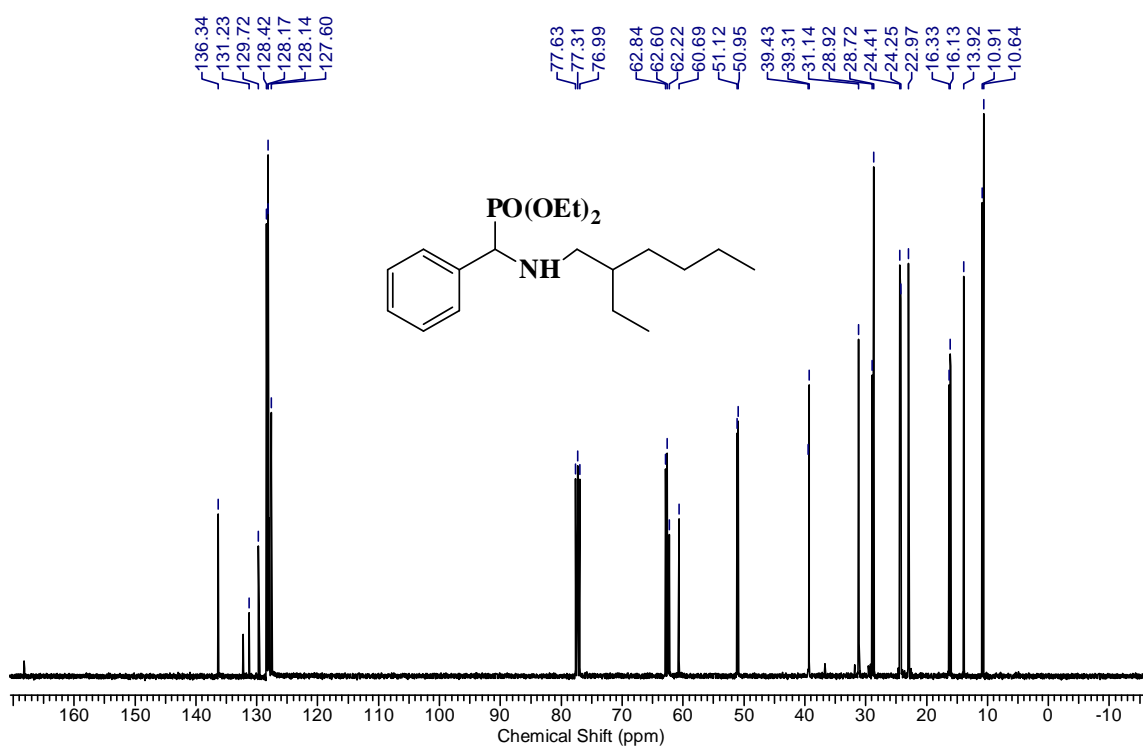
¹³C NMR of compound 3al (CDCl₃, 100 MHz)
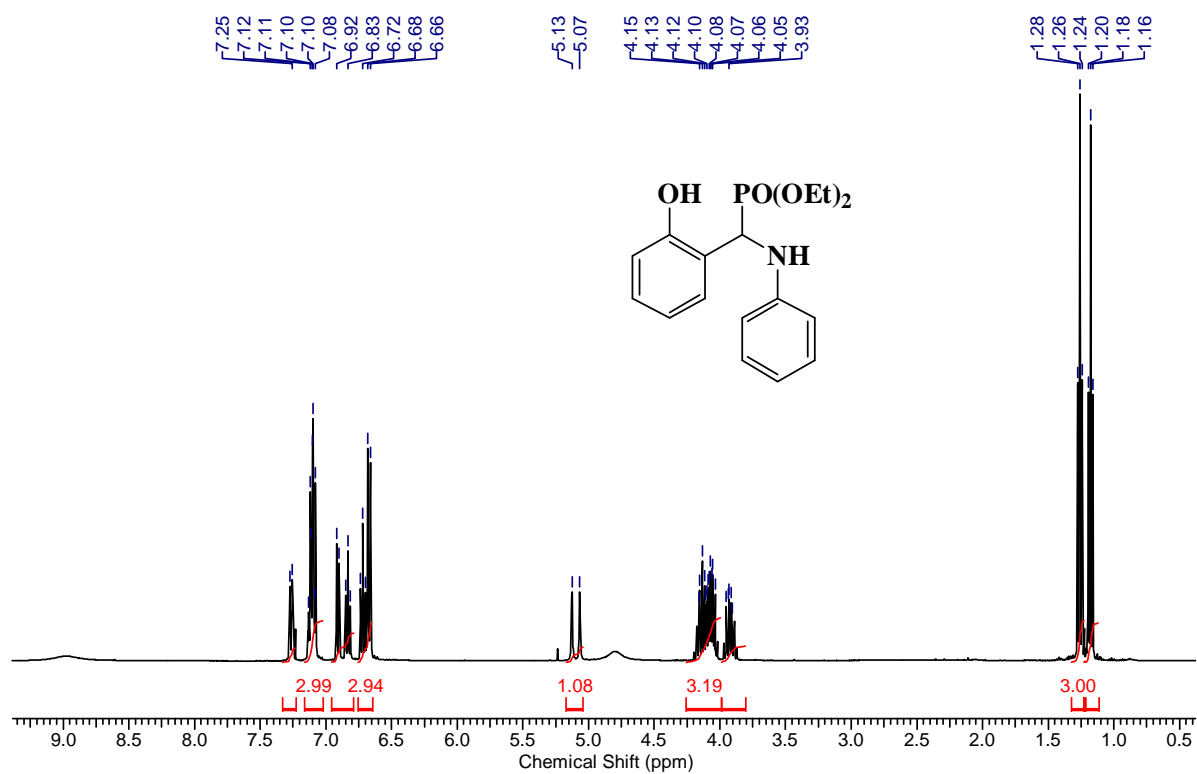
1H NMR of compound 3ba (CDCl3, 400 MHz)
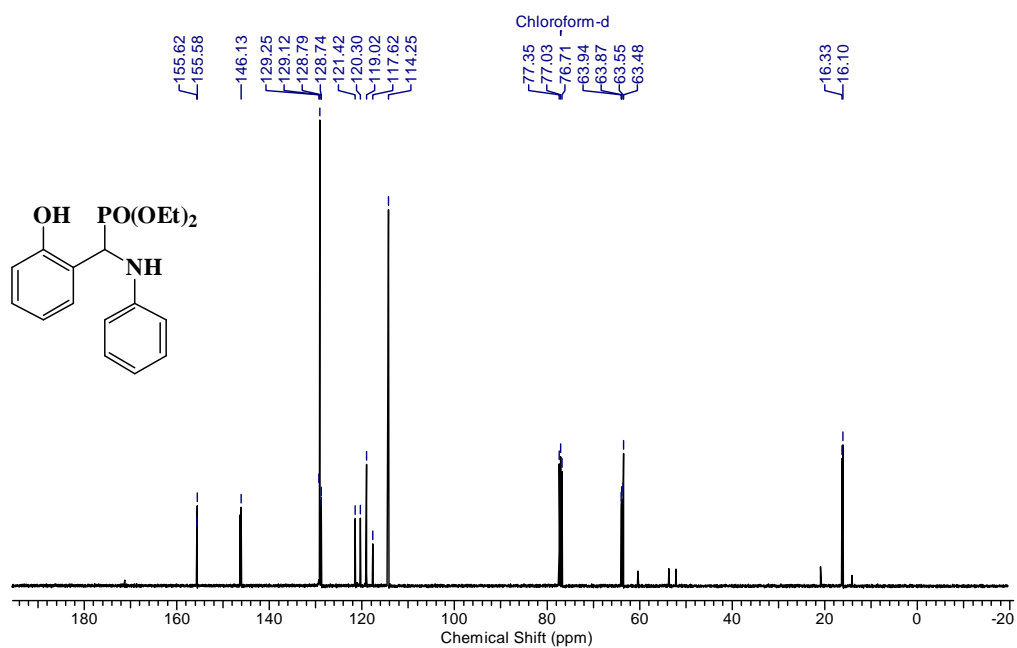
13C NMR of compound 3ba (CDCl3, 100 MHz)
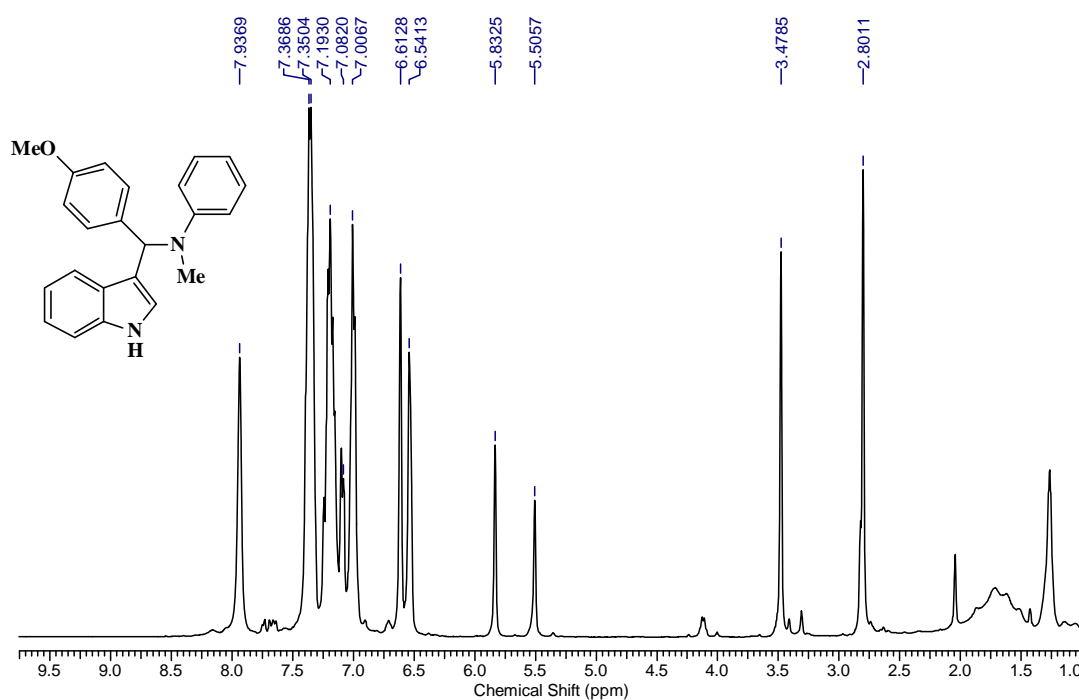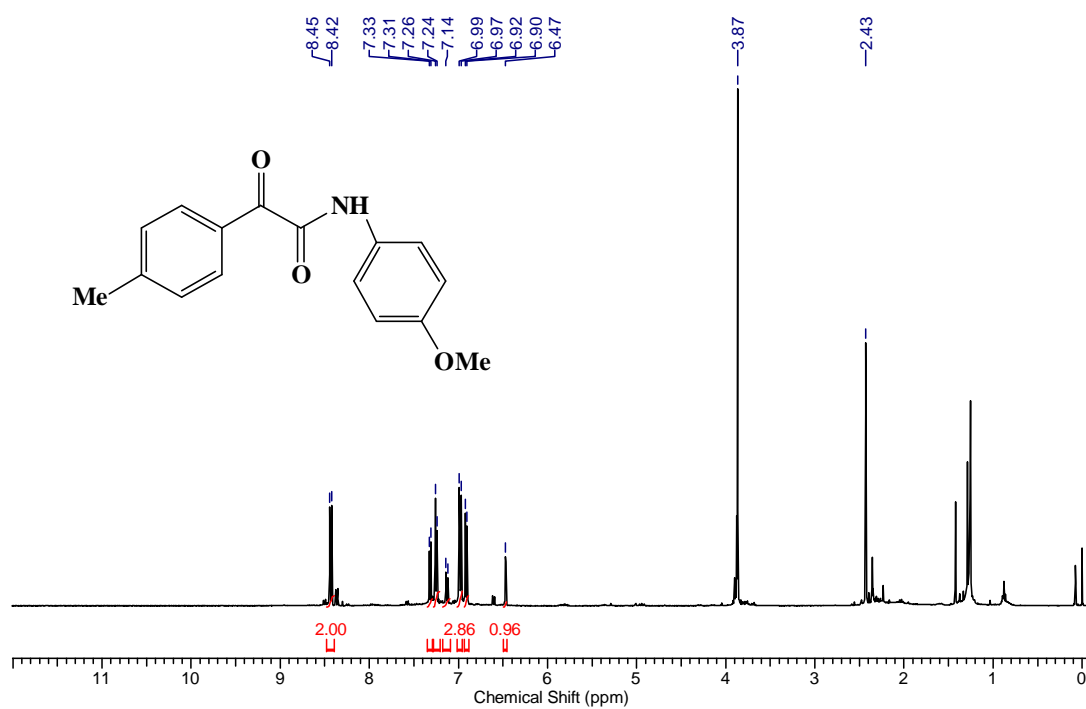
¹H NMR of compound 3a (CDCl₃, 400 MHz)
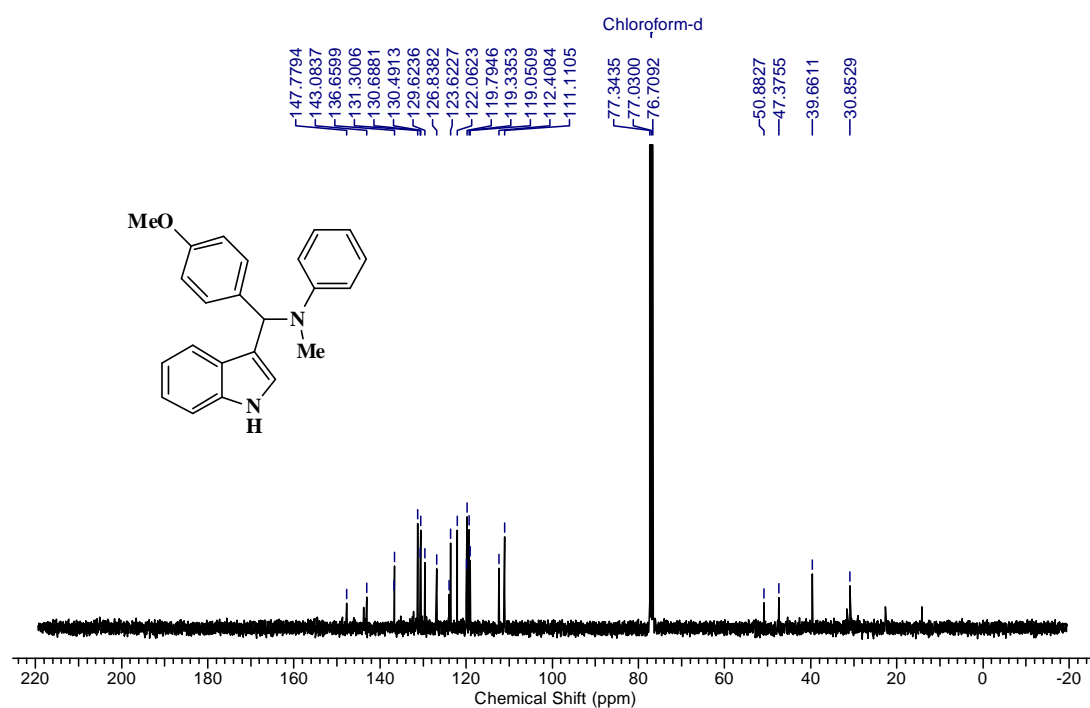
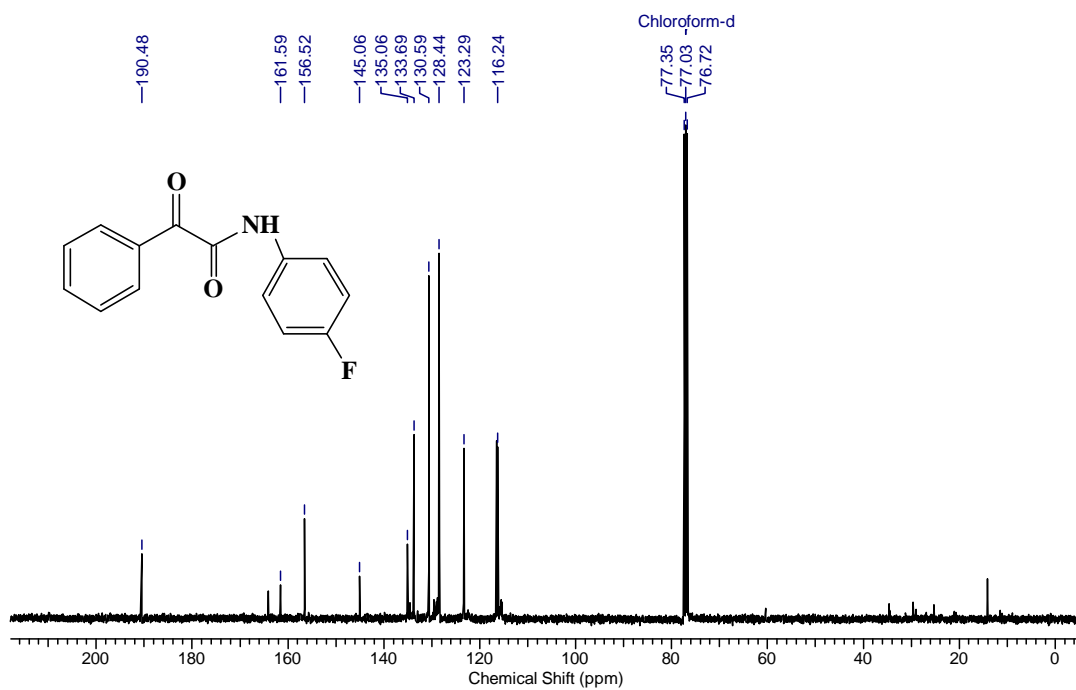*¹³C NMR of compound 3a (CDCl₃, 100 MHz)*
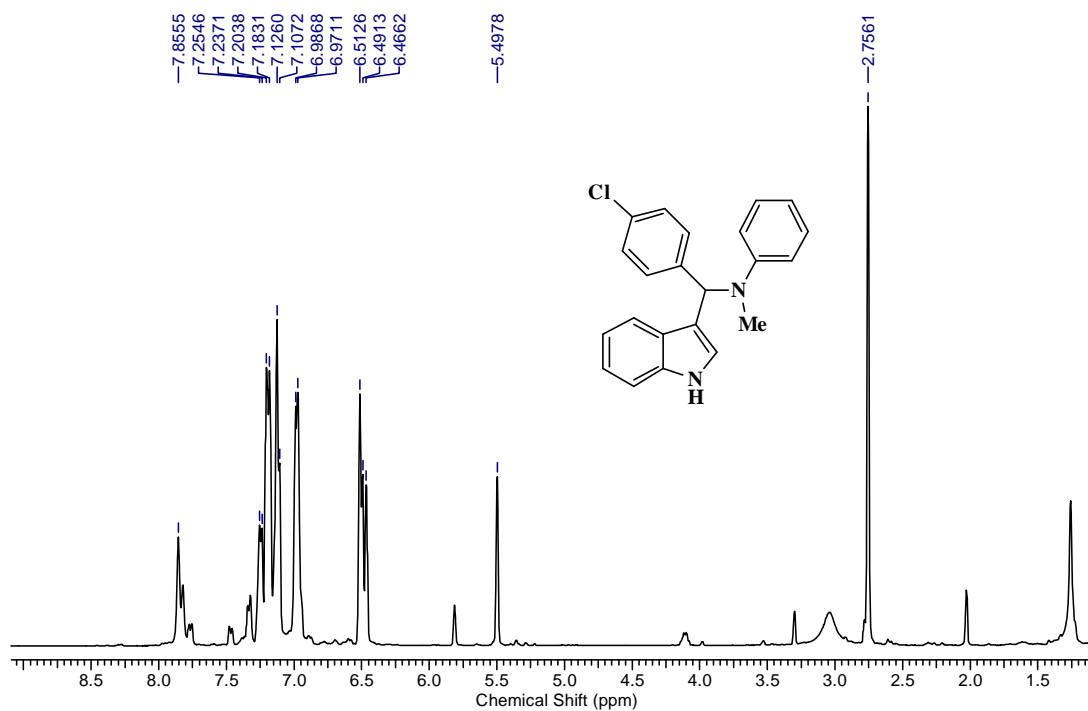
¹H NMR of compound 6a (CDCl₃, 400 MHz)
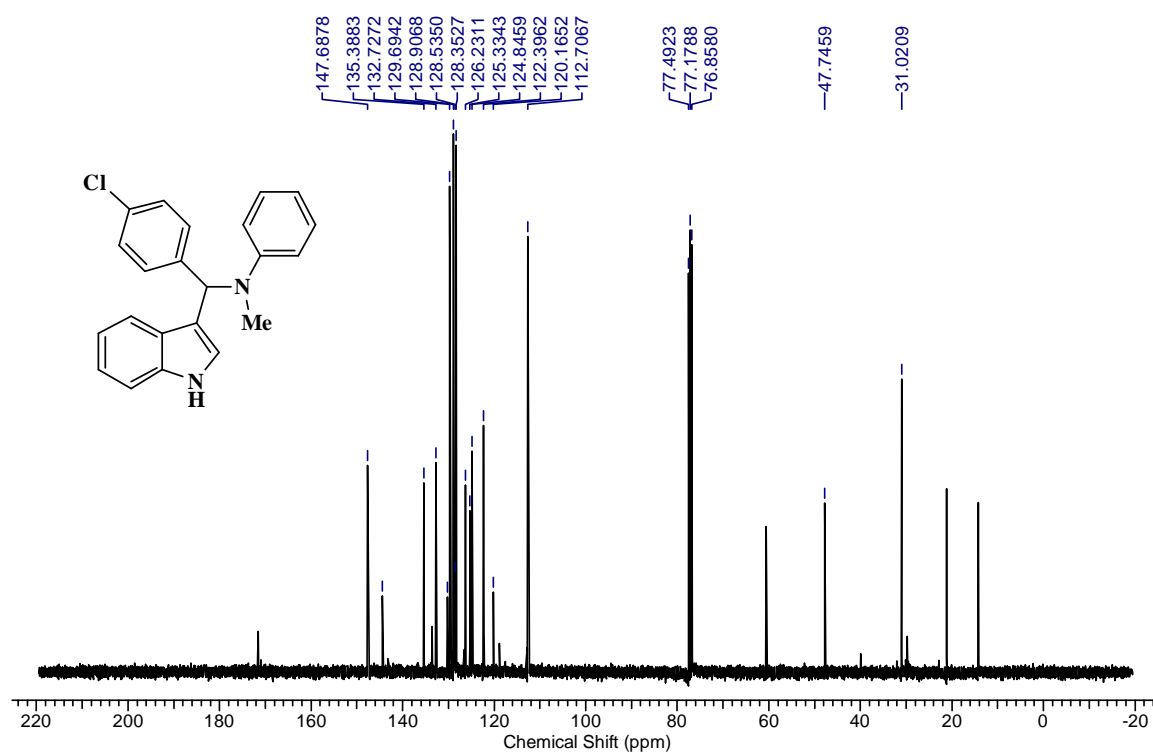
¹³C NMR of compound 6a (CDCl₃, 100 MHz)
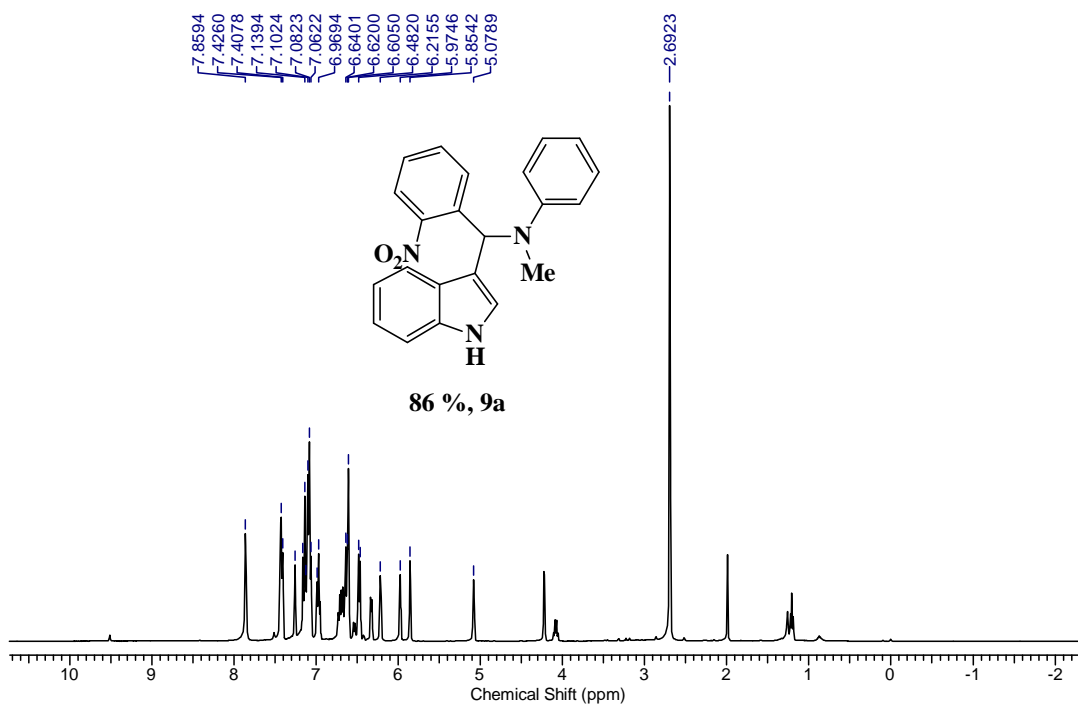
¹H NMR of compound 9a (CDCl₃, 400 MHz)
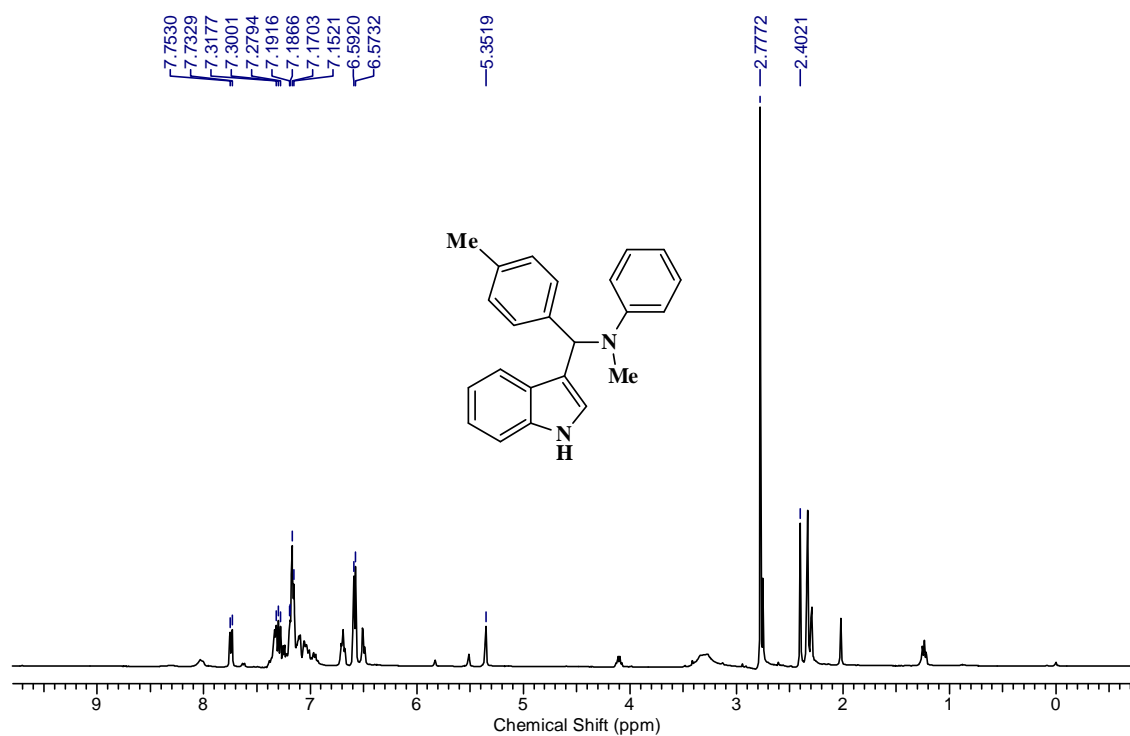
¹H NMR of compound 2a (CDCl₃, 400 MHz)

Appendix *B*

Chapter 3

Characterization NMR Data quinoxaline derivatives (Table 3.3)
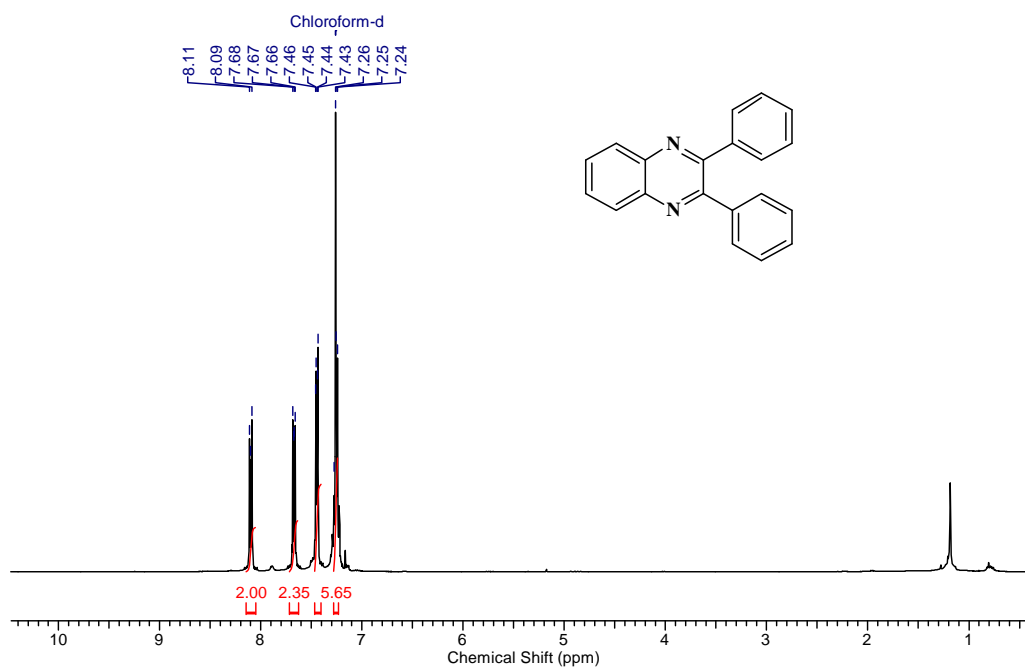
1H NMR of compound En-1 (CDCl3, 400 MHz)
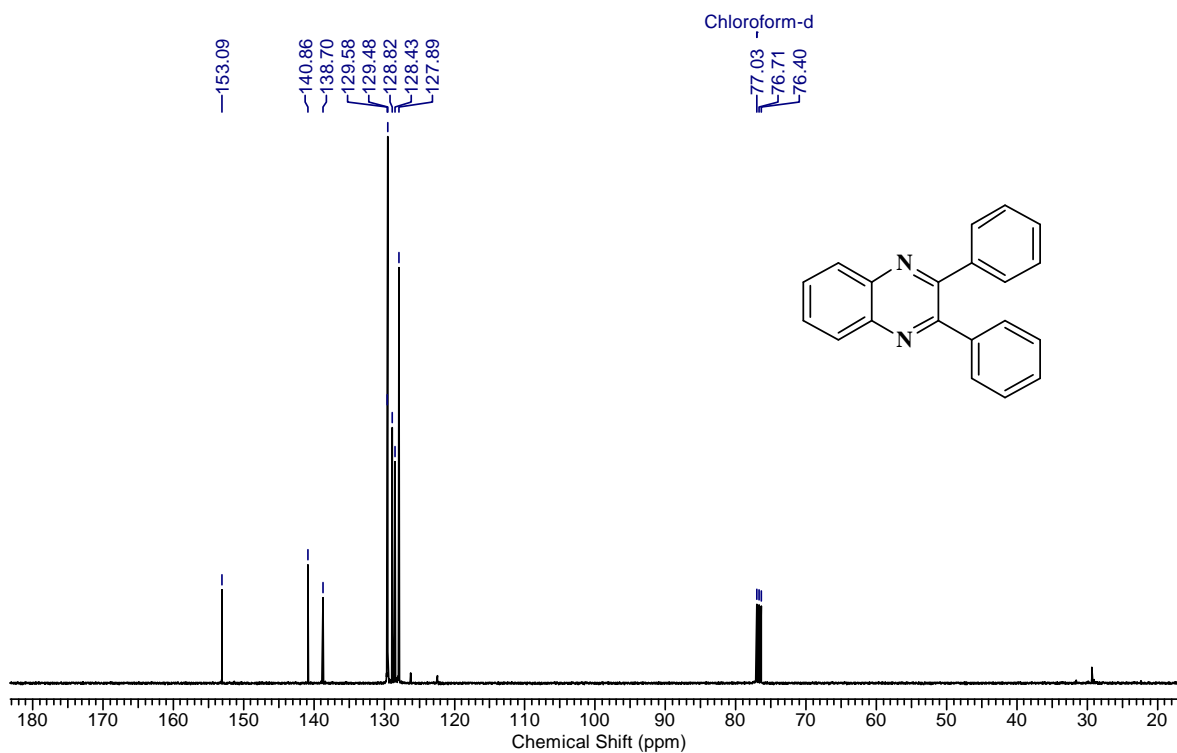
13C NMR of compound En-1 (CDCl3, 100 MHz)
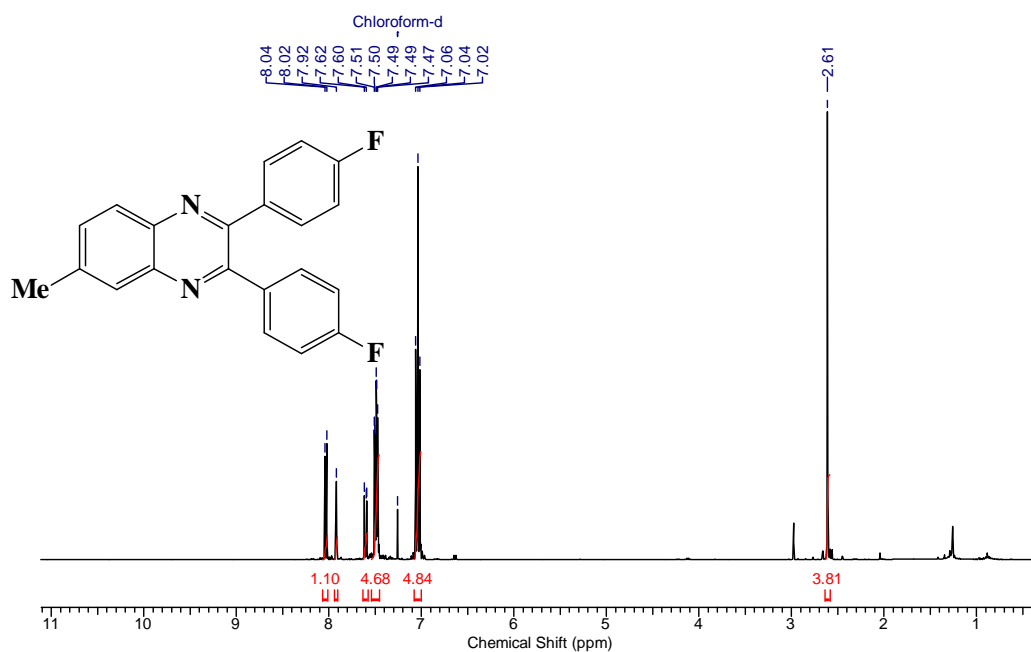
^1H NMR of compound En-4 (CDCl$_3$, 400 MHz)
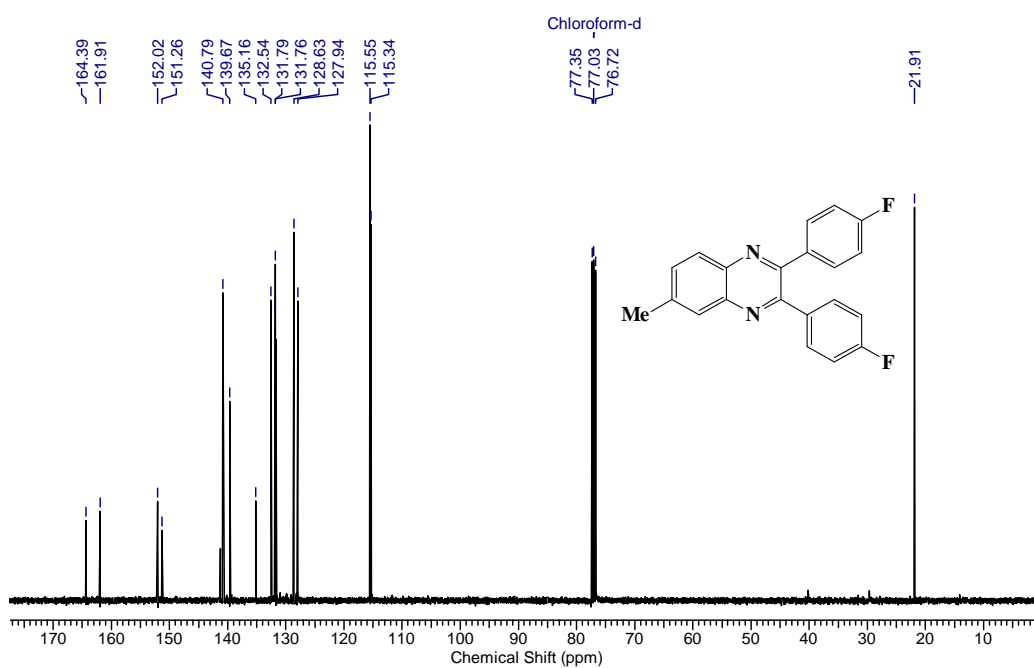
^{13}C NMR of compound En-4 (CDCl$_3$, 100 MHz)
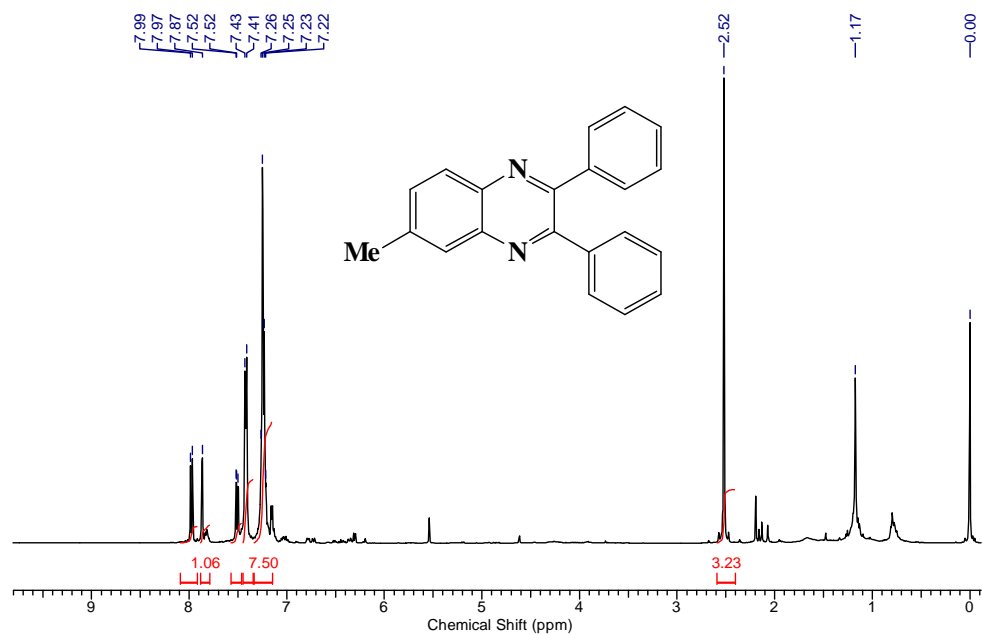
1H NMR of compound En-2 (CDCl₃, 400 MHz)
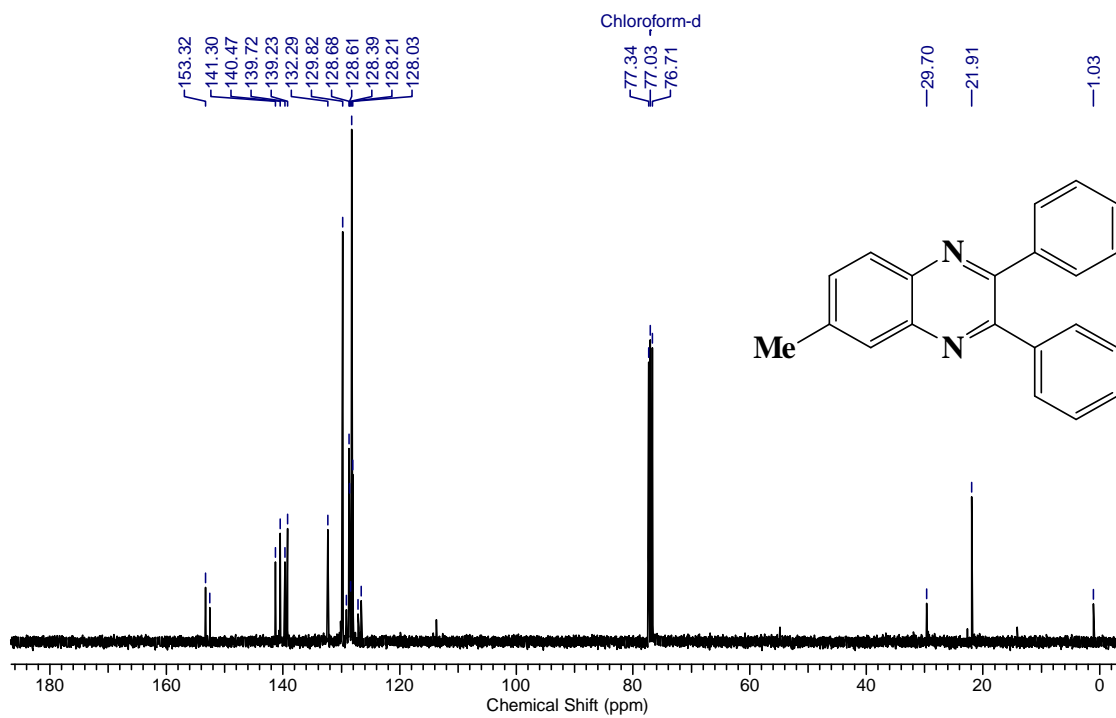
13C NMR of compound En-2 (CDCl₃, 100 MHz)
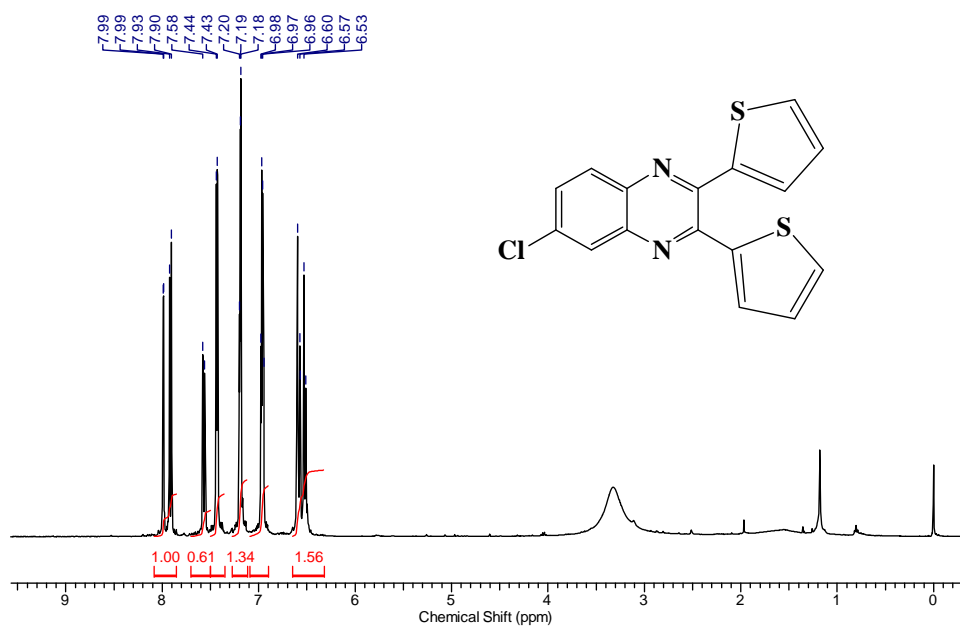
¹H NMR of compound En-9 (CDCl₃, 400 MHz)
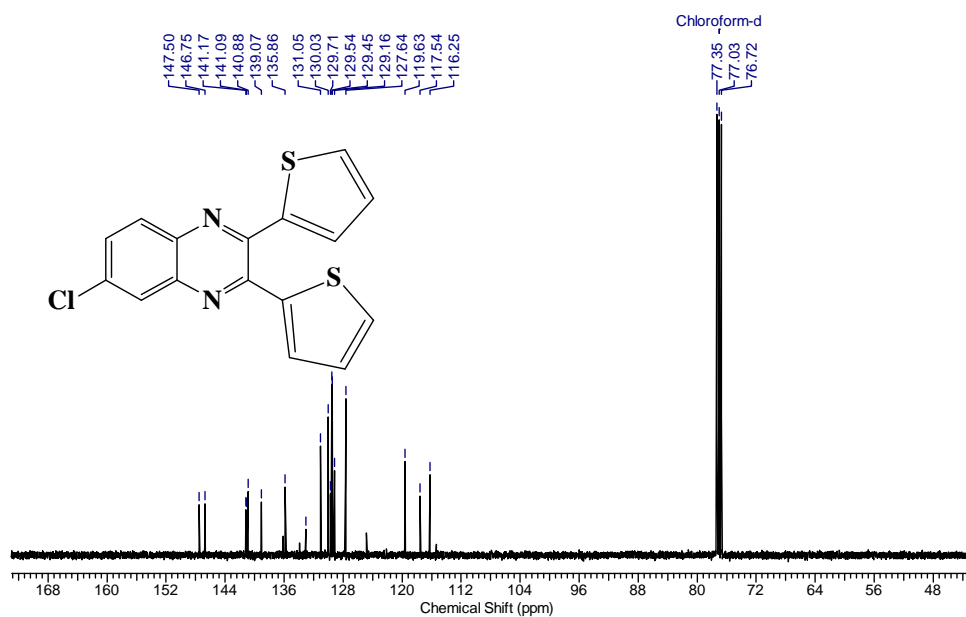
¹³C NMR of compound En-9 (CDCl₃, 100 MHz)
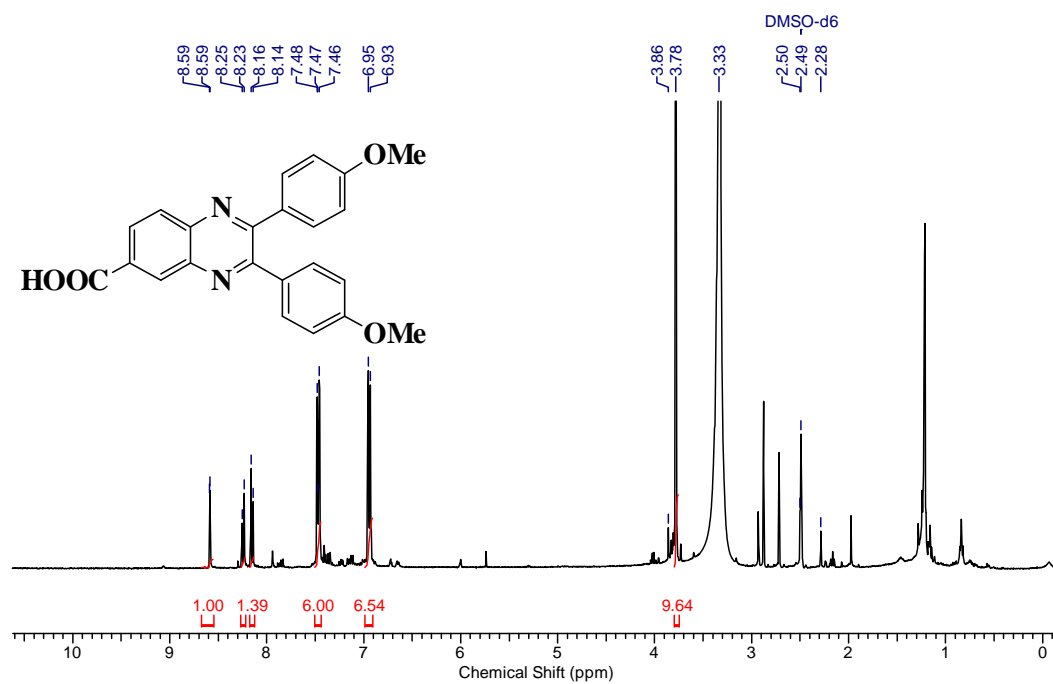
¹H NMR of compound En-8 (CDCl₃, 400 MHz)
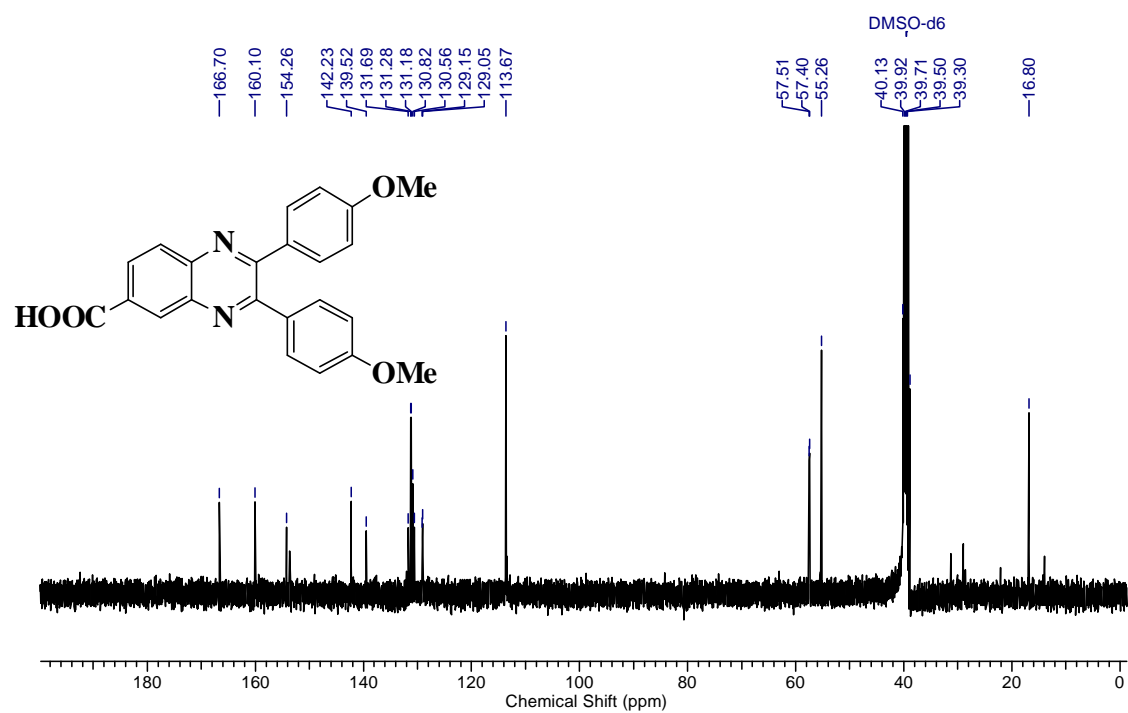
¹³C NMR of compound En-8 (CDCl₃, 100 MHz)
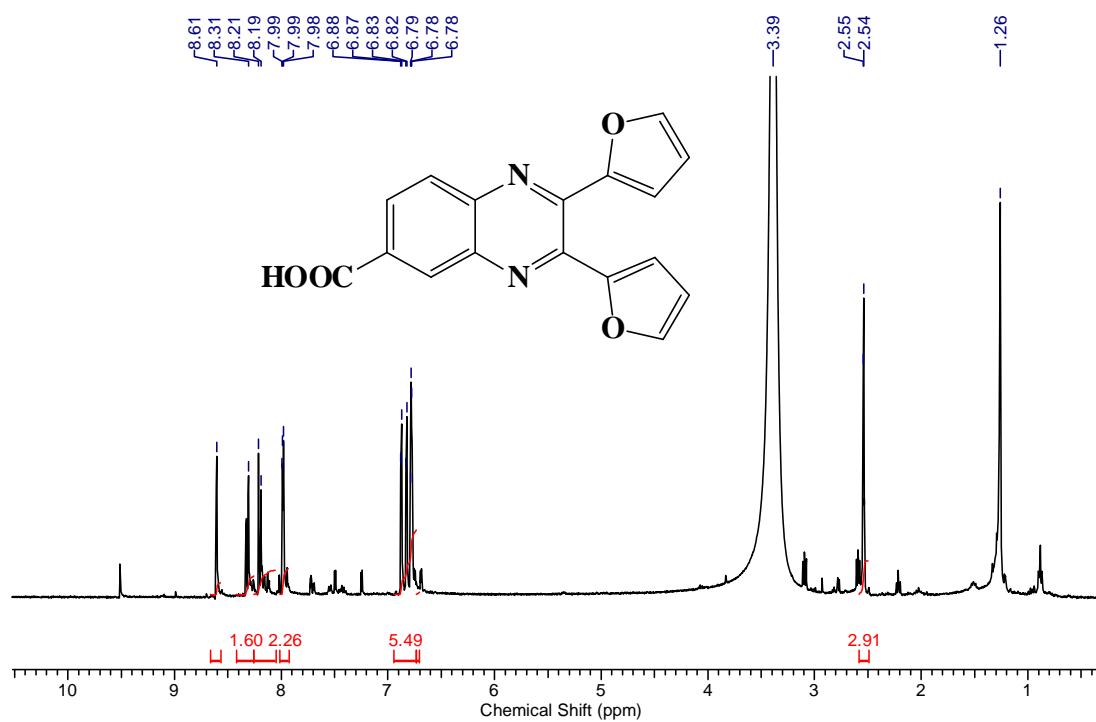
^{1}H NMR of compound En-13 (CDCl$_3$, 400 MHz)
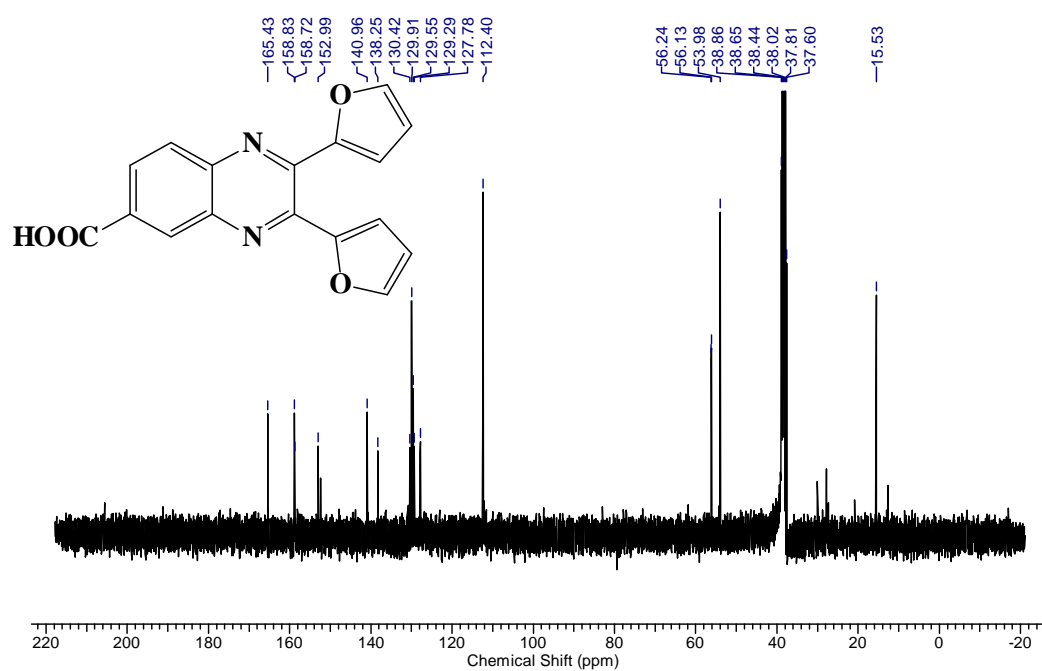
^{13}C NMR of compound En-13 (CDCl$_3$, 100 MHz)

¹H NMR of compound En-11 (CDCl₃, ^1H *NMR of compound En-11 (CDCl_3,* **400 MHz)**
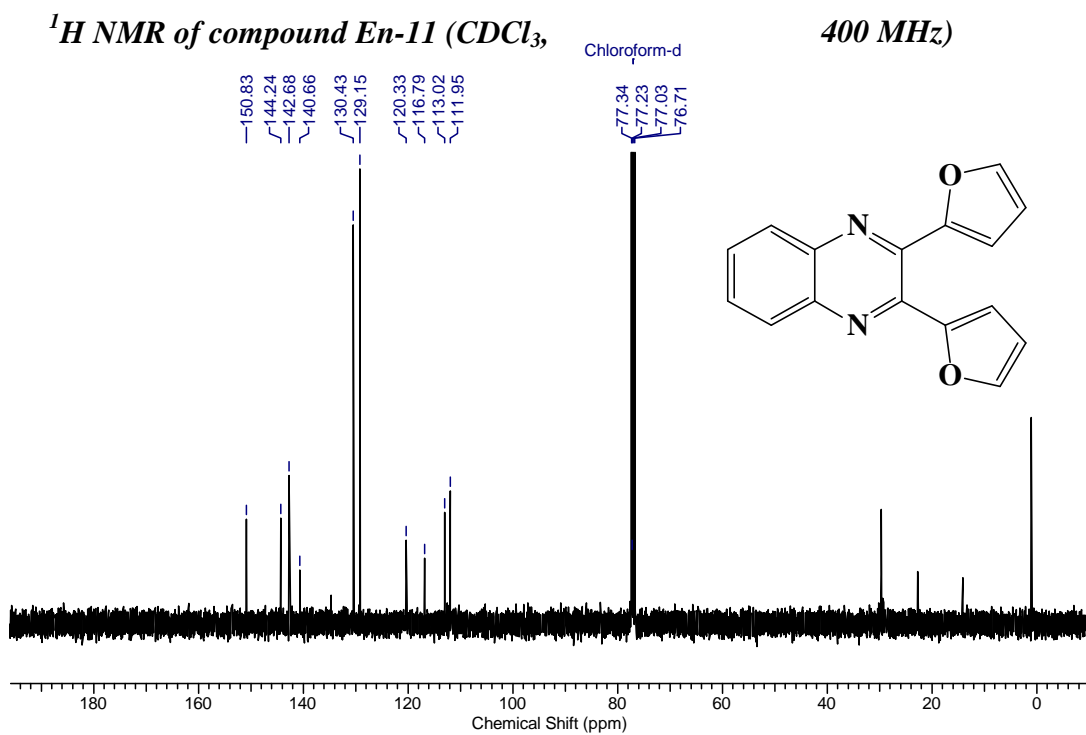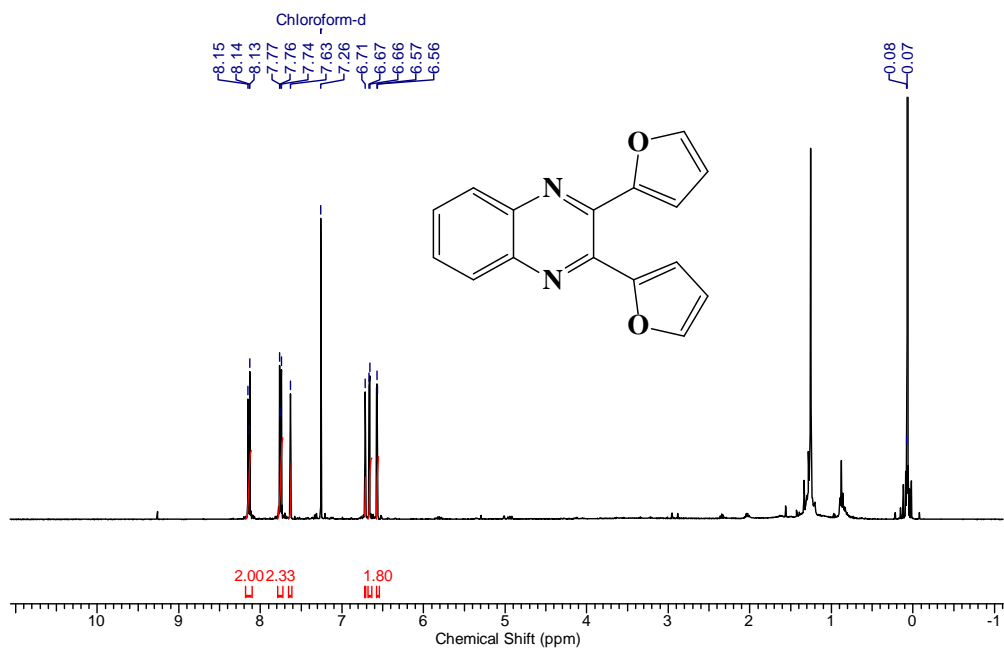
¹³C NMR of compound En-11 (CDCl₃, 100 MHz)
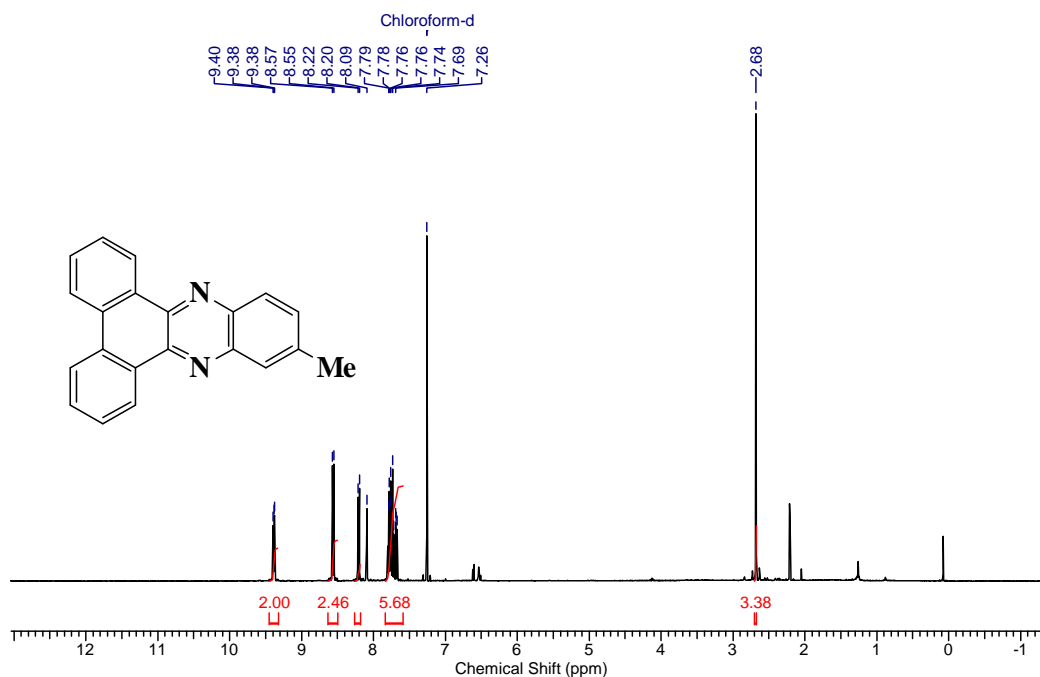
¹H NMR of compound En-17(CDCl₃, 400 MHz)
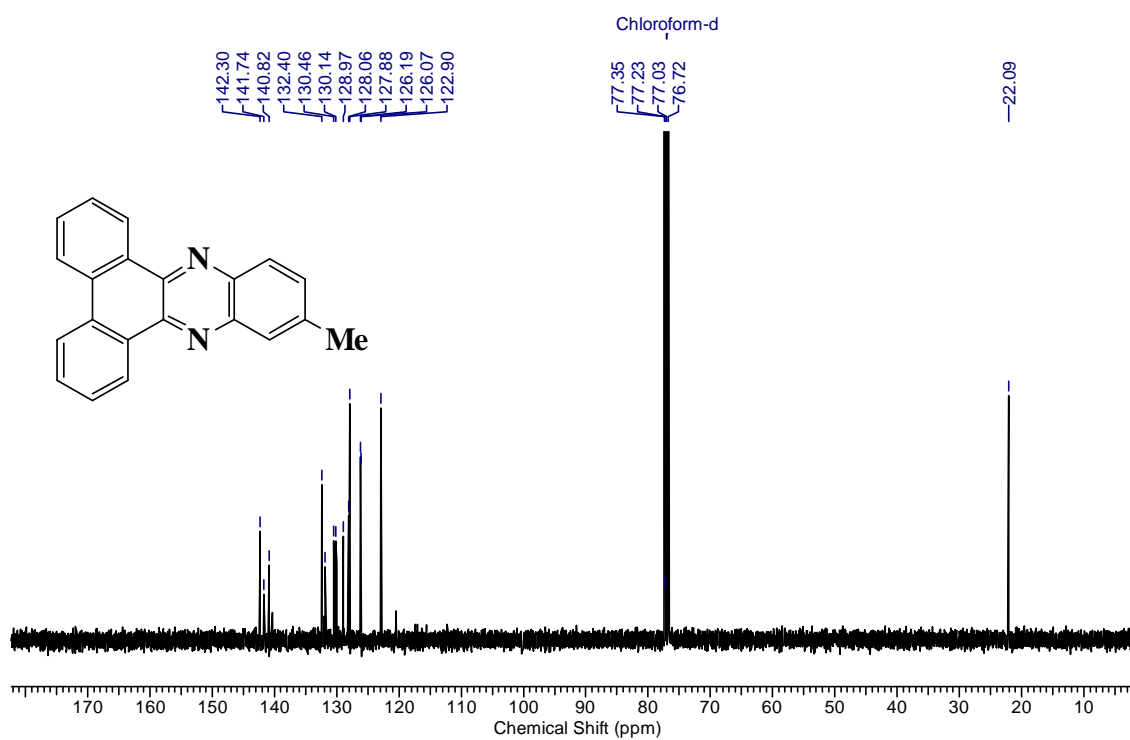
¹³C NMR of compound En-17 (CDCl₃, 100 MHz)
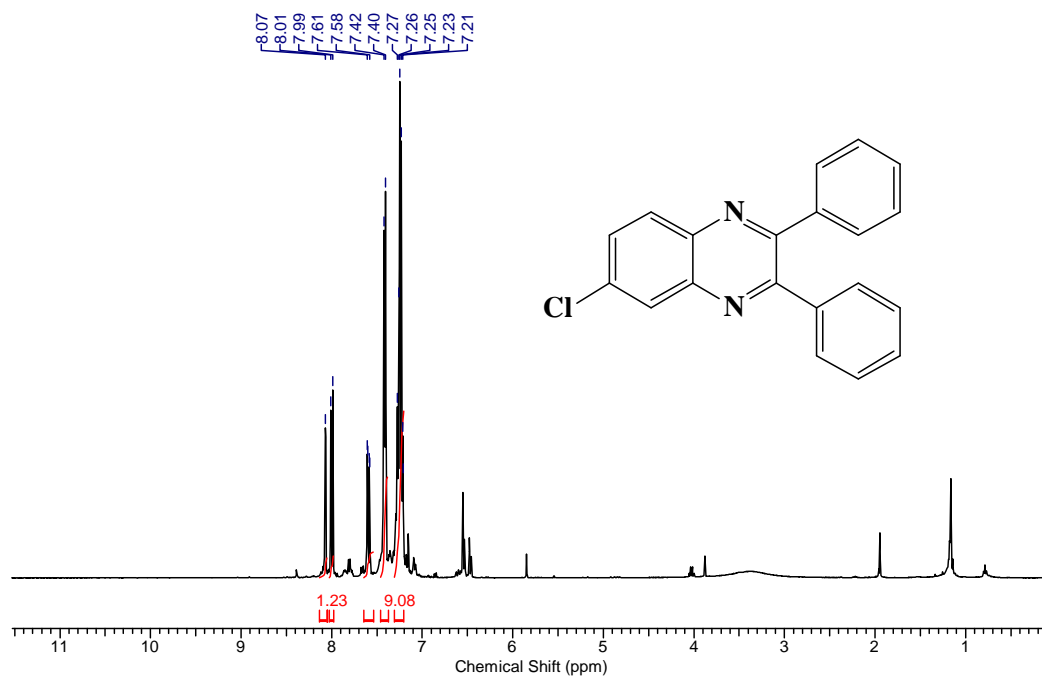
¹H NMR of compound En-3 (CDCl₃, 400 MHz)
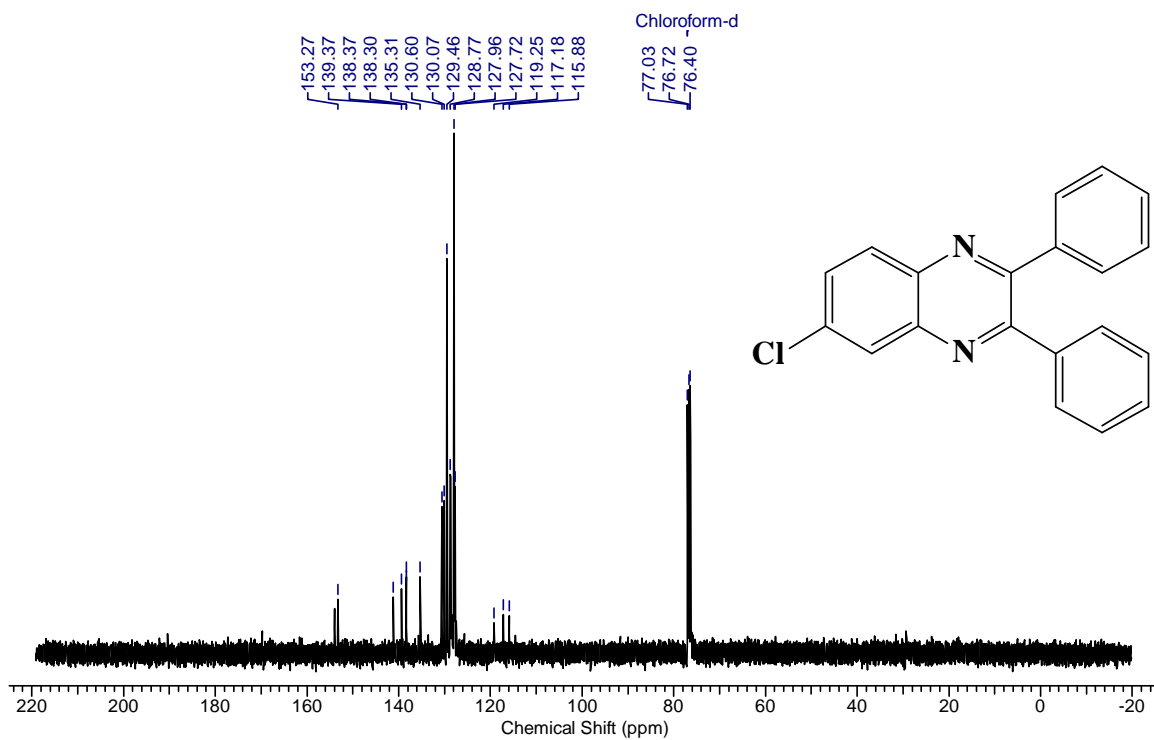
¹³C NMR of compound En-3 (CDCl₃, 100 MHz)
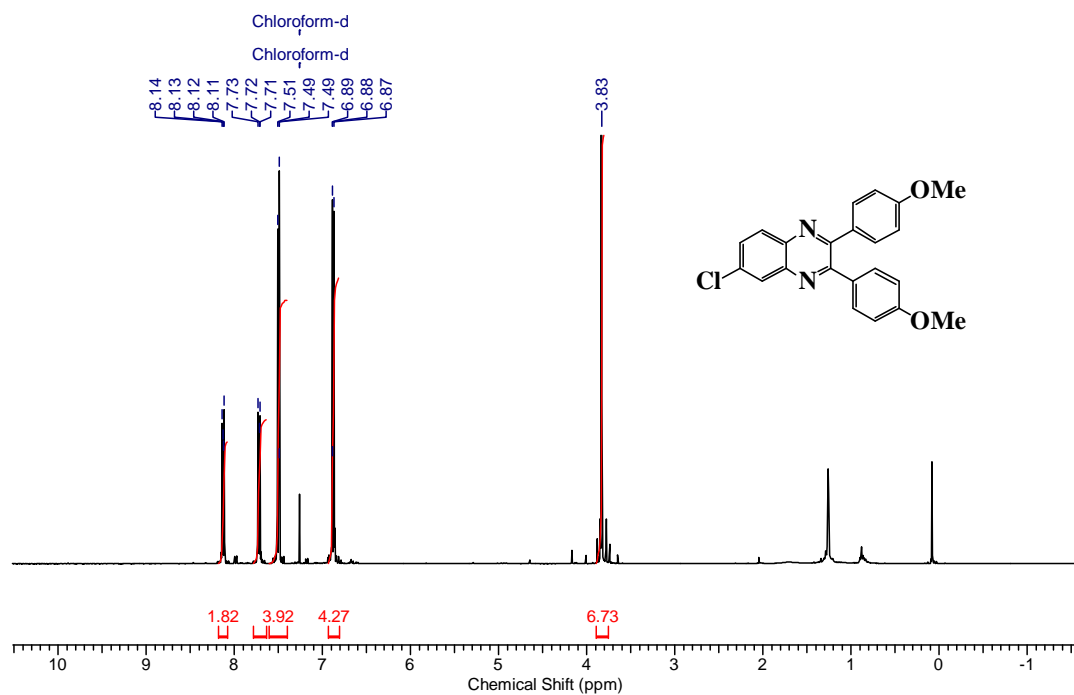
¹H NMR of compound En-7 (CDCl₃, 400 MHz)
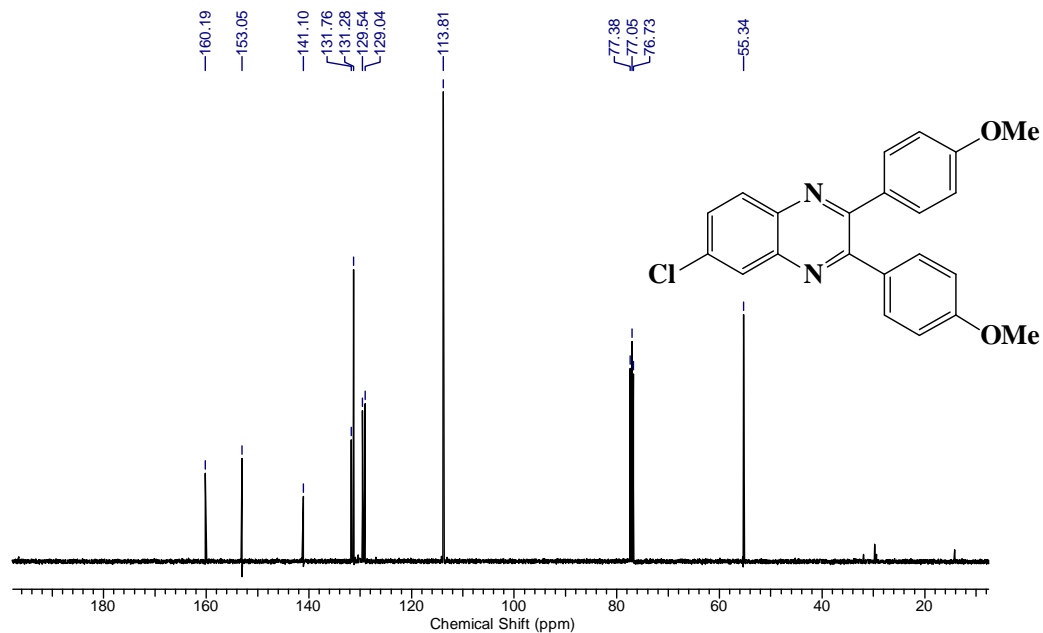
¹³C NMR of compound En-7 (CDCl₃, 100 MHz)

Appendix C

Chapter 4

Characterization data of α-keto esters, α-keto phosphonates and β-keto esters

Table 4.2 and Table 4.3
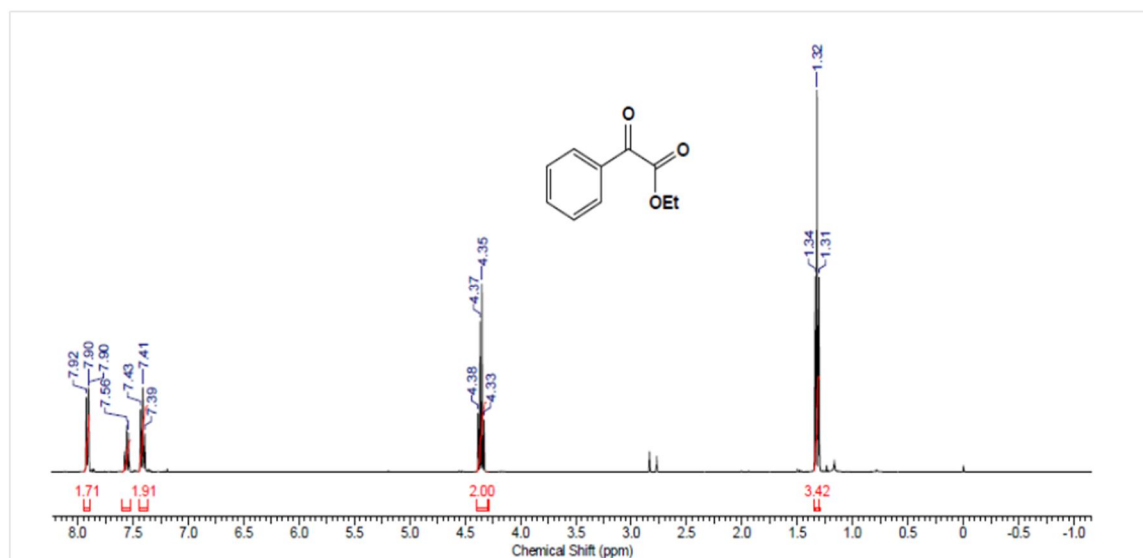
¹H NMR of compound 2a (CDCl₃, 400 MHz)
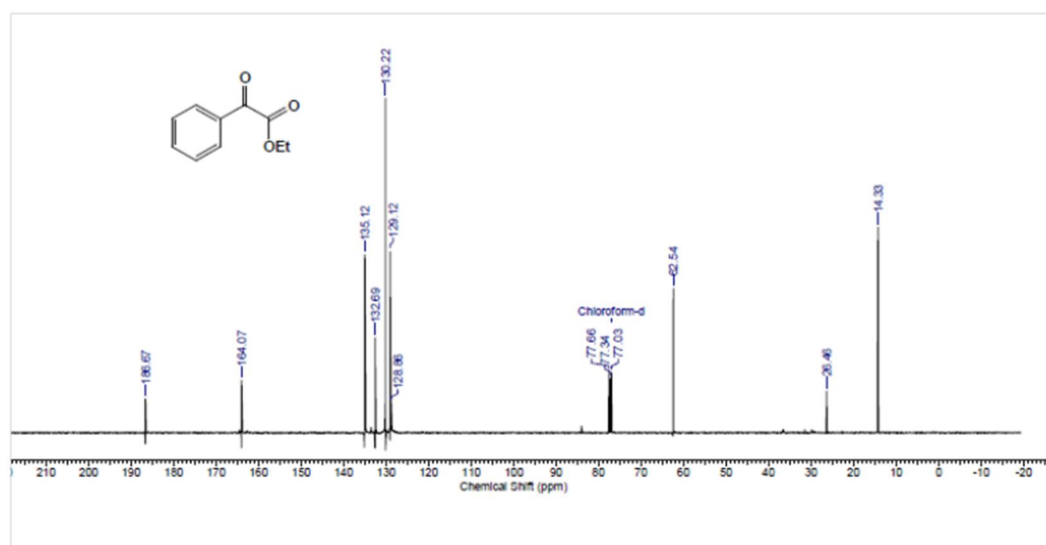
¹³C NMR of compound 2a (CDCl₃, 100 MHz)
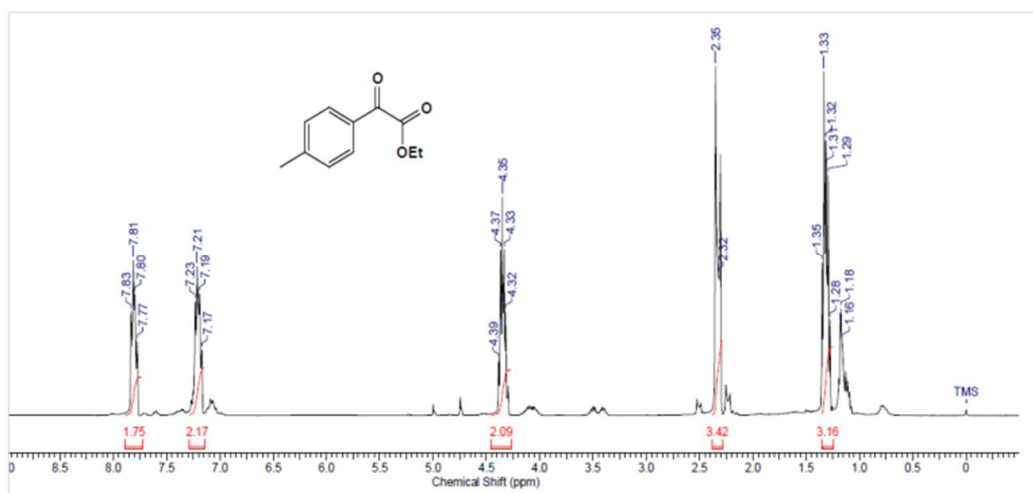
1H NMR of compound 2b (CDCl3, 400 MHz)
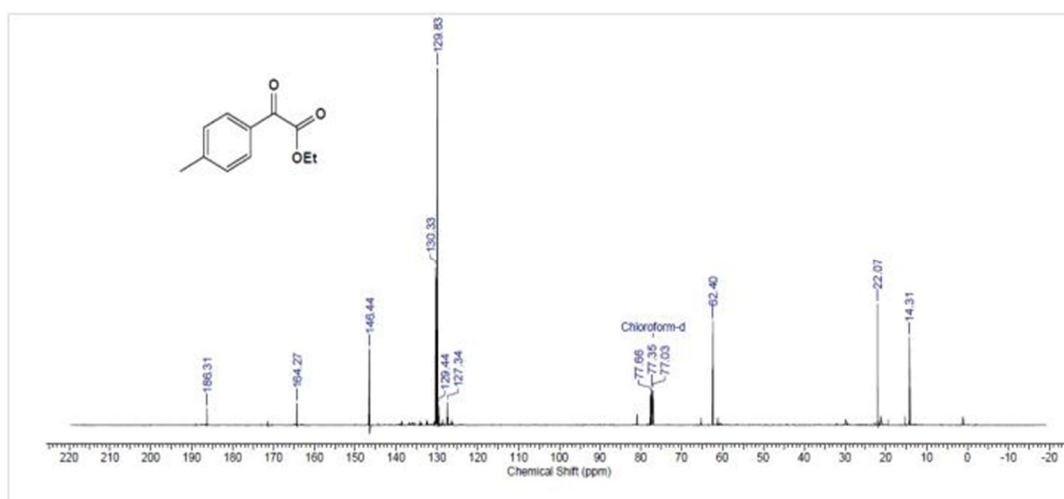
13C NMR of compound 2b (CDCl3, 100 MHz)
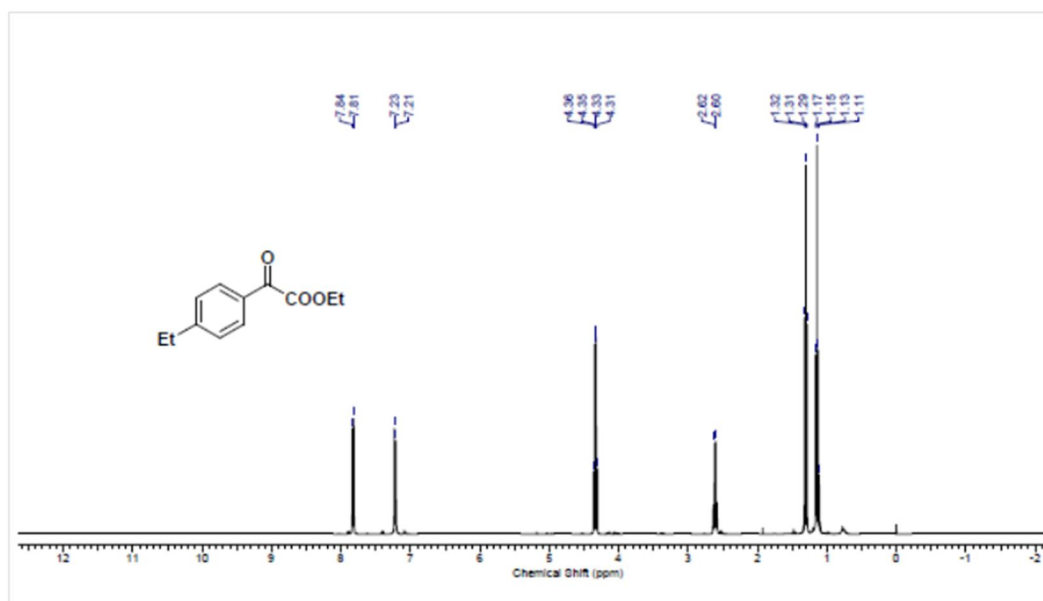
¹H NMR of compound 3c (CDCl₃, 400 MHz)
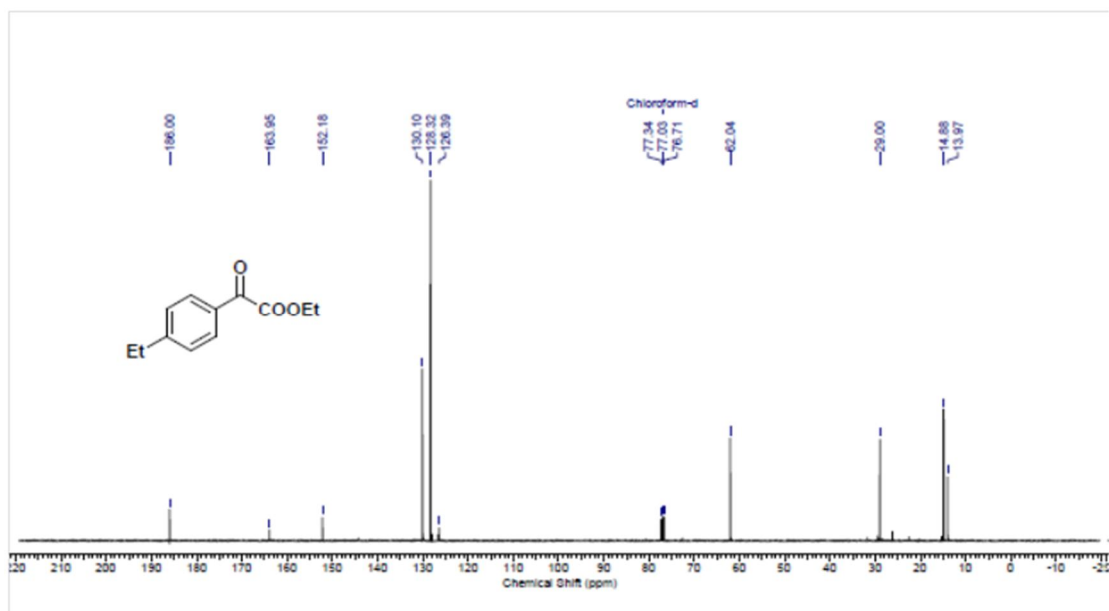
¹³C NMR of compound 2c (CDCl₃, 100 MHz)
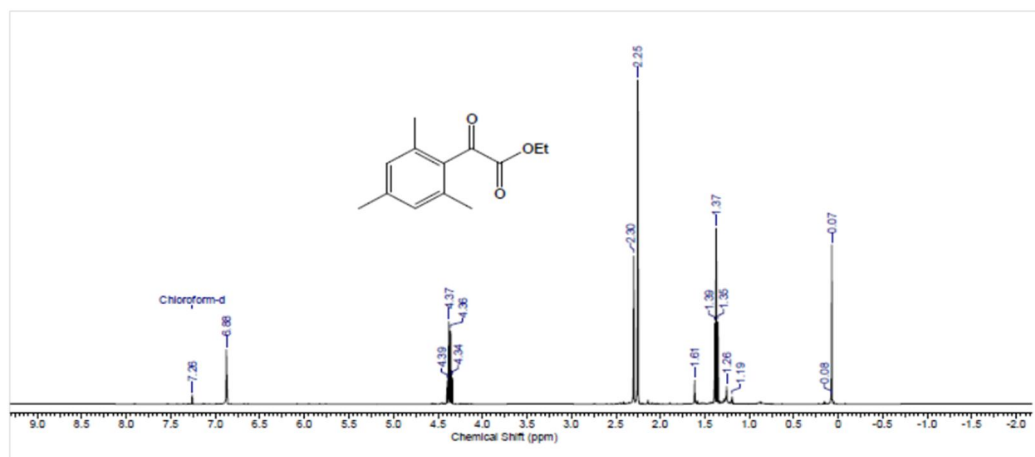
¹H NMR of compound 2g (CDCl₃, 400 MHz)
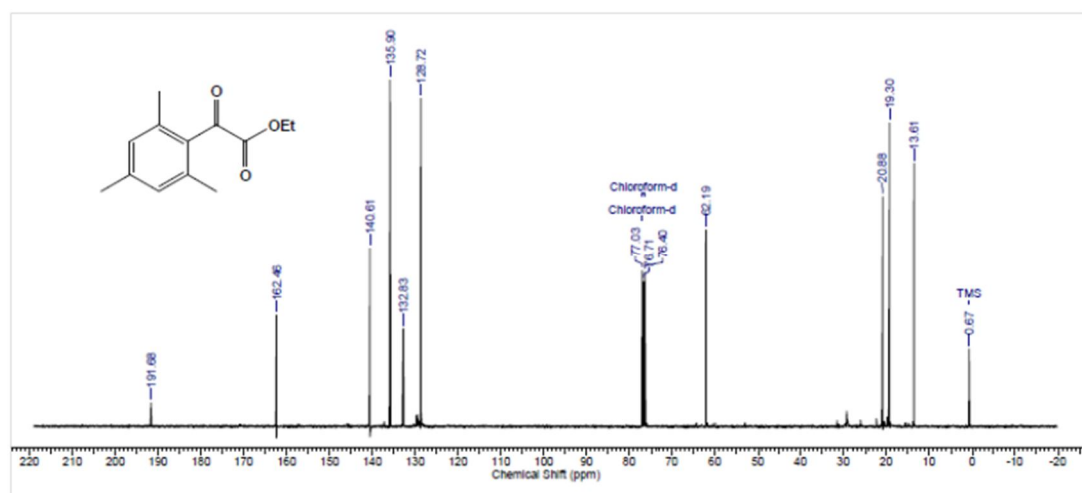
¹³C NMR of compound 2g (CDCl₃, 100 MHz)
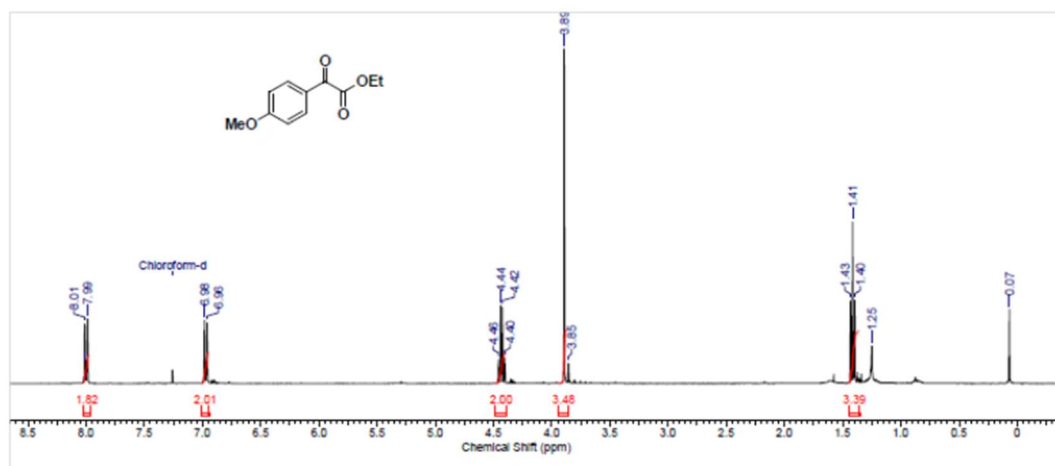
¹H NMR of compound 2d (CDCl₃, 400 MHz)
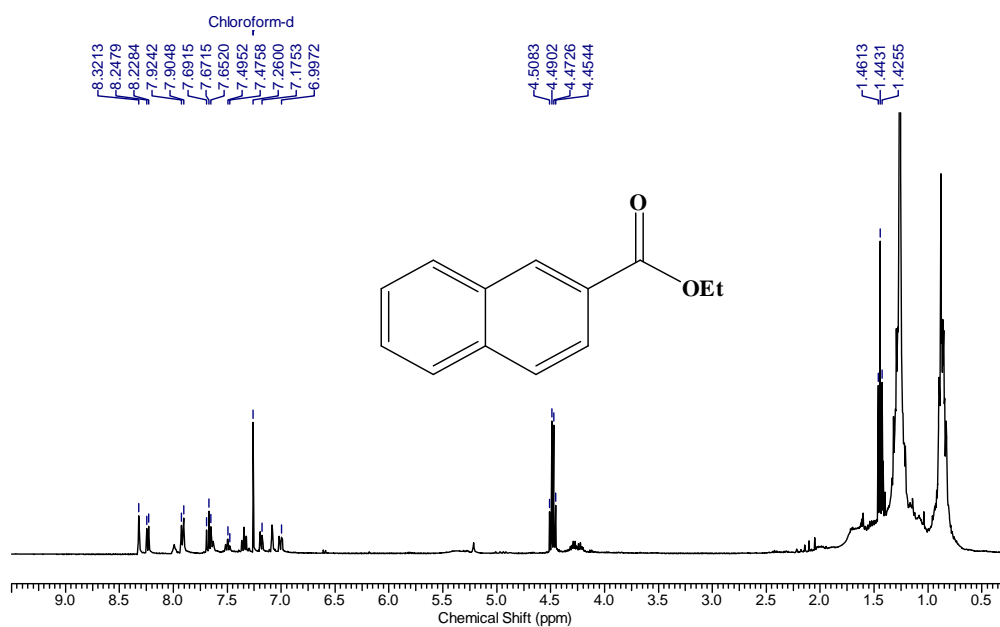
¹H NMR of compound 2d (CDCl₃, 400 MHz)
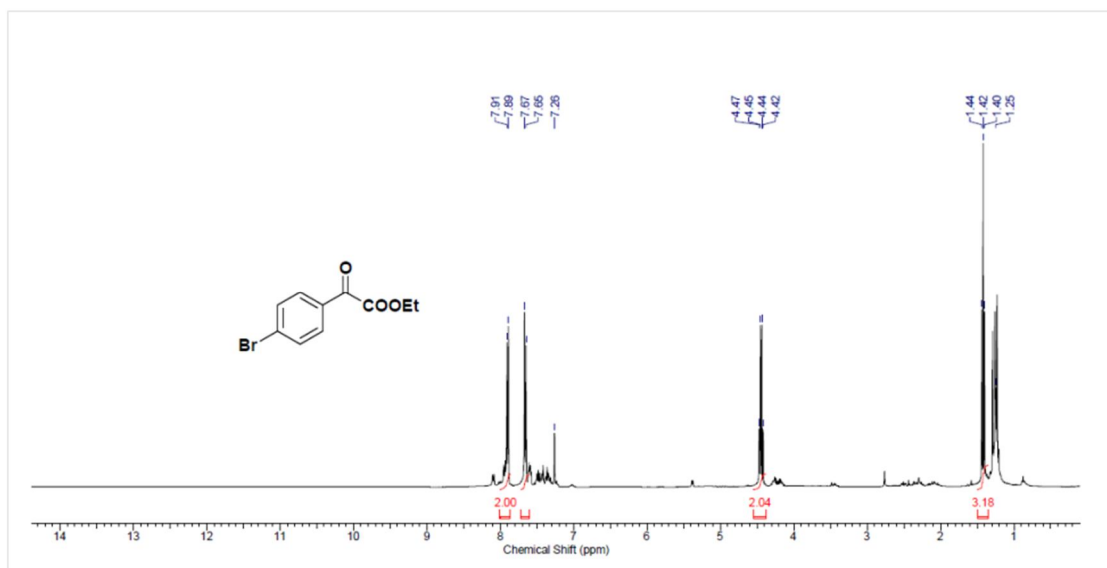
¹H NMR of compound 2e (CDCl₃, 400 MHz)
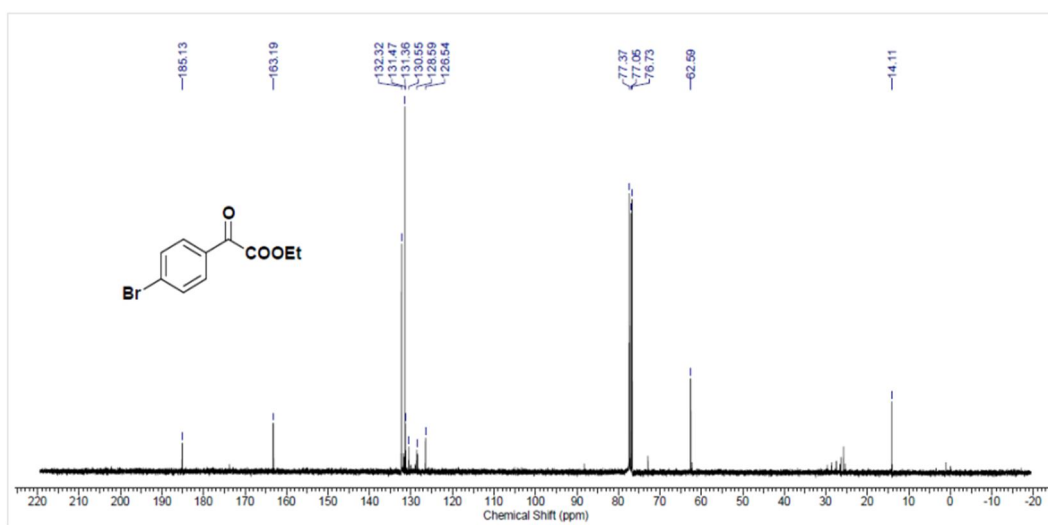
¹³C NMR of compound 2e (CDCl₃, 100 MHz)
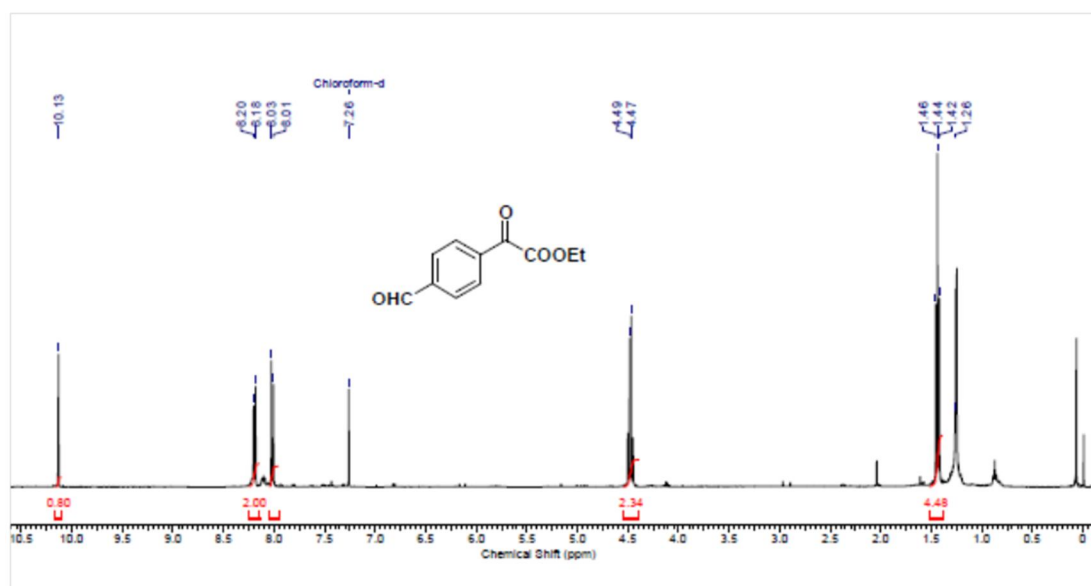
¹H NMR of compound 2i (CDCl₃, 400 MHz)
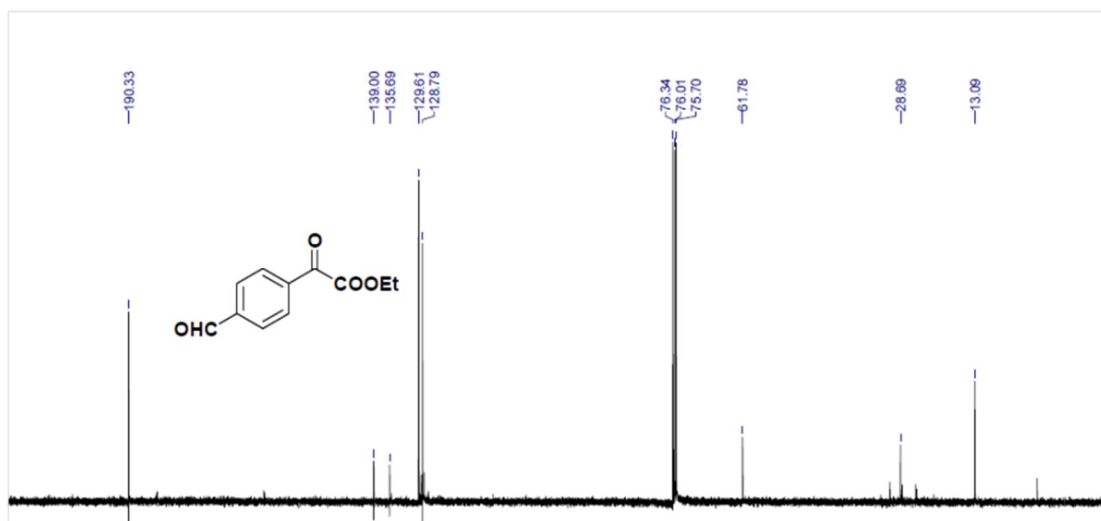
¹³C NMR of compound 2i (CDCl₃, 100 MHz)
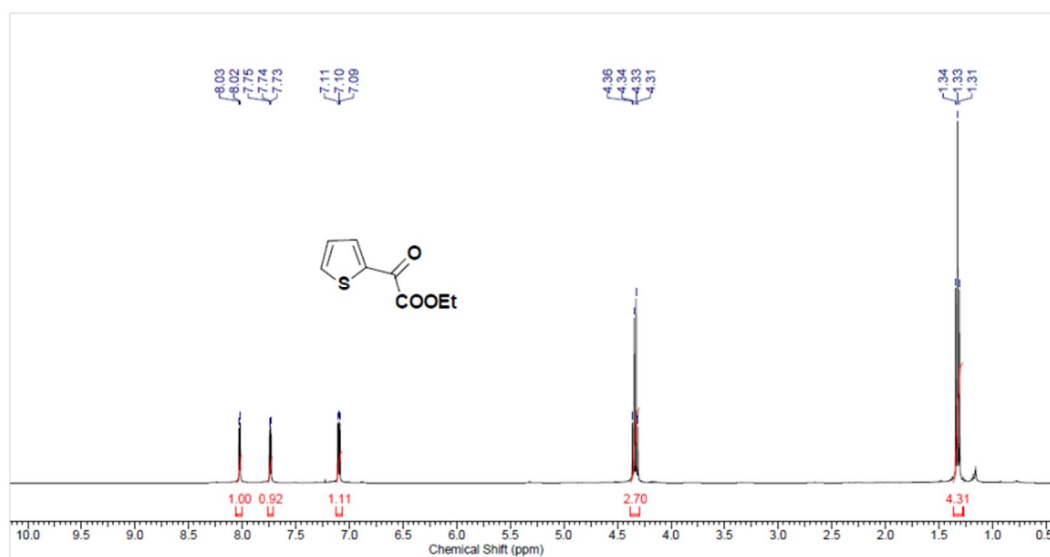
1H NMR of compound 2k (CDCl3, 400 MHz)
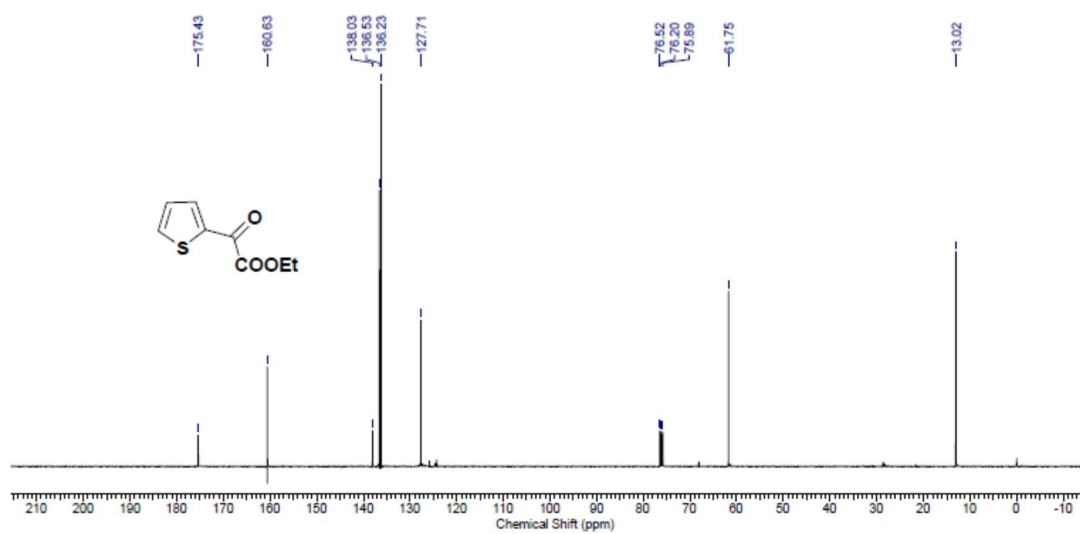
13C NMR of compound 2k (CDCl3, 100 MHz)
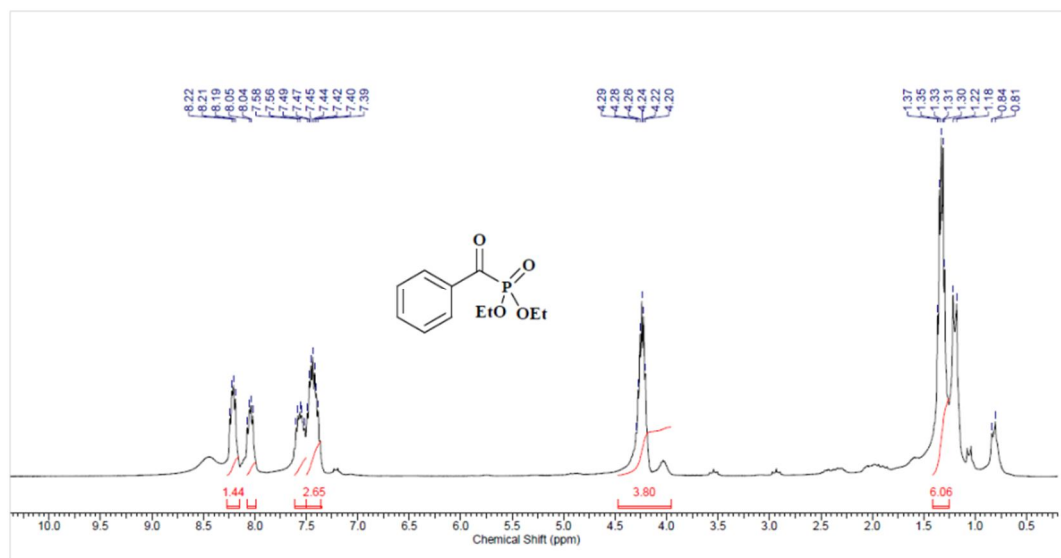
¹H NMR of compound 4a (CDCl₃, 400 MHz)
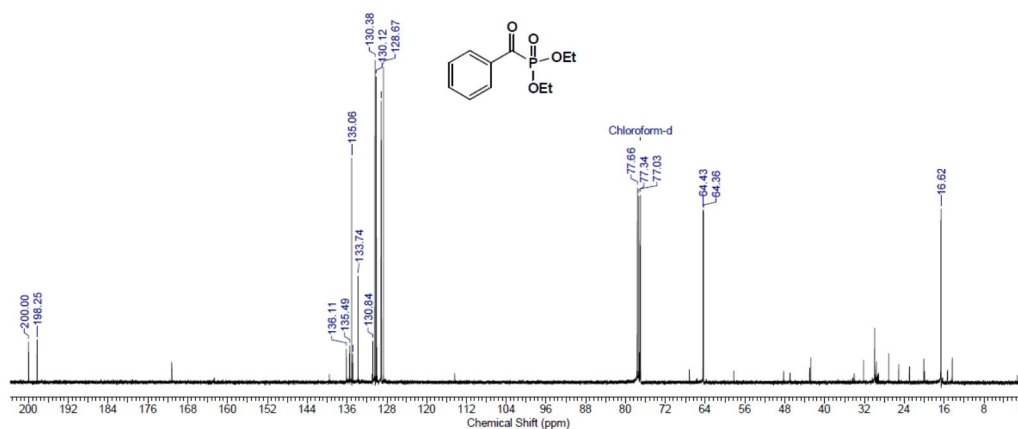
¹³C NMR of compound 4a (CDCl₃, 100 MHz)
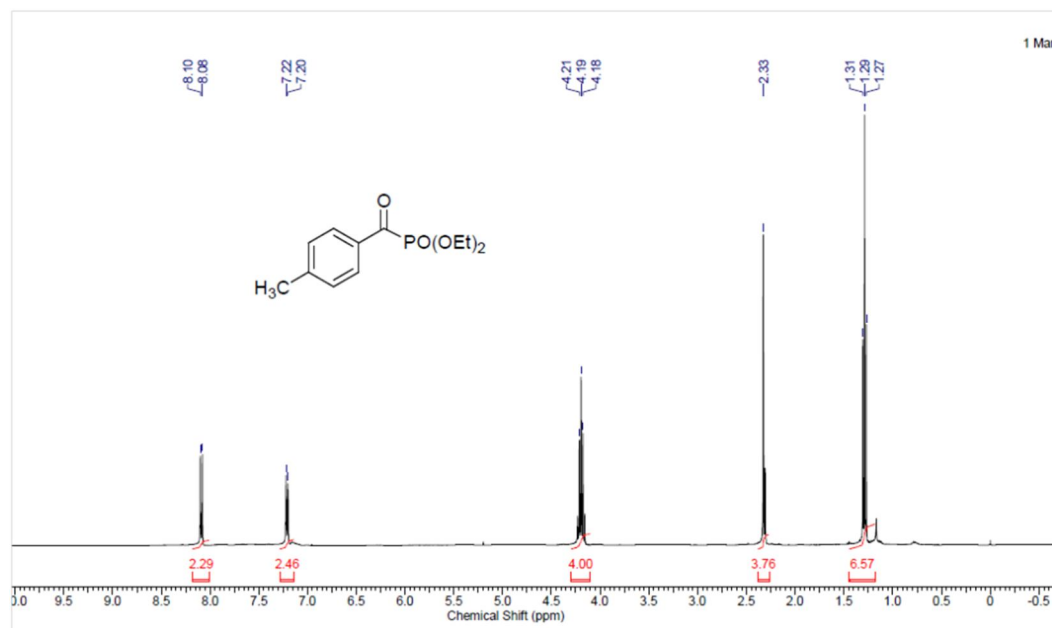
¹H NMR of compound 4b (CDCl₃, 400 MHz)
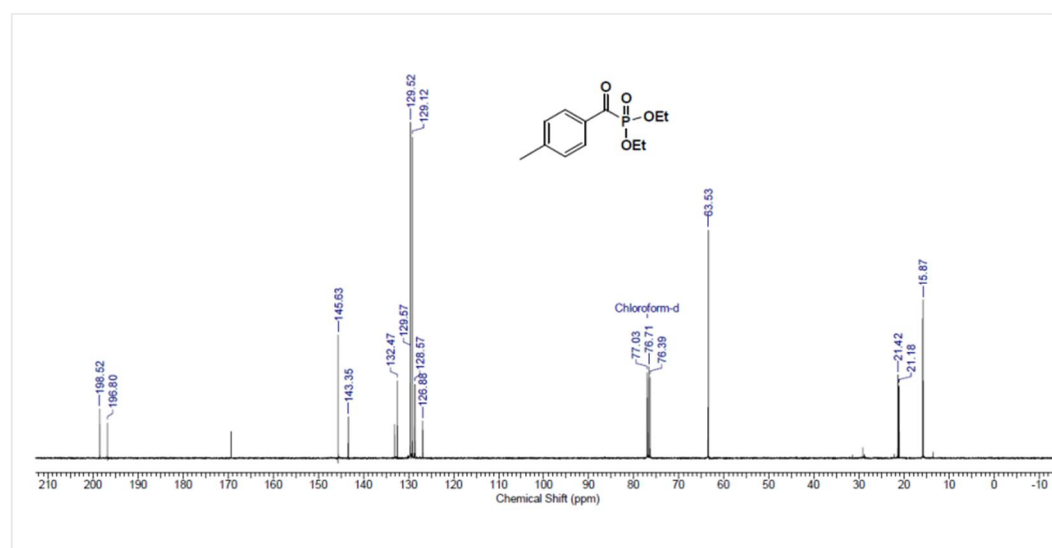
¹³C NMR of compound 4b (CDCl₃, 100 MHz)
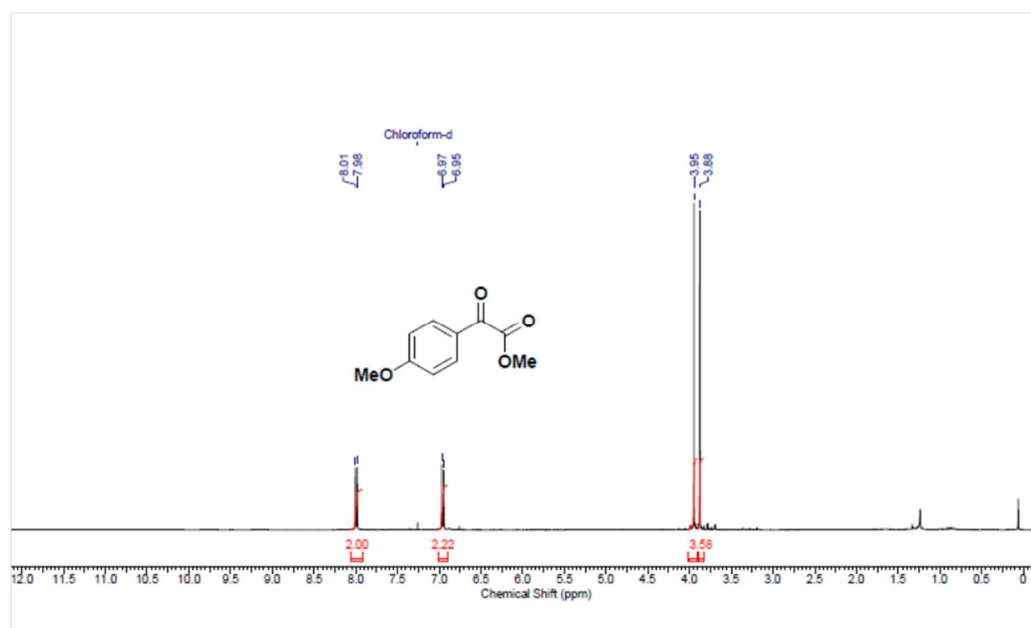
¹H NMR of compound 2q (CDCl₃, 400 MHz)
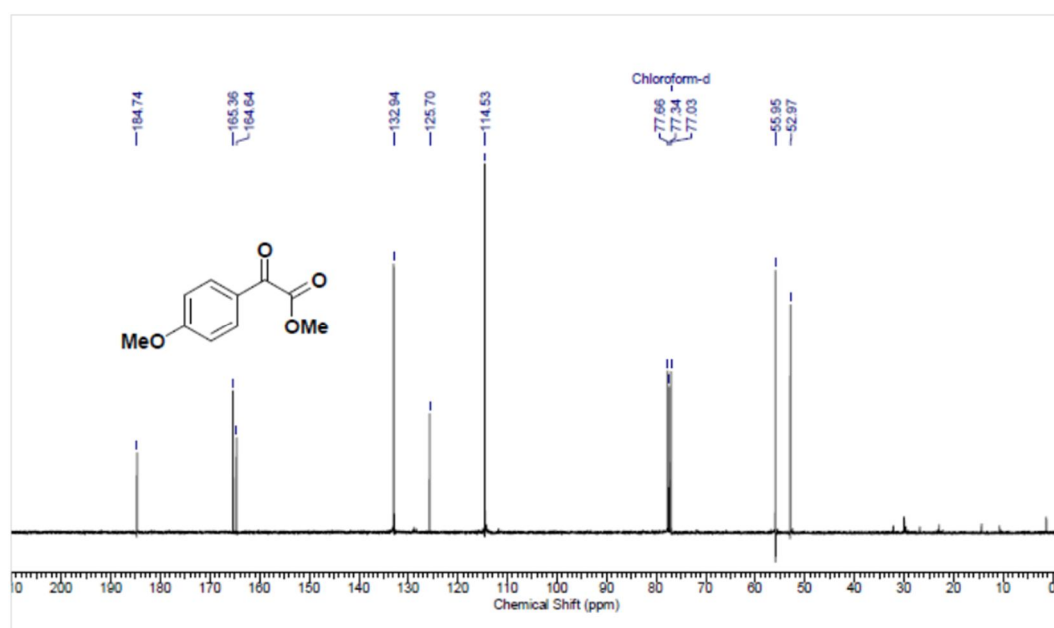
¹³C NMR of compound 2q (CDCl₃, 100 MHz)
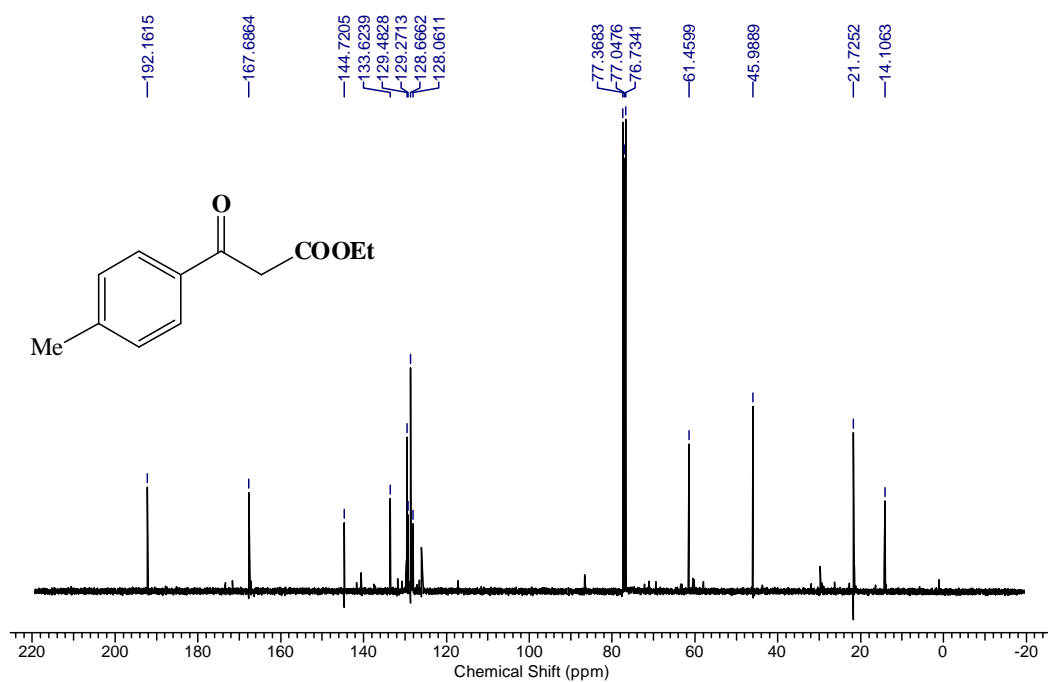
¹H NMR of compound 2m (CDCl₃, 400 MHz)
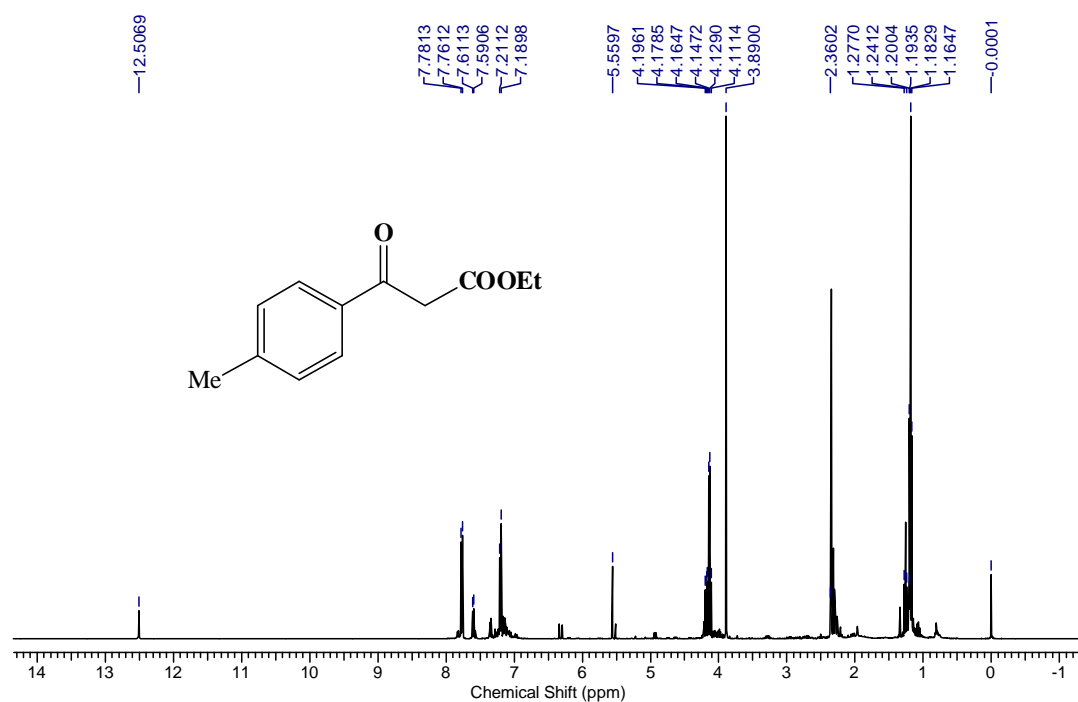
¹³C NMR of compound 2m (CDCl₃, 100 MHz)

Appendix D

Chapter 5

Characterization data of α-keto amide derivatives Table-5.4 and Table 5.5

¹H NMR of compound 3af (CDCl₃, 400 MHz)
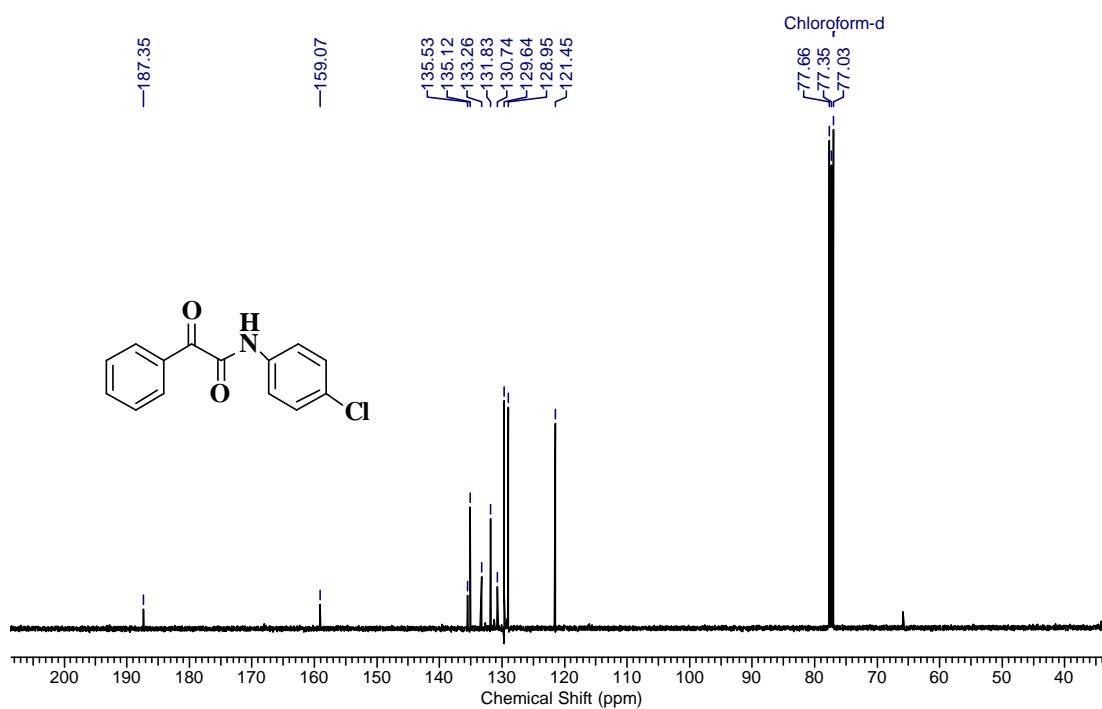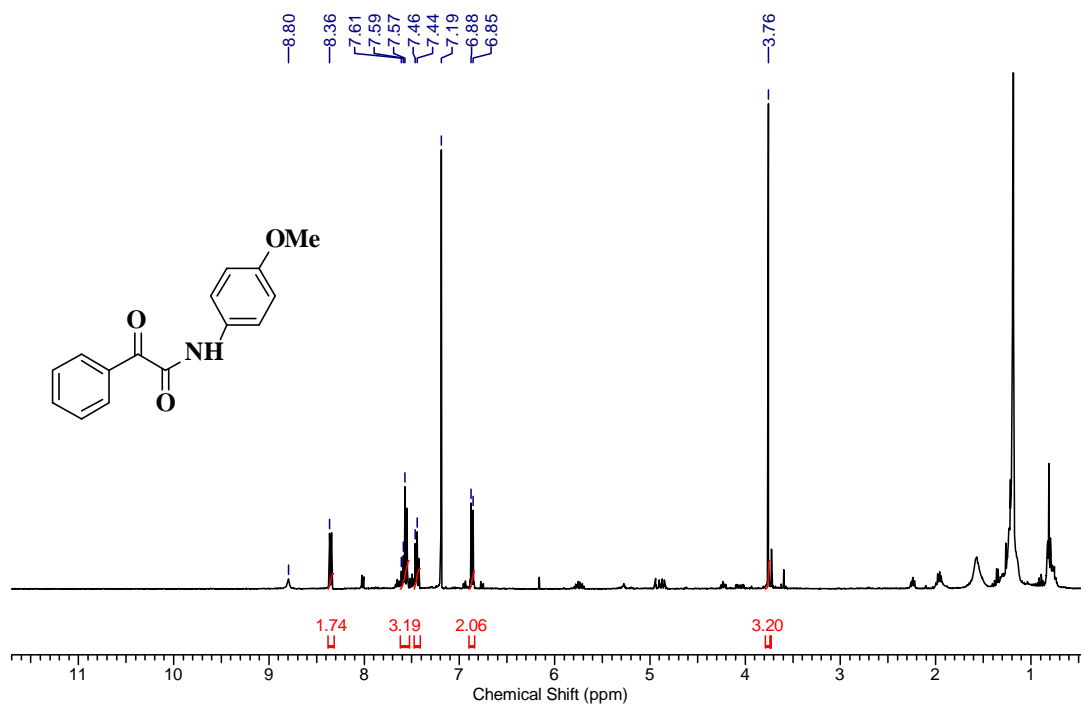
¹³C NMR of compound 3af (CDCl₃, 100 MHz)

225

¹H NMR of compound 3ae (CDCl₃, 400 MHz)
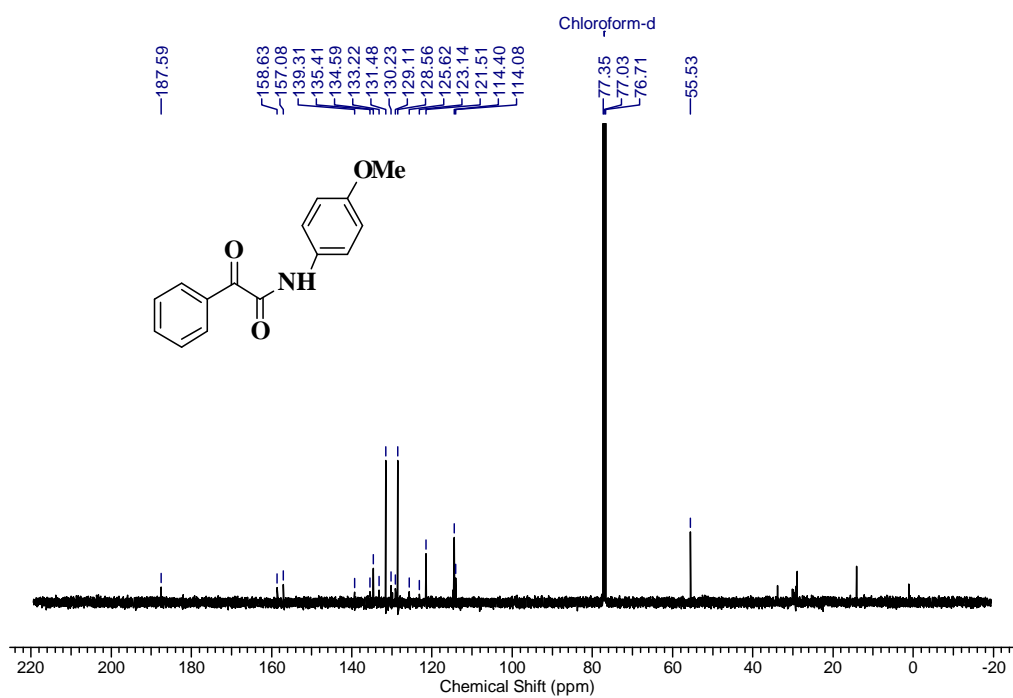
¹³C NMR of compound 3ae (CDCl₃, 100 MHz)
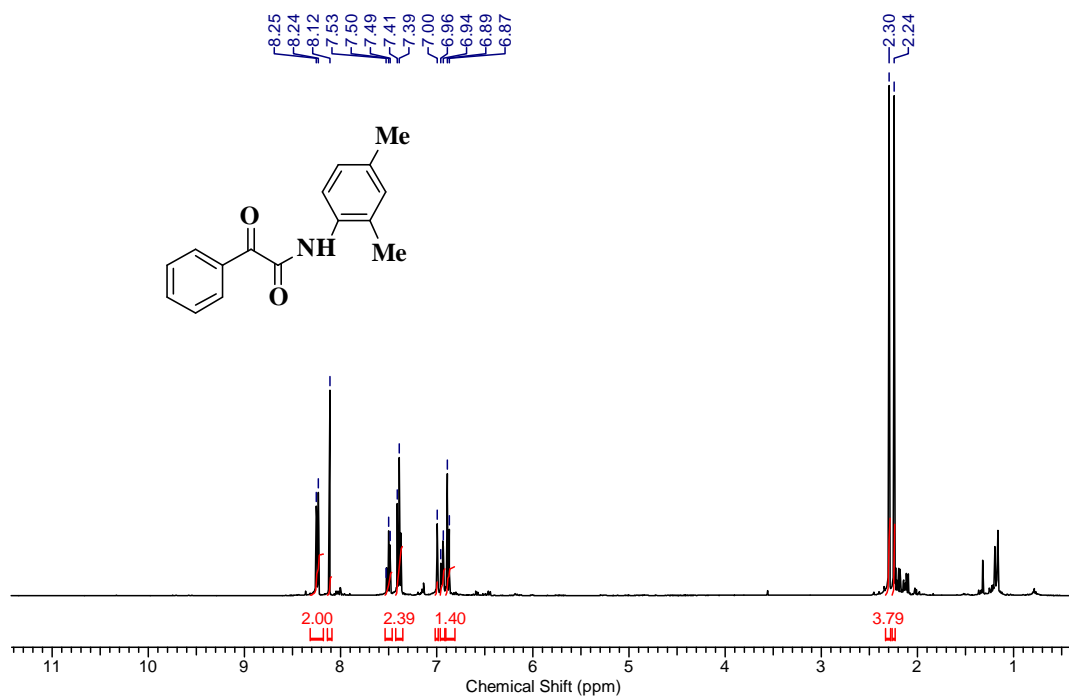
*¹H NMR of compound **3ag** (CDCl₃, 400 MHz)*
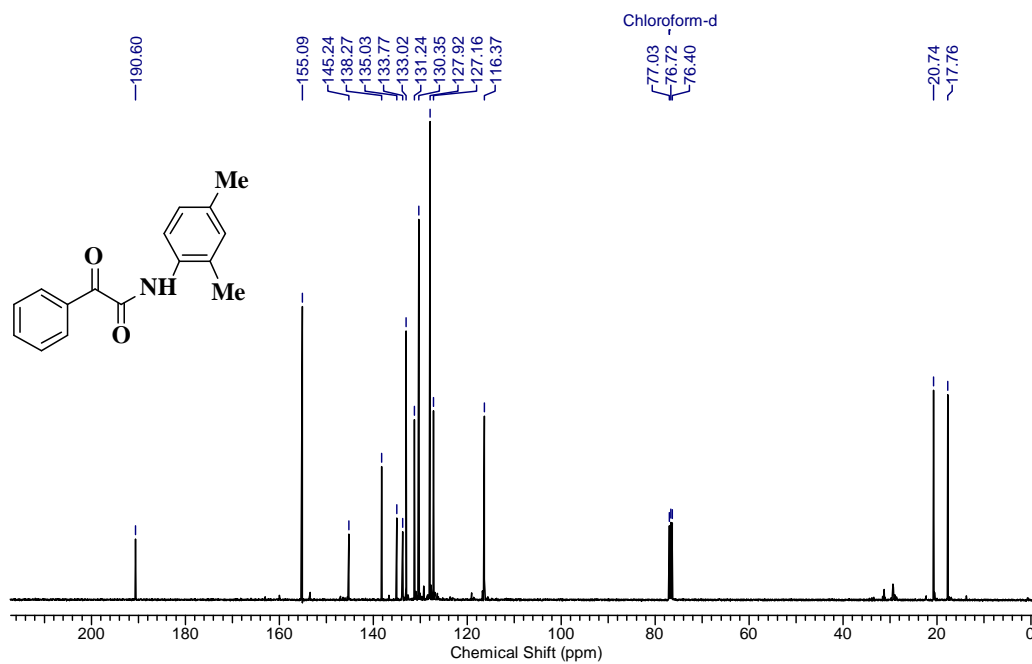
¹³C NMR of compound 3ag (CDCl₃, 100 MHz)
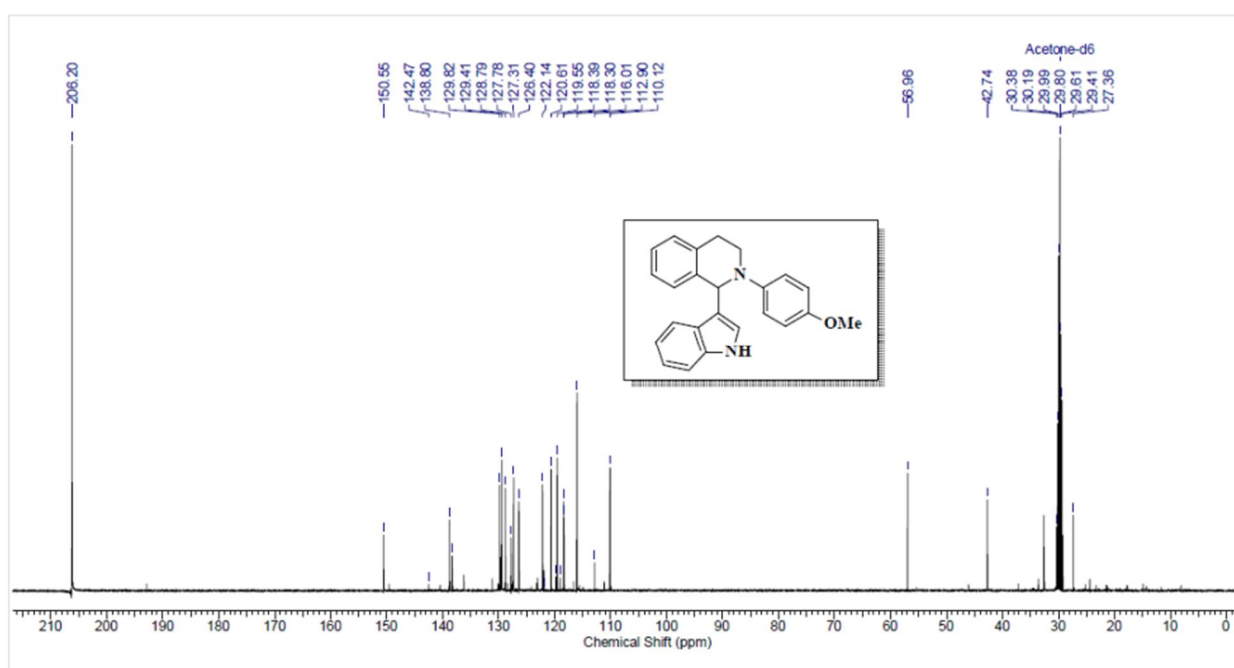
¹H NMR of compound 3ah (CDCl₃, 400 MHz)

¹³C NMR of compound 3ah (CDCl₃, 100 MHz)
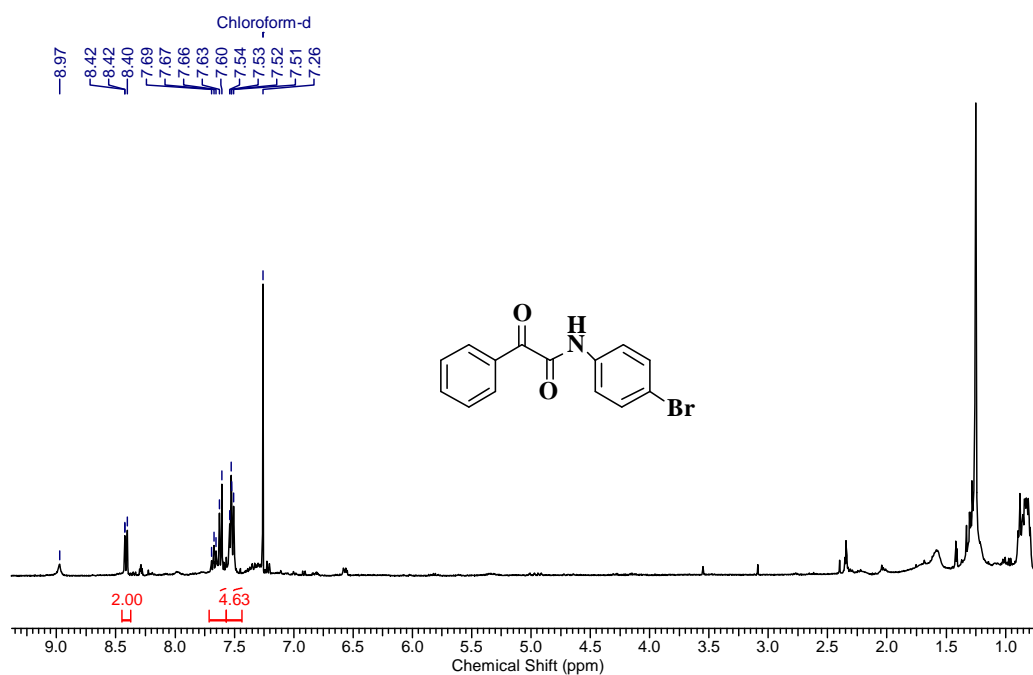
¹H NMR of compound 3ad (CDCl₃, 400 MHz)
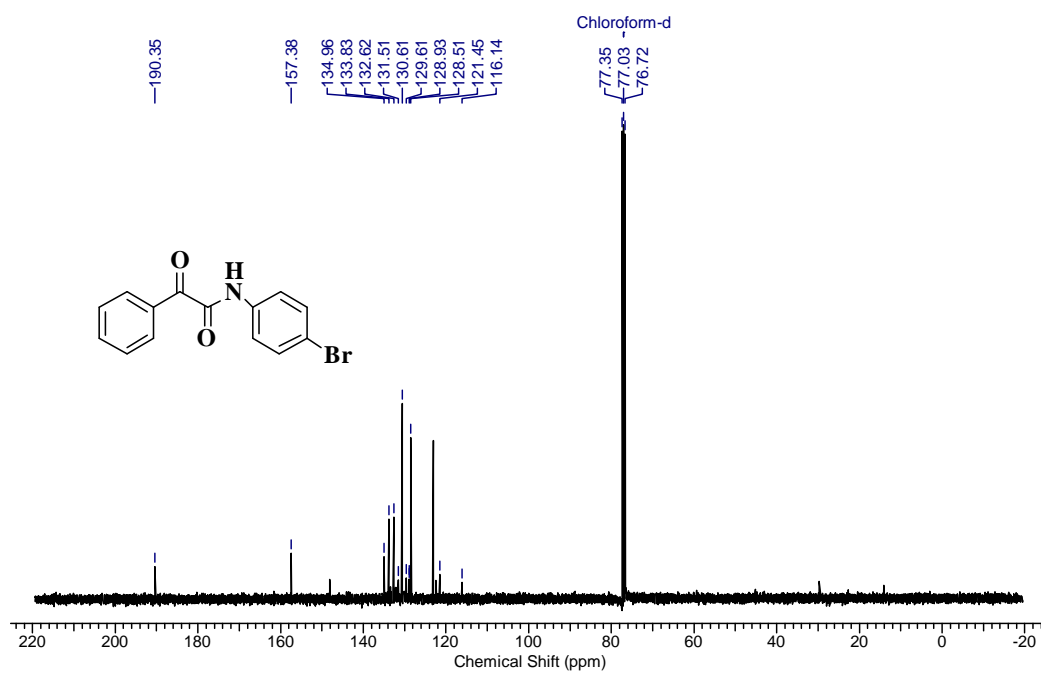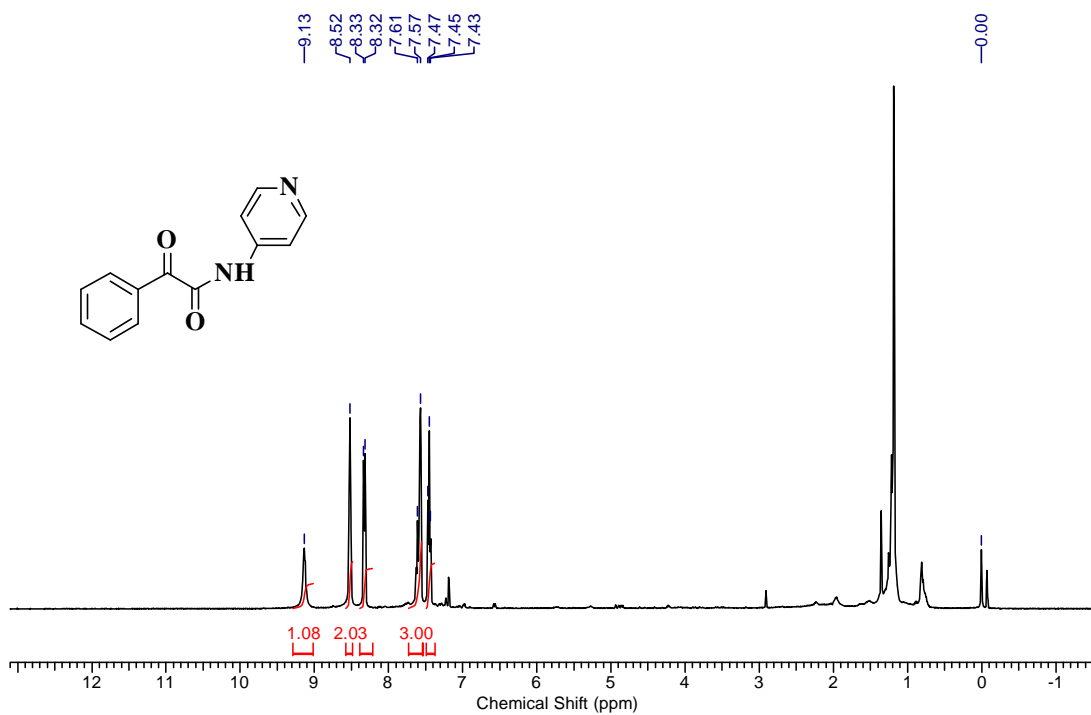
¹³C NMR of compound 3ad (CDCl₃, 100 MHz)

¹H NMR of compound 3ag (CDCl₃, 400 MHz)
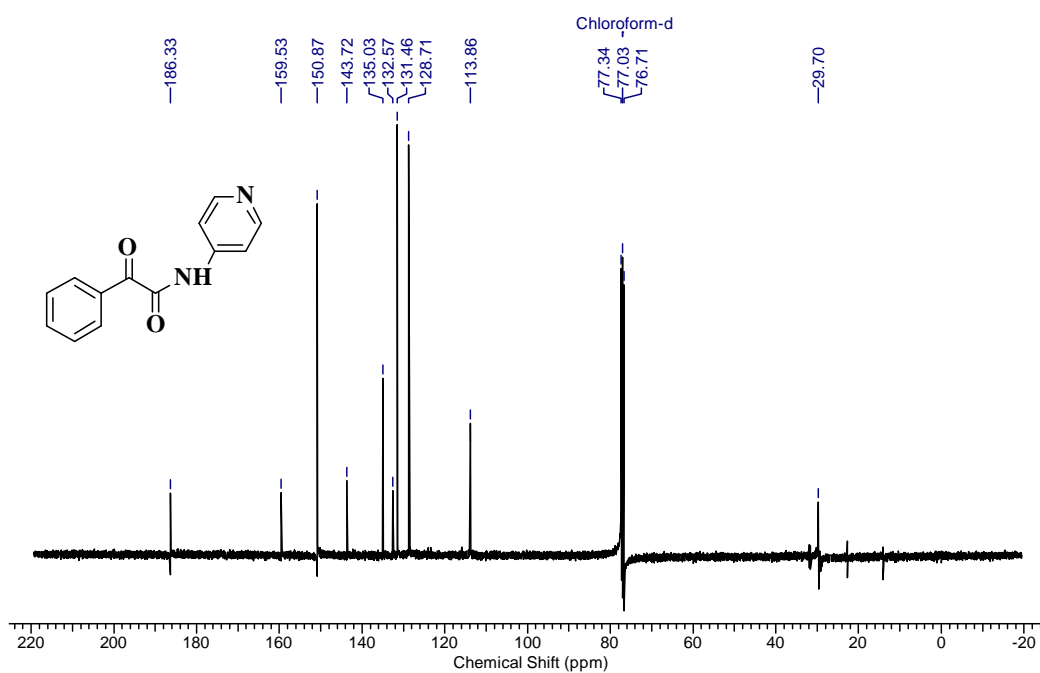
¹³C NMR of compound 3ag (CDCl₃, 100 MHz)
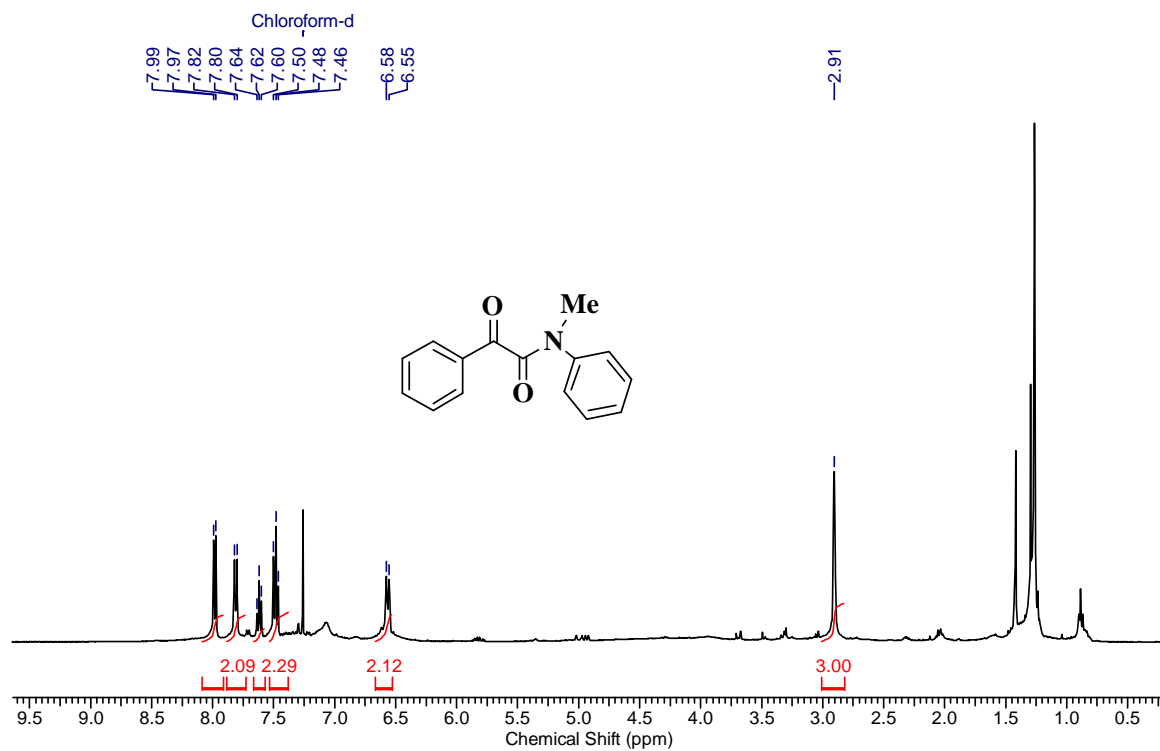
¹H NMR of compound 3ai (CDCl₃, 400 MHz)
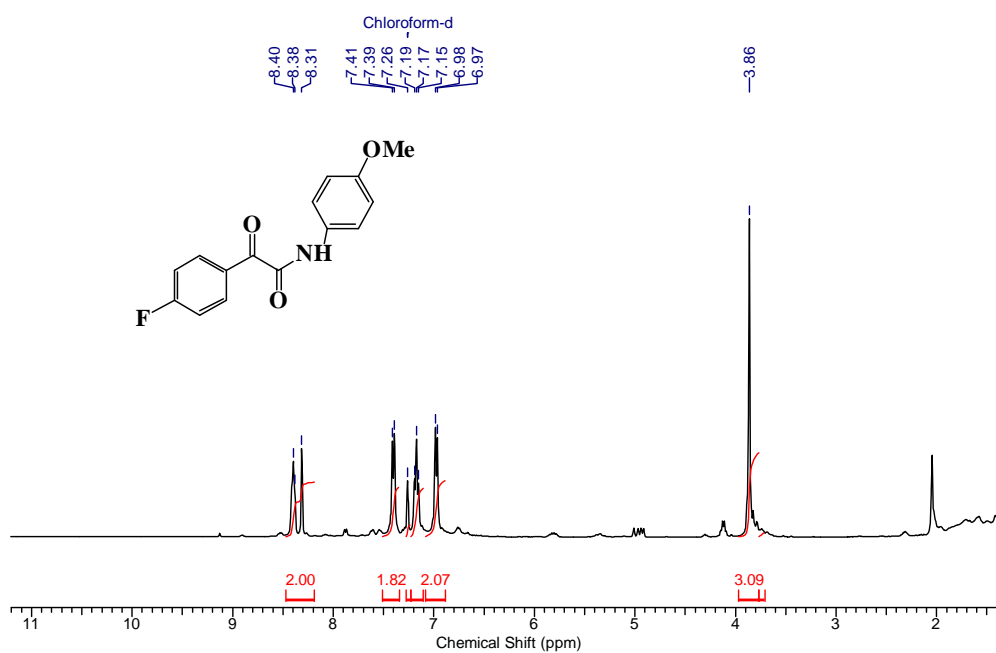
^{1}*H NMR of compound 3dj (CDCl$_3$, 400 MHz)*
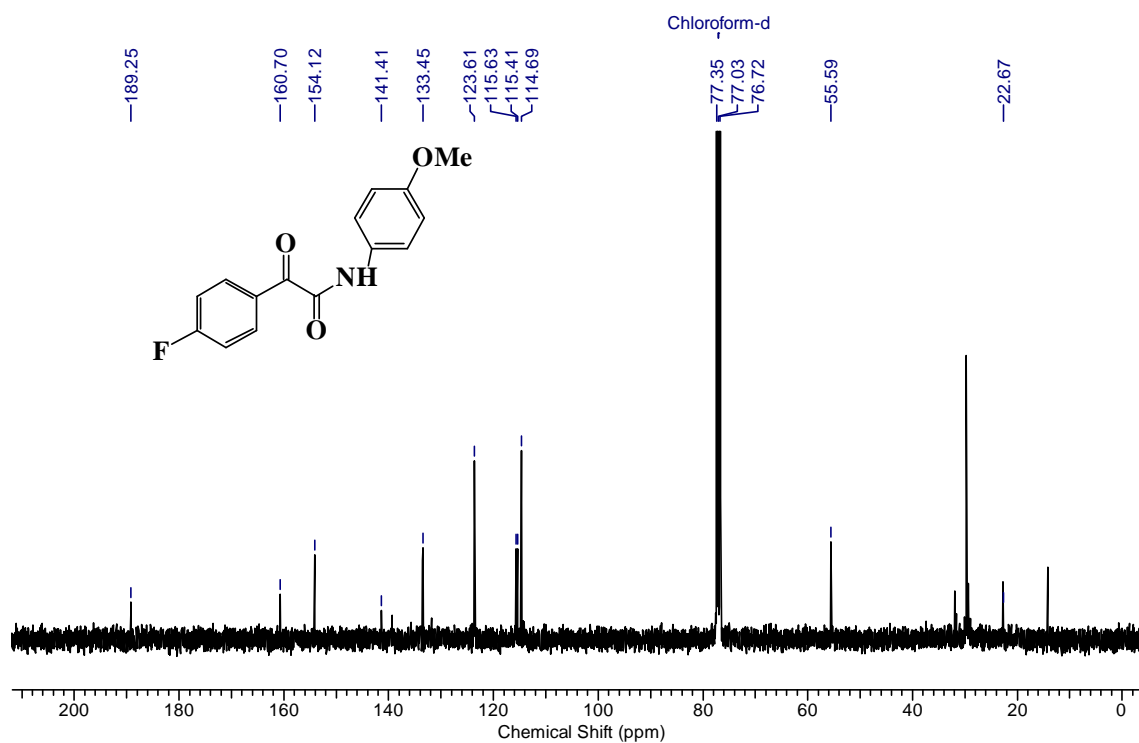
^{13}*C NMR of compound 3dj (CDCl$_3$, 100 MHz)*

¹H NMR of compound 3ei (CDCl₃, 400 MHz)

¹³C NMR of compound 3ei(CDCl₃, 100 MHz)
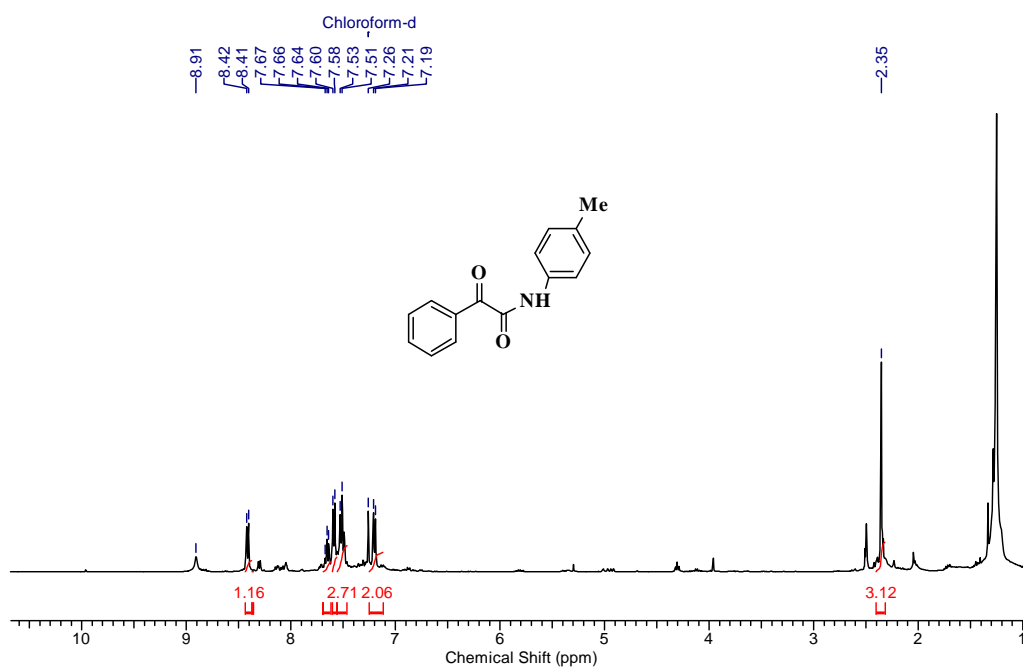
^{1}H NMR of compound 3ae (CDCl$_3$, 400 MHz)
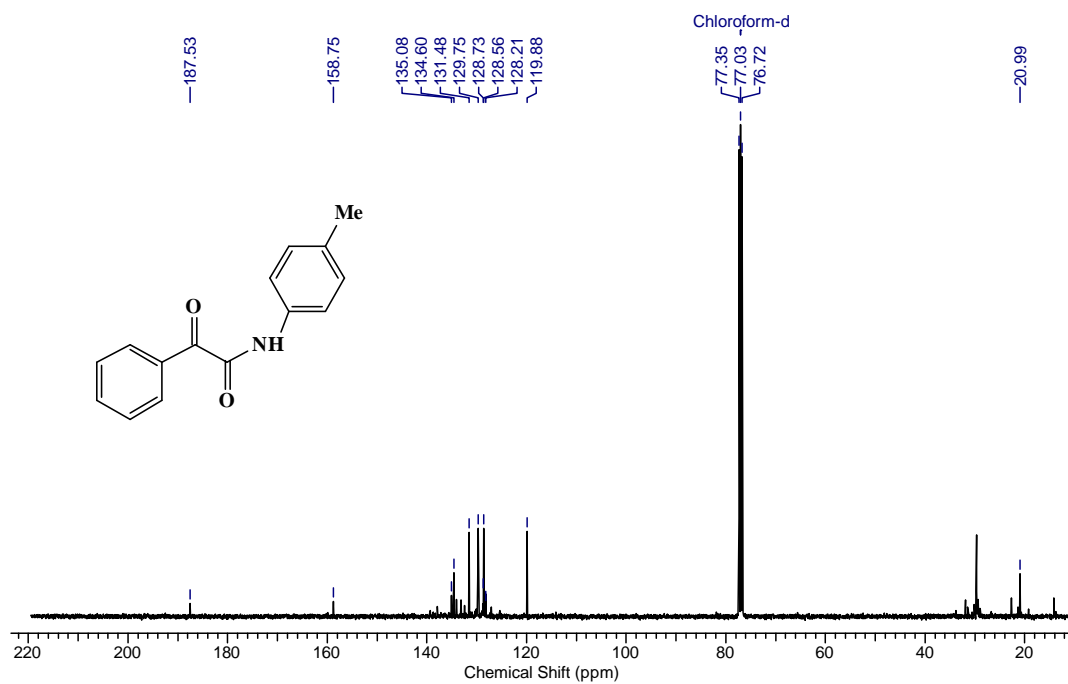
^{13}C NMR of compound 3ae (CDCl$_3$, 100 MHz)

^{1}H NMR of compound 3be (CDCl$_3$, 400 MHz)
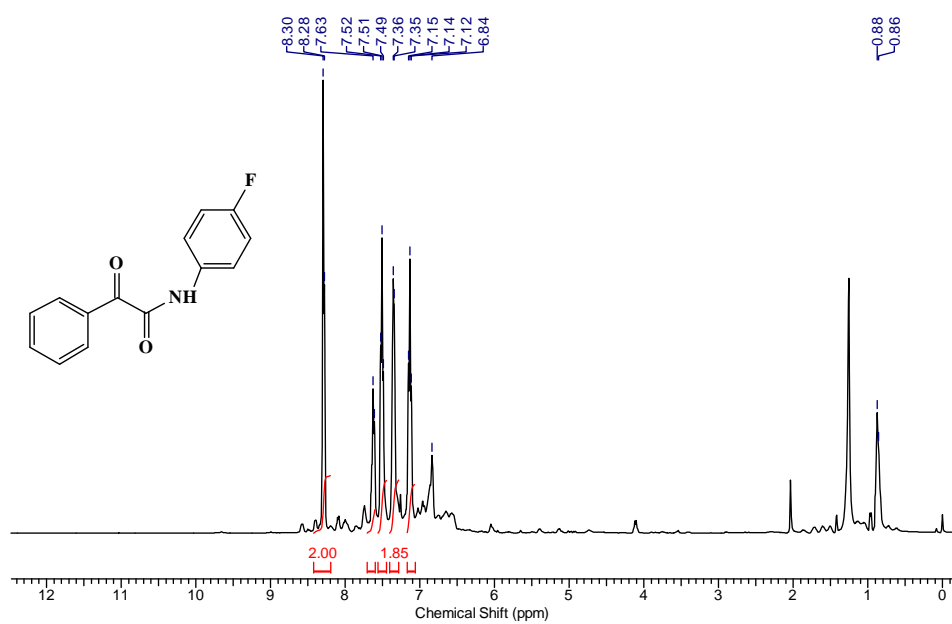
¹H NMR of compound 3ak (CDCl₃, 400 MHz)

¹³C NMR of compound 3ak (CDCl₃, 100 MHz)
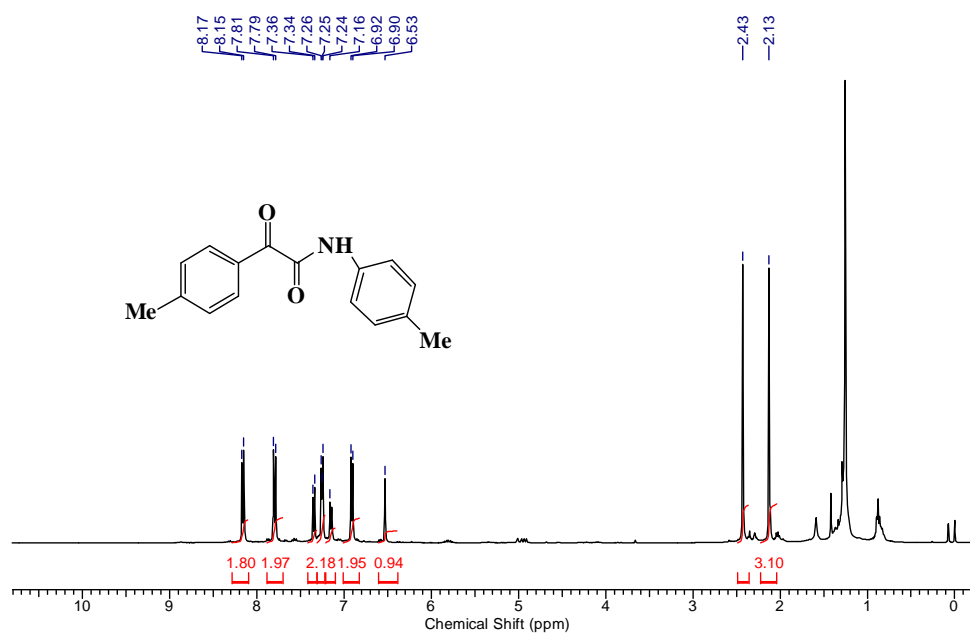
¹H NMR of compound 3ei (CDCl₃, 400 MHz)
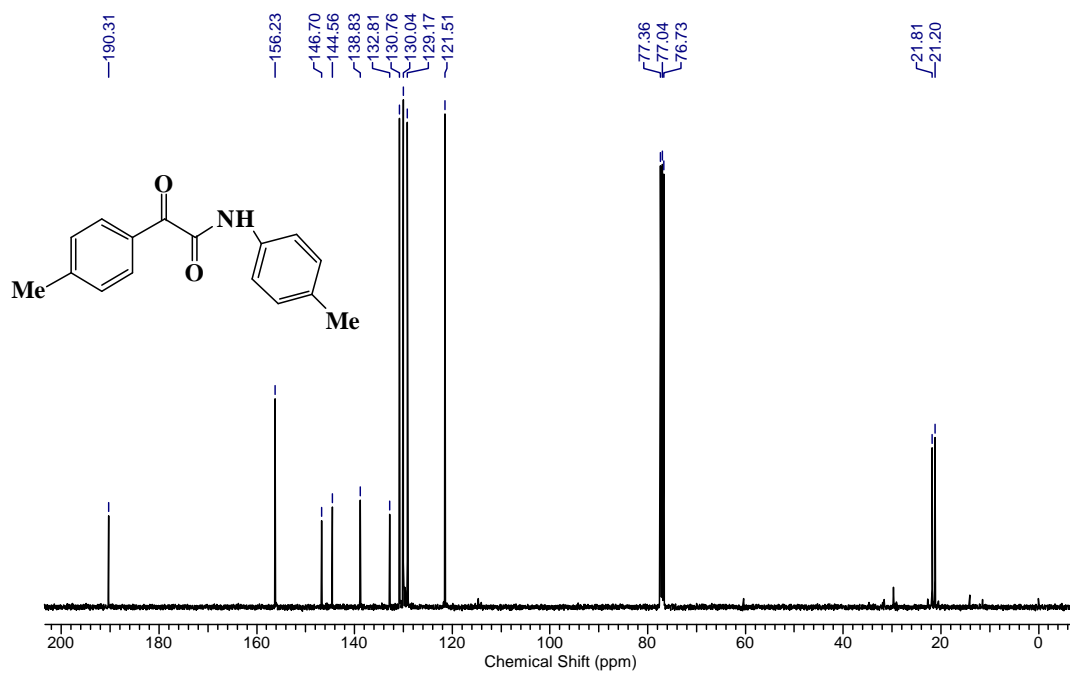
¹³C NMR of compound 3dj (CDCl₃, 100 MHz)

Appendix E

Chapter 6

Characterization data coupled products of N-Phenyl-tertraisoquinolines Table 6.3
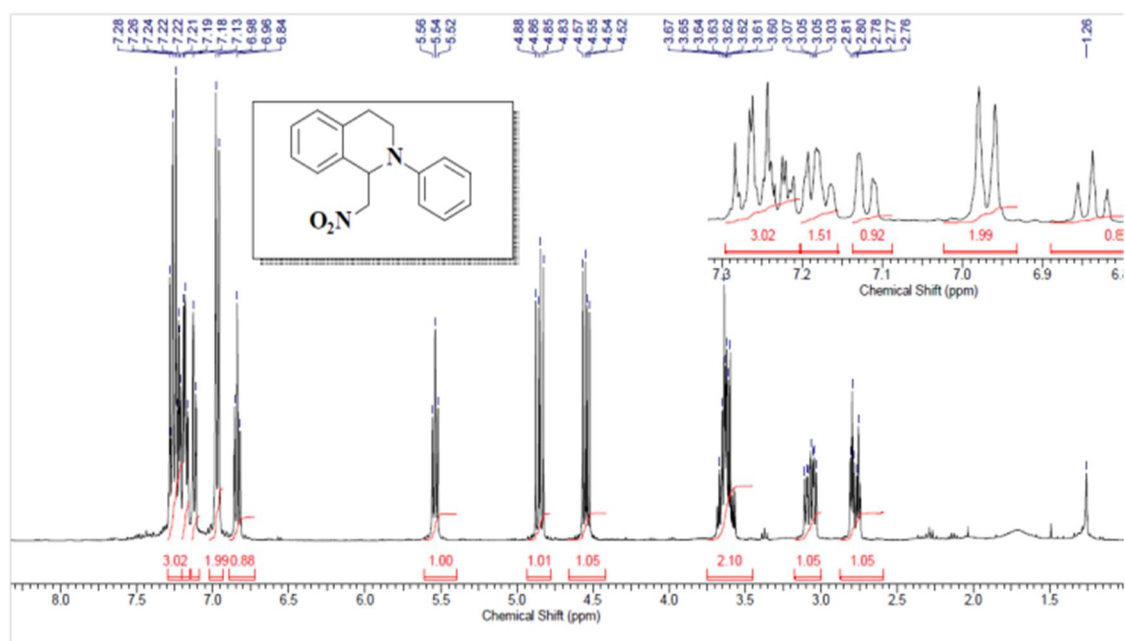
^{1}H NMR of compound **3ab** *(CDCl$_3$, 400 MHz)*
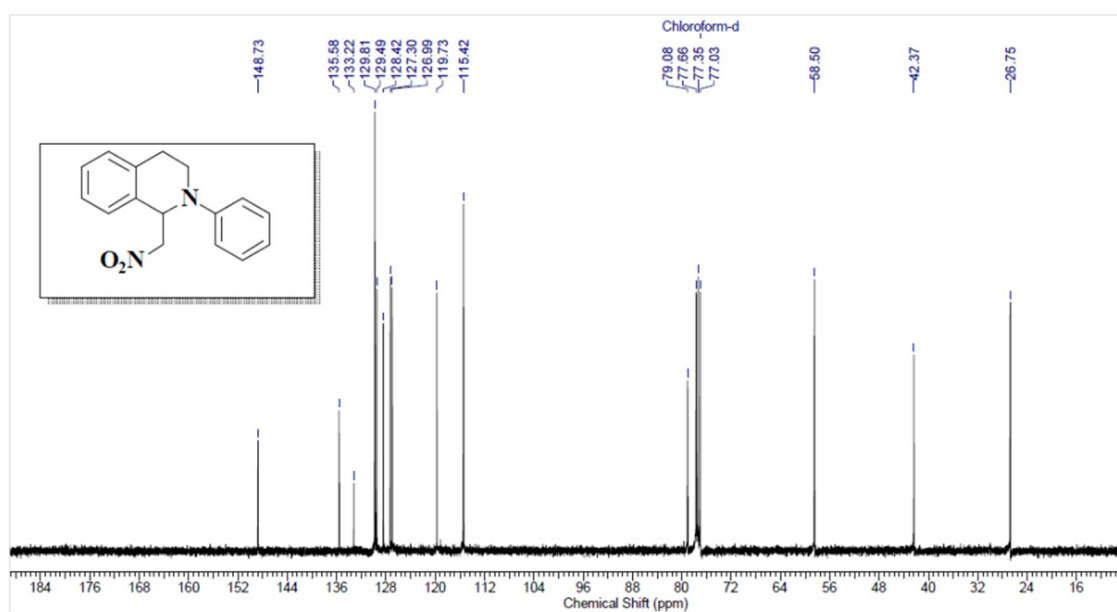
^{13}C NMR of compound **3ab** *(CDCl$_3$, 100 MHz)*
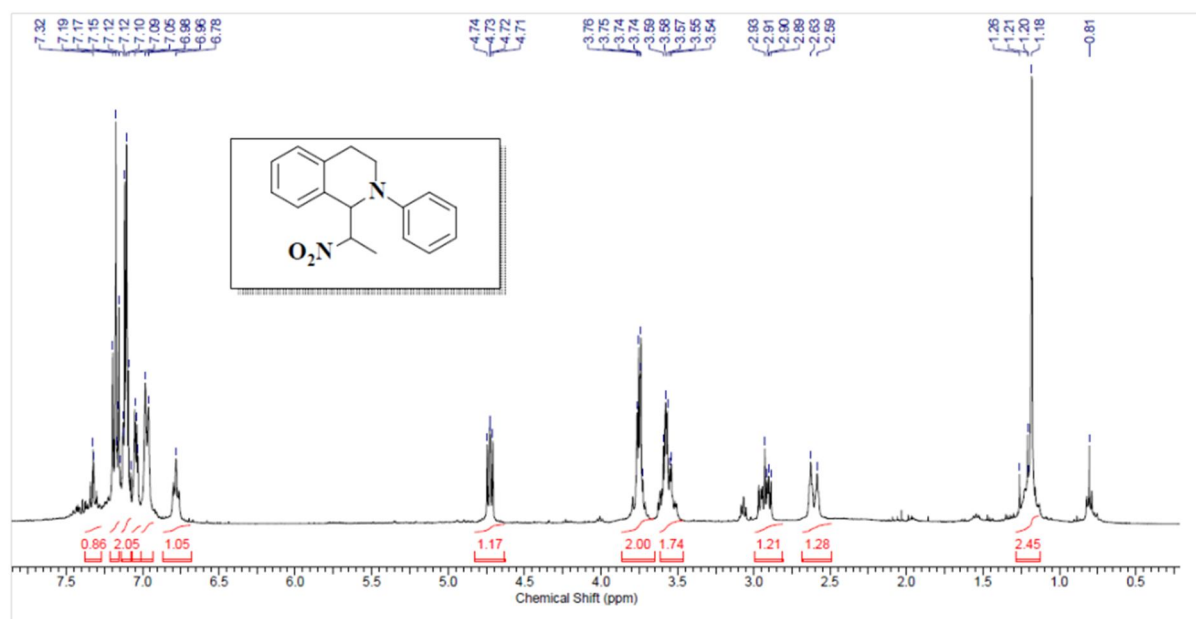
^1H NMR of compound **3ae** (CDCl$_3$, 400 MHz)
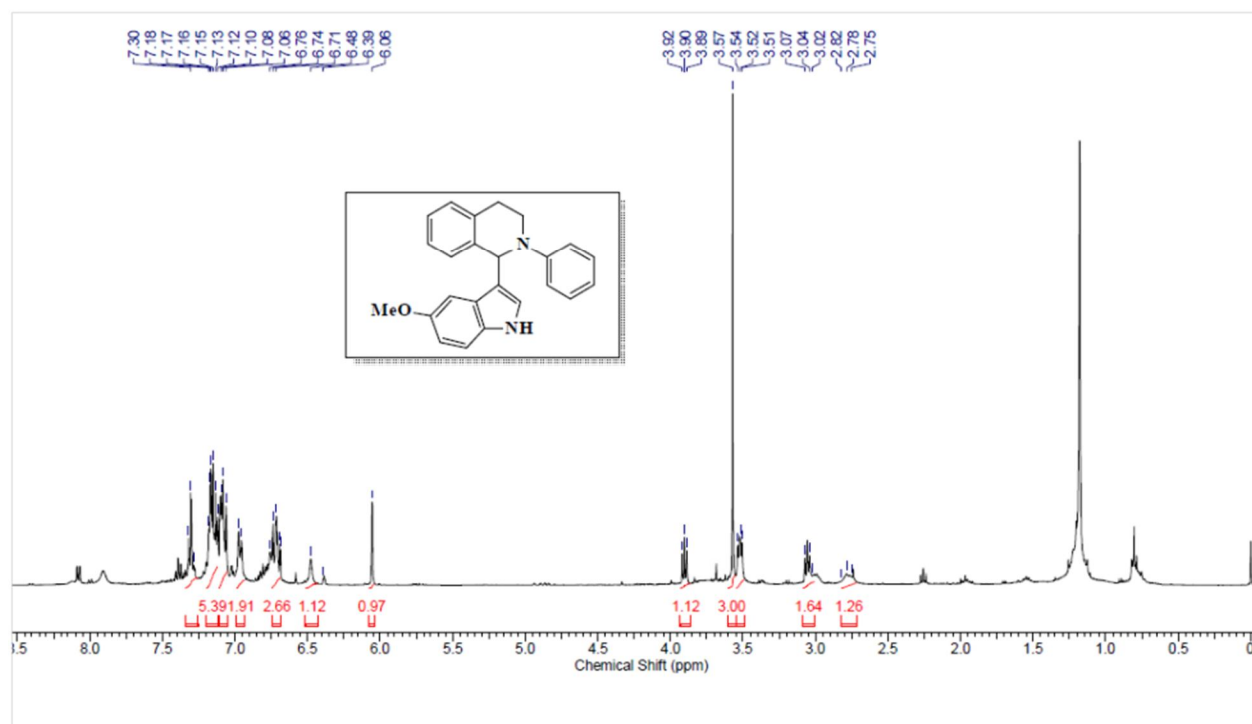
^1H NMR of compound **3ag** (CDCl$_3$, 400 MH
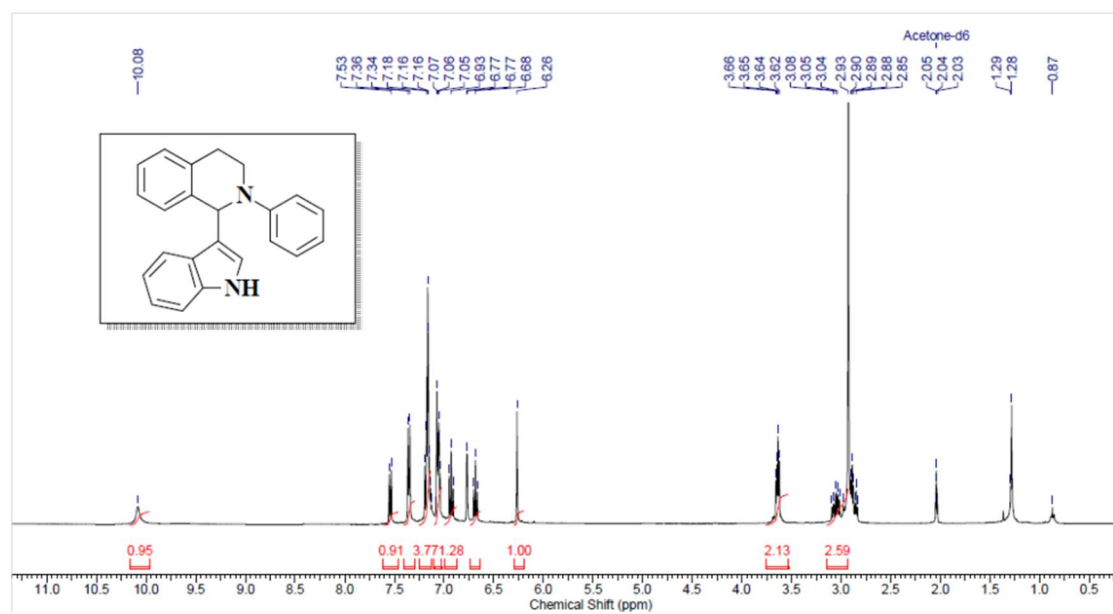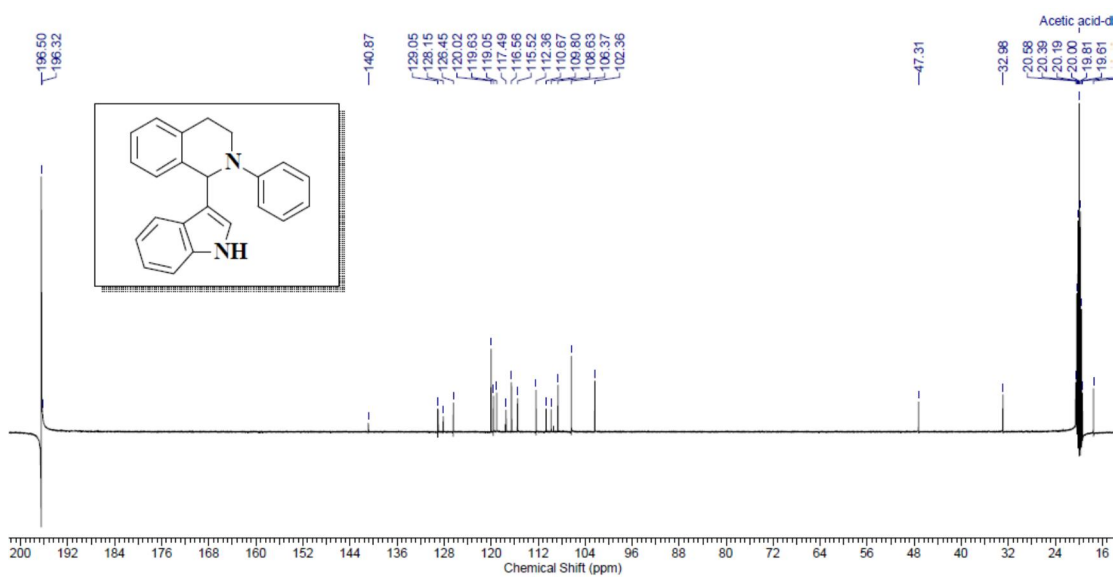
240

^{1}H NMR of compound **3ac** (CDCl₃, 400 MHz)

^{13}C NMR of compound **3ac** (CDCl₃, 100 MHz)

*¹H NMR of compound **3ad** (CDCl₃, 400 MHz)*
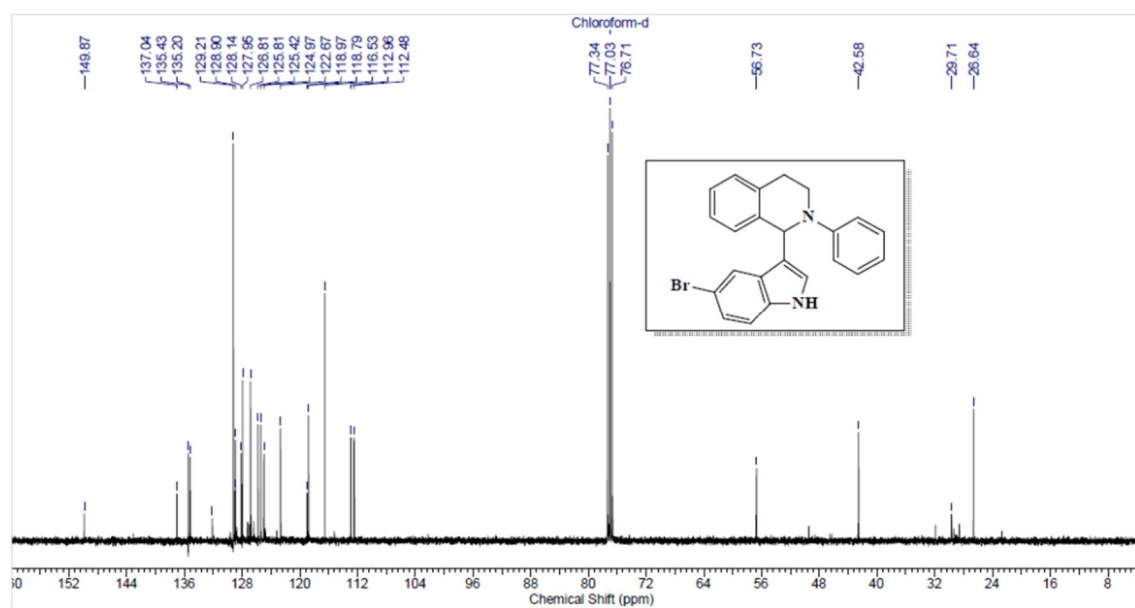

*¹³C NMR of compound **3ac** (CDCl₃, 100 MHz)*

242
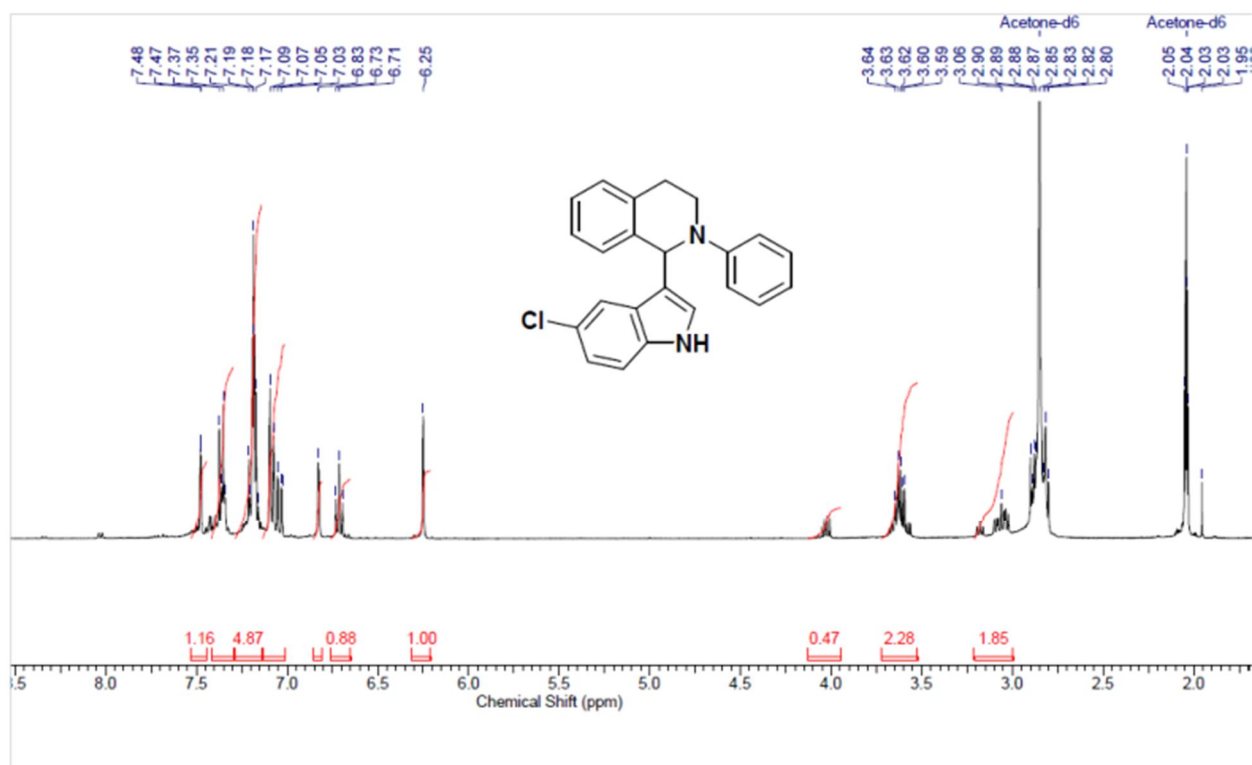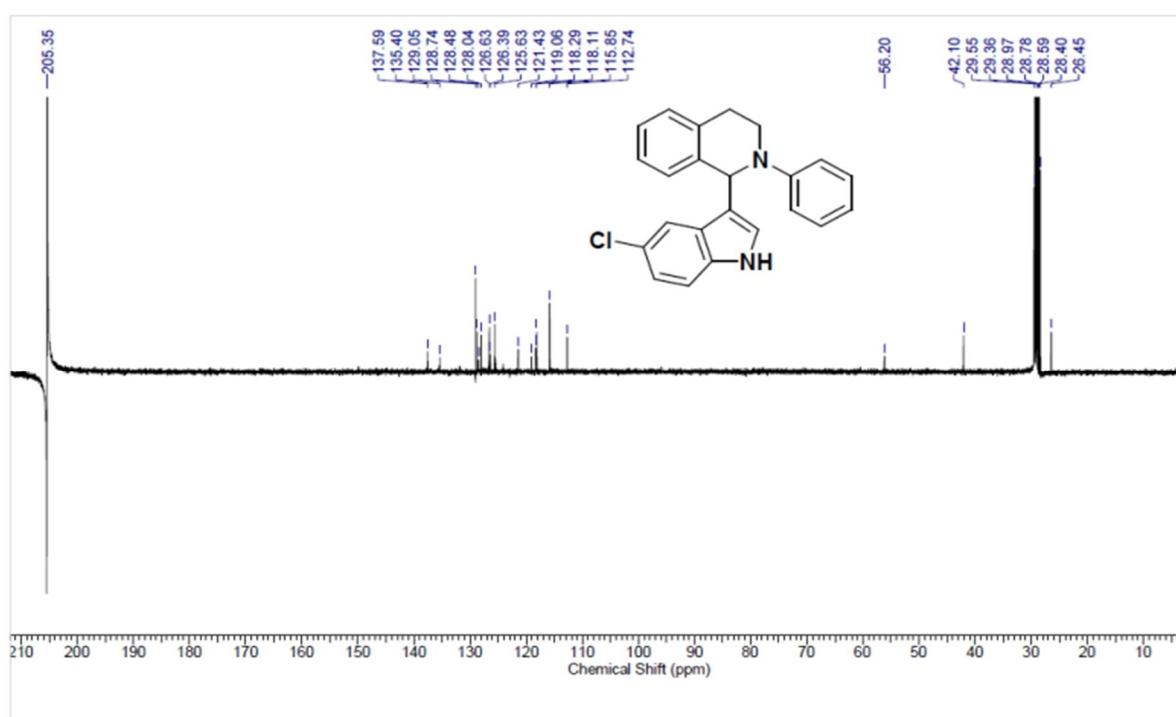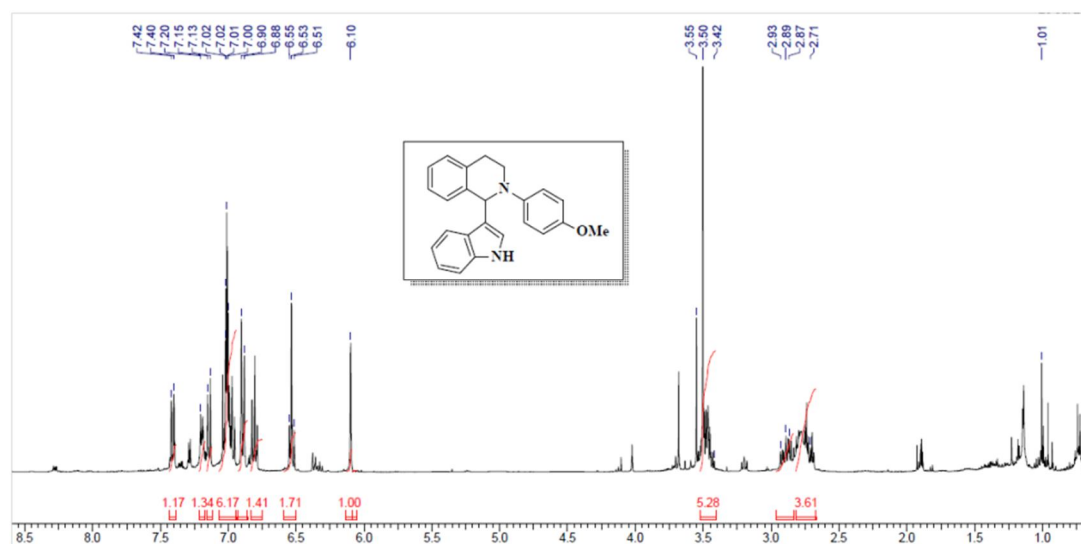
^1H NMR of compound **3cc** (CDCl$_3$, 400 MHz)

^{13}C NMR of compound **3cc** (CDCl$_3$, 100 MHz)
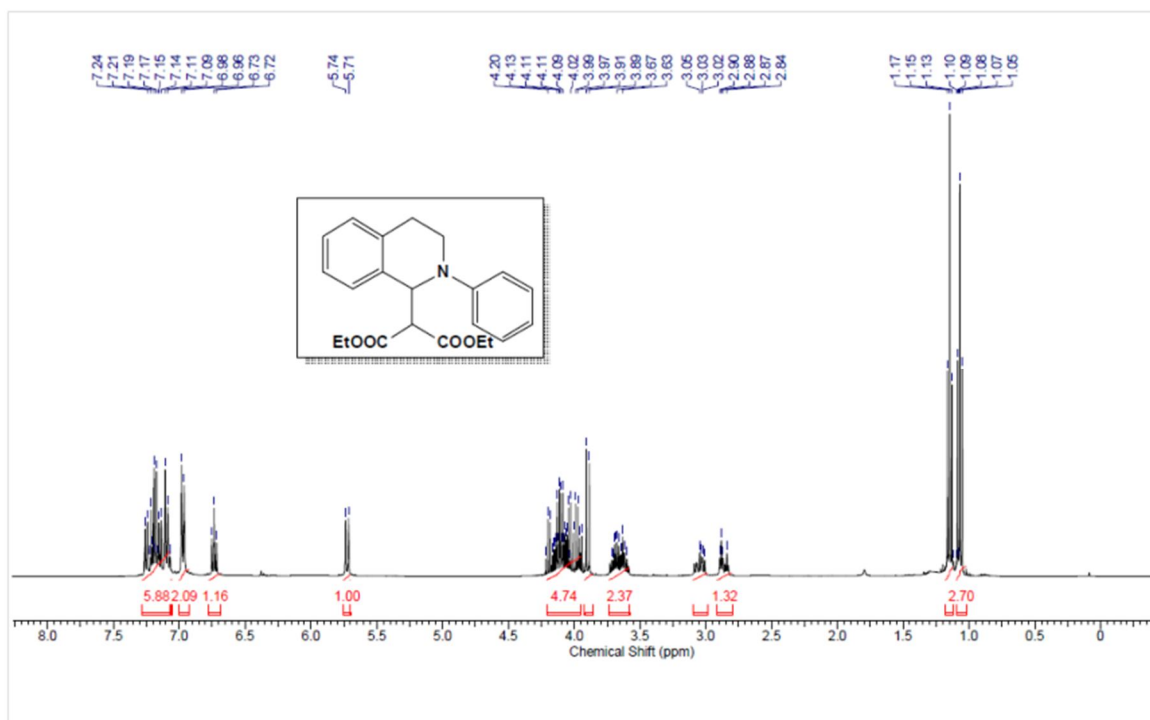
*¹H NMR of compound **3af** (CDCl₃, 400 MHz)*
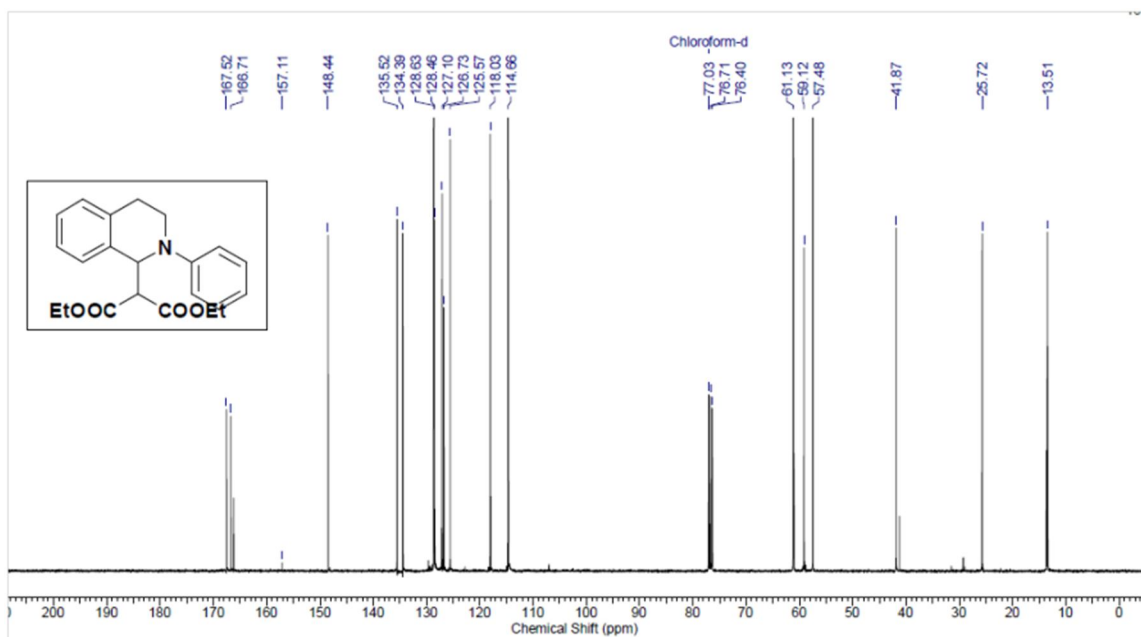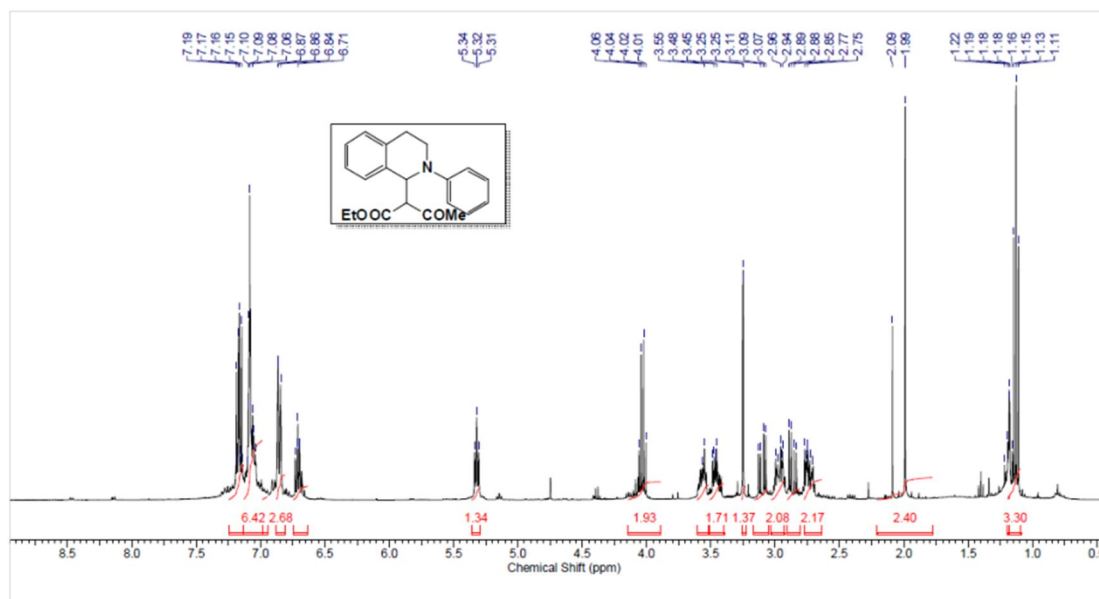
*¹³C NMR of compound **3af** (CDCl₃, 100 MHz)*
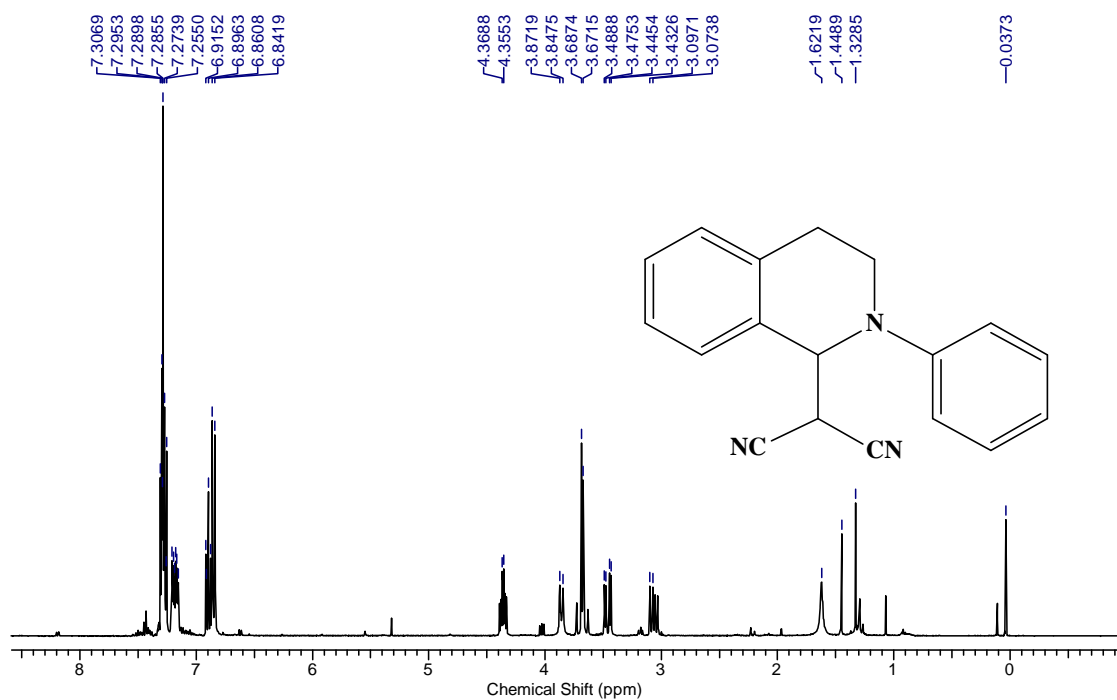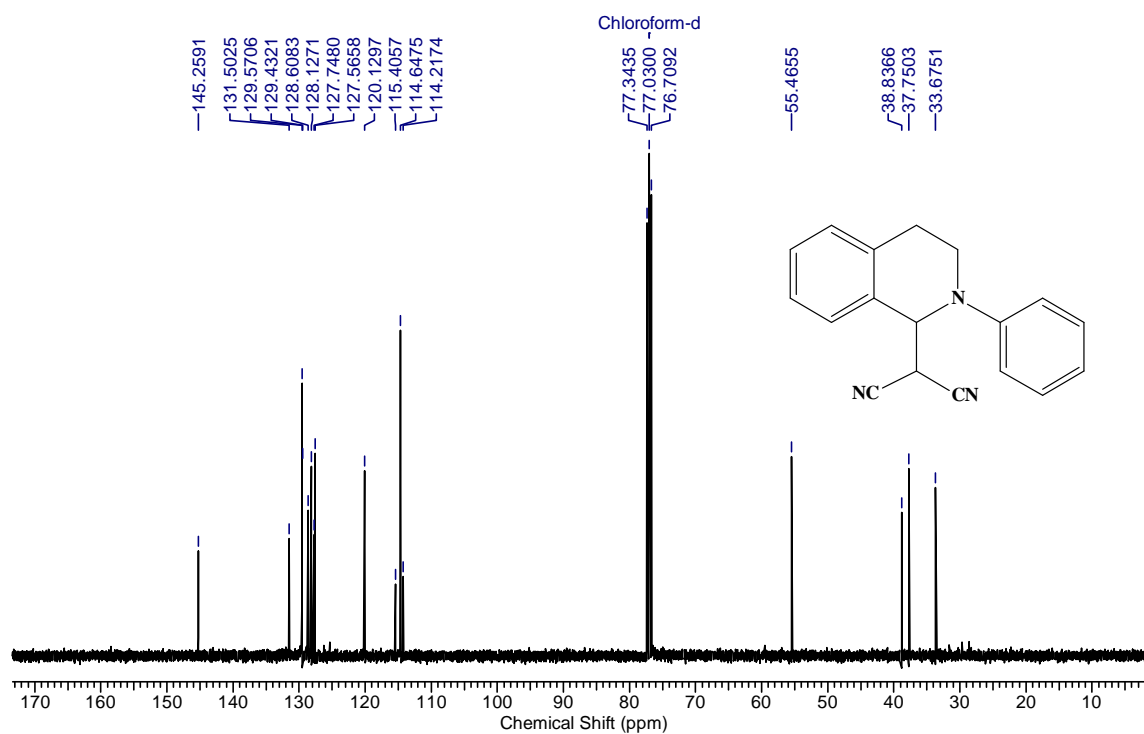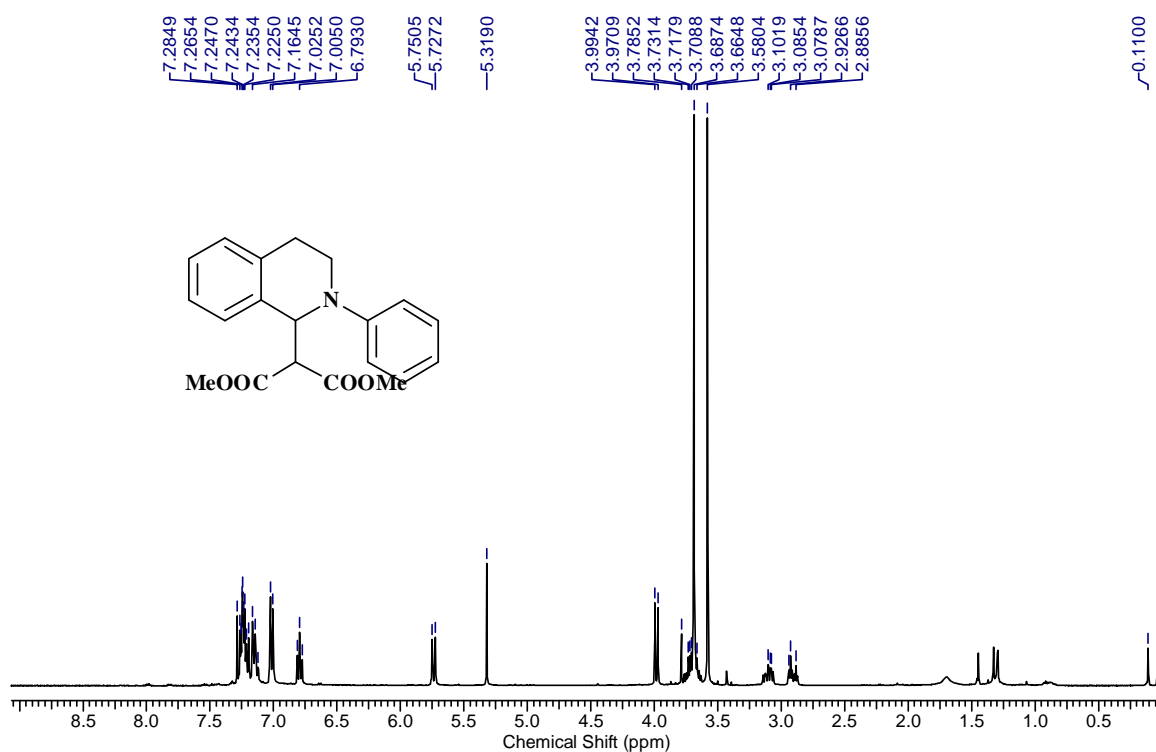
^1H NMR of compound **3af** (CDCl$_3$, 400 MHz)
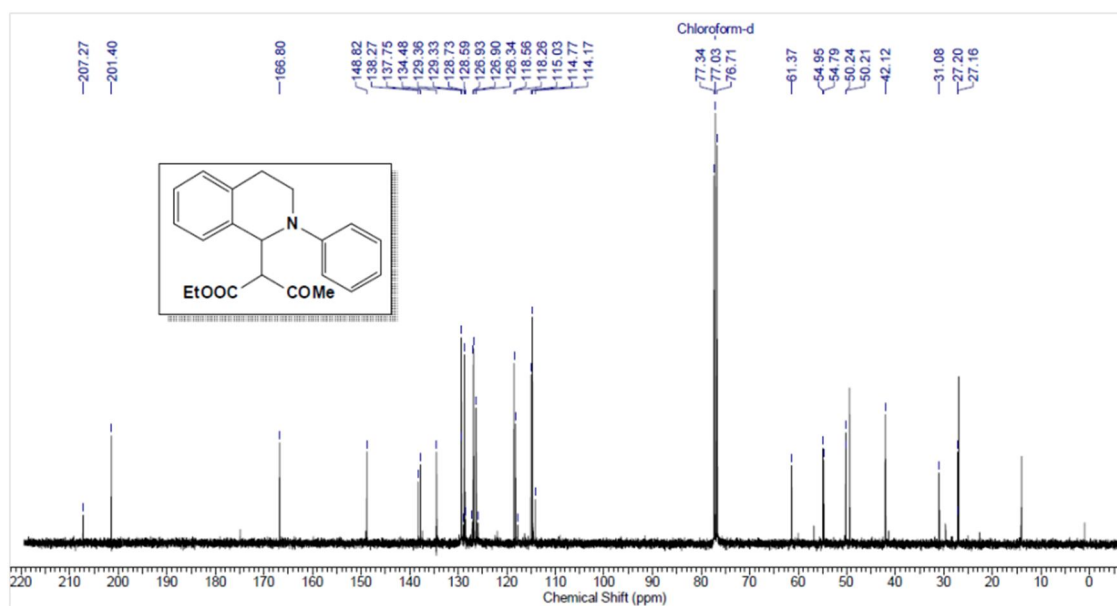
^{13}C NMR of compound **3af** (CDCl$_3$, 100 MHz)
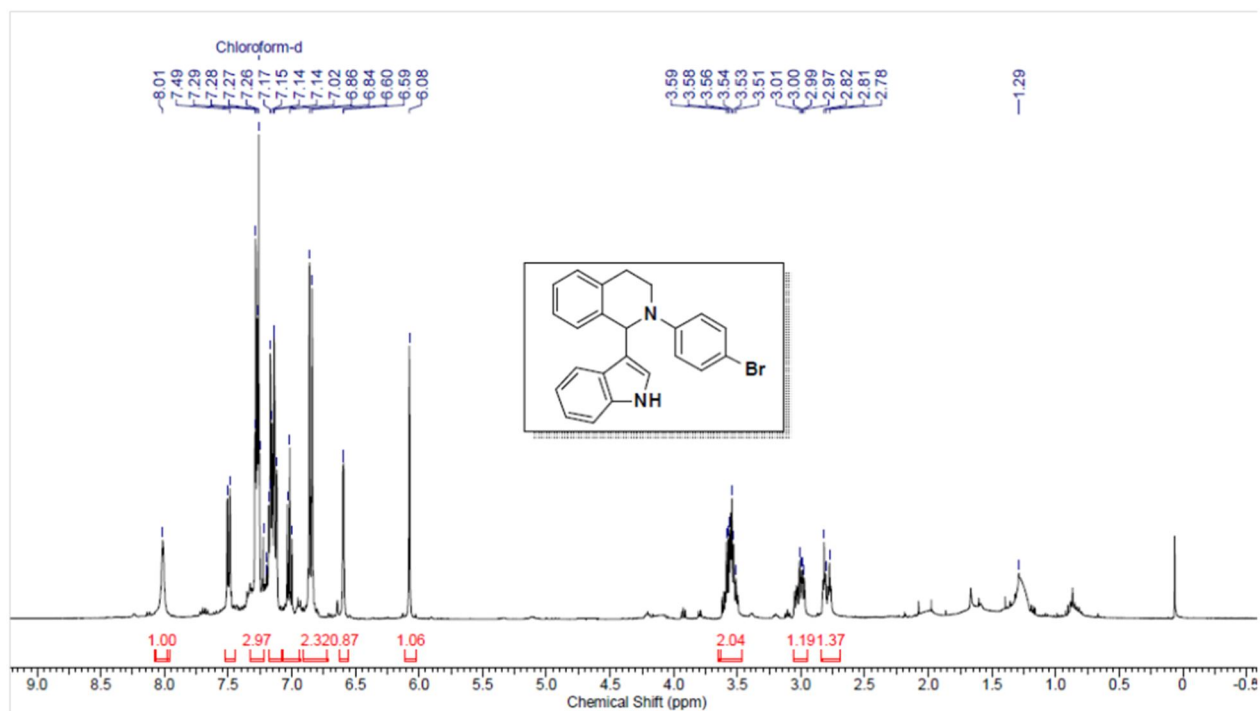
1H NMR of compound 3bc (CDCl3, 400 MHz)
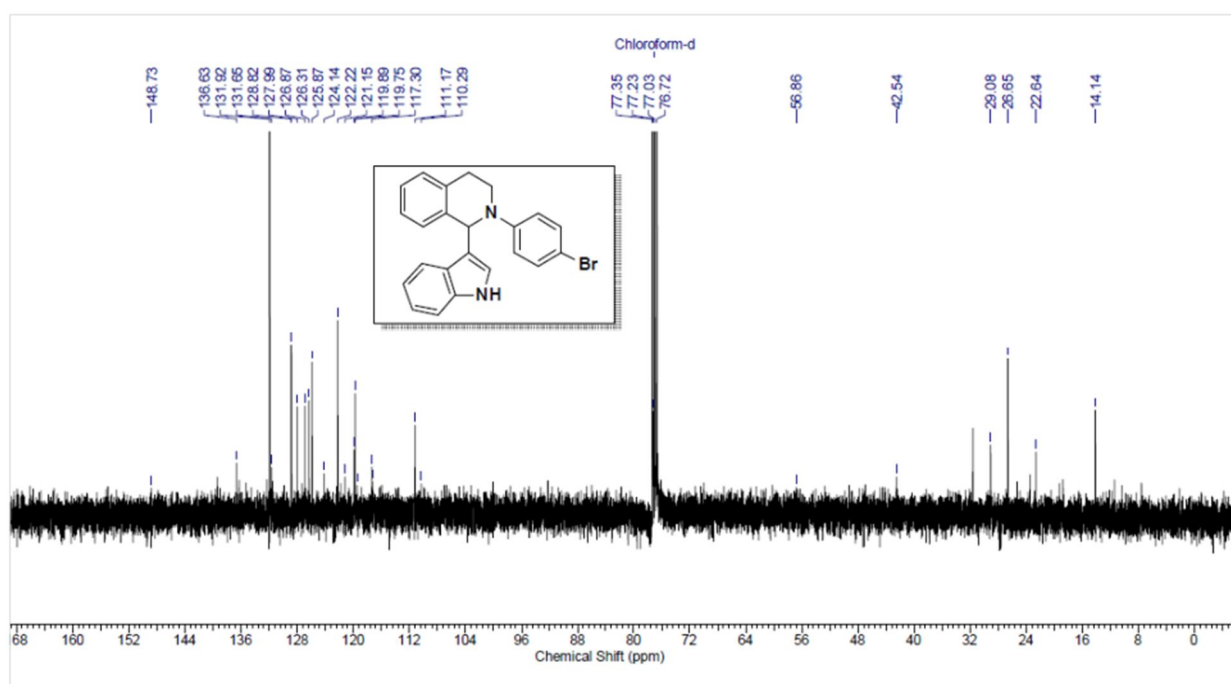
13C NMR of compound 3bc (CDCl3, 100 MHz)
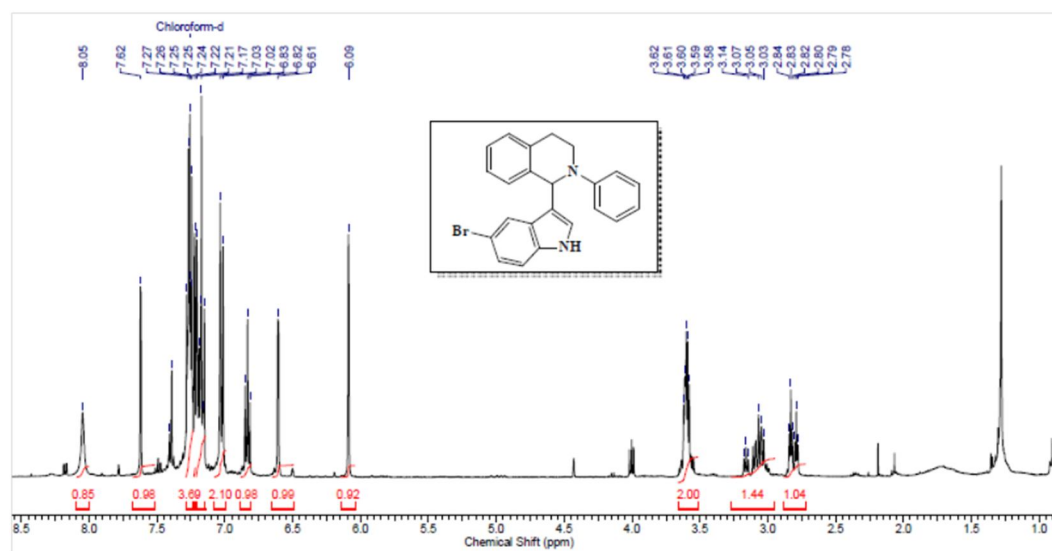
^{1}H NMR of compound **3ai** (CDCl$_3$, 400 MHz)

^{13}C NMR of compound **3ai** (CDCl$_3$, 100 MHz)

^{1}H NMR of compound **3am** (CDCl$_3$, 400 MHz)

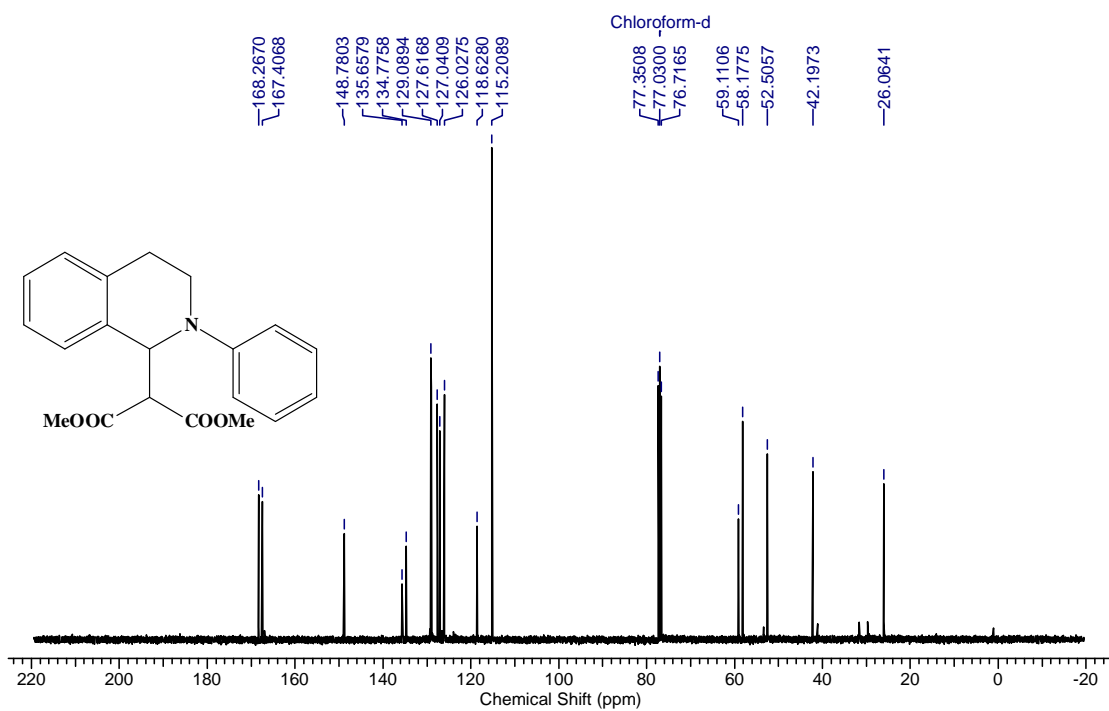^{13}C NMR of compound **3am** (CDCl$_3$, 100 MHz)

^1H NMR of compound **3ah** (CDCl$_3$, 400 MHz)

^{13}C NMR of compound **3ah** (CDCl$_3$, 100 MHz)